



QUANTITATIVE ANALYSIS OF WEAK INTERMOLECULAR INTERACTIONS IN COUMARIN-3-CARBOXYLATE DERIVATIVES

Ahsan Elahi^[a] and Rajni Kant^{[a]*}

Keywords: coumarin3-carboxylate; lattice energy; intermolecular interactions; PIXEL.

The study of nature of intermolecular interactions and their control is extremely important in the area of crystal engineering, in order to design a new material of desirable properties and also for crystal structure prediction. A better understanding of these interactions and their influence on the crystal packing can be obtained by evaluating the energetics associated with these interactions. In this regard, we have identified from the literature a series of coumarin-3-carboxylate derivatives and extracted molecular pairs from the crystal packing providing maximum stability to the crystal structure. The lattice energy of all the compounds have been calculated by using PIXELC module in Coulomb-London-Pauli (CLP) package and is partitioned into corresponding coulombic, polarization, dispersion and repulsion contributions. It is found that the weak intermolecular interactions like C-H...O, π ... π and C-H... π play an important role in the stabilization of the crystal packing.

*Corresponding Authors

Fax: +91 191 243 2051

E-Mail: rkvk.paper11@gmail.com

[a] Department of Physics& Electronics, Jammu University ,
Jammu Tawi -180 006, India.

Introduction

Coumarins (2H-1-benzopyran-2-ones) belong to the family of lactones containing benzopyrone skeletal framework that have enjoyed isolation from plant as well as total synthesis in the laboratory.¹ Coumarins have been extensively investigated due to their applications in the fields of biological, chemical and physical sciences.^{2,3} Coumarin in itself possess broad range of biological activities namely antioxidant,^{4,5} cytostatic,⁶ anti-hyperglycemic,⁷ casein kinase 2 inhibitor,⁸ vasorelaxant,⁹ and antitubercular¹⁰ activities. In view of the immense biological importance of coumarins, we have identified from the literature a few Coumarin-3-carboxylate derivatives and calculated theoretically their lattice energies. The Crystallographic Information File (CIF) for each compound was obtained through the CSD licensed access. All the molecular pairs involved in the crystal packing were extracted and their energies were determined using PIXEL.¹¹ PIXEL calculations were performed in order to estimate the nature and energies associated with the intermolecular interactions which will enable us to explore the role of these interactions in the stabilization of the crystal lattice. A representative illustration of the coumarin moiety indicating the atomic numbering scheme used for the present work is shown in Fig.1.

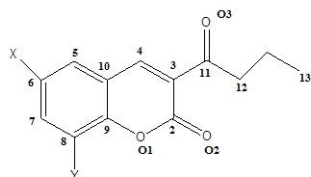


Figure 1. Coumarin moiety and the numbering scheme used

The chemical name, molecular code, position of the substituent(s) and precise crystallographic data for each compound are presented in Table 1a and 1b, respectively.

Table 1a. List of compounds and the position of substituent(s)

Chemical name	Substituent	
	X	Y
Ethyl-2H-benzopyran-2-oxo-3-carboxylate (M-1) ¹²	H	H
Ethyl 6-chloro-2-oxo-2H-chromene-3-carboxylate (M-2) ¹³	Cl	H
Ethyl 6-bromo-2-oxo-2H-chromene-3-carboxylate (M-3) ¹³	Br	H
Ethyl 8-methoxy-2-oxo-2H-chromene-3-carboxylate (M-4) ¹⁴	H	OC H ₃

Table 1b. Precise crystal data for coumarin-3-carboxylate derivatives

Data	M-1	M-2	M-3	M-4
	C ₁₂ H ₁₀ O ₄	C ₁₂ H ₉ ClO ₄	C ₁₂ H ₉ BrO ₄	C ₁₃ H ₁₂ O ₅
M, g mol ⁻¹	218.20	252.64	297.10	248.23
Crystal System	Monoclinic	Monoclinic	Monoclinic	Monoclinic
Space Group	P21/c	P21/c	P21/c	P21/n
a(Å)	7.916(1)	5.7982(5)	5.8432(6)	6.8572(14)
b(Å)	15.736(2)	13.0702(12)	13.2073(14)	10.644(2)
c(Å)	8.737(8)	15.5540(12)	15.6959(15)	15.780(3)
α (°)	90	90	90	90
β (°)	108.11(6)	108.191(3)	109.327(3)	100.153(14)
γ (°)	90	90	90	90
Z	4	4	4	4
R	0.0696	0.055	0.045	0.044

Theoretical calculations

The lattice energies of all the compounds were calculated by PIXELC module in Coulomb-London-Pauli (CLP) computer program package (version 13.2.2012).¹¹ The total lattice energy is partitioned into its coulombic, polarization, dispersion and repulsion contributions (Table 2).

Table 2. Lattice energy from CLP (in kcal mol⁻¹)

Molecule	E_{Cou}	E_{Pol}	E_{Disp}	E_{Rep}	E_{Tot}
M-1	-11.08	-4.11	-28.15	17.13	-26.22
M-2	-12.35	-4.34	-31.59	19.26	-29.039
M-3	-12.64	-4.2065	-31.09	19.33	-28.58
M-4	-14.86	-5.47	-35.25	25.40	-30.18

In CLP, the coulombic terms are handled by Coulomb's law while the polarization terms are calculated in the linear dipole approximation, with the incoming electric field acting on local polarizabilities and generating a dipole with its associated dipole separation energy; dispersion terms are simulated in London's inverse sixth power approximation, involving ionization potentials and polarizabilities; repulsion is presented as a modulated function of wavefunction overlap. All the stabilizing molecular pairs involved in crystal packing were selected from the mlc output file, which is generated after PIXEL energy calculations and were analysed with their interaction energies. The symmetry operator and centroid-centroid distance along with coulombic, polarization, dispersion, repulsion and total interaction energies between the molecular pairs are presented in Table 3. The molecular pairs are arranged in decreasing order of their stabilization energies. The PIXEL method has been preferred for the quantification of intermolecular interactions, primarily because of the following reasons: (1) It is computationally less demanding.¹¹ (2) It allows partitioning of total interaction energy into corresponding coulombic, polarization, dispersion, and repulsion contribution which facilitates a better understanding of the nature of intermolecular interactions contributing towards the crystal packing.^{15,16} (3) The energies obtained from PIXEL calculation are generally comparable with high level quantum mechanical calculations.^{17,18}

Results and discussion

Ethyl-2H-benzopyran-2-oxo-3-carboxylate (M-1)

Molecular pairs of M-1 (a-i) extracted from crystal structure along with their respective interaction energies are shown in Fig. 2. The maximum stabilization to the crystal structure comes from C-H... π intermolecular interaction involving H12 with C8 and C9 of Cg2 (where Cg2 is the centroid of benzene ring) and C-C molecular stacking forming dimer related by centre of symmetry. The stabilization energy of the pair is -10.25 kcal mol⁻¹ (Fig. 2a) obtained using PIXEL.

Another molecular pair (Fig. 2b) involves molecular stacking to generate dimers across the centre of symmetry having an interaction energy of -8.41 kcal mol⁻¹. The next two stabilized pairs show the presence of bifurcated

C-H...O hydrogen bonding. Motif c involves bifurcated donor atom H8 interacting with O1 and O2 (Fig. 2c) whereas in motif d, acceptor atom O2 (interacting with H6 and H7) and donor atom H6 (interacting with O2 and O3) is bifurcated (Fig. 2d). The stabilization energy of the two pairs being -7.05 kcal mol⁻¹ and -4.73 kcal mol⁻¹ respectively and the stabilization mainly comes from the coulombic component (Table 3). Motif e shows the presence of C-H... π (involving H13 and C6 of Cg2 ring) and provides stabilization of -2.08 kcal mol⁻¹ (Fig. 2e). Additional stabilization to the structure comes from molecular pair (Fig. 2f) showing the presence of C-H...H-C (involving H5 and H13) with H...H distance being 2.478 Å, forming dimer having an interaction energy of -1.98 kcal mol⁻¹. Molecular pairs g, h and i having interaction energies -1.79, -1.38 and -1.31 kcal mol⁻¹, respectively, also contribute towards the stability of crystal packing.

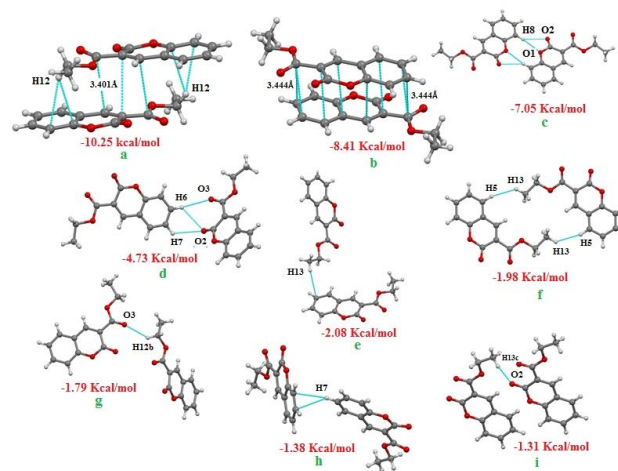


Figure 2. Molecular pairs (a-i in Table 3) along with their interaction energies calculated with Pixel (values in red) in M-1.

Ethyl-6-chloro-2-oxo-2H-chromene-3-carboxylate (M-2)

The extracted molecular pairs (a-f) of M-2 are shown in Fig. 3 along with their stabilization energies. The most stabilized molecular pair in M-2 shows the presence of bifurcated acceptor C-H...O hydrogen bonding (involving O3 with H4 and H5) forming dimers related by centre of symmetry with an interaction energy of -10.27 kcal mol⁻¹ (Fig. 3a) and the interaction is mainly coulombic in nature (Table 3). The next most stabilized pair involves C=O... π and C-H... π intermolecular interaction, involving O3 with Cg1 (centre of gravity of pyrone ring) and H12a with Cg2 (centre of gravity of benzene ring) and hence form dimer having an interaction energy of -10.04 kcal mol⁻¹ (Fig. 3b). The combined nature of these interactions is mainly dispersive in nature (Table 3). Molecular pair c shows the presence of C-H...O interaction involving bifurcated acceptor atom O2 with H7 and H8 and donor atom H13a with O1 resulting in a stabilization energy of -5.73 kcal mol⁻¹ (Fig. 3c). Another C-H...O (involving H4 and O2) interaction generates a molecular pair having an interaction energy of -4.8 kcal mol⁻¹ (Fig. 3d). Another molecular pair (Fig. 3e) involves the interaction of carbon atom C2 of carbonyl bond of Cg1 with chlorine atom Cl1 of another molecule with C...Cl distance being 3.456 Å.

Table 3. PIXEL interaction energies (I.E.) (kcal/mol) between molecular pairs related by a symmetry operation and the associated intermolecular interactions in the crystal

Motif	Centroid distance, Å	E_{Coul}	E_{Pol}	E_{Disp}	E_{Rep}	E_{Tot}	Symmetry	Important interactions
M-1								
a	3.788	-4.66	-1.649	-4.756	7.98	-10.25	2-x,-y,2-z	C12-H12... π , stacking
b	4.237	-3.18	-1.12	-12.78	8.65	-8.41	1-x,-y,2-z	Stacking
c	8.117	-4.92	-1.36	-3.44	2.67	-7.05	1-x,-y,1-z	C8-H8...O1, C8-H8...O2
d	9.188	-3.25	-0.95	-2.605	2.08	-4.73	1-x,1/2+y,1.5-z	C6-H6...O2, C6-H6...O3, C7-H7...O2
e	9.366	-0.54	-0.21	-2.05	0.74	-2.08	2-x,-1/2+y,2.5-z	C13-H13...C6(π)
f	8.722	0.19	-0.597	-3.94	2.36	-1.98	2-x,-y,3-z	C5-H5...H13-C13
g	8.513	-0.43	-0.88	-2.007	1.52	-1.79	x,1/2-y,-1/2+z	C12-H12b...O3
h	9.494	-0.09	-0.33	-2.31	1.36	-1.38	x,-1/2-y,1/2+z	C7-H7... π
i	8.737	-0.64	-0.19	-0.59	0.12	-1.31	x,y,1+z	C13-H13c...O2
M-2								
a	6.251	-8.84	-2.72	-6.91	8.22	-10.27	2-x,-y,1-z	C4-H4...O3, C5-H5...O3
b	4.463	-3.72	-1.69	-13.69	9.05	-10.04	1-x,-y,1-z	C11=O3... Cg1, C12-H12a...Cg2
c	8.787	-3.89	-1.17	-4.08	3.41	-5.73	-x,1/2+y,1/2-z	C7-H7...O2, C8-H8...O2, C13-H13a...O1
d	5.798	-1.05	-0.78	-5.4	2.44	-4.8	-1+x,y,z	C4-H4...O2
e	7.569	-0.382	-0.525	-5.97	2.92	-3.97	1-x,1/2+y,1/2-z	C6-C11...C2=O2
f	13.070	-0.47	-0.215	-2.46	1.21	-1.96	x,-1+y,z	C12-H12b...C11, C13-H13c...C11
M-3								
a	6.437	-8.67	-2.6	-7.07	7.88	-10.46	2-x,-y,1-z	C4-H4...O3, C5-H5...O3
b	5.437	-3.75	-1.60	-13.26	8.55	-10.06	1-x,-y,1-z	C11=O3... Cg1, C12-H12a...Cg2
c	9.147	-3.91	-1.19	-4.08	3.37	-5.80	-x,1/2+y,1/2-z	C7-H7...O2, C8-H8...O2, C13-H13a...O1
d	5.843	-1.05	-0.78	-5.37	2.53	-4.68	1+x,y,z	C4-H4...O2
e	7.59	-0.54	-0.43	-5.73	2.89	-3.8	1-x,-1/2+y,1/2-z	C6-Br1...C2=O2
f	13.207	-0.50	-0.167	-2.22	1.12	-1.76	x,1+y,z	C12-H12b...Br1, C13-H13c...Br1
M-4								
a	4.906	-6.59	-2.31	-14.77	12.97	-10.71	2-x,-y,1-z	π ... π , C14-H14...O3
b	4.726	-3.991	-1.745	-15.6	10.8	-10.54	1-x,-y,1-z	π ... π , C14-H14...O4
c	9.037	-4.25	-1.57	-5.8	4.34	-7.26	-1/2+x,1/2-y, 1/2+z	C13-H13...O5, C12-H12...O5, C14-H14a...O4, C14-H14b...O2
d	7.194	-4.37	-1.72	-4.63	3.53	-7.19	1.5-x, -1/2+y, 1/2-z	C4-H4...O3, C5-H5...O3, C12-H12...O2
e	8.830	-0.07	-0.215	-1.5	0.76	-1.07	1/2-x,1/2+y, 1/2-z	C13-H13...C5
f	12.228	0.12	-0.26	-1.81	0.95	-1.003	1.5-x, -1/2+y,1.5-z	C14-H14... π , C6-H6...C14

Cg1- centre of gravity of pyrone ring (O1-C2-C3-C4-C10-C9); Cg2- centre of gravity of benzene ring (C5-C6-C7-C8-C9-C10)

The stabilization energy of the pair is $-3.97 \text{ kcal mol}^{-1}$ with major contribution from dispersion component (Table 3). Finally the least stabilized pair involves bifurcated C-H...Cl (involving Cl1 with H13c and H12b) interaction having an interaction energy of $-1.96 \text{ kcal mol}^{-1}$ (Fig.3f).

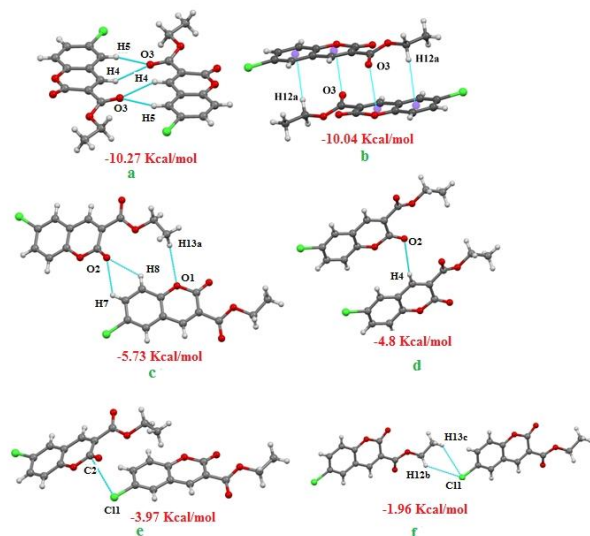


Figure 3. Molecular pairs (a-j in Table 3) along with their interaction energies calculated with Pixel (values in red) in M-2.

Ethyl 6-bromo-2-oxo-2H-chromene-3-carboxylate (M-3)

Molecular pairs (a-f) extracted from M-2 along with their respective interaction energies are shown in Fig. 4. The only difference between M-2 and M-3 is the presence of different halogen atom (Br in place of Cl). The packing features of M-3 were almost similar to those observed for M-1 and results in the generation of similar packing motifs. The energy of molecular pairs involving bifurcated C-H...O hydrogen bond (Fig. 4a,c) of M-3 were similar to those observed in M-1 (Table 3).

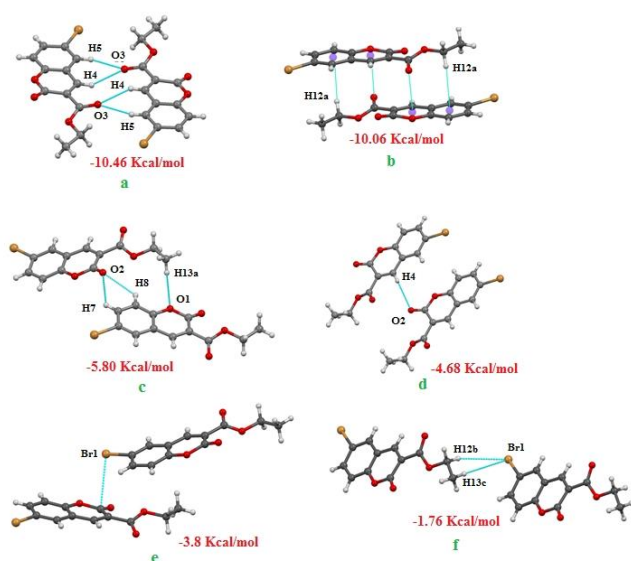


Figure 4. Molecular pairs (a-f in Table 3) along with their interaction energies calculated with Pixel (values in red) in M-3.

An important striking feature is that an interaction in which Cl is involved in M-2 is replaced by the similar interaction with Br in M-3. The molecular pairs in which Br1 is involved are motifs e and f with their stabilization energies being -3.8 and $-1.76 \text{ kcal mol}^{-1}$ and are dispersive in nature.

Ethyl 8-methoxy-2-oxo-2H-chromene-3-carboxylate (M-4)

The molecular pairs (a-f) which provide maximum stabilization to the packing in M-4 are shown in Fig. 5. The two most stabilized pairs (a and b) show the presence of $\pi \dots \pi$ interaction, a packing feature which is not observed in M-1, M-2 and M-3. Molecules in both the motifs are arranged in antiparallel manner and show the presence of double ring stacking (Cg1-Cg2). Along with this interaction both the pairs also involve C-H...O interaction and hence forming dimers (Fig. 5a,b) having stabilization energies of -10.71 and $-10.54 \text{ kcal mol}^{-1}$ respectively. The combined nature of these interactions is mainly dispersive in nature. Molecular pair c involves the interaction of bifurcated acceptor atom O3 with H13 and H12. This pair also involves the interaction of H14a with O4 and H14b with O2 and hence resulting in a total stabilization energy of $-7.26 \text{ kcal mol}^{-1}$ (Fig. 5c). The next stabilized interacting pair also interacts via C-H...O interaction (involving bifurcated acceptor atom O3 with H4 and H5 and O2 with H12) with an interaction energy of $-7.19 \text{ kcal mol}^{-1}$ (Fig. 5d). Molecular pairs e and f having an interaction energy -1.07 and $-1.003 \text{ kcal mol}^{-1}$ respectively provides additional stabilization to the crystal structure.

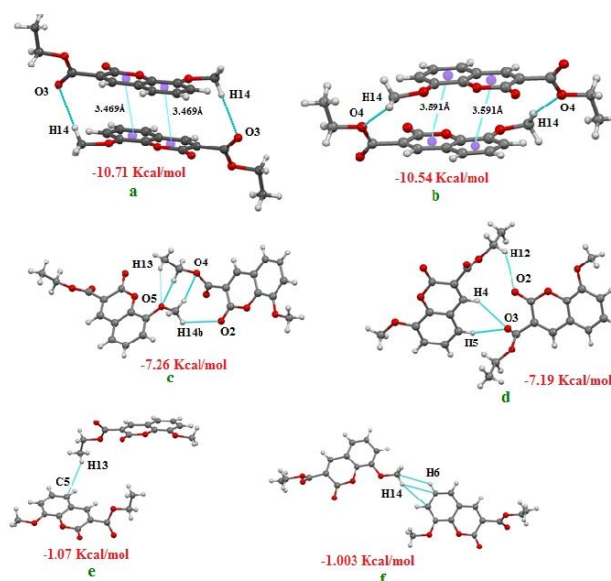


Figure 5. Molecular pairs (a-f in Table 3) along with their interaction energies calculated with Pixel (values in red) in M-4.

Conclusions

The field of investigation of the crystal and molecular structures has advanced to an extent wherein it is possible to exploit the role of weak intermolecular interactions which aid crystal packing. PIXEL calculations suggest the presence of different key structural motifs which aid in the

stabilization of crystal packing. Analysis of different structural motifs shows that C-H...O and $\pi\cdots\pi$ intermolecular interactions are the major contributors that stabilize the crystal packing in addition to C-H... π and C-H...X (Cl or Br). It is of interest to extend such studies in other complex structures which will enable to exploit the role of intermolecular interactions.

References

- ¹Olayinka, O. A., Obinna, C. N., *J. Heterocycl. Chem.*, **2010**, *47*, 179-187.
- ²Trenor, S. R., Shultz, A. R., Love, B. J., Long, T. E., *Chem. Rev.*, **2004**, *104*, 3059-3077.
- ³Yu, T. Z., Yang, S. D., Zhao, Y. L., Zhang, H., Han, X. Q., Fan, D. W., Qiu, Y. Q., Chen, L. L., *J. Photochem. Photobiol.*, **2010**, *A214*, 92-99.
- ⁴Borges, F., Roleira, F., Milhazes, N., Santana, L., Uriarte, E., *Curr. Med. Chem.*, **2005**, *12*, 887-916.
- ⁵Kontogiorgis, C., Hadjipavlou-Litina, D., *J. Med. Chem.*, **2005**, *48*, 6400-6408.
- ⁶Kostova, I., *Curr. Med. Chem.*, **2005**, *5*, 29-46.
- ⁷Ramesh, B., Pugalendi, K.V., *J. Med. Food*, **2006**, *9*, 562-566.
- ⁸Chilin, A., Battistutta, R., Bortolato, A., Cozza, G., Zanatta, S., Poletto, G., Mazzorana, M., Zagotto, G., Uriarte, E., Guiotto, A., Pinna, L. A., Meggio, F., Moro, S., *J. Med. Chem.*, **2008**, *51*, 752-759.
- ⁹Vilar, S., Quezada, E., Santana, L., Uriarte, E., Yanez, M., Fraizp, *Bioorg. Med. Chem. Lett.*, **2006**, *16*, 257-261.
- ¹⁰Karali, N., Kocabalkanli, A., Gursoy, A., Ates, O., *Farmaco.*, **2002**, *57*, 589-593.
- ¹¹Gavezzotti, A., *New J. Chem.*, **2011**, *35*, 1360-1368.
- ¹²Madegowda, M., Beeranahally, H. D., Sridhar, M. A., Prasad, J. S., Vishal, P. N., Yogesh, T. N., Shah, A., *Analytical Sciences*, **2003**, *19*, x33- x34.
- ¹³Santos-Contreras, R. J., Martinez, F. J., Garcia-Baez, E. V., Padilla-Martinez, I. I., Peraza, A. L., Herbert, H., *Acta Cryst.*, **2007**, *C63*, o239 - o242.
- ¹⁴Takahashi, H., Takechi, H., Kubo, K., Matsumoto, T., *Acta Cryst.*, **2006**, *E62*, o2553-o2555.
- ¹⁵Dunitz, J. D., Gavezzotti, A., *Cryst. Growth Des.*, **2012**, *12*, 5873-5877.
- ¹⁶Dunitz, J. D., Gavezzotti, A., *Cryst. Growth Des.*, **2005**, *5*, 2180-2189.
- ¹⁷Maschio, L., Civaleri, B., Ugliengo, P., Gavezzotti, A., *J Phys Chem A*, **2011**, *115*, 11179-11186.
- ¹⁸Dunitz, J. D., Gavezzotti, A., *Chem. Soc. Rev.*, **2005**, *38*, 2622-2633.

Received: 31.03.2014.

Accepted: 06.05.2014.



AN EFFICIENT SYNTHESIS OF SOME NOVEL 5,7-DIARYLPYRIDO[4,3-d]PYRIMIDINES

V. Vijayakumar^[a], P. Karthikeyan^[a] and S. Sarveswari^{*[a]}

Keywords: Synthesis; 4-oxo-N, 2, 6-triphenylpiperidine-3-carboxamides, 5,6,7,8-tetrahydro-4-hydroxy-5,7-diarylpyrido[4,3-d]pyrimidin-2(3H)-ones, 2-amino-5,6,7,8-tetrahydro-5,7-diarylpyrido[4,3-d]pyrimidin-4-ols.

The 4-oxo-N,2,6-triphenylpiperidine-3-carboxamides (**3a-f**) were synthesized using arylaldehydes, ammonium acetate and acetoacetanilide, which in turn converted into 5,6,7,8-tetrahydro-4-hydroxy-5,7-diarylpyrido[4,3-d]pyrimidin-2(3H)-ones (**4a-f**), 2-amino-5,6,7,8-tetrahydro-5,7-diarylpyrido[4,3-d]pyrimidin-4-ols (**5a-f**) by condensing with guanidine carbonate and urea respectively.

* Corresponding Authors

Fax: +91 416 220 3091

E-Mail: sarveswari@gmail.com

[a] Centre for Organic and Medicinal Chemistry, VIT University, Vellore-632014, Tamilnadu, India.

continuation of the earlier interest,¹⁷ herein we report the synthesis of diarylpyrido[4,3-d]pyrimidine derivatives which are hitherto unreported.

Introduction

The piperidine ring is an ubiquitous structural feature of many alkaloid natural products and drug candidates. Watson et al. asserted that during a recent 10-year period there were thousands of piperidine compounds mentioned in clinical and preclinical studies.¹ Piperidones are somewhat less prominent, but often they serve a role as advanced intermediates prior to their conversion to piperidines. Reviews updating progress in the stereoselective syntheses of substituted piperidines have appeared recently.² One of the review presents synthetic methodologies on the basis of diversity and stereocontrol.³

Compounds with piperidin-4-one nucleus were reported to have various important biological properties such as antiviral, anti-inflammatory, local anesthetic, anticancer, antimicrobial activity.³⁻⁷ The piperidones were also reported to act as neurokinin receptor antagonists, analgesic and anti-hypertensive agents.⁸⁻¹⁴ The importance of piperidin-4-one as intermediates in the synthesis of a diversity of compounds with potent physiological activity has been reviewed by Prostavok and Gaivoronskaya.¹⁵ The studies undertaken on 4-piperidones have direct relation to the synthesis of drug molecules. The effect of substituent at second, third and sixth position particularly, aryl substituent at second and/or sixth positions with regard to its biological activity have been well documented. The preparation of pharmaceutically active compounds of this kind remains a major challenge in synthetic organic chemistry. Due to the demand for improved selectivity and reduction of side effects of potential drugs in pharmaceutical research, compounds with increasing molecular complexity. However, the biological properties of piperidines are highly dependent on the type and locations of substituent on the heterocyclic ring continue to drive the search for new methodologies. Similarly imidazole, oxazole and pyrazole were also exhibiting several activities and the fused bicycles of 4-piperidones with imidazole, pyrazole, oxazole and pyrimidine were expected to show interesting bio activities. In

Experimental

Synthesis of compound 3a-f was done according to the procedure available in literature .¹⁷

General Procedure for the synthesis of (4a-f)

5,6,7,8-Tetrahydro-4-hydroxy-5,7-diarylpyrido[4,3-d]pyrimidin-2(3H)-ones (**4a-f**) are synthesized by the condensation of **3a-f** with urea in ethanol. A mixture of 4-piperidone (0.003246 mol, 1.2 g) in ethanol and Urea (0.003246 mol, 0.2g) was refluxed on a water bath for 6 hr. The reaction mixture was cooled to room temperature; the solid product was washed with ethanol-ether (1:5). The product was recrystallized using ethanol. The purity of the product was checked through TLC and the melting point was recorded. The formation of the product was confirmed by the absence of carbonyl stretching frequency in IR spectrum which appeared in the piperidones. The yield and other physical parameters of **4a-f** are given in the Table-1.

General Procedure for the synthesis of (5a-f)

2-Amino-5,6,7,8-tetrahydro-5,7-diarylpyrido[4,3-d]pyrimidin-4-ols (**5a-f**) are synthesized by the condensation of **3a-f** with guanidine carbonate in ethanol. A mixture of (0.003246 mol, 1.2 g) of 4-piperidone in ethanol solution and 0.003246 mol, 0.4g of guanidine carbonate was refluxed on a water bath for 8 hr. The reaction mixture was cooled to room temperature; the obtained solid product was washed with mixture of ethanol-ether (1:5). The crude product was recrystallized using ethanol. The purity was checked through TLC and the melting point was observed in open capillaries. The formation of the product was confirmed by the absence of carbonyl peaks which appeared in the piperidones. The yield and other physical parameters are given in the Table 1 for all the compounds **5a-f**.

Spectral data of newly prepared compounds

4a: Yield (89 %), m.p = 175 °C. IR data in cm^{-1} : 3289 (NH str), 3167, 3068 (Aromatic str), 3452 (Aromatic OH str), 1653 (N-CO-N str). $^1\text{H-NMR}$ (400MHz, CDCl_3): δ 1.90 (s, 1H), 1.51-1.70 (t, 2H), 2.51 (t, 1H), 3.30 (d, 1H), 3.70 (s, 1H), 4.0 (t, 1H), 5.35 (d, 1H), 7.27-7.32 (m, 6H), 7.45 (d, 4H), 8.0 (s, 1H). $\text{C}_{19}\text{H}_{19}\text{N}_3\text{O}_2$ (Calculated) C, 71.01; H, 5.96; N, 13.08; Found C, 71.21; H, 6.06; N, 12.88; GC-Mass Base Peak = 92.

4b: Yield (86 %), m.p=220. IR data in cm^{-1} : 3265 (NH str), 3173, 3064 (Aromatic str), 3328 (Aromatic OH str), 1645 (N-CO-N str), 1573 (C-O-C str). $^1\text{H-NMR}$ (400MHz, CDCl_3): δ 1.90 (s, 1H), 1.62-1.70 (t, 2H), 2.50 (t, 1H), 3.36 (d, 1H), 3.65 (s, 1H), 3.89 (s, 6H), 3.93 (t, 1H), 5.30 (d, 1H), 6.95(d, 4H), 7.20 (d, 4H), 8.0 (s, 1H). ES-MS: 381.17[M⁺]; $\text{C}_{21}\text{H}_{23}\text{N}_3\text{O}_4$ (Calculated): C, 66.13; H, 6.08; N, 11.02; Found: C, 66.33; H, 5.18; N, 11.01.

4c: Yield (88 %), m.p =217 °C. IR data in cm^{-1} : 3283 (NH str), 3376 (Aromatic OH str), 1639 (N-CO-N str), 1584 (C-O-C str), 3125 C-C str (furan). $^1\text{H-NMR}$ (400MHz, CDCl_3): δ 1.90 (s, 1H), 1.60-1.70 (t, 2H), 2.50 (t, 1H), 3.65 (s, 1H), 4.1 (t, 2H), 5.35 (d, 1H), 6.45-6.50 (m, 4H), 7.65 (d, 2H), 8.0 (s, 1H). $\text{C}_{15}\text{H}_{15}\text{N}_3\text{O}_4$ (Calculated): C, 59.79; H, 5.02; N, 13.95; O, 21.24; Found: C, 60.02; H, 4.05; N, 13.95; ES MS: 301.10.

4d: Yield (82 %), m.p = 192 °C. IR data in cm^{-1} : 3397 (NH str), 3251, 3192 (Aromatic str), 3459 (Aromatic OH str), 1669 (N-CO-N str). $^1\text{H-NMR}$ (400MHz, CDCl_3): δ 1.90 (s, 1H), 1.62-1.70 (t, 2H), 2.50 (t, 1H), 3.36 (d, 1H), 3.65 (s, 1H), 3.89 (s, 6H), 3.93 (t, 1H), 5.30 (d, 1H), 6.95(d, 4H), 7.20 (d, 4H), 8.0 (s, 1H). $\text{C}_{19}\text{H}_{17}\text{N}_3\text{O}_2\text{Cl}_2$ (Calculated): C, 66.13; H, 6.08; N, 11.02; Found; C, 66.15; H, 6.88; N, 11.12; ES-MS: 381.

4e: Yield (84 %), m.p = 186 °C. IR data in cm^{-1} : 3386 (NH str), 3254, 3194 (Aromatic str), 3459 (Aromatic OH str), 1672 (N-CO-N str). $^1\text{H-NMR}$ (400MHz, CDCl_3): δ 1.90 (s, 1H), 1.62-1.70 (t, 2H), 2.50 (t, 1H), 3.36 (d, 1H), 3.65 (s, 1H), 3.89 (s, 6H), 3.93 (t, 1H), 5.30 (d, 1H), 6.95(d, 4H), 7.20 (d, 4H), 8.0 (s, 1H). $\text{C}_{19}\text{H}_{17}\text{N}_3\text{O}_2\text{Cl}_2$ (Calculated): C, 66.13; H, 6.08; N, 11.02; Found; C, 65.93; H, 5.48; N, 11.06.

4f: Yield (82%), m.p = 192 °C. IR data in cm^{-1} : 3397 (NH str), 3251, 3192 (Aromatic str C-Cl str), 3459 (Aromatic OH str), 1669 (N-CO-N str), 694 (C-Cl str). $^1\text{H-NMR}$ (400MHz, CDCl_3): δ 1.90 (s, 1H), 1.62-1.70 (t, 2H), 2.50 (t, 1H), 3.36 (d, 1H), 3.65 (s, 1H), 3.89 (s, 6H), 5.40 (s, 1H), 7.50-7.62 (m, 8H), 8.0 (s, 1H). $\text{C}_{19}\text{H}_{17}\text{N}_3\text{O}_2\text{Cl}_2$ (Calculated): C, 58.47; H, 4.39; Cl, 18.17; N, 10.77; Found; C, 58.40; H, 5.58; N, 10.01; ES-MS: 390.26; GC-Mass Base Peak = 138.

5a: Yield (80%), m.p =270 °C. IR data in cm^{-1} : 3250 (NH str), 3176, 3065 (Aromatic str), 3368 (Aromatic OH str), 1654 (C-N str). $^1\text{H-NMR}$ (400MHz, CDCl_3): δ 1.90 (s, 1H), 2.80-2.98 (t, 2H), 4.30 (t, 1H), 5.23 (s, 1H), 7.0 (s, 2H), 7.28-7.40 (m, 10H), 11.0 (s, 1H). GC-Mass Base Peak = 187, $\text{C}_{19}\text{H}_{18}\text{N}_4\text{O}$; (Calculated) C, 71.68; H, 5.70; N, 17.60; Found: C, 71.81; H, 4.69; N, 16.78.

5b:Yield (75 %), m.p =258 °C. IR data in cm^{-1} : 3265 (NH str), 3271 (Aromatic str), 3043 (Aromatic OH str), 336 (C-N str), 1673, 1546 (C-O-C str). $^1\text{H-NMR}$ (400MHz, CDCl_3): δ 1.93 (s, 1H), 2.80-3.03 (t, 2H), 3.83 (s, 6H), 4.30 (t, 1H), 5.18 (s, 1H), 6.87-6.97 (m, 6H), 7.15-7.21 (m, 4H), 11.0 (s, 1H). $\text{C}_{21}\text{H}_{22}\text{N}_4\text{O}_3$. (Calculated) C, 66.65; H, 5.86; N, 14.81; O, 12.68. Found C, 67.12; H, 5.86; N, 14.51.

5c: Yield (79 %), m.p =283 °C. IR data in cm^{-1} : 3226 (NH str), 3365 (Aromatic OH str), 1652 (C-N str), 3143 (C-C str furan). $^1\text{H-NMR}$ (400MHz, CDCl_3): δ 1.93 (s, 1H), 2.80-2.94 (t, 2H), 4.56 (t, 1H), 5.46 (s, 1H), 6.18 (d, 1H), 6.45-6.50 (m, 3H), 7.0 (s, 2H), 7.68(d, 2H), 11.0 (s, 1H). $\text{C}_{15}\text{H}_{14}\text{N}_4\text{O}_3$ (Calculated) C, 60.40; H, 4.73; N, 18.78; O, 16.09; Found C, 60.50; H, 3.76; N, 18.88.

5d: Yield (72 %), m.p =258 °C. IR data in cm^{-1} : NH str 3265, Aromatic str 3271, 3043, Aromatic OH str 336, C-N str 1673, C-O-C str 1546. $^1\text{H-NMR}$ (400MHz, CDCl_3): δ 1.93 (s, 1H), 2.80-3.03 (t, 2H), 3.83 (s, 6H), 4.30 (t, 1H), 5.18 (s, 1H), 6.87-6.97 (m, 6H), 7.15-7.21 (m, 4H), 11.0 (s, 1H). $\text{C}_{21}\text{H}_{22}\text{N}_4\text{O}_3$ (Calculated) C, 66.65; H, 5.86; N, 14.81; O, 12.68; Found C, 66.25; H, 4.16; N, 14.21.

5e: Yield (75 %), m.p =258 °C. IR data in cm^{-1} : NH str 3265, Aromatic str 3271, 3043, Aromatic OH str 336, C-N str 1673, C-O-C str 1546. $^1\text{H-NMR}$ (400MHz, CDCl_3): δ 1.93 (s, 1H), 2.80-3.03 (t, 2H), 3.83 (s, 6H), 4.30 (t, 1H), 5.18 (s, 1H), 6.87-6.97 (m, 6H), 7.15-7.21 (m, 4H), 11.0 (s, 1H). $\text{C}_{21}\text{H}_{22}\text{N}_4\text{O}_3$ (Calculated) C, 66.46; H, 5.66; N, 14.71; Found C, 66.61; H, 4.66; N, 13.71.

5f: Yield (68 %), m.p =292°C. IR data in cm^{-1} : 3278 (NH str), 3176, 3076 (Aromatic str), 342 (Aromatic OH str), 1657 (C-N str), 694 (C-Cl str). $^1\text{H-NMR}$ (400MHz, CDCl_3): δ 1.93 (s, 1H), 2.80-3.0 (t, 2H), 4.30 (t, 1H), 5.20 (s, 1H), 7.0 (s, 2H), 7.20-7.24 (d, 2H), 7.41-7.50 (m, 6H), 11.0 (s, 1H). $\text{C}_{19}\text{H}_{16}\text{N}_4\text{OCl}_2$ Calculated C, 58.93; H, 4.16; Cl, 18.31; N, 14.47; O, 4.13; Found C, 58.83; H, 3.73; N, 14.40.

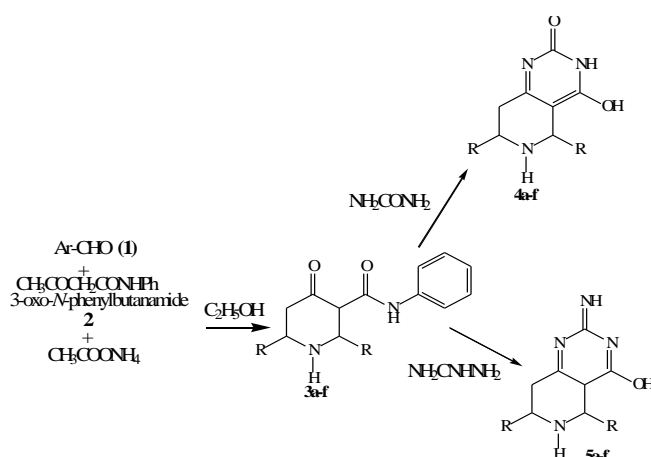
Results and Discussion

The 2, 6-diaryl-4-piperidones (**3a-f**) were synthesised by the procedure available in the literature.¹⁷

5,6,7,8-Tetrahydro-4-hydroxy-5,7-diarylpyrido[4,3-d]pyrimidin-2(3H)-ones (**4a-f**) are synthesized by the condensation of **3a-f** with urea in ethanol. A mixture of 4-piperidone (0.003246 mol, 1.2 g) in ethanol and urea (0.003246 mol, 0.2 g) was refluxed on a water bath for 6 hr. 2-Amino-5,6,7,8-tetrahydro-5,7-diarylpyrido[4,3-d]pyrimidin-4-ols (**5a-f**) were synthesized by the condensation of **3a-f** with guanidine carbonate in ethanol. A mixture of 0.003246 mol, (1.2 g) 4-piperidone in ethanol and 0.003246 mol (0.4 g) of guanidine carbonate was refluxed on a water bath for 8 h. The formation of desired products was confirmed by spectral data (included in experimental section).

Table 1. Physical data of the compounds (**4a-f**), (**5a-f**) and (**3a-f**)

S. No	R	M.P °C	Yield, %
4a	Phenyl	175-78	79
4b	4-Methoxyphenyl	220-22	86
4c	Furfural	217-19	88
4d	3-Methoxyphenyl	217-20	88
4e	2-Methoxyphenyl	218-19	83
4f	4-Chlorophenyl	192-94	72
5a	Phenyl	270-72	80
5b	4-Methoxyphenyl	259-62	75
5c	Furfural	227-30	78
5d	3-Methoxyphenyl	258-60	75
5e	2-Methoxyphenyl	254-56	75
5f	4-Chlorophenyl	292-95	68

**Scheme 1.** Synthesis of diarylpyrido[4,3-d]pyrimidine derivatives

Conclusion

In conclusion, synthesis of some fused heterocycles with 4-piperidone moiety and 4,5,6,7-tetrahydro-4,6-diaryl-2H-pyrazolo[4,3-c]pyridin-3-ols, 4,5,6,7-tetrahydro-4,6-diaryl-2H-pyrazolo[4,3-c]pyridin-3-ols were attempted successfully, the compounds with fused pyrazole were proved as biologically important molecules. In the present work molecules with pyrazole moiety were obtained using a simple reaction protocol with moderate yield. The synthesized compounds were characterized by IR spectrum, GC-MS spectrum, ¹H NMR spectrum and elemental analysis.

Acknowledgements

Authors gratefully acknowledge the management of VIT University for providing required basic facilities and SAIF (IITM) for providing the spectral data to carry out the present work.

References

- Watson, P. S.; Jiang, B.; Scott, B., *Org. Lett.* **2000**, *2*, 3679.
- (a) Bailey, P. D.; Millwood, P. A.; Smith, P. D., *J. Chem. Soc., Chem. Commun.*, **1998**, 633. (b) Mitchinson, A.; Nadin, A., *J. Chem. Soc., Perkin Trans. 1*, **2000**, 2862. (c) Laschat, S.; Dickner, T., *Synthesis*, **2000**, 1781.
- Kallstrom, S., and Reko Leino, *Bioorg. Med. Chem.*, **2008**, *16* 601.
- Vijayakumar, V., Sundaravadivelu, M., Perumal, S., *Magn Reson. Chem.*, **2001**, *39*, 101.
- Vijayakumar, V., Rajesh, K., Suresh, J., Narasimhamurthy, T., Lakshman, P. L. N., *Acta Cryst.*, **2010**, *66E*, 170.
- Aridoss, G., Balasubramanian, S., Parthiban, P., Kabilan, S., *Eur. J. Med. Chem.*, **2007**, *42*, 851.
- Priya, S., Sinha, S.S., Vijayakumar, V., Narasimhamurthy, T., Vijay, T., Rathore, R.S., *Acta Cryst.*, **2006**, *E62*, 5367.
- Schon, U., Messinger, J., Buckendahl, M., Prabhu, M. S., Konda, A., *Tetrahedron Lett.* **2007**, *48*, 2519.
- Ramalingam, C., Balasubramanian, S., Kabilan, S., *Eur. J. Med. Chem.*, **2004**, *39*, 527.
- Thenmozhiyal, J. C., Venkatraj, M., Ponnuswanmy, S., Jeyaraman, R., *Indian. J. Chem.*, **2007**, *46B*, 1526.
- Ramalingam, C., Balasubramanian, S., Kabilan, S., *Indian. J. Chem.*, **2002**, *41B*, 2402.
- Aridass, G. Balasubramanian, S. Parthian, P. Kablian, S., *Eur. J. Med. Chem.*, **2006**, *41*, 268.
- Chow, Y. L. Colon, C. J., Tam, J. N. S., *Can. J. Chem.*, **1968**, *46*, 282.
- Sander, P., Bottger, E. C., *Chemotherapy*, **1999**, *45*, 95.
- Arthur, M., Courvalin, P., *Antimicrob. Agents Chemother.*, **1993**, *37*, 1563.
- Kuznetsov, V. V., Prostakov, N. S., *Chem. Heterocycl. Compd.* **1994**, *1*, 3.
- Karthikeyan, P., Vijayakumar, V., and Sarveswari, S., *Eur. Chem. Bull.*, **2014**, *3(4)*, 333.

Received: 30.03.2014.

Accepted: 09.05.2014.



PYRIDAZINE AND ITS RELATED COMPOUNDS. PART 37.¹

SYNTHESIS AND APPLICATION OF SOME HETEROARYLAZO DISPERSE DYES DERIVED FROM PYRAZOLO[3,4-c]- PYRIDAZINE

Ali Deeb,^[a,*] Salah Shaqra,^[b] Taha Abo Elfotoh^[a] and Sameh Dief^[a†]

Keywords: 3-diazo-4,5-diphenyl-3*H*-pyrazolo[3,4-*c*]pyridazine; active methylenes; color fastness.

3-Diazopyrazolo[3,4-*c*]pyridazine was synthesized and its transformations were investigated. With reactive methylene compound the corresponding hydrazones were formed. The prepared azo disperse dyes were applied to polyester fabric, and their spectral and color fastness properties measured.

* Corresponding Authors

E-Mail: dralideeb@hotmail.com

[a] Department of Chemistry, Faculty of Science, Zagazig University, Egypt

[b] Textile Department, National Research Center, Dokki, Cairo, Egypt

† Abstracted in part from the master's thesis of Sameh Dief, Zagazig University, 2014.

Introduction

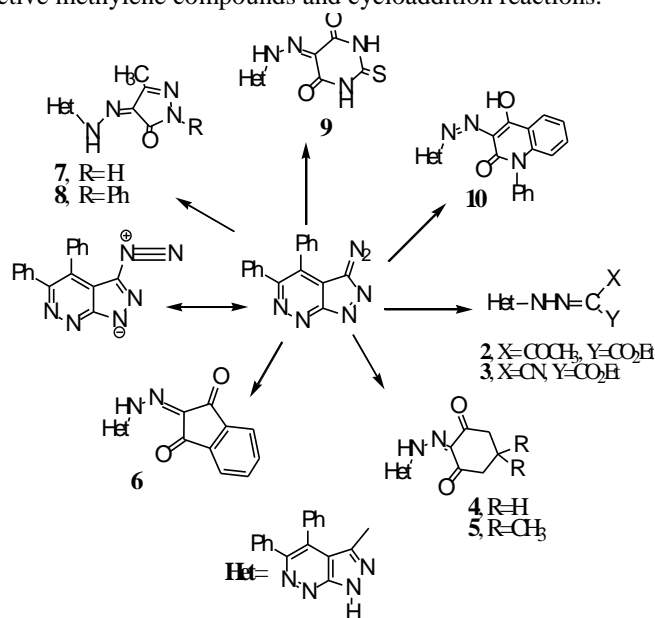
Azo compounds have for a great many years occupied a dominant position in the field of colouring matters due to their versatility. A large volume of publications and patents have appeared describing their synthesis and dyeing properties.^{2,3} Among these, azodyes using heterocyclic amines have become important as they give brighter and stronger results than those based on aniline-based diazo compounds.^{4,5}

The pyrazole derivatives based azo dyes are known as disperse dyes with excellent brightness of shade. This class of dyes was established as an alternative to more expensive anthraquinone dyes.⁴ On the other hand heterocyclic annulated pyridazines continue to attract considerable attention which mainly arises from the large variety of interesting pharmacological activities observed with pyridazine derivatives.⁶ Recently, our researches have been devoted to the synthesis of condensed tricyclic systems of potential biological activity with a pyrazole ring as the central nucleus.⁷⁻⁹ As a continuation of these studies we report here the synthesis of some 3-(4,5-diphenyl-1*H*-pyrazolo[3,4-*c*]pyridazin-3-yl)hydrazono derivatives and an evaluation of their properties on polyester fibers.

Results and Discussion

Our synthesis began with the preparation of 3-diazo-4,5-diphenyl-3*H*-pyrazolo[3,4-*c*]pyridazine **1** following the literature procedure by the diazotization of 3-amino-4,5-diphenyl-1*H*-pyrazolo[3,4-*c*]pyridazine with sodium nitrite in glacial acetic acid at room temperature.¹⁰

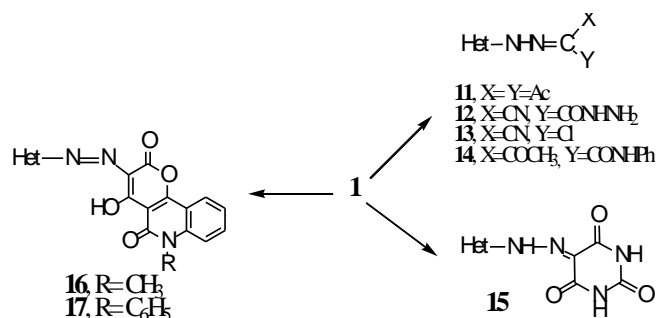
We reported the synthesis of 3-(4,5-diphenyl-1*H*-pyrazolo[3,4-*c*]pyridazin-3-yl)hydrazono derivatives **2-10** based on coupling reaction of 3-diazo-4,5-diphenyl-3*H*-pyrazolo[3,4-*c*]pyridazine **1** with active methylene compounds such as ethyl 3-oxobutanoate, ethyl 2-cyanoacetate, cyclohexane-1,3-dione, 5,5-dimethylcyclohexane-1,3-dione, 1*H*-indene-1,3(2*H*)-dione, 3-methyl-1*H*-pyrazol-5(4*H*)-one, 3-methyl-1-phenyl-1*H*-pyrazol-5(4*H*)-one, 2-thioxodihydropyrimidine-4,6(1*H*,5*H*)-dione, and 4-hydroxy-1-phenylquinolin-2(1*H*)-one.^{10,11} In continuation of this work, we report here the results of our further investigation on the reaction of compound **1** with further active methylene compounds and cycloaddition reactions.



Scheme 1. Reactions of 3-diazo-4,5-diphenyl-3*H*-pyrazolo[3,4-*c*]pyridazine

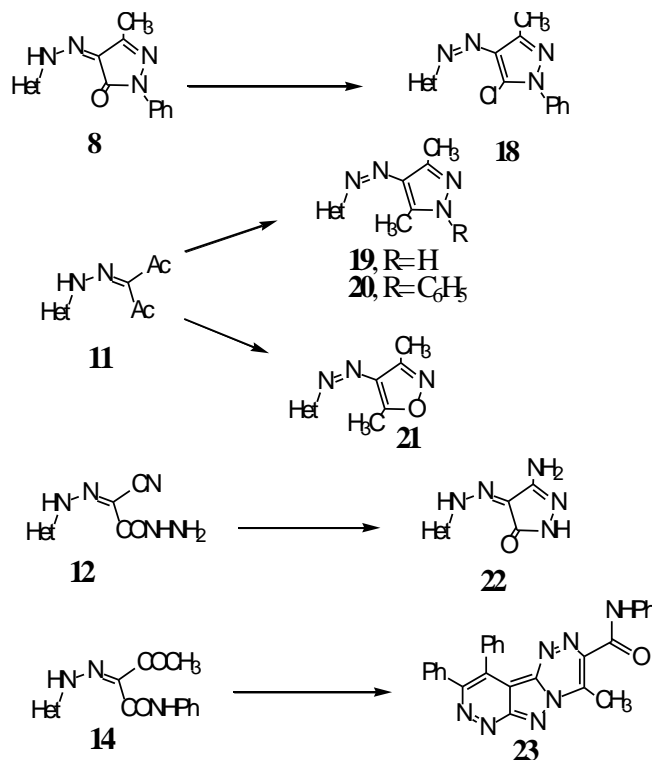
The reaction of **1** with pentane-2,4-dione, 2-cyanoacetohydrazide, 2-chloroacetonitrile, 3-oxo-*N*-phenylbutanamide, 4-hydroxy-6-methyl-2*H*-pyrano[3,2-*c*]quinoline-2,5(6*H*)-dione, 4-hydroxy-6-phenyl-2*H*-pyrano[3,2-*c*]quinoline-2,5(6*H*)-dione, and pyrimidine-2,4,6(1*H*,3*H*,5*H*)-trione formed easily the corresponding

hydrazone compounds **11-17**. For all compounds of this type several tautomeric forms can be written. For example compounds of the types **11**, **12**, and **13** can be regarded as azo compounds or as hydrazones, and the carbonyl part can be written in the keto or enolized form. The end of the reaction was judged by the disappearance of the diazo compound according to TLC analysis. The reaction time varied from a few minutes to several hours. The reaction products were isolated in high yield and gave satisfactory elemental analysis. The spectroscopic properties of the products were in excellent agreement with the proposed structures.



Scheme 2. Reaction routes to form hydrazone compounds

With view of studying some of the reaction of the hydrazones **8**, **11**, **12** and **14** that were allowed to react with some reagents. Treatment of compound **8** with phosphoryl chloride at refluxing temperature gave the corresponding chloro derivative **18**. Hydrazone **11** undergoes a smooth reaction with hydrazine hydrate and with phenyl hydrazine produced pyrazole derivative **19** and **20**, also reacts with hydroxyl amine hydrochloride in refluxing absolute ethanol in the presence of anhydrous potassium carbonate gave the isoxazole derivative **21**.



Scheme 3. Transformation of hydrazones

Similarly carbohydrazone hydrazone **12** was reacted with hydrazine hydrate producing aminopyrazolone derivative **22**. Compound **22** also was obtained by condensing hydrazone **3** with hydrazine hydrate.

The hydrazone **14** was also readily cyclized in ethanol at 78 °C to give the 4-methyl-N,9,10-triphenylpyridazino [3',4':3,4]pyrazolo[5,1-c][1,2,4]triazine-3-carboxamide derivative **23**. The assignment of the cyclic compound involves the intramolecular nucleophilic attack of pyrazole ring 2-nitrogen to the ketonic carbonyl with elimination of water molecule.

Dyeing of polyester fabrics and dyeing properties

Color measurement

The effect of the nature of different substituents on dyeing behavior, color hue, and depth was investigated. This investigation depends on some spectral data of the dyed materials. The most commonly used function $f(R)$ is that developed theoretically by Kubelka and Munk. In their theory, the optical properties of a sample are described by two values: K is the measure of the light absorption, and S is a measure of the light scattering. On textiles, K is determined primarily by the dyestuffs and S only by the substrate. From the wavelength, Kubelka and Munk calculate Eq. (1) for the reflectance R of thick, opaque samples with the constants of K and S :

$$\frac{K}{S} = \frac{(1-R)^2}{2R} \quad (1)$$

In this equation R is used as a ratio, e.g., 32 % reflectance as 0.32. The K/S value at λ max was taken as a measure of color depth. On the other hand, the psychometric coordinates (L^* , a^* , b^*) for each dyed sample were obtained to illustrate the color hues, where L^* is the lightness, ranging from 0 to 100 (0 for black and 100 for white); a^* is the red-green axis, (+) for red, zero for grey, and (-) for green; and b^* is the yellow-blue axis, (+) for yellow, zero for gray, and (-) for blue.

The parent dyestuff in each group is taken as the standard in color difference calculation (ΔL^* , ΔC^* , ΔH^* and ΔE^*).

The results are measured using CIE-LAB techniques and given in Tables 2-6, where ΔL^* is the lightness difference, ΔC^* the chroma difference, ΔH^* the hue and ΔE^* the total color difference. A negative sign of ΔL^* indicates that the dyed fiber becomes darker than the standard, but a positive sign indicates that the dyed fiber becomes lighter than the standard. A negative sign of ΔC^* indicates that the dyed fiber becomes duller than the standard, but a positive sign indicates that the dyed fiber becomes brighter than the standard. A negative sign of ΔH^* indicates that the color directed to red color, while a positive sign indicates that the color directed to yellowish. The values of K/S of **2-22** vary from 5.97 to 50.48. The introduction of different couplers in dyes **2-22** varies the strength of K/S values (Table 1).

Table 1. Optical measurements, *K/S* and color coordinates, of dyes **2-22** on polyester fibers at sun light wavelength (D65/10), tungsten wavelength (A/10) and fluorescent wave length (F11/10).

Coordinates	<i>L</i> *	<i>a</i> *	<i>b</i> *	<i>C</i> *	<i>H</i>	<i>X</i>	<i>Y</i>	<i>Z</i>	<i>x</i>	<i>y</i>	<i>K/S</i>
Compound 2											
D65/10	74.46	5.43	14.67	15.65	69.68	46.87	47.42	37.84	0.3547	0.3589	20.98
A/10	76.03	8.93	16.34	18.62	61.34	59.33	49.94	12.69	0.4865	0.4095	
F11/10	75.29	5.91	16.72	17.74	70.54	52.94	48.75	22.83	0.4252	0.3915	
Compound 3											
D65/10	86.12	-4.30	60.87	61.02	94.04	62.80	68.22	20.51	0.4145	0.4502	37.85
A/10	88.58	5.52	59.93	60.18	84.74	84.48	73.29	7.68	0.5106	0.4430	
F11/10	87.86	-1.19	65.65	65.66	91.03	73.96	71.78	11.97	0.4690	0.4551	
Compound 4											
D65/10	71.15	3.10	40.27	40.39	85.60	41.21	42.40	17.85	0.4061	0.4179	50.84
A/10	73.63	10.95	40.54	41.99	74.88	55.75	46.13	6.52	0.5143	0.4255	
F11/10	72.61	4.71	45.82	46.06	84.14	48.03	44.57	10.03	0.4679	0.4343	
Compound 5											
D65/10	84.99	-0.46	29.21	29.21	90.89	62.36	65.98	40.82	0.3686	0.3900	13.08
A/10	86.67	6.08	29.35	29.97	78.29	80.28	69.34	14.17	0.4902	0.4233	
F11/10	86.01	1.32	32.55	32.58	87.68	71.27	68.00	24.14	0.4361	0.4161	
Compound 6											
D65/10	84.92	1.44	40.38	40.40	87.96	63.06	65.86	32.01	0.3919	0.4092	13.39
A/10	87.31	8.17	42.07	42.85	79.01	82.91	70.64	11.08	0.5036	0.4291	
F11/10	86.63	2.39	44.39	44.46	86.92	73.11	69.26	19.10	0.4528	0.4289	
Compound 7											
D65/10	87.87	-2.00	20.81	20.91	95.50	67.15	71.79	53.18	0.3495	0.3737	5.63
A/10	88.96	3.59	20.81	21.11	80.22	84.31	74.08	18.08	0.4778	0.4198	
F11/10	88.47	-0.50	23.16	23.16	91.24	75.62	73.05	31.72	0.4192	0.4050	
Compound 8											
D65/10	87.58	0.16	27.46	27.46	89.67	67.57	71.19	46.30	0.3651	0.3847	7.61
A/10	89.25	6.05	27.99	28.63	77.80	86.39	74.70	15.91	0.4881	0.4220	
F11/10	88.66	1.46	31.06	31.09	87.31	77.04	73.46	27.35	0.4332	0.4130	
Compound 9											
D65/10	82.61	5.53	51.58	51.86	84.08	60.47	61.43	22.29	0.4194	0.4261	23.71
A/10	85.81	12.20	54.00	55.36	77.27	81.59	67.61	7.90	0.5193	0.4304	
F11/10	84.89	5.69	57.21	57.50	84.32	71.05	65.80	13.05	0.4740	0.4389	
Compound 10											
D65/10	87.47	4.90	26.25	26.70	79.42	69.53	70.97	47.26	0.3703	0.3780	6.21
A/10	89.61	8.86	28.88	30.21	72.95	88.87	75.47	15.82	0.4933	0.4189	
F11/10	88.96	4.78	29.27	29.65	80.72	79.41	74.09	28.63	0.4360	0.4068	
Compound 11											
D65/10	85.49	-2.02	37.77	37.82	93.07	62.62	66.98	34.66	0.3812	0.4077	17.91
A/10	87.39	5.45	38.02	38.41	81.85	81.61	70.80	12.13	0.4960	0.4303	
F11/10	86.71	0.3	41.05	41.05	89.58	72.25	69.42	20.65	0.4451	0.4277	
Compound 12											
D65/10	80.86	7.08	23.08	24.14	72.94	58.05	58.21	24.29	0.3715	0.3726	12.28
A/10	83.08	10.80	25.95	28.11	67.40	74.64	62.31	13.38	0.4965	0.4145	
F11/10	82.34	6.53	25.96	26.77	75.88	66.26	60.94	39.99	0.4374	0.4023	

Contg. Table 1.

Coordinates	L*	a*	b*	C*	h	X	Y	Z	x	y	K/S
Compound 13											
D65/10	88.17	4.67	13.96	14.72	71.51	70.82	72.42	60.97	0.3468	0.3546	
A/10	89.62	7.38	15.68	17.33	64.79	88.04	75.48	20.28	0.4790	0.4107	9.32
F11/10	89.04	4.85	15.73	16.46	72.87	79.63	74.25	37.09	0.4170	0.3888	
Compound 14											
D65/10	89.28	-5.04	36.27	36.62	97.91	68.54	74.75	41.10	0.3717	0.40054	
A/10	90.79	3.28	34.96	35.12	84.64	88.58	78.02	14.60	0.4889	0.4306	16.28
F11/10	90.28	-2.07	40.39	40.44	92.94	78.80	76.90	23.91	0.4387	0.4282	
Compound 15											
D65/10	88.49	-0.87	27.84	27.85	91.78	68.89	73.08	47.40	0.3638	0.3859	
A/10	90.07	5.02	28.02	28.74	79.85	87.79	76.45	16.34	0.4862	0.4233	8.6
F11/10	89.60	0.28	31.78	31.78	89.50	78.51	75.45	27.84	0.4318	0.4150	
Compound 16											
D65/10	87.26	4.93	27.65	28.08	79.89	69.12	70.53	45.63	0.3731	0.3807	
A/10	89.47	9.18	30.29	31.65	73.13	88.70	75.16	15.32	0.4950	0.4195	9.02
F11/10	88.74	5.14	30.71	31.14	80.50	79.11	73.62	27.61	0.4386	0.4082	
Compound 17											
D65/10	82.84	8.28	25.78	27.08	72.20	62.14		61.87	40.59	0.3775	0.3759
A/10	85.33	12.14	29.04	31.47	67.32	80.44		66.66	13.60	0.5005	0.4148
F11/10	84.42	7.99	28.85	29.93	74.53	71.18		64.87	24.63	0.4430	0.4037
Compound 18											
D65/10	82.58	5.40	33.62	34.05	80.87	60.43		61.37	34.00	0.3879	0.3939
A/10	85.11	10.75	35.87	37.44	73.32	79.18		66.22	11.68	0.5041	0.4216
F11/10	84.34	5.32	37.68	38.05	81.97	69.74		64.73	20.32	0.4505	0.4182
Compound 19											
D65/10	89.18	-0.38	28.21	28.21	90.76	70.51		74.55	48.18	0.3649	0.3858
A/10	90.84	5.08	29.01	29.45	80.07	89.74		78.13	16.45	0.4869	0.4239
F11/10	90.44	0.44	31.22	31.22	89.18	80.47		77.25	28.97	0.4310	0.4138
Compound 20											
D65/10	86.81	2.44	33.40	33.49	85.82	67.11		69.63	39.95	0.3798	0.3941
A/10	89.02	7.83	35.09	35.96	77.42	86.84		74.22	13.69	0.4970	0.4247
F11/10	88.51	2.38	37.27	37.35	86.34	77.17		73.13	23.94	0.4429	0.4197
Compound 21											
D65/10	88.29	-6.81	49.71	50.18	97.80	65.82		72.68	29.54	0.3917	0.4325
A/10	90.15	2.87	47.93	48.02	86.58	86.77		76.62	10.85	0.4980	0.4398
F11/10	89.64	-3.50	55.10	55.21	93.63	76.65		75.53	16.81	0.4536	0.4469
Compound 22											
D65/10	85.15	4.20	17.18	17.69	76.27	64.70		66.30	52.13	0.3533	0.3621
A/10	86.74	7.76	19.03	20.55	67.82	81.34		69.47	17.39	0.4836	0.4130
F11/10	86.11	4.27	19.24	19.70	77.49	72.92		68.21	31.62	0.4221	0.3948

Assessment of color fastness

Most influences that can affect fastness are light, washing, heat, perspiration, crabbing and atmospheric pollution. Conditions of such tests are chosen to correspond closely to treatments employed in manufactu-

re and ordinary use conditions.¹² Results are given after usual matching of tested samples against standard reference (the grey scale).¹² The results revealed that these dyes have good fastness properties (Table 7).

Table 2. Color differences between dyes (**4, 5, 6, 9, 13, 15**) using **14** as a standard on polyester fibers at sun light wavelength (D65/10), tungsten wavelength (A/10) and fluorescent wavelength (F11/10).

	Reference dye 14				Batch is
	ΔE^*	ΔL^*	ΔC^*	ΔH^*	
Compound 4					
D65/10	7.722	-5.674	2.119	-4.790	Darker less green yellow
A/10	7.601	-5.346	3.258	-4.311	Darker redder yellow
F11/10	7.237	-5.503	2.805	-3.770	Darker less green yellow
Compound 5					
D65/10	4.710	-1.497	-3.486	-2.791	Darker less green less yellow
A/10	4.109	-1.436	-2.527	-2.905	Darker redder less yellow
F11/10	4.504	-1.492	-3.558	-2.322	Darker less green less yellow
Compound 6					
D65/10	5.271	-1.422	1.940	-4.690	Darker less green yellow
A/10	4.921	-1.103	3.780	-2.951	Darker redder yellow
F11/10	3.784	-1.159	1.937	-3.037	Darker less green yellow
Compound 9					
D65/10	10.473	-2.439	6.764	-7.614	Darker less green less yellow
A/10	10.537	-1.826	9.234	-4.736	Darker redder yellow
F11/10	9.096	-1.976	7.190	-5.209	Darker less green yellow
Compound 13					
D65/10	11.937	-0.431	-9.995	-6.512	Darker less green less yellow
A/10	10.553	-0.489	-8.445	-6.309	Darker redder less yellow
F11/10	11.838	-0.503	-10.416	-5.602	Darker less green less yellow
Compound 15					
D65/10	4.614	-0.273	-3.866	-2.505	Darker less green less yellow
A/10	3.695	-0.243	-2.958	-2.200	Darker redder less yellow
F11/10	3.961	-0.227	-3.638	-1.551	Darker less green less yellow

Table 3. Color differences between dyes (**12, 22**) using **3** as a standard on polyester fibers at sun light wavelength (D65/10), tungsten wavelength (A/10) and fluorescent wavelength (F11/10).

	Reference dye 3				Batch is
	ΔE^*	ΔL^*	ΔC^*	ΔH^*	
Compound 12					
D65/10	15.963	-2.174	-12.993	-9.014	Darker less green less yellow
A/10	14.425	-2.227	-11.343	-8.630	Darker redder less yellow
F11/10	15.323	-2.254	-13.343	-7.189	Darker less green less yellow
Compound 22					
D65/10	16.404	0.203	-15.481	-5.421	Darker less green less yellow
A/10	15.749	-0.161	-14.388	-6.401	Darker redder less yellow
F11/10	16.641	-0.115	-15.909	-4.882	Darker less green less yellow

Table 4. Color differences between dyes (**19**, **20**, **21**) using **11** as a standard on polyester fibers at sun light wavelength (D65/10), tungsten wavelength (A/10) and fluorescent wavelength (F11/10).

	Reference dye 11				Batch is
	ΔE^*	ΔL^*	ΔC^*	ΔH^*	
Compound 19					
D65/10	5.277	1.067	-4.804	-1.903	Lighter less green less yellow
A/10	4.678	1.006	-4.243	-1.694	Lighter redder less yellow
F11/10	4.876	1.098	-4.670	-0.873	Lighter less green less yellow
Compound 20					
D65/10	4.915	0.150	-2.397	-4.288	Lighter less green less yellow
A/10	3.541	0.298	-1.311	-3.276	Lighter redder less yellow
F11/10	3.203	0.335	-2.019	-2.464	Lighter less green less yellow
Compound 21					
D65/10	6.053	0.922	5.560	2.207	Lighter greener yellow
A/10	5.165	0.918	4.397	2.550	Lighter less red yellow
F11/10	6.613	0.978	6.172	2.162	Lighter greener yellow

Table 5. Color differences between dyes (**7**, **8**, **18**) using **2** as a standard on polyester fibers at sun light wavelength (D65/10), tungsten wavelength (A/10) and fluorescent wavelength (F11/10).

	Reference dye 2				Batch is
	ΔE^*	ΔL^*	ΔC^*	ΔH^*	
Compound 7					
D65/10	13.563	5.188	3.628	11.995	Lighter less red yellow
A/10	11.393	4.971	1.641	10.119	Lighter less red yellow
F11/10	11.821	5.083	3.587	10.052	Lighter less red yellow
Compound 8					
D65/10	14.328	4.941	8.181	10.675	Lighter less red yellow
A/10	13.191	4.952	6.462	10.379	Lighter less red yellow
F11/10	13.846	5.022	8.752	9.481	Lighter less red yellow
Compound 9					
D65/10	13.963	3.137	11.956	6.495	Lighter red yellow
A/10	14.499	3.469	11.308	8.384	Lighter red yellow
F11/10	14.545	3.464	12.389	6.787	Lighter less red yellow

Table 6. Color differences between dyes (**10**, **17**) using **16** as a standard on polyester fibers at sun light wavelength (D65/10), tungsten wavelength (A/10) and fluorescent wavelength (F11/10).

	Reference dye 16				Batch is
	ΔE^*	ΔL^*	ΔC^*	ΔH^*	
Compound 10					
D65/10	2.054	0.561	-0.926	1.745	Lighter redder less yellow
A/10	1.864	0.449	-1.205	1.349	Lighter redder less yellow
F11/10	1.909	0.514	-0.939	1.581	Lighter redder less yellow
Compound 17					
D65/10	3.192	-1.431	-0.810	-2.735	Darker redder less yellow
A/10	3.023	-1.367	-0.543	-2.641	Darker redder less yellow
F11/10	2.911	-1.426	-0.891	-2.376	Darker redder less yellow

Table 7. Fastness properties of compounds 2-22

Dyes	Fiber	Washing fastness			Crabbing fastness			Perspiration fastness, basic			Light fastness, 40 h
		Alt.	S. W	S. F	Alt.	S. W	S. F	Alt.	S. W	S. F	
2	Polyester	3	4	4	3	4	4	3	4	4	3
3	Polyester	4	4	4	4	4	4	4	4	4	1
4	Polyester	3-4	4	4	3-4	4	4	3-4	4	4	4
5	Polyester	4	4	4	4	4	4	4	4	4	2
6	Polyester	3-4	4	4	3-4	4	4	3	4	4	3
7	Polyester	3-4	4	4	3-4	4	4	3-4	4	4	4
8	Polyester	4	4	4	3-4	4	4	3-4	4	4	4
9	Polyester	3-4	4	4	3-4	4	4	3-4	4	4	1-2
10	Polyester	4	4	4	3-4	4	4	4	4	4	1
11	Polyester	4	4	4	4	4	4	4	4	4	3
12	Polyester	3	4	4	3	4	4	3	4	4	3-4
13	Polyester	3	4	4	3	4	4	3	4	4	2-3
14	Polyester	3-4	4	4	4	4	4	4	4	4	3
15	Polyester	4	4	4	3-4	4	4	3-4	4	4	2-3
16	Polyester	3-4	4	4	3-4	4	4	3-4	4	4	3
17	Polyester	3	4	4	3	4	4	3	4	4	3
18	Polyester	4	4	4	4	4	4	4	4	4	4
19	Polyester	4	4	4	4	4	4	4	4	4	4
20	Polyester	4	4	4	4	4	4	4	4	4	4
21	Polyester	3-4	4	4	3-4	4	4	3-4	4	4	3-4
22	Polyester	3	4	4	3-4	4	4	3-4	4	4	4

Alt = Alteration, S.W = Staining on wool, S.F = Staining on polyester..

Experimental

All melting points were determined on a Gallenkamp electric melting point apparatus. Thin-layer chromatography (TLC) analysis was carried out on silica gel 60 F254 precoated aluminum sheets.

Infrared spectra were recorded on FTIR 5300 Spectrometer and Perking Elmer Spectrum RXIFT-IR System, using the potassium bromide wafer technique. ¹H-NMR spectra were recorded on Varian Gemini 200 MHz spectrometer using the indicated solvents and tetramethylsilane (TMS) as an internal reference. Electron impact mass spectra were obtained at 70 eV using a GC-MS–qp1000 EX Shimadzu spectrometer. Elemental analysis (C, H, N) were carried out at the Micro-Analytical Center of Cairo University, Giza, Egypt.

The dyeing assessment fastness tests, and color measurements were carried out at Misr Company for Spinning and Weaving, El-Mahala El-Kobra, Egypt.

General procedure for the preparation of coupling products from 3-diazo-4,5-diphenylpyrazolo[3,4-c]pyridazine 1 and active methylene compounds.

A solution of compound 1 (0.6 g, 2.0 mmol) in ethanol (30 mL) was treated with the corresponding active methylene compounds (2.0 mmol). The reaction mixture was stirred at room temperature for such time. The colored azo-dye precipitated was filtered, dried, and recrystallized from ethanol. In this manner the following compounds were prepared.

3-((4,5-Diphenyl-1H-pyrazolo[3,4-c]pyridazin-3-yl)diazenyl)-pentane-2,4-dione 11.

Prepared from pentane-2, 4-dione, and reaction time: 45 minutes, yellow crystals in 73 % yield, m.p. 250-252 °C. IR: 3500, 3300 (NH), 3060 (CH_{arom}), 2925 (CH_{aliph}), 1700 (C=O), 1630 (C=N), 1510 (C=C) cm⁻¹. ¹H-NMR (DMSO-*d*₆): δ = 7.9-7.2 (m, 10H, 2Ph) and 2.9 (s, 6H, 2CH₃). Anal. Calcd for C₂₂H₁₈N₆O₂: C, 66.32; H, 4.55; N, 21.10, Found: C, 66.20; H, 4.40; N, 20.90.

2-Cyano-2-((4,5-diphenyl-1H-pyrazolo[3,4-c]pyridazin-3-yl)diazenyl) acetohydrazide. 12

Prepared from 2-cyanoacetohydrazide, reaction time: 6 hours, reddish brown crystals in 69 % yield, m.p.: 180-182 °C. IR: 3345, 3197 (NH₂ & NH), 3030(CH_{arom}), 2928 (CH_{aliph}), 2259 (CN), 1687(C=O) cm⁻¹; MS: m/z 397 [M⁺, 1.35%]. Anal. Calcd for C₂₀H₁₅N₉O: C, 60.45; H, 3.80; N, 31.72. Found: C, 59.35; H, 3.78; N, 30.12.

(4,5-Diphenyl-1H-pyrazolo[3,4-c]pyridazin-3-yl) carbonocyanidohydrazonic chloride. 13

Prepared from 2-chloroacetonitrile, reaction time: 2 hours, brown crystals in 67 % yield, m.p.: 208-210 °C. IR: 3165(NH), 3105(CH_{arom}), 2900 (CH_{aliph}), 2130 (CN), 1651(C=N), cm⁻¹; MS: m/z 373.3 [M⁺, 10.75%], 374.5 [M⁺+1, 10.19%], 337.1 [M⁺-Cl, 9.65%] 273.2 [M⁺-N=NCH(CN)Cl]. Anal. Calcd for C₁₉H₁₂ClN₇: C, 61.05; H, 3.24; N, 26.23. Found: C, 61.03; H, 3.19; N, 26.25.

5-((4,5-Diphenyl-1*H*-pyrazolo[3,4-*c*]pyridazine-3-yl)hydrazono-3-oxo-*N*-phenylbutanamide 14.

Prepared from 3-oxo-*N*-phenylbutanamide, reaction time: 2 hours, yellow crystals in 65 % yield, m.p. 279-281°C. IR: 3400 (NH), 1690 (C=O), 1650 (C=O amide), 1530 cm⁻¹; Anal. Calcd for C₂₇H₂₁N₇O₂: C, 68.20; H, 4.45; N, 20.62. Found: C, 68.30; H, 4.30; N, 20.70.

5-(2-(4,5-Diphenyl-1*H*-pyrazolo[3,4-*c*]pyridazin-3-yl)hydrazono)pyrimidine-2,4,6(1*H*,3*H*,5*H*)-trione. 15

Prepared from pyrimidine-2,4,6(1*H*, 3*H*, 5*H*)-trione, the reaction time: 3.5 hours yellow crystals 90 % yield. m.p.: 310-312 °C. IR: 3168 (NH), 1713, 1674 (C=O), 1534 (C=N) cm⁻¹. MS: m/z 426.4 [M⁺, 8.97%], 427.4 [M+ 1, 3.18], 456 [M-Cl, 22.45]. Anal. Calcd for C₂₁H₁₄N₈O₃: C, 59.15; H, 3.31; N, 26.28. Found: C, 59.10; H, 3.26; N, 26.14.

3-((4,5-Diphenyl-1*H*-pyrazolo[3,4-*c*]pyridazin-3-yl)diazenyl)-4-hydroxy-6-methyl-2*H*-pyrano[3,2-*c*]quinoline-2,5(6*H*)-dione. 16

Prepared from, 4-hydroxy-6-methyl-2*H*-pyrano[3,2-*c*]quinoline-2,5(6*H*)-dione, the reaction time: 2 hours, orange crystals in 50 % yield, m.p.: 285-287 °C; IR: 3436 (NH and OH), 3078 (CH_{aromatic}), 2975 (CH_{aliphatic}), and 1645 (C=O) ester and 1606 (C=O) amide, cm⁻¹; MS: m/z 542.3 [M⁺, 0.31%]. Anal. Calcd for C₃₀H₁₉N₇O₄: C, 66.54; H, 3.54; N, 18.11. Found: C, 66.46; H, 3.50; N, 18.10.

3-((4,5-Diphenyl-1*H*-pyrazolo[3,4-*c*]pyridazin-3-yl)diazenyl)-4-hydroxy-6-phenyl-2*H*-pyrano[3,2-*c*]quinoline-2,5(6*H*)-dione. 17

Prepared from, 4-hydroxy-6-phenyl-2*H*-pyrano[3,2-*c*]quinoline-2,5(6*H*)-dione, the reaction time: 4 hours, orange crystals in 81 % yield, m.p.: 280-282 °C; IR: 3419 cm⁻¹ (-OH), 3146 (-NH), 3060 (CH_{aromatic}), 2789 (CH_{aliphatic}) 1647 (C=O) ester, 1608 cm⁻¹ (C=O) amide ring carbonyl, cm⁻¹; MS: m/z 604.40 [M⁺, 2.55 %]. Anal. Calcd for C₃₅H₂₁N₇O₄: C, 69.65; H, 3.51; N, 16.24. Found: C, 69.58; H, 3.48; N, 16.20.

3-((5-Chloro-3-methyl-1-phenyl-1*H*-pyrazol-4-yl) diazenyl)-4,5-diphenyl-1*H*-pyrazolo[3,4-*c*]pyridazine 18.

A mixture of 4-((4,5-diphenyl-1*H*-pyrazolo[3,4-*c*]pyridazin-3-yl)diazenyl)-3-methyl-1-phenyl-1*H*-pyrazol-5(4*H*)-one **8** (0.5g, 1.05 mmol) and phosphorylchloride (25 mL) was refluxed for 3h. The reaction mixture was cooled to room temperature and poured into crushed ice, the solid product was filtered, dried and recrystallized from ethanol. Brown crystals in 77 % yield, m.p.: 250-252 °C; IR: 3317 (NH), 3050 (CH_{arom}), 2968 (CH_{aliph}), 1591 (C=N) cm⁻¹. MS: m/z 491 [M⁺, 22.35 %], 492 [M+ 1, 17.53], 456 [M-Cl, 22.45]. Anal. Calcd for C₂₇H₁₉ClN₈: C, 66.05; H, 3.90; N, 22.28. Found: C, 65.86; H, 3.84; N, 22.42.

3-((3,5-Dimethyl-1*H*-pyrazol-4-yl)diazenyl)-4,5-diphenyl-1*H*-pyrazolo[3,4-*c*]pyridazine 19.

To a solution of 3-((4,5-diphenyl-1*H*-pyrazolo[3,4-*c*]pyridazin-3-yl)diazenyl)pentane-2,4-dione **11** (0.8 g, 2.0 mmol) in acetic acid (20 mL), hydrazin hydrate (85 %, 1.0 mL) was added. The reaction mixture was refluxed for 3 h. The yellow solid product was filtered and recrystallized from methanol, yellow crystals in 81 % yield. m.p.: 281-282 °C; IR: 3170 (NH), 3068 (CH_{arom}), 2928 (CH_{aliph}) 1625 (C=N), 1590 (PhN) and 1535 (C=C) cm⁻¹, ¹H-NMR (DMSO-*d*₆) δ= 7.9-7.2 (m, 10H, 2Ph) and 2.9 (s, 6H, 2CH₃). Anal. Calcd for C₂₂H₁₈N₈: C, 66.99; H, 4.60; N, 28.4. Found: C, 66.80; H, 4.50; N, 28.30.

3-((3,5-Dimethyl-1-phenyl-1*H*-pyrazol-4-yl)diazenyl)-4,5-diphenyl-1*H*-pyrazolo[3,4-*c*]pyridazine. 20

A mixture of 3-((4,5-diphenyl-1*H*-pyrazolo[3,4-*c*]pyridazin-3-yl)diazenyl)pentane-2,4-dione **11** (0.8 g, 2.0 mmol) and phenyl hydrazine (0.22 g, 2.0 mmol) in acetic acid (20 mL) was refluxed for 5 h. The cooled reaction mixture was poured into water (100 mL). The solid product obtained was filtered, and recrystallized from ethyl acetate, yellow crystals in 84 % yield, m.p.: 272-273 °C; IR: 3170 (NH), 3088 (CH_{arom}), 2918 (CH_{aliph}) 1625 (C=N), 1590 (PhN) and 1535 (C=C) cm⁻¹; ¹H NMR(DMSO-*d*₆): δ= 14.9 (br s, 1H, NH), 7.7 (s, 5H, PhN) 7.4-6.8 (m, 10H, 2Ph) and 2.3 (s, 3H, CH₃), 1.9 (s, 3H, CH₃). Anal. Calcd for C₂₈H₂₂N₈: C, 71.74; H, 4.71; N, 23.8. Found: C, 71.30; H, 4.60; N, 23.70.

4-((4,5-Diphenyl-1*H*-pyrazolo[3,4-*c*]pyridazin-3-yl)diazenyl)-3,5-dimethylisoxazole 21.

A mixture of 3-((4,5-diphenyl-1*H*-pyrazolo[3,4-*c*]pyridazin-3-yl)diazenyl)pentane-2,4-dione **11** (0.8 g, 2.0 mmol) and hydroxylamine hydrochloride (0.14 g, 2.0 mmol) in pyridine (15 mL) was refluxed for 10 h. The reaction mixture was poured onto water (100 mL). The solid product obtained was filtered, and recrystallized from ethanol. Yellow crystals in 73 % yield, m.p.: 214-215 °C; IR: 3210 (NH), 3060 (CH_{arom}), 2948 (CH_{aliph}), 1630 (C=N), 1590 (PhN) and 1520 (C=C) cm⁻¹. ¹H NMR (DMSO-*d*₆): δ =11.8 (s, 1H, NH), 7.6-6.8 (m, 10H, 2Ph) 2.1 (s, 3H, CH₃), 1.9 (s, 3H, CH₃). Anal. Calcd for C₂₂H₁₇N₇O: C, 66.82; H, 4.33; N, 24.80. Found: C, 66.70; H, 4.20; N, 24.70.

3-Amino-4-((4,5-diphenyl-1*H*-pyrazolo[3,4-*c*]pyridazin-3-yl)-diazenyl)-1*H*-pyrazol-5(4*H*)-one 22.

To a solution of ethyl 2-cyano-2-(2-(4,5-diphenyl-1*H*-pyrazolo[3,4-*c*]pyridazin-3-yl)hydrazono)acetate **3** (0.82 g, 2.0 mmol) in ethanol (50 mL), hydrazine hydrate (85 %, 1.0 mL) was added. The reaction mixture was refluxed for 3 h. Upon cooling the precipitated product was filtered and recrystallized from ethanol. Deep red crystals in 81 % yield, m.p.: >300 °C; IR: 3355, 3280, 3210, 3140 (NH₂ & NH), 1680 (C=O), 1620 (C=N) and 1570 (C=C) cm⁻¹;

¹H NMR (DMSO-*d*₆): δ = 7.8-7.2 (m, 10H, 2Ph) and 3.4 (br s, 2H, NH₂). Anal. Calcd for C₂₀H₁₅N₃O: C, 60.44; H, 3.80; N, 31.72. Found: C, 60.30; H, 3.70; N, 31.60.

4-Methyl-N,9,10-triphenyl pyridazino [3',4':3,4] pyrazolo[5,1-c][1,2,4]triazine-3-carboxamide **23**.

Compound **14** (0.8 g) was heated in ethanol (20 mL) for 30 minutes, after concentration, the solid crystals was filtered. Greenish yellow in 58% yield. M.p.: 279-281 °C; IR: 3342 (NH) , 1689 cm⁻¹ (amide C=O). Ms: m/z 457.15 [M⁺, 100%], 458.15[M+ 1, 32.67], 442.10 [M-CH₃, 5.68], 337.05[M-CONHPh, 24.57] 100%. Anal. Calcd for C₂₇H₁₉N₇O: C, 70.88; H, 4.19; N, 21.43. Found: C, 70.68; H, 4.16; N, 21.14.

Dyeing procedures

Preparation of dye dispersion

The required amount of dye (2 % shade) was dissolved in DMF and added dropwise with stirring to a solution of Dekol-N (2 g dm⁻³), an anionic dispersing agent of BASF, then the dye was precipitated in a fine dispersion ready for use in dyeing.

Dyeing of polyester at 130°C under pressure using Levegal PT (carrier of Bayer)

The dye bath (1:20 liquor ratio), containing 5 g dm⁻³ Levegal PT (Bayer) as carrier, 4 % ammonium sulfate, and acetic acid at pH 5.5, was brought to 60 °C, the polyester fabric was entered and run for 15 min. The fine dispersion of the dye (2 %) was added, and the temperature was raised to boiling within 45 min, dyeing was continued at boiling temperature for about 1 h, then the dyed material was rinsed and soaped with 2 % nonionic detergent to improve wet fastness.

Assessment of color fastness (Table 7)

Fastness to washing, perspiration, light, and crabbing was tested according to the reported methods.

Fastness to washing

A specimen of dyed polyester fabric was stitched between two pieces of undyed samples (one from wool and the other one from the same fibre under test "polyester"), all of equal diameter, and then washed at 50 °C for 30 min. The staining on the undyed adjacent fabric was assessed according to the following grey scale: 1-poor, 2-fair, 3-moderate, 4-good, and 5-excellent.

Fastness to Crabbing

A composite specimen was made by sewing a piece of dyed fabric between two equal weight pieces of undyed samples (one from wool and the other one from the same fiber under test "polyester"). The composite specimen was boiled at 100 °C in water for 2 minutes.

Fastness to perspiration (basic):

The AATCC standard test method 15-1960 was used. For each dyed sample two composite specimens were prepared by stitching a piece of dyed sample between two undyed samples (one from wool and the other one from the same fiber under test "polyester"). Each one of the two composite specimens were immersed in alkaline solution for 30 minutes with occasional agitation and squeezing to ensure complete wetting, then squeezed to about 200-300 % regain and put between the plastic plates of the perspiration tester in such a way that the specimens should be in a vertical position when placed in the oven. The loaded sample was kept in an oven at 38 °C for 6-8 hours, after which the sample was dried by conventional means. Change in color of the dyed samples and staining of the undyed ones were assessed using "International Geometric Grey Scale" (1-5).

The alkaline solution (pH= 8-8.5) contained sodium chloride (10 g l⁻¹), ammonium carbonate (4 g l⁻¹), disodium orthophosphate (1 g l⁻¹) and histidine monohydrochloride (0.25 g l⁻¹).

Fastness to Light

Dyed sample and standard Blue Scale samples were exposed to the sun light for 40 h. After exposure, the sample and standard were allowed to lie in the dark at room temperature for about 2h in order to cool off and regain normal moisture from air.

Light fastness of the dyed sample was given by comparison the change in color with relative "International Geometric Grey Scale" (1-5): 1-poor, 2-fair, 3-moderate, 4-good, 5-excellent.

Color assessment

Table 1 reports the color parameters of the dyed fabrics assessed by tristimulus colorimetry. The color parameters of the dyed fabrics were determined using a SPECTRO multichannel photodetector (model MCPD1110A), equipped with a D65 source and barium sulfate as a standard blank.

The values of (the chromaticity coordinates, luminance factor, and the position of the color in the CIE-LAB color solid are reported Tables 2-6).

Conclusions

A set of **21** disperse dyes **2-22** were synthesized by reaction of 3-diazo-4,5-diphenyl-3H-pyrazolo[3,4-c]-pyridazine **2** with active methylene compounds and their derivatives. All of them were investigated for their dyeing characteristics on polyester. The dyed fabrics exhibit moderate to good (3-4) washing, crabbing, and perspiration fastness properties (Table 7). The remarkable degree of levelness and brightness after washing is indicative of good penetration and excellent affinity of these dyes for fabric due to accumulation of polar groups. This in combination with the ease of preparation makes them particularly valuable.

References

- ¹Part 36: Deeb, A. Mahgoub, S., *Med. Chem. Res.*, accepted, **2014**.
- ²Catino, S. C. and Farris, R. E., in: *Concise Encyclopedia of Chemical Technology*, Ed. M. Gryson, N.Y.: J. Wiley and Sons, **1985**.
- ³ Fedda, A. A., Etman, H. A., Amer, F. A., Barghout, M. and Mohammed, K. S. *J. Chem. Technol. Biotechnol.*, **1994**, *61*, 343.
- ⁴Towns, A. D., *Dyes Pigm.*, **1999**, *42*, 3.
- ⁵Griffiths, G., *Rev. Prog. Color.*, **1981**, *11*, 37.
- ⁶Heinish, G. and Kopelent, H., *Progress in Medicinal Chemistry: Pharmacologically Active Pyridazine Derivatives*, **1992**, Part 2, Vol. 29, 141. Ed. By G P Ellis and G B West Amsterdam:Elsevier Science Publishers, **1992**.
- ⁷Hosny, M., El-Mariah, F., Deeb, A., *Phosph., Sulfur, Silicon*, **2007**, *182*, 1475-1482.
- ⁸Deeb, A. Morad, E. Elenany, D., *Phosph., Sulfur, Silicon*, **2010**, *185*, 222-231.
- ⁹Deeb, A., El-Mariah, F., Hosnym M., *Bioorg. Med. Chem., Lett.*, **2004**, *14*, 5013-5017.
- ¹⁰Deeb, A. Bayoumy, B. Hataba, A. and Fikry, R., *Heterocycles*, **1991**, *32*, 901.
- ¹¹ Deeb, A. Kotb, M., *Heterocycles*, **2004**, *83*, 1143.
- ¹²Society of Dyes and Colorists: *Standard Methods for the Determination of Color Fastness of Textiles and Leather*, 5th edn. Society of Dyes and Colorists, Bradford **1990**.
- ¹³ Ho, Y. W. and Wang, I. J., *Dyes Pigm.*, **1995**, *29*, 117-129.

Received: 27.03.2014.

Accepted: 09.05.2014.



BIOSYNTHESIS OF L-METHIONINE IN *Corynebacterium glutamicum* X300

Subhadeep Ganguly and Kunja Bihari Satapathy

Keywords: S-adenosylmethionine; methyl group donor; homocysteine; L-methionine; methylcobalamin homocysteine transmethylase

Enzymes leading to the methylation of homocysteine to produce L-methionine in the mutant *Corynebacterium glutamicum* X300 were investigated in this present study. S-adenosyl methionine served as a methyl group donor to homocysteine to form L-methionine. The enzymatic pathway examined in this present study was cobalamin-independent pathway. No methylcobalamin homocysteine transmethylase activity was detected in this microorganism.

Corresponding Authors

E-Mail: res_biol@rediffmail.com

[a] Post-Graduate Department of Botany, Utkal University, Vani Vihar, Bhubaneswar-751004, Odisha

ZnSO₄·7H₂O, 1.6 mg; CaCO₃, 1.5 g; Na₂MoO₄·2H₂O, 5.0 mg; MnSO₄·4H₂O, 2.5 mg; biotin, 80 mg and thiamine-HCl, 70 µg.¹⁰

Introduction

Trials for microbial production of L-methionine were initiated in 1970s in Japan using *Corynebacterium glutamicum*.^{1,2} Cystathione, an intermediate of biosynthesis of L-methionine in microorganism follow two alternative pathways, namely: (1) trans-sulfuration pathway and (2) direct sulfhydration pathway.^{3,4} Several reports are available on the microbial synthesis of L-methionine.^{3,5,6} In our present investigation, we are intended to investigate the enzymatic pathway for L-methionine production in the mutant *Corynebacterium glutamicum*X300.

Materials and methods

Selection of microorganism: A regulatory mutant *Corynebacterium glutamicum* XI (accumulated only 0.6 mg mL⁻¹ L-methionine) developed in our laboratory from its parent strain *Corynebacterium glutamicum* (basically a L-glutamic acid producing bacterium which does not accumulate L-methionine) which was isolated from North Bengal soil was subjected for mutational study.⁷

Optimum cultural conditions: Volume of medium, 25 ml; initial pH, 7.0; shaker's speed, 150 rpm; age of inoculum, 48 h; optimum cell density, 4.0x10⁸ cells mL⁻¹; temperature, 28 °C and period of incubation, 72 h.⁸

Composition of basal salt medium for L-methionine fermentation: L-methionine production was carried out using the following basal salt medium (per litre): glucose, 60 g; (NH₄)₂SO₄, 1.5 g; K₂HPO₄, 1.4 g; MgSO₄·7H₂O, 0.9 g; FeSO₄·7H₂O, 0.01 g; biotin, 60 µg.⁹

Composition of synthetic medium (per liter): glucose, 100 g; (NH₄)₂SO₄, 8.0 g (in terms of nitrogen); K₂HPO₄, 2.2 g; MgSO₄·7H₂O, 1.5 g; FeSO₄·7H₂O, 0.03 g; KH₂PO₄, 2.0 g;

Analysis of L-methionine: Descending paper chromatography was employed for detection of L-methionine in culture broth and was run for 18 hours on Whatman No.1 Chromatographic paper. Solvent system used includes n-butanol: acetic acid: water (2:1:1). The spot was visualized by spraying with a solution of 0.2 % ninhydrin in acetone and quantitative estimation of L-methionine in the suspension was done using colorimetric method.¹¹

Preparation of cell free extract for enzymatic assay: Freshly harvested cells of *Corynebacterium glutamicum* X300 was suspended in 20 mM potassium phosphate buffer (pH 8.0) containing 2-mercaptoethanol (7 mM) and was ruptured by two passages through a French pressure cell using a pressure of 7800 lb in⁻² (53.8 MN m⁻²) as described by French and Milner (1955).¹² The crude extract was then centrifuged at 30,000 rpm for 15 minutes and the supernatant was used as a source of enzymes. The protein content was spectrophotometrically determined by the method as described by Layne.¹³ The estimation of cobalamin and enzymes involved in L-methionine biosynthesis and S-adenosylmethionine as described by Salem *et al.*¹⁴

Statistical analysis: All the data were expressed as mean ± SEM, where n=6.

All the chemicals used in this study were analytical grade (AR) grade and obtained from E mark. Borosil glass goods and triple distilled water used throughout the study.

Results and Discussion

Blakley reported the methylation of homocysteine for L-methionine production in *Escherichia coli*.¹⁵ Serine or glycine may serve as a methyl donor for L-methionine production.¹⁶ Guest *et al.* and Whitfield *et al.* claimed that an Mg²⁺ (or Mn²⁺) dependent transmethylase catalyze the

transfer of methyl group from a conjugated 5-methyl tetrahydrofolate to homocysteine.^{17,18} Guest *et al.* also reported that CH₃H₄PteGlu₃ or 5-CH₃H₄PteGlu₁ may donate methyl group to homoserine only in presence of cobalamin in the medium.¹⁷ The cobalamin content of the mutant *Corynebacterium glutamicum* X300 was measured by the method as described by Foster *et al.*¹⁹ The mutant cell contained 827.3±1.618 ng of cobalamin g⁻¹ dry cell weight. The methyl group donor for homocysteine was serine in the mutant when H₄Pteglu₃ was added as folate coenzyme. The comparatively low activity of H₄Pteglu₁ proved that at least one reaction in the methionine synthesis was specific for polyglutamate folate. The activities of 5,10-methylenetetrahydrofolate reductase and 5-methyltetrahydrofolate homocysteine transmethylase were extensively investigated in *Corynebacterium glutamicum* X300 for the conversion of serine and homocysteine into L-methionine. The production of L-methionine was stimulated in this organism on addition of H₄Pteglu₃ or H₄Pteglu₁ (Table 1), suggesting thereby the common occurrence of 5,10-methylenetetrahydrofolate homocysteine transmethylase in the supernatant was indicated by improved L-methionine accumulation. But this activity requires a polyglutamate folate.

Table 1. 5,10-methylene tetrahydrofolate reductase and 5-methyltetrahydrofolate homocysteine transmethylase activity in *Corynebacterium glutamicum* X300

Source of folate	L-methionine (nmol)
H ₄ Pteglu ₁	21.6±0.913
H ₄ Pteglu ₃	43.2±0.883

Values were expressed as mean±SEM, where n=6. Each sample contained 4.8 mg of protein which were incubated in a vial containing serine and homocysteine as suggested by Salem *et al.*¹⁴ Incubations were carried out at 28 °C for 60 min under H₂. The endogenous folates were removed by passing through the columns of Dowex 1 resin (Cl⁻ form)].

The transmethylase activity in extracts was examined by using 5-[¹⁴C]methyltetrahydrofolate as a methyl group donor to homocysteine. 5-CH₃H₄PteGlu₃. Transmethylation from 5-CH₃H₄PteGlu₁ was not initiated by incubating under H₂ even though the addition of different cofactors like S-adenosylcobalamin and reductase system (H) was resulted.

Table 2. 5-CH₃H₄PteGlu₃-homocysteine transmethylase activity in *Corynebacterium glutamicum* X300

Nature of folate compound	L-methionine (nmol h ⁻¹ mg ⁻¹ of protein)
5- ¹⁴ CH ₃ H ₄ PteGlu ₁	21.4±1.136
5- ¹⁴ CH ₃ H ₄ PteGlu ₃	45.8±0.981

Values were expressed as mean± SEM, where n=6. Cell extracts (8 mg of protein) were incubated at 28 °C for 1 h in a mixture containing MgSO₄·7H₂O (5 mM), DL-homocysteine (25 mM) and either 5-¹⁴CH₃H₄PteGlu₁ or 5-¹⁴CH₃H₄PteGlu₃ (2 mM; 0.7 μCi μmol⁻¹), S-adenosylmethionine (10 μM), FAD (100 nmol), NAD (100 nmol), ethanol (100 nmol), H₄PteGlu₃ (10mM) and alcohol dehydrogenase 100 μg.

Extract was tested for the ability to use methylcobalamin as a methyl group donor to homocysteine. No methylcobalamin homocysteine transmethylase activity was detected in this microorganism. S-adenosylmethionine was also tested to examine its ability to donate methyl group to

homocysteine for L-methionine biosynthesis in this mutant. Production was increased 16nmol h⁻¹ mg⁻¹ of protein with S-adenosylmethionine, suggesting thereby it was considered as a methyl group donor to homocysteine for L-methionine biosynthesis. Shapiro in *Aerobacter aerogenes*, Balish and Shapiro, Mardon and Balish in *Candida albicans*, Shapiro, Shipiro *et al.* and Botsford and Parks in *Saccharomyces cerevisiae* reported similar pattern of methyl group transfer.^{1-4,8,20} Thus, synthesis of L-methionine occurs by transmethylation to homocysteine from a polyglutamate folate. 5,10-methylene tetrahydrofolate reductase transferred methyl group from either a conjugated folate or monoglutamate folate. From this present study, it can be tentatively concluded that the mutant used S-adenosylmethionine as a methyl group donor to homocysteine to form L-methionine. The enzymatic pathway examined in this present study was cobalamine-independent pathway in this mutant similar to *E.coli* as suggested by Woods *et al.*⁹

References

- Kase, H. and Nakayama, K., *Agric. Biol.Chem.*, **1974**, *38*, 2021-2030.
- Kase, H. and Nakayama, H., *Agric. Biol. Chem.*, **1975**, *39*, 687-693.
- Hwang, B. J., Yeom, H. J., Kim, Y. and Lee, H. S., *J.Bacteriol.*, **2001**, *184*, 1277-1286.
- Lee, H. S. and Hwang, B. J., **2003**, *Appl. Microbiol.Biotechnol.*, *62*, 459-467.
- Ruckert, C., Puhler, A. and Kalinowski, *J.Biotechnol.*,**2003**, *104*, 213-228.
- Kovaleva, G. Y. and Gelfand, M. S., *Mol. Biol.*, **2007**, *41*, 126-136.
- Ganguly, S., Satapathy, K. B. and Banik, A. K., *Res. J. Pharm. Dose Forms Technol.*, **2014**, *6*, 303-310.
- Ganguly, S., Satapathy, K. B., *J. Bioproc. Technol., Photon*, **2013**, *98*, 303-307.
- Iwata, M., Made, M. and Ishiwa, H., *Appl. Environ. Microbiol.*, **1986**, *52*, 392-393.
- Ganguly, S. and Satapathy, K. B., *Int. J. Multidiscipl. Educ. Res.*, **2013**, *2*, 252-261.
- Ganguly, S. and Banik, A. K., *J. Pure Appl. Microbiol.*, **2012**, *6*, 271-279.
- French, C. S. and Milner, H. W., *Methods Enzymol.*, **1955**, *1*, 64.
- Layne, E., *Methods Enzymol.*, **1957**, *3*, 451.
- Salem, A. R., Pattison, J. R. and Foster, M. A., *Biochem J.*, **1972**, *126*, 993.
- Blakley, R. C., *Biochem. Folic Acid Relat. Pteridines*, **1969**, *30*, 332-353.
- Salem, A. R. and Foster, M. A., *Biochem. J.*, **1972**, *127*, 845-853.
- Guest, J. R., Foster, M. A. and Woods, D. D., *Biochem. J.*, **1964**, *92*, 488.
- Whitfield, C. D., Steers, E. J. Jr. and Weissbach, H., *J. Biol. Chem.*, **1970**, *245*, 390.
- Foster, M. A., Tejerina, G., Guest, J. R. and Wood, D. D., *Biochem. J.*, **1964**, *92*, 476.
- Sharpiro, S. K., Yphantis, D. A. and Almenas, A., *J. Biol. Chem.*, **1964**, *239*, 1551.

Received: 05.04.2013.

Accepted: 12.05.2014.



CHROMATOGRAPHY OF ANTICANCER DRUGS. PART 3

Tibor Cserhádi^[a] and Mária Szógyi^[a]**Keywords:** chromatography; natural and synthetic anticancer drugs;

Various chromatographic techniques applied for the separation and quantitative determination of synthetic anticancer drugs and natural anticancer compounds are reviewed.

Corresponding Authors

E-Mail: szogyim t-online.hu

[a] Research Center for Natural Sciences, Hungarian Academy of Sciences, Budapest, Hungary

Introduction

Various chromatographic techniques have been extensively applied not only for the separation and quantitative determination of synthetic anticancer drugs but also for the analysis of natural anticancer compounds present in complicated accompanying organic and inorganic matrices. The same chromatographic techniques were employed for the analysis of synthetic drugs as for the investigation of natural products. These methods have been reviewed.

Discussion

Liquid chromatography combined with tandem mass spectrometry (LC/MS/MS) was successfully employed for the separation and quantitative determination of doxorubicin and its main metabolite doxorubicinol (DOXol). Solid phase extraction was applied for the prepurification and preconcentration of samples, the validated calibration ranged from 5.00-to 1000 ng mL⁻¹ and from 0.50 to 50.0 ng mL⁻¹. The data proved the the good accuracy and precisicy of the method. It was established that the procedure can be used for the analysis of DOX and DOXol in whole cells, nuclear enriched fraction and organelle-enriched fraction. It was further found that the method is suitable for the determination of analytes in subcellular compartments.¹

A HPLC-MS procedure was developed for the study of the efficacy of a non-hypercalcemic vitamin-D2 derived anti-cancer agent (MT19c). The measurements established the antitumor activity of the new preparation. It was stated that the compound shows marked antitumor effect and can be applied for the design of vitamin-D based anticancer molecules. It was further proposed for the developing of MT19c as a therapeutic agent for malignant ovarian tumors by targeting oncogenic de novo lipogenesis.²

An LC-MS method was developed for the investigation of the anticancer prodrug combretastatin A1 phosphate (OXi4503, CA1P), the active CA1 and its glucuronide metabolites in human urine and CA1 in plasma.

Validated methods were applied for the determination of CM1, the active agent derived from the prodrug CA1P, for the analysis of three glucuronides CA1G1, CA1G2 and CA1DG. Solid phase extraction was employed for the preconcentration of human plasma samples while urine samples were not pretreated. Validations were carried out in concentration ranges of 5 – 1000 nM (plasma CA1); 50 – 2000 nM (urine samples). The mean correlation coefficients were over 0.997. Mean recoveries were 101% (CA1 from plasma, 97% from urine), The measurements revealed the presence of two monoglucuronides and a diglucuronide.³

Optimization of the inclusion complex formation of the hydrophobic anticancer drug cifelin was studied in detail. It was established that the inclusion of the drug is stealth liposomes decreases toxicity and enhanced the circulation of the drug in the blood stream. The optimal composition of the liposome was found to be 165:8:1 w/w phosphatidylcholine:cholesterol. The composition of the liposomes was controlled by thin-layer chromatography (TLC) using butanol:glacial acetic acid:water (12:3:5, v/v) as mobile phase. The measurements indicated that the efficacy of inclusion complex formation was 98.3 %.⁴

Size exclusion chromatography (SEC) or dialysis were employed for the characterization of niosomal formulations of doxorubicin aimed to obtain a potential brain targeted delivery system. Formulations were functionalized with the glucose derivative N-palmitoylglucosamine (NPG). Various physicochemical methods such as light scattering, transmission electron microscopy, HPLC, thin layer evaporation, were employed for the study of the characteristics of the doxorubicin formulations. The concentration of drug was determined in blood and various organs. It was established that the new formulation may help the better understanding of the mechanism of drug transport of functionalized niosomes.⁵

The influence of sodium thiosulfate (STS) on the side effect of the anticancer drug cisplatin (CP) was investigated in detail. Measurements were carried out by SEC combined with inductively coupled plasma atomic emission spectrometer (ICP-AES). It was found that the addition of STS modified considerably the decomposition rate of CP decreasing the side effect of CP. It was further suggested that similar measurements may help the decrease of side-effects of Pt based anticancer drugs.⁶

The influence of anticancer drug treatment on the protein map of pancreatic cancer cells was determined. Protein composition was analysed by two-dimensional (2-D), and nano-high performance liquid chromatography electrospray ionization time of flight mass spectrometry/mass spectrometry. It was stated that the distribution and concentration of protein fractions can be used for the detection and identification of protein fractions.⁷

LC-MS-MS was employed for the elucidation of the structure of the main unknown oxygenated metabolites of the new anticancer drug EAPB0203. The structure of metabolites were compared with those of synthetic standards. One- and two-dimensional H-1 NMR spectroscopies has also been applied for the elucidation of the structure of the new anticancer agent and its main metabolites.⁸

The separation and quantitative determination of the anticancer drug CYC in rat plasma was achieved by employing LC-MS methodology. Analyte was extracted from plasma samples using liquid-liquid extraction (ethyl acetate:water). Chromatographic analysis was carried out on a C18 column (150 mm x 4.6. mm i.d., particle size, 5 μm). The isocratic flow rate was set to 0.8 mL min^{-1} . Mobile phase consisted of acetonitrile-water-formic acid (23.5:76.5:0.1 v/v). The calibration curve of the drug was linear in the concentration range of 5-2.500 ng mL^{-1} ($r = 0.9955$). The main recovery ranged from 90.0 % to 110 %. The intra- and interday precisions were lower than 11.8 and 6.6 %, respectively. The accuracy of the method was within ± 5.8 %. The investigations indicated that the method can be successfully applied for the study the pharmacokinetics of CYC-116 in rats after oral administration.⁹

A repeat dose study of the novel pro-apoptotic chemotherapeutic agent α -tocopheryloxyacetic acid (α -TEA) was assessed using male and female mice. It was established that α -TEA suppress tumor growth in various murine and human xenograft tumor models, including melanoma, breast, lung, prostate and ovarian cancers. Mice were treated with 100, 300, and 1500 mg $\text{kg}^{-1} \text{d}^{-1}$ α -TEA. The serum levels were determined by LC-MS. No mortality was found, and no clinical signs of toxicity. Histopathological evaluation revealed no significant lesions. The half-life of orally administered α -TEA was determined as 52 h. It was stated that the results may facilitate the design of clinical trials to evaluate the safety and antitumor efficacy of α -TEA in patients with cancer.¹⁰

Bioreducible and core-cross-linked hybrid micelles were prepared from trimethoxysilyl-ended poly(ϵ -caprolactone)-S-S-poly(ethylene oxide) block copolymers. The structure of the novel copolymers were determined by various physicochemical methods such as FTIR, ¹H NMR, gel permeation chromatography, differential scanning calorimetry, wide-range X-ray diffraction, dynamic light scattering (DLS), transmission electron microscopy. It was proposed that the copolymers can be applied for the fabrication of bioreducible and core-crosslinked hybrid micelles potential for anticancer drug delivery system.¹¹

The pharmacokinetics of 5-fluorouracil (5-FU) and cyclophosphamide (CP) in depression rats was investigated in detail. The effect of mood disorder on the drug metabolism process was assessed by the determination of the plasma drug concentration by HPLC for 5-FU and with

HPLC-MS/MS for CP. The results revealed significant differences between the pharmacokinetic parameters of 5-FU and CP between in depression model rats and control group ($p < 0.05$).¹²

A complex of cyclohexane-1,2-diaminoplatinum with an amphiphilic biodegradable polymer was prepared and applied as a drug carrier. The composition of the complex was analysed by HPLC combined with inductively coupled plasma mass spectrometry and X-ray photoelectron spectroscopy. It was stated that this novel complex may have a great potential application in clinical use.¹³

A new method was developed for the preparation of a drug loaded PLGA/PEVA composite (containing paclitaxel as model compound). It was established that the mixture of PLGA poly(lactide-co-glycolide) and PEVA (ethylene vinyl acetate) form an ideal carrier for paclitaxel (PTX). The morphology of the coating material was analysed by scanning electron microscopy, the release pattern of PTX was determined by HPLC.¹⁴

Fluorinated and pegylated polyaspartamide derivatives were prepared and employed to enhance the solubility and biological efficacy of flutamide. The characteristics of the novel copolymers based on polyaspartamide were investigated by size exclusion chromatography, light scattering analysis, and scanning electron microscopy.¹⁵

Star-block copolymers consisting of a hyperbranched polyethyleneimine, a poly(t -glutamic acid) inner shell and a polyethylene outer shell were synthesized and characterized by H-1 NMR, GPC and TEM. It was found that the complexes showed relatively high temporal stability at physiological pH and the release of the encapsulated compounds decreased at higher pH values.¹⁶

A novel type of folic-acid (FA) based copolymers were synthesized and their characteristics were investigated by using H-1 NMR, GPC, TEM, DLS and confocal laser scanning microscopy. It was established that FA conjugated micelles could be excellent nanocarrier to deliver anticancer drugs specially inside the cell via FA-receptor-mediated endocytosis.¹⁷

The influence of process parameters on the co-precipitation of PTX and poly(L-lactic acid) was investigated by supercritical antisolvent process (SAS). The particle samples were characterized by XRD, SEM, HPLC, laser diffraction particle size analyzer. The results indicated that the solvent and the solvent ratio exert a marked influence on the particle morphologies. The best operating conditions for the experimental system were as follows: DCM/EtOH 50/50, v/v; 35 $^{\circ}$; 10-12 MPa; PLLA, 5 g L^{-1} ; solution flow rate 0.5 mL min^{-1} .¹⁸

A novel series of molecularly imprinted polymers (MIPs) based on acrylonitrile:methacrylic acid (AN:MAA) was synthesized and their characteristics were investigated by various physicochemical methods such as elemental analysis (EA), attenuated total reflectance infrared spectroscopy (ATR FT-IR), RAMAN spectroscopy, SEC, thermogravimetric analysis (TGA), DSC, and batch rebinding tests. It was concluded from the measurements that -COOH functional groups play a considerable role in the imprinting process. The target molecule was diosgenin an important anticancer and antileukemia compound.¹⁹

Preparation and optimization of media employing Pluronic micelles to enhance the solubilization of the drug sirolimus an antiinflammatory/antiproliferative and immunosuppressive bioactive compound. The influence of the composition of the drug release medium was investigated in detail. The measurements indicated that the buffer composition (acetate or phosphate buffer) influenced considerably the behaviour of the drug sirolimus in aqueous environment. It was further found that the type and concentration of the micelles also influence the in-vitro release profile of sirolimus. It was further established that the critical micellization temperature (CMT), DLS, hydrodynamic size of micelles also influences the release profile of sirolimus.²⁰

The impact of polyamine depletion of the anticancer activity of a trinuclear Pt-compound was determined. The polyamine concentration in the samples was reduced by adding α -difluoromethylornithine (DFMO) or N-1,N-11-diethylnorspermine (DENSPM) to the samples. The anticancer activity of the drug was determined by HPLC analysis can increase the toxicity The results suggested that the combination of polyamine synthesis inhibitors with trinuclear Pt compound can enhance the antitumor activity of the trinuclear compound. It was assumed that the combination of polyamine synthesis inhibitors with trinuclear anticancer drug increases the toxicity of a trinuclear Pt compound.²¹

Liquid chromatography combined with tandem mass spectrometry was employed for the analysis of XMT-1001, a novel, polymeric topoisomerase I inhibitor. HPLC was applied for the determination of XMT-1001, conjugate release products, CPT-20-O-N-succinidimido-glycinate; CPT-SI and CPT-20-O-N-succinilamido glycinate. It was established that conjugated drug shows enhanced antitumor efficacy compared macromolecular camptothecin drug conjugate.²²

Novel amphiphilic, biodegradable, and biocompatible cross-linked copolymers were synthesised and the drug deliver capacity was assessed. Copolymers were prepared with 2-methylene-1,3-dioxypene (MDO), poly(ethylene glycol)methylether methacrylate (PEGMA) and 7-(2-metacryloyloethoxy)-4-methylcoumarin metacrylate (CMA). The copolymers were investigated by H-1-NMR, C13 NMR, GPC, DLS, and TEM. The hydrolytic degradation and enzymatic decomposition of the polymers were also determined. DOX was employed as target compound. The measurements indicated that these new copolymers can serve as promising nanocarriers for the delivery of anticancer drugs.²³

Another anticancer drug delivery system was developed applying lactosyl-norcantharidin-associated N-trimethyl-chitosan nanoparticles (Lac-NCTD). The concentration of the drug in the samples were determined by HPLC. It was concluded from the data that the concentration of the anticancer drug in the samples depended on the temperature, pH value of the environment and the composition of the anticancer drug delivery system. It was further found that the polymer can penetrate the plasma membrane of CaCo-2 cells.²⁴

The synthesis and biochemical characterization of a novel multifunctional biopolymer was reported. The drug delivery system contained the anticancer drugs daunorubicin and

methotrexate. GnRH-III decapeptide served as targeting moiety. Bioconjugates were prepared from amino acids: [(4)Lys]-GnRH-III (Glp-His-Trp-Lys-His-Asp-Trp-Lys-Pro-Gly-NH₂). The concentration of anticancer drugs in the samples were determined by LC-MS. It was established that the biological efficacy of the preparation containing two anticancer drugs was higher than those containing only one anticancer drug.²⁵

A novel drug delivery system was developed, characterized and its characteristics were investigated in detail. The novel amphiphilic graft polymer was prepared by using poly lactic acid and monomethyl polyethylene glycol. The characteristics of the novel copolymers were determined by 1-H NMR, FTIR, GPC, TEM, DLS, and CMCs The anticancer drug DOX was loaded into the micelles. The measurements suggested that the anticancer efficacy of the DOC loaded preparation was higher than those of free drug. It was further established that these micelles can be employed as promising potential carriers for delivering anticancer drugs.²⁶

Multiaarm poly(acrylic) star polymer was prepared and applied in sustained delivery of cisplatin and a nitrogen oxide prodrug. The product showed excellent water solubility and markedly low viscosity. The hydrophilic drug cisplatin and a hydrophobic nitric oxide was selected as model compounds. It was concluded from the results that the multiaarm poly(acrylic acid star) polymer is suitable for the sustained release of cisplatin and a nitrogen oxid product.²⁷

Micellar electrokinetic chromatography-laser-induced fluorescence method (MEKC-LIF) was employed for the analysis of DOX in biological samples. The migration buffer of the system consisted of 10 mM borate, 100 mM sodium dodecyl sulfate (SDS) (pH 9.3). Responses were linear in the range of 11.3-725 ng mL⁻¹; limit of quantitation (LOQ) was 43.1 ng mL⁻¹, limit of detection (LOD) was 6.36 ng mL⁻¹. It was stated that the MEKC-LIF method can be applied as a powerful diagnostic tool for monitoring the intracellular DOX distribution influencing cytotoxicity.²⁸

The correlation between the chromatographic behaviour and antitumor activity of curcuminoids was investigated by using high performance liquid chromatography-electrospray ionization tandem mass spectrometry (HPLC-ESI-MS/MS). The data were evaluated by the method of orthogonal partial least squares (OPLS) and by canonical correlation analysis (CCA). The method was proposed for the discovery of antitumor active constituents.²⁹

A validated HPLC method was developed for the determination of the encapsulation efficacy of curcumin in poly(lactic-co-glycolic acid) (PLGA) and poly(lactic-co-glycolic acid) - polyethylene glycol (PLGA-PEG) nanoparticles. HPLC analyses were carried out under reversed phase conditions using C18 column (250 mm x 4.6 mm, 5 μ m particle size). Isocratic mobile phase consisted of ethanol:water:acetonitrile (v/v/v) at the flow rate of 0.8 mL min⁻¹. The excitation and emission wavelengths were 365 and 512 nm, respectively. The selectivity, linearity, precision, accuracy, robustness, LOD and LOQ were determined. LOD and LOQ values were 9.65 and 50 ng mL⁻¹. The intra- and inter-assay coefficients of variation were less than 3.73 %. The maximum relative

standard deviation was 3.08 %. The data indicated that the method can be successfully applied for the determination of curcumin in PLGA and PLGA-PEG nanoparticles³⁰

The antitumor activity of free and nanosponge-encapsulated camptothecin was investigated using human prostate cancer cells as model compounds. The objectives of the measurements were the enhancement of the poor water solubility of the anticancer drug. It was found that the activity of β -cyclodextrin nanosponge encapsulated camptothecin showed higher anticancer activity. HPLC measurements indicated that the biological efficacy of the bioactive anticancer drug is higher in encapsulated form.³¹

Integrated rapid resolution LC-MS was employed for the screening and identification of the metabolites of the potential anticancer agent 3,6,7-trimethoxyphenanthroindolizidine (CAT) in rat urine. Analyses were performed by employing combination of multi-period product ion-scan (mpMS/MS) with high resolution characteristic extracted ion chromatograms. It was further found that the method allowed the separation and identification of 21 metabolites and the determination of the structure of 9 metabolites.³²

cDNA cloning, overexpression, purification and pharmacological evaluation for anticancer activity of ribosomal protein L23A gene (RPL23A) from giant panda (*Alluopoda melanoleuca*) was performed. The expression product was further purified by Ni chelating affinity chromatography.³³

Capillary electrophoresis technologies are frequently used in the analysis of various organic and inorganic components present in complicated accompanying matrices. The newest methods has been recently discussed including the separation and quantitative determination of a wide variety of analytes such as impurity profiling, quality control, quality control of pharmaceutical formulations, lipophilicity determination, interaction between metallodrugs and proteins or nucleotides, characterization and quantification of metabolites in biological matrices and real-world samples, etc.³⁴

The pharmacokinetic of the complex EAK-EPT was investigated in detail (EAK amino acid pairing peptide), (EPT anticancer agent). The measurements was carried out by HPLC, and indicated that EAK can serve as a suitable carrier to increase the bioavailability of EPT.³⁵

The differences between the physical properties of the inner and outer leaflet of membranes was elucidated by using a combined chromatography/cyclodextrin procedure suitable for the selective labelling of outer and inner leaflet. It was assumed that selective labelling influence the curvature of the membrane.³⁶

The synthesis of a new kind of amphiphilic, biodegradable, biocompatible, cross-linkable copolymers was reported and their application for drug delivery was elucidated. Copolymers were characterized by H-1 NMR, C-13 NMR, DLS, TEM and GPC. The capacity of the polymers to deliver the anticancer drug doxorubicin was also investigated. The measurements indicated that the composition of polymers exerts a marked influence on the drug release behaviour. It was assumed that these novel

copolymers can serve as promising nanocarriers for the delivery of anticancer drugs.³⁷

The antimicrobial activity of essential oils (EO) against *Streptococcus* mutant was investigated in detail. Twenty EO were included in the experiments. Active ingredients were achieved by hydrodistillation and chemical methods. The minimum inhibitory concentration (MIC) and bactericidal (MBC) were also determined. Chemical analyses were carried out by employing thin-layer chromatography and gas chromatography/mass spectrometry. The data indicated that some fractions of EO contained fractions with marked antiproliferative effect.³⁸

A novel class of anticancer prodrugs were prepared and experimentally applied. Styryl conjugated 2-nitrobenzyl derivatives were introduced as phototrigger to reduce the drug release. Chlorambucil was employed as model compound. The drug release was followed by measuring UV-vis absorption, FT-IR, and HPLC spectra. It was further established that the release of chlorambucil can be regulated by the modification of external light condition.³⁹

The chemopreventive activities of 3,6-dihydroxyflavone (3,6-DHF) against mammary carcinogenesis was studied in detail. The bioavailability of 3,6-DHF in rats was determined by HPLC. The results indicated that the oral administration of 3,6-DHF suppressed the breast carcinogenesis induced 1-methyl-1-nitrosourea (MNU). It was found that 3,6-DHF decreased the cancer incidence by 35.75 %. It was concluded from the results that 3,6-DHF is a potent natural chemopreventive agent influencing the anticancer mechanism of flavonoids.⁴⁰

The stability of 5-fluorouracil a chemotherapeutic agent was investigated under different conditions. HPLC and infrared spectroscopy were applied for the separation and quantitative determination of the analytes. HPLC measurements were carried out on a C18 column using 40 mM KH_2PO_4 mobile phase. The analytes were detected at 260 nm wavelength. The correlation coefficient was 0.9995. The R.S.D. values for intra-day and inter-day precisions were lower than 0.2 % and 1 %, respectively. It was established that the drug is not stable under alkaline conditions, but stable when exposed to UV irradiations.⁴¹

The analytical methods used for the determination of metallodrugs have been previously reviewed. The advantages and disadvantages of the various up-to date separation technologies have been enumerated and discussed in detail. The applicability of ICP-MS (inductively coupled plasma mass spectrometry) ICP-MS in the various field of the analysis of metallodrugs in biological samples.⁴²

The characterization of recombinant human IL-15 deamidation was followed by RP-HPLC/ESI-MS measurements. It was found that the deamidation rate depended considerably on the pH value of the mobile phase, on the temperature and composition of the solvent phase.⁴³

HPLC-UV method was employed for the study of the chemical composition of acetone extract of the lichens *Parmelia caperata*, *P. saxatilis* and *P. sulcata*. The antioxidant, antimicrobial and anticancer activities of the

main metabolites were also investigated. It was established that the main phenolic compounds in the extracts were protocetraric and usnic acid (*P. caperata*) and depsidone salazinic acid. Moreover, some samples contained atranorin and chloroatranorin. The investigations demonstrated the marked antioxidant, antimicrobial and anticancer activity of some extracts. The results indicated that these lichens can be applied as new sources of natural antimicrobial agents, antioxidants, and anticancer compounds.⁴⁴

The efficacy of various chromatographic technologies for the separation and quantitative determination of proteins was compared. It was found that SDS-PAGE is not suitable for this type of analysis. The results indicated that high performance size exclusion chromatography (HP-SEC), strong anion exchange (SAX), weak cation exchange (WCX) can be applied for the analysis of ovalbumin, myoglobin, and bovine serum albumin (BSA). The RSD values (peak areas day-to-day) were similar for each stationary phase: SEC<1.9 %; SAX>5 %; RP>2 %; WCX<3.5 %. The analysis of an IgG1 type antibody was also included in the experiments.⁴⁵

The presence of bioactive peptides in marine organism, the methods for their separation and purification using different chromatographic technologies have been previously discussed. Peptides with antimicrobial, antitumoral and antiviral activity were discovered and isolated. Various phyla such as *Porifera*, *Cnidaria*, *Nemertina*, *Crustacea*, *Mollusca*, *Echinodermata*, and *Cramata* were investigated for their biological activity.⁴⁶

HPLC combined with mass spectrometry was employed for the affinity screening of bioactive component from herb medicine. The bioactive compounds paclitaxel, resveratrol, ketoprofen and penicillin G were included in the investigation. It was established that the three-dimensional cell bioreactor coupled with HPLC/MS can be successfully applied for affinity screening and analysis of bioactive components interacting with cells.⁴⁷

HPLC-MS was employed for the separation and quantitative determination of the anticancer prodrug combretastatin A1 phosphate (OX4503, CAIP) active CA1, and its glucuronide metabolites in human urine and of CA1 in plasma. Solid phase extraction was applied for the preconcentration of CA1 from plasma, while urine samples were analysed without pretreatment. Assays were validated between 50-2000 nM (CAIP), 25-2000 nM (CAI), 50-40.000 nM CA1G1 and CA1G2, 25-4000 CAIDG. Main recoveries varied between 92 and 101 %.⁴⁸

The mass balance, excretion and metabolism of [C-14] ASA404 was investigated in cancer patients in a phase I trial. Measurements were carried out by HPLC. ASA404 was involved in the investigation because of its tumour vascular disrupting capacity. It was established that the method identified two novel metabolites not detected with other methods.⁴⁹

A specific and sensitive enzyme-linked immunosorbent assay (ELISA) was developed for the pharmacokinetic studies of vindesine (VDS). The results were compared with those measured by HPLC. It was found that the results obtained by ELISA and HPLC were commensurable. It was

further established that the method showed a very weak cross-reactivity with other vinca alkaloids such as vincristine (0.18 %) and vinblastine (0.11 %). The measurements proved that the sensitivity of ELISA method was 50-fold higher than the HPLC procedure. It was assumed that the ELISA procedure can be successfully used for the pharmacokinetic studies of VDS.⁵⁰

The efficacy of quercetin and liposomal quercetin was compared using PEGylated nanomaterials containing polyethyleneglycol-2000-distearoyl phosphatidylethanolamine. The data were evaluated by TEM and HPLC/UV spectroscopy. The investigations indicated that liposomal formulation of quercetin is more effective drug delivery vehicle in vivo as tumor-targeted drug carriers.⁵¹

It is well known that the low water solubility and bioavailability limits the application of curcumin in clinical practice. A new nanoparticle curcumin preparation was developed and its pharmacokinetics and safety was investigated employing various physicochemical and biophysical methods such as HPLC. It was further assumed that the novel preparation can improve the bioavailability of curcumin in human subjects.⁵²

The antitumor and angiostatic activity of frog skin excretions of *Phyllomedusa bicolor* (South American tree frog) was investigated. The crude skin exudate was further purified by SEC and HPLC. The measurements indicated that two peptides belonging to the dermaseptin family were responsive for the antitumor and angiostatic activity. It was stated that these compounds can be used for the development of novel class of anticancer drugs.⁵³

The anticancer and immunostimulator activity of the conjugate of paclitaxel and a non-toxic derivative of LPS was investigated by HPLC, NMR and IR. It was established that the stability of the preparation depended considerably on the pH and temperature. It was further found that the conjugate exhibited chemotherapeutic and immunotherapeutic activity in vitro. It was concluded from the results that this conjugate is a potential chemo-immunotherapeutic preparation showing high anticancer activity, and less toxicity and easy of delivery.⁵⁴

The influence of betulin enriched birch extracts on human carcinoma cells and ear inflammation was investigated in detail. A novel more effective extraction procedure was developed and applied for the analysis of the active components in the samples. The extracts were further investigated by HPLC-MS, Raman, SERS and C-13 NMR. The antiviral activity of the extracts were determined on skin epidermoid carcinoma, ovarian carcinoma, cervix adenocarcinoma, and breast adenocarcinoma. Each extract showed marked anticancer activity. The measurements further indicated that each extract contains considerable antiproliferative and anti-inflammatory activity too.⁵⁵

RP-HPLC method was developed for the analysis of camptothecin (CPT) incorporated into solid nanoparticles (SLN). The concentration of CPT in some rat organs (brain, heart, kidneys, liver, lung, spleen) was determined. The temperature of separation was 30 °C. Analytes were separated by gradient elution, mobile phase consisted of triethylamine buffer pH 5.5 and acetonitrile at a flow-rate

1.2 mL min⁻¹. Running time was 16 min. Analytes were detected by fluorometric method the excitation and emission wavelength being 360 and 440 nm. The calibration curves were linear in each case ($r > 0.9999$) between 1-200. It was stated that the new method is reliable, precise, accurate and suitable for the analysis of CPT in rat organ samples in physical mixture with SLN, and incorporated in SLN.⁵⁶

Because of their cancer preventive activity the lipophilic compounds of wheat bran were extensively investigated employing HPLC technologies. It was established that fractions containing unsaturated free fatty acid, phytosteroids, and alkylresorcinols showed high cytotoxic activity. The anticancer effect of the pure fractions was determined on human prostate adenocarcinoma (PC3) cells. It was further established that pure compounds 5-heptadecylresorcinol (IC₅₀=22.5 µg mL⁻¹); 5-(16-heneicosenyl)resorcinol (trans) (IC₅₀ = 13.7 µg mL⁻¹); 5-(14-nonadecenyl)resorcinol (trans) IC₅₀ = 42.2 µg mL⁻¹; 5-(2-oxotocosanyl)resorcinol (IC₅₀ = 10.9 µmol) showed marked anticancer activity. It was concluded from the results that alkylresorcinols are important in the cancer preventive activity of wheat bran. It was further concluded from the data that other components such as free fatty acids and phytosterols also influence the anticancer activity of wheat bran.⁵⁷

MEKC-LIF technique (micellar electrokinetic chromatography) combined with laser-induced fluorescence was employed for the investigation of the subcellular localization of DOX in biological samples. The migration buffer consisted of 10 mM borate, 100 mM SDS sodium dodecyl sulfate (SDS) (pH 9.3). The correlation between the chromatographic parameters and the concentration of the analyte in the mobile phase was linear between 11.3-725, the limit of quantitation (LOQ) was 43.1 mg mL⁻¹; the limit of detection (LOD) was 6.36 ng mL⁻¹. The measurements indicated that liposomal carriers enhance the efficiency of liposomal carrier in delivering DOX into the nucleus. It was established that subcellular fractionation followed by liquid-liquid extraction and MEKC-LIF. The method was proposed for the investigation of the intracellular distribution of DOX.⁵⁸

A GC/MS method was developed and successfully applied for the analysis of the components of *Flammulina velutipes* (FVS), a potential antitumor agent. The objectives of the investigation was the determination of the growth inhibition activity of FVS against certain human cancer cell lines (gastric SGC and colon LoVo) and the study of the pharmacokinetics of encapsulated FVS. The components separated and quantitatively determined were: ergosterol (54.8 %), and 22,23-dihydroergosterol (27.9 %). The measurements indicated that the preparation showed strong in vitro proliferative activity against SGC cells. It was concluded from the results that FVS can be a possible candidate for the development of an anticancer drug preparation. Using microemulsion formulation FVS can be applied for the development of bioavailable preparations.⁵⁹

Liquid chromatography/radiodetection/mass spectrometry was employed for the preclinical evaluation of the metabolism and disposition of RRx-001, a novel anticancer agent. Investigations revealed the presence of four main metabolites.⁶⁰

Supercritical carbon dioxide followed with LC was applied for the extraction of ar-turmerone (aromatic volatile turmeric oil from *Curcuma longa* Linn). It was established that aromatic turmerone showed marked anticancer activity with 50 % inhibitory concentrations of 64.8±7.1; 102.5±12.5 and 122.7.6 against HepG2, Huh-7 and Hep3B cells. The data suggested that ar-turmerone deserves further investigations as a natural anticancer and cancer-preventive agent.⁶¹

The metabolic profile of the anticancer drug panobinostat was determined by LC followed with radiometric detection and LC-tandem mass spectrometry. Radioactivity was recovered after 7 days (44-77% in feces and 29.51% in urine). The results indicated that panobinostat and its metabolites were excreted in similar amounts through the kidneys and liver with good dose of recovery.⁶²

The mutagenic and antimutagenic activity of the methanol leaf extract of *Myristica fragrans* was investigated by both in vivo and in vitro methods. Gas chromatography/mass spectrometry was employed for the separation and quantitative determination of phytochemicals. It was assumed that phytochemical compounds with antioxidant activity may be responsible for the biological activity.⁶³

The metabolism and accumulation of the lipophilic deoxynucleoside analogues cytarabine and gemcitabine was investigated by using TLC and HPLC. The results suggested that these compounds are suitable for novel clinical applications.⁶⁴

A new LC-MS/MS analytical method was developed and validated for the separation and quantitative determination of seven anticancer drugs (cyclophosphamide, ifosfamide, irinotecan, etoposide, gemcitabine, carboplatin and pemetrexed) in human plasma. Analytes were extracted with two different methods and separated on a C18 column (2.1 mm x 100 mm x 3 µm particle size) with gradient elution. Positive electrospray ionization was used as ionization source. The mobile phase consisted of acetonitrile-water (0.1% formic acid and 10 mM ammonium acetate). Flow rate was set to 0.2 mL min⁻¹. Linear correlation coefficients were >0.992 for each anticancer drug. The accuracy was ±10.5 %. The mean recovery ranged from 50.0 to 81.0 %. The method was successfully applied to clinical samples of cancer patients.⁶⁵

The application of GC with electron capture detection, GC-MS and HPLC for the analysis of clioquinol (5-chloro-7-iodo-8-quinolinol) has been previously discussed. The mechanism of action and the clinical uses in neurodegenerative disorders have also been reviewed.⁶⁶

The conjugation of anticancer drugs through endogenous monoclonal antibody cysteine residues has been discussed in detail. It was stated that the conjugates can be readily analyzed by HPLC methods.⁶⁷

The synthesis of podophyllotoxin, by an endophytic fungus *Fusarium solani* was previously reported and the its separation and quantitative determination by HPLC was achieved.⁶⁸

The anti-tumor activity of the methanolic extract of *Salvia mentifolia* was investigated. It was established that all the organs showed anti-tumor activity. HPLC measurements proved the presence of polyphenols. Rosmarinic acid, caffeic acid, luteolin-7-O-glucoside and quercitrin were present in each sample. The measurements indicated that genus *Salvia* is a natural source of anti-tumor agents, however, the amount of anticancer agents show considerable differences.⁶⁹

The influence of depression on the pharmacokinetic of 5-fluorouracil (5-FU) and cyclophosphamide (CP) was investigated using female Sprague-Dawley rats. The concentration of anticancer drugs were followed by HPLC-MS/MS. It was concluded from the measurements that depression mode disorder might alter drug metabolism process.⁷⁰

Abbreviations

AN	acrylonitrile
CCA	canonical correlation analysis
CMT	critical micellization temperature
CMCs	critical micelle concentration
CP	cisplatin
CPT	camptotecin
CP	cyclophosphamide
3,6-DHF	3,6-dihydroxyflavone
DLS	dynamic light scattering
DOX	doxorubicin
DOX ol	doxorubicinol
EA	elemental analysis
ATR FT-IR	attenuated total reflectance infrared spectroscopy
5-FU	5-fluorouracil
GPC	gel permeation chromatography
HP-SEC	high performance size exclusion chromatography
ICP-AES	inductively coupled plasma atomic emission spectrometer
LC/MS/MS	liquid chromatography tandem-mass spectrometry
LOD	limit of detection
LOQ	limit of quantitation
Maa	methacrylic acid
MNU	1-methyl-1-nitrosourea
NPG	N-palmitoylglucosamine
MEKC-LIF	micellar electrokinetic chromatography-laser-induced fluorescence
MBC	minimum bactericidal concentration
MIPs	molecularly imprinted polymers
OPLS	orthogonal partial least squares
PEVA	ethylene vinyl acetate
PLGA	poly(lactide-co-glycolide)
PTX	paclitaxel

RP-HPLC	reversed phase high performance liquid chromatography
SAX	strong anion exchange
SDS	sodium dodecyl sulfate
SEC	size exclusion chromatography
SLN	solid lipid nanoparticles
STS	sodium thiosulfate
AS	supercritical antisolvent process
TLC	thin layer chromatography
TEM	transmission electron microscopy
TGA	thermogravimetric analysis
WCX	weak cation exchange

References

- Xu, J. H., Liu, Y., Yu, Y., Ni, Q. J., Chen, Y., *Anal. Lett.*, **2012**, *45*, 1980-1994.
- Moore, R. G., Lange, T. S., Robinson, K., Kim, K. K., Uzun, A., Horan, T. C., Kavar, N., Yano, N., Chu, S. R., Mao, Q. F., Brard, L., DePaepe, M. M., Padbury, J. F., Arnold, L. A., Brodsky, A., Shen, T. L., Singh, R. K., *Plos One* **2012**, WOS:0003048005900032. E34443.
- Stratford, M. R. L., Folkes, L. K., *J. Chrom. B, Anal. Technol., Biomed. Life Sci.*, **2012**, *898*, 1-6.
- Kolova, E. A., Polozkova, A. P., Denisova, T. V., Krasnyuk, I. I., Oborotova, N. A., *Pharm. Chem. J.*, **2012**, *45*, 746-749.
- Bragagni, M., Mennini, N., Ghelardini, C., Mura, P., *J. Pharm. Pharm. Sci.*, **2012**, *15*, 184-196.
- Sooriyaachchi, M., Narendran, A., Gailer, J., *Metallomics*, **2012**, *4*, 960-967.
- Takata, T., Ishigaki, Y., Shimasaki, T., Tsuchida, H., Motoo, Y., Hayashi, A., Tomosugi, N., *Oncol. Rep.*, **2012**, *28*, 1968-1976.
- Lafaille, F., Banaigs, B., Inguibert, N., Enjambal, C., Doulain, P. E., Bonnet, P. A., Masquefa, C., Bressole, F. M. M., *Anal. Chem.*, **2012**, *84*, 9865-9872.
- Su, J., Chen, X. H., Li, Q., Yu, Z. G., Guan, X. D., Geng, L. L., Bi, K. S., *Chromatographia*, **2012**, *75*, 263-268.
- Hahn, T., Akporiaye, E. T., *Anti-Cancer Drugs*, **2012**, *23*, 455-464.
- Wang, Y. J., Dong, C. M., *J. Polym. Sci. Part A-Polym. Chem.*, **2012**, *50*, 1645-1656.
- Duan, J., Zhou, T., Chen, X., Wang, Y., Wen, Y. G., Xu, F., *Eur. Rev. Med. Pharmacol. Sci.*, **2012**, *16*, 427-436.
- Xiao, H. H., Zhou, D. F., Liu, S., Zheng, Y. H., Huang, Y. B., Jing, X. B., *Acta Biomater.*, **2012**, *8*, 1859-1868.
- Yuk, S. H., Oh, K. S., Park, J., Kim, S. J., Kim, J. H., Kwon, I. K., *Sci. Technol., Adv. Mater.*, **2012**, *13*, article number 025005.
- Piccioneo, A.P., Pitarresi, G., Pace, A., Triolo, D., Picone, P., Buscemi, S., Giammona, G., *J. Drug Targ.*, **2012**, *20*, 433-444.
- Huang, H. H., Li, J. Y., Liao, L. H., Li, J. H., Liao, L. H., Li, J. H., Wu, L. X., Dong, C. K., Lai, P.P., Liu, D. J., *Eur. Polym. J.*, **2012**, *48*, 696-704.
- Ma, G. L., Zhao, S. X., Jin, X., Chen, M. M., Zhang, Z. P., Song, C. X., *Chem. J. Chinese Univ.*, **2012**, *33*, 1854-1859 (English Abstract).

- ¹⁸Li, W. F., Liu, G., J., Li, L. X., Wu, J., Lu, Y. X., Jiang, Y. B. *Chinese J. Chem. Eng.*, **2012**, *20*, 803-813.
- ¹⁹Dima, S. O., Sarbu, A., Dobre, T., Purcar, V., Nicolae, C. A., *Mater. Plast.*, **2012**, *49*, 106-113.
- ²⁰Raval, A., Parmar, A., Raval, A., Bahadur, P., *Coll. Surf. B-Bioint.*, **2012**, *93*, 180-187.
- ²¹Kjellstrom, J., Oredsson, S., M., Wenneberg, J., *Cancer Cell Int.*, **2012**, *12*, 12-20.
- ²²Walsh, M. D. Hanna, S. K., Sen, J., Rawal, S., Cabral, C. B., Yurkovetskiy, A. V., Fram, R. J., Lowinger, T. B., Zambony, W. C., *Clin. Cancer Res.*, **2012**, *18*, 2591-2602.
- ²³Jin, Q., Maji, S., Agarwal, S., *Polym. Chem.*, **2012**, *3*, 2785-2793.
- ²⁴Guan, M., Zhu, Q. L., Liu, Y., Bei, Y., Y., Gu, Z. L., Zhang, X., N., Zhang, Q., *Int. J. Nanomed.*, **2012**, *7*, 1921-1930.
- ²⁵Leurs., Lajko, E., Mezo, G., Orban, E., Ohlsclager, P., Marquardt, Kohidai, L., Manea, M., *Eur. J. Med. Chem.*, **2012**, *52*, 173-183.
- ²⁶Yu, Z. X., He, B., Long, C. Y., Liu, R., Sheng, M. M., Wang, G. G. Tang, J. Z., Gu, Z. W., *Macromol. Res.*, **2012**, *20*, 250-258.
- ²⁷Duan, S., F., C ai, S., Xie, Y., M., Bagby, T., Ren, S. Q., Forrest, M. L., *J. Polym. Sci. Part A-Polym. Chem.*, **2012**, 2715-2724.
- ²⁸Ho, J. A. A., Fan, N. C., Jou, A. F. J. Wu, L. C. Sun, T. P., *Talanta*, **2012**, *99*, 683-688.
- ²⁹Jiang, J. L., Jin, X. L., Zhang, H., Su, X., Qiao, B., Yuan, Y. J., *J. Pharm. Biomed. Anal.*, **2012**, *70*, 664-670.
- ³⁰do Nascimento, T. C. F., Casa, D. M., Dalmolin, L. F., de Mattos, A. C., Khalil, N. M., Mainardes, R. M., *Curr. Pharm. Anal.*, **2012**, *8*, 324-333.
- ³¹Minelli, R., Cavalli, R., Ellis, L., Pettazoni, P., Trotta, F., Ciamporcerio, E., Barrera, G., Fantozzi, R., Dianzani, Pili, R. *Eur. J. Pharm. Sci.*, **2012**, *47*, 686-694.
- ³²Tian, Y. P., He, J. M., Zhang, R. P., Lv, H. N., Ma, S. G., Chen, Y. H., Yu, S. S., Chen, Y. G., Wu, Y., He, W. Y., Abliz, Z., *Anal. Chim. Acta*, **2012**, *731*, 60-67.
- ³³Sun, B., Hou, Y. L., Hou, W. R., Zhang, S. N., Ding, X., Su, X. L. *Int. J. Mol. Sci.*, **2012**, *13*, 2133-2147.
- ³⁴Bytzek, A., K., Hartinger, C. G., *Electrophoresis*, **2012**, *33*, 622-634.
- ³⁵Ma, W. N., Lu, S., Pan, P., Sadatmousavi, P., *Plos One*, **2012**, *7*, e-43684.
- ³⁶Chintia, S., Kymchenko, A. S. London, E., *Biochim. Biophys. Acta-Biomembr.*, **2012**, *1818*, 1284-1290.
- ³⁷Jin, Q., Maji, S., Agarwal, S., *Polym. Chem.*, **2012**, *3*, 2785-2793.
- ³⁸Garvao, L. C. D., Furletti, F. F., Bersan, S. M. F., da Cunha, M. G., Ruiz, A. L. T. G., de Carvalho, J. E., Sartoratto, A., Rehder, V. L. G., Figueira, G. M., Duarte, M. C. T., Ikegaki, M., de Alencar, S. M., Rosalen, P. L., *Evidence-based Compl. Altern. Med.*, **2012**, Article number: 751435.
- ³⁹Bao, C. Y., Jin, M., Li, B., Xu, Y. D., Jin, J. Y., Zhu, L., Y., *Org. Bioorg. Chem.*, **2012**, *10*, 5238-5244.
- ⁴⁰Chang, H., Fu, Y. J., Juan, L. J., Yi, L., Xu, H. X., Zhou, Y., Zhu, J. D., Zhang, Q., Y., Mi, M. T., *Breast. Cancer Res.*, **2012**, *14*, R80.
- ⁴¹Yadav, N., Singh, P., Mehrotra, R., *Curr. Pharm. Anal.*, **2012**, *8*, 49-55.
- ⁴²Timerbaev, A., Sturup, S., *Curr. Drug Metabol.*, **2012**, *13*, 272-283.
- ⁴³Nellis, D. F., Michiel, D. F., Jiang, M. S., Esposito, D., Davis, R., Jiang, H. G., Korrell, A., Knapp, G. C., Lucernoni, L., E., Nelson, R. L., Pritt, E. M., Procter, L. V., Rogers, M., Sumpter, T. L., Vyas, V. V., Waybright, T. J., Yang, X. Y., Zheng, A. M., Yovandovich, J. L., Gilly, A., Mitra, G., Zhu, J. W., *Pharm. Res.*, **2012**, *29*, 722-738.
- ⁴⁴Manojlovic, N., Rankovic, B., Kosanic, M., Vasiljevic, P., Stanojkovic, T., *Phytomedicine*, **2012**, *19*, 1166-1172.
- ⁴⁵Grotefend, S., Kaminski, L., Wroblewitz, S., El Deeb, S., Kuhn, N., Reichl, S., Limberger, M., Watt, S., Watzig, H., *J. Pharm. Biomed. Anal.*, **2012**, *71*, 127-138.
- ⁴⁶Lazcano-Perez, F., Roman-Gonzalez, S. A., Sanchez-Puig, N., Arreguin-Espinosa, R., *Protein. Peptide Lett.*, **2012**, *19*, 700-707.
- ⁴⁷Mou, Z. L., Qi, X. N., Liu, R. L., Zhang, J., Zhang, Z. Q., *J. Chrom. A*, **2012**, *1243*, 33-38.
- ⁴⁸Stratford, M. R. L., Folkes, L. K., *J. Chrom. B, Anal. Techn. Biomed. Life Sci.*, **2012**, *898*, 1-6.
- ⁴⁹McKeage, M. J., Fong, P. C., Hong, X., Flarakos, J., Mangold, J., Du, Y., Tanaka, C., Schran, H., *Cancer Chemother. Pharm.*, **2012**, *69*, 1145-1154.
- ⁵⁰Nakano, Y., Saita, T., Fujito, H. *Yakugaku Zasshi*, **2012**, *132*, 727-732.
- ⁵¹Gang, W., Jie, W., J., Ping, Z. L., Ming, D. S. Ying, L. Y., Lei, W., Fang, Y., *Expert Opin. Drug Deliv.*, **2012**, *9*, 599-613.
- ⁵²Kanai, M., Imaizumi, A., Otsuka, Y., Sasaki, H., Hashiguchi, M., Tsujiko, K., Matsumoto, S., Ishiguro, H., Chiba, T., *Cancer Chemother. Pharm.*, **2012**, *69*, 65-70.
- ⁵³van Zoggel, H., Hamma-Kourbali, Y., Galanth, C., Ladram, A., Nicolas, P., Courty, J., Amiche, M., Delbe, J., *Amino Acids* **2012**, *42*, 385-395.
- ⁵⁴Roy, A., Chandra, S., Mamilapally, S., Upadhyay, P., Bhaskar, S., *Pharm. Res.*, **2012**, *29*, 2294-2309.
- ⁵⁵Dehelean, C. E., Soica, C., Ledeti, I., Aluas, M., Zupko, I., Galuscan, A., Cinta-Pinzaru, S., Munteanu, M., *Chem. Centr. J.*, **2012**, *6*, 157.
- ⁵⁶Martins, S. M., Wendling, T., Goncalves, V., M., F., Sarmiento, B., Ferreira, D. C., *J. Chrom. B-Anal. Technol. Biomed. Life Sci.*, **2012**, *880*, 100-107.
- ⁵⁷Liu, L., Winter, K. M., Stevenson, L., Morris, C., Leach, D. N. D. N., *Food Chem.*, **2012**, *130*, 156-164.
- ⁵⁸Ho, J. A. A., Fan, N. C., Jou, A. F. J., Wu, L. C., *Talanta*, **2012**, *99*, 683-688.
- ⁵⁹Yi, C. X., Zhong, H., Tong, S. S., Cao, X., Firempong, C. K., Liu, H. F., Fu, M., Yang, Y., Feng, Y. S., Zhang, H. Y., Xu, X. M., Yu, J. N., *Int. J. Nanomed.*, **2012**, *7*, 5067-5078.
- ⁶⁰Scicinski, J., Oronsky, B., Taylor, M., Luo, G., Musick, T., Marini, J., Adams, C. M., Fitch, W. L., *Drug. Metab. Disp.*, **2012**, *40*, 1810-1816.
- ⁶¹Cheng, S. B., Wu, L. C., Hsieh, Y. C., Wu, C. H., Chan, Y. J., Chang, L. H., Chang, C. M. J., Hsu, S. L., Teng, C. L., Wu, C. C., *J. Agric. Food Chem.*, **2012**, *60*, 9620-9630.
- ⁶²Clive, S., Woo, M. M., Nydam, T., Kelly, L., Sqier, M., Kagan, M., *Cancer Chemother. Pharm.*, **2012**, *70*, 513-522.
- ⁶³Akinboro, A., Bin Mohamed, K., Asmawi, M. Z., Othman, A. S., Ying, T.H., *Drug. Chem. Toxic.*, **2012**, *35*, 412-422.
- ⁶⁵Zhou, J. Y., Gao, S. H., Zhang, F., Jiang, B., Zhan, Q., Cai, F., Li, J. X., Chen, W. S., *J. Chrom. B-Anal. Technol. Biomed. Life Sci.*, **2012**, *906*, 1-8.
- ⁶⁶Bareggi, S. R., Cornelli, U., *CNS Neurosci. Ther.*, **2012**, *18*, 41-46.
- ⁶⁷Lyon, R. P., Meyer, D. L., Setter, J. R., Senterm P. D., *Methods Enzymol.*, **2012**, *502*, 123-138.

- ⁶⁸Nadeem, M., Ram, M., Alam, P., Ahmad, M. M., Mohammad, A., Al-Quarainy, F., Khan, S., Abdin, M. Z., *African J. Microbiol. Res.*, **2012**, 6, 2493-2499.
- ⁷⁰Duan, J. J., Zhou, T., Chen, X., Wang, Y., Wen, Y. G., Xu, F., *Eur. Rev. Med. Pharm. Sci.*, **2012**, 16, 427-436
- ⁶⁹Fiore, G., Massarelli, P., Sajeve, M., Franchi, G. G., *Rev. Bras. Farm.*, **2012**, 22, 381-388.

Received: 07.05.2014.
Accepted: 12.05.2014.



A COMPARATIVE STUDY FOR CHELATION OF IRON(II) AND IRON(III) WITH LEVODOPA - AN ANTIPARKINSONIAN DRUG MOLECULE

Syed Zafar Abbas Zaidi^[a] and Nasreen Fatima^[a]

Keywords: Levodopa; iron(II) and iron(III) chelate; UV-VIS study

In the present study interaction of Fe(II) and Fe(III) with antiparkinsonian drug molecule, Levodopa (LD), is investigated using potentiometry and spectrophotometry. Identical spectra of both of Fe(II) and Fe(III) complexes of the drug provide an evidence that similar stoichiometry was followed. Molar absorptivities of the complexes, found to be more than $100 \text{ M}^{-1} \text{ cm}^{-1}$, showed charge transfer spectra. Addition of an antioxidant decolorized the initial intensive color of the Fe(III) complex, which was evidence of high oxidation state of iron. Catecholic ligands, being strong reductants, chelate a metal ion in high oxidation state and show LMCT bands. These observations lead to conclude that iron has high oxidation state, regardless of initial source of metal.

*Corresponding Authors

Tel: 03153237699 and 03002659510

E-Mail: mehar_zafar@yahoo.com

[a] Department of Chemistry, University of Karachi, B-12 Eastern square, Federal – B area, block-1, Karachi, Pakistan

INTRODUCTION

Dopamine analogs and iron have an unquestionable and significant role in brain function.¹⁻⁵ Iron storing protein, ferritin⁶⁻⁷ is known to be present in axons of neuronal cells. Dopamine is an important neurotransmitter and its deficiency is considered to be the basic factor responsible for behavioral changes in neuro-disorders like Parkinson's disease. On the other hand iron is also considered to be one of the symptom of Parkinson disease as its accumulation is observed in Parkinsonian brain.⁸ However, it has been reported that iron chelators have an ability to reduce the symptoms of Parkinson.¹⁻²

Levodopa (-)-3-(3,4-dihydroxyphenyl)alanine³⁻⁵ is a precursor of dopamine and norepinephrine⁹ in the biosynthetic pathways for these neurotransmitters and these derivatives regulate a variety of physiological functions in the human body.¹⁰ It may act as chelator for iron and is present in the different medications used for the Parkinson's disease. It has two binding sites, a catecholic and an alanine site (Fig.1). In the present study chelation ability of Levodopa towards iron has been explored.

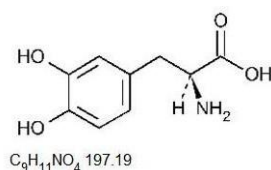


Figure 1. Structure of (-)-3-(3,4-dihydroxyphenyl)alanine (Levodopa)

The most important factor of the bioavailability of iron depends upon food sources that may restrain its absorption in the human body.¹¹⁻¹³ Iron exists in two forms in a living system. These are its reduced form Fe(II) and the oxidized one Fe(III). Fe(II) is the bioessential oxidation state of this metal.

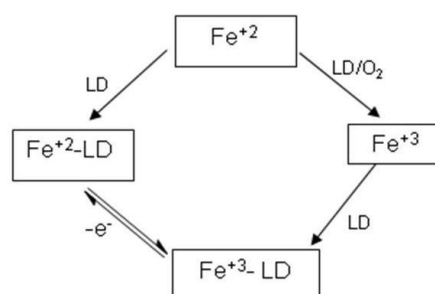


Figure 2. Possible redox reactions in the Fe-Levodopa system

The present literature lacks in the studies related to the interaction of iron and dopamine or its analogues. Therefore we selected to investigate the chelation capabilities of different oxidation states of iron with Levodopa. Spectral characteristics of some similar complexes and their stoichiometry have already been reported.¹⁴⁻¹⁵ Using these data the kinetic aspects of these complexes have also been looked into.

EXPERIMENTAL

Reagents of analytical grade were used for all the reactions. Iron salts ($\text{FeCl}_3 \cdot 6\text{H}_2\text{O}$ and $\text{Fe}(\text{NH}_4)_2(\text{SO}_4)_2 \cdot 6\text{H}_2\text{O}$) were of Merck and Levodopa was obtained from Wild Wind. For the preparation of the stock and sample solutions, CO_2 free distilled deionised water was used.

Potentiometric titrations

Experiment, for both cases, was performed in triplicate, having the constant ligand/metal mole ratio, i.e. 5:1, at 25 ± 1 °C. 0.05 mmol metal solution was mixed with 0.25 mmol of LD solution. The volume of reaction mixture was made up to 50.0 ml with deionised distilled water, taken in a double walled titration cell kept on a magnetic stirrer. The rubber stopper on the cell had holes for the addition of standard base, thermometer and for a glass electrode. Aliquots of standard NaOH (0.1 M) were added with the help of a micropipette.

The pH changes, recorded on a JENWAY 370, were then plotted against added volume of standard NaOH solution. The equilibrium constants for each specie (ML_1 , ML_2 and ML_3), were calculated by circle fitting method. Furthermore, the pK values were calculated through the pH titration curves. The pK_1 , pK_2 and pK_3 were also calculated by using the graphical method (Table 1) to correlate with the reported Levodopa ((-)-3-(3,4-dihydroxyphenyl)-L-alanine) pK values.¹⁷

Table 1. pK values evaluated by potentiometric titration method.

Complex	pK_1	pK_2	pK_3
Fe(II)-LD	Unidentified	7.21	9.94
Fe(III)-LD	6.42	6.60	13.81

Unidentified = the case in which humps are so close that it cannot be distinguish

Absorbance maxima

Absorbance maxima of the complex, was explored by mixing 0.005 mmol of the salt solution, with enough excess of levodopa solution. It was prepared in deionized distilled water. Following that the solution was subjected to scanning in UV-visible region on GENESYS 6 (Thermo Electron Corporation) and that λ_{max} were established to be as 430 and 730 nm, for both cases i.e. Fe(II) and Fe(III) complexes. The metal and ligand solutions have no absorbance at these wavelengths. All further work was carried out on both λ_{max} .¹⁴⁻¹⁵

Molar extinction coefficients (Serial Dilution)

Solutions of different dilutions were prepared in the de-ionized distilled water. Absorbance was recorded for all diluted solutions at selected wavelengths i.e. 430 and 730 nm. Plot of absorbance for different dilutions against metal concentration, provided the slope for determining molar extinction coefficient.

Mole ratio

Accurate amounts of the metal salts, Fe(III) and Fe(II) and the ligand were taken to prepare respective solutions in deionized distilled water. Different aliquots of ligand solution were added in 0.005 mmol metal solution and volume was kept constant for all. The absorbance was recorded at 730 nm, while temperature was maintained at 25 ± 1 °C.¹⁵

Slope ratio

For this method the working solution was such that the sequence of the complex solution was split in two halves. In one half volume of 5×10^{-4} M Fe(II) was kept constant, while varying the volume of 5×10^{-3} M Levodopa, and in the other half of the samples sequence, LD was kept constant, with variable concentration of metal. The complex samples were scanned at the respective λ_{max} and the recorded absorbance was plotted versus concentration of varying specie. Similar process was followed for Fe(III) and slope of each straight line was evaluated. The ratio of the slopes helped to establish the stoichiometry of the respective complexes.

Job's plot

The solutions were prepared by mixing metal and ligand solution by continuous increase of one ingredient with the similar decrease of second ingredient. Absorbance of all samples was recorded at the λ_{max} and by plotting graph between metal composition and respective absorbances, stoichiometry was determined.

Kinetics

For the determination of rate of reaction, different concentrations of Fe(II) and Fe(III) complex solutions were observed at different time intervals. Kinetics of Fe(III)-LD complex was followed on RX20000 Rapid kinetics accessories Stop flow apparatus of Applied Photo Physics. k_{obs} was then evaluated from the slope of plot drawn between $\ln|A_t - A_\infty|$ and time.

RESULTS AND DISCUSSION

Potentiometric titrations

Potentiometric curve of Levodopa is shown in Figure 3. The plot of pH change on addition of standard NaOH to Fe(II) complex solution shows two prominent curves near pH 4.5 and 7.5. Depression in titration curve of the complex as compared to the ligand was very prominent, which confirmed the complex formation (Fig.4). These results substantiate the varying stoichiometry with the change of pH. Against that for the case of Fe(III), depression and twists in titration curves were found at pH 3, 4 and 11 (Fig.5).

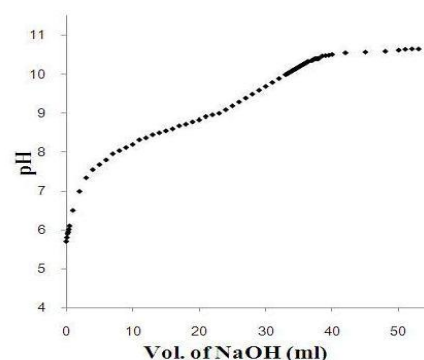


Figure 3. Potentiometric titration plot of Levodopa with NaOH

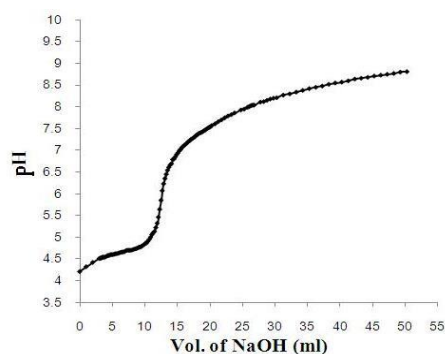


Figure 4. Potentiometric titration plot of Fe(II)-Levodopa with NaOH

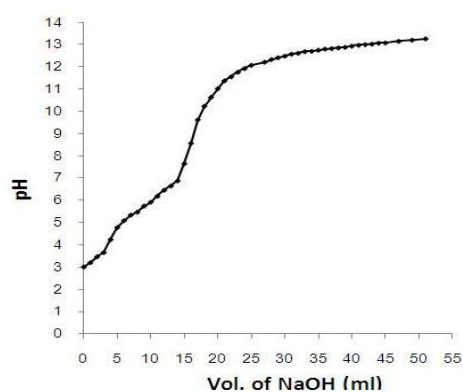


Figure 5. Potentiometric titration plot of Fe(II)-Levodopa with NaOH

Absorbance maxima

U.V. visible spectroscopy was used to investigate the spectral characteristics, complexation of Fe(II) and Fe(III) with Levodopa. For this purpose iron complexes of LD in the volumetric ratio of 1:5 were scanned spectrophotometrically in the range of 300 to 800 nm.

A green colored complex of Fe(II) and levodopa was formed at 25±1 °C within 3 to 4 minutes with continuous increase of absorbance while in the case of Fe(III) the color appears abruptly within seconds and fades sharply. Absorbances were recorded at both the selected wavelengths. Observed spectras revealed that Fe(II) and Fe(III) complexes of LD show an absorbance maxima in the visible region (Fig.6).

In order to confirm the hypothesis that green colored complex with Levodopa is formed in +3 oxidation state of iron, complex of Fe(II)-LD was treated with a reducing agent (ascorbic acid). This resulted into immediate color loss, indicating that Fe(II) was first converted to Fe(III) by the aerial oxidation and that Levodopa worked as catalyst for this reaction. Distinct peaks of Fe(II) and Fe(III) complexes of LD were observed at 430 and 730 nm.

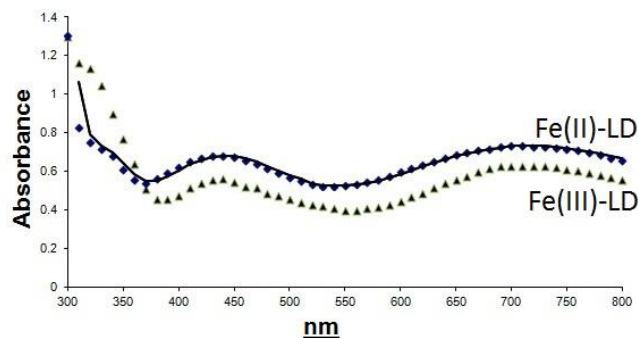


Figure 6. UV-VIS spectra of Fe(II)-LD and Fe(III)-LD complexes

Molar extinction coefficients (serial dilution)

Molar absorptivity of Fe(II)-LD complex was investigated using serial dilution method (Table 2). Absorption maxima in a non buffered aqueous medium were identified to be at 430 nm and 730 nm. At 430 nm molar absorptivity was found to be 237.03 M⁻¹ cm⁻¹. The trend line at 730 nm is comparatively higher than that of 430 nm and provides a molar absorptivity of about 302.6 M⁻¹ cm⁻¹ (Fig.7).

Table 2. Molar extinction coefficients by serial dilution method.

Complex	Wavelength (nm)	ϵ (M ⁻¹ cm ⁻¹)
Fe(II)-LD	430 nm	237
Fe(II)-LD	730 nm	302.6

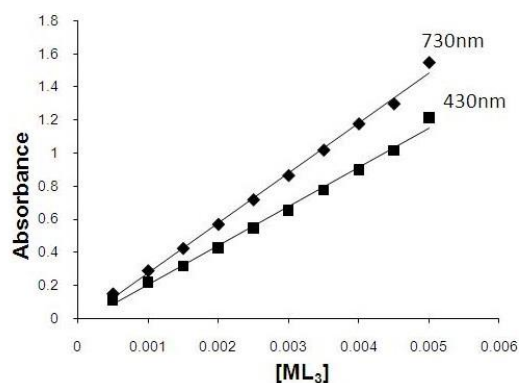


Figure 7. Molar absorptivity by serial dilution method in non-buffered medium; [Fe(II)-LD₃]=5.0×10⁻⁴ M, =25±1 °C; λ_{max} =430 and 730 nm.

Mole ratio

The plots of absorbances against the mole ratio of Fe(II) and Fe(III) complex with LD guide us to suggest a mole ratio of 1:3 for Fe(II)-LD as well as for the complex of Fe(III)-LD (Fig.8-10). The complexation of Fe(III) with Levodopa is faster than that of Fe(II) complexation. The study was therefore verified through a stop flow apparatus and the same mole ratio was found. Molar absorptivity (Table 3) and formation constant (Table 5) were also evaluated by mole ratio method.

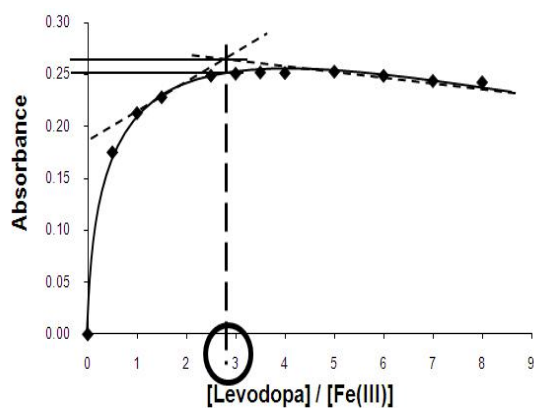


Figure 8. Stoichiometry by mole ratio method of Fe(III)-LD in non-buffered medium; $[Fe(III)]=5.0 \times 10^{-4}$ M; $T=25 \pm 1$ °C; $\lambda_{max}=430$ nm

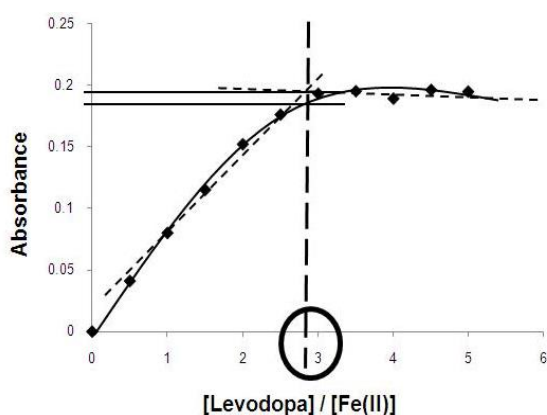


Figure 9. Stoichiometry by mole ratio method of Fe(II)-LD in non-buffered medium; $[Fe(II)]=5.0 \times 10^{-4}$ M; $T=25 \pm 1$ °C; $\lambda_{max}=430$ nm

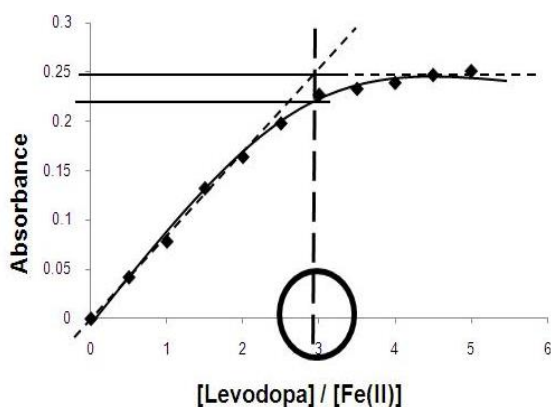


Figure 10. Stoichiometry by mole ratio method of Fe(II)-LD in non-buffered medium; $[Fe(II)]=5.0 \times 10^{-4}$ M; $T=25 \pm 1$ °C; $\lambda_{max}=730$ nm

Table 3. Molar extinction coefficients by mole ratio method.

Complex	Wavelength	ϵ ($M^{-1} cm^{-1}$)
Fe(III)-LD	730 nm	788
Fe(II)-LD	430 nm	380
Fe(II)-LD	730 nm	498

Slope ratio

The stoichiometric results from slope ratio method were found 1:3 (Table 4), in good agreement with mole ratio method (Fig.11-12).

Table 4. Stoichiometry by slope ratio method of Fe(III)-LD and Fe(II)-LD in non-buffered medium.

Metal Complex	Wavelength (nm)	Stoichiometry from slope ratio (L/M)
Fe(III)-LD	730	3.1
Fe(II)-LD	730	2.9

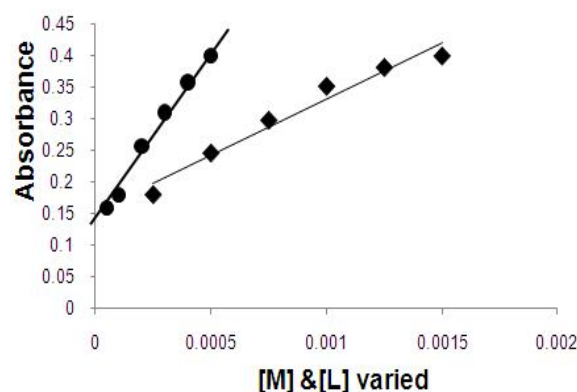


Figure 11. Plots of slope ratio method of Fe(III)-LD, in non-buffered medium; Absorbance vs. concentration of variable reagent, $T=25 \pm 1$ °C; $\lambda_{max}=730$ nm; Variable: ◆ [LD]; ● [Fe(III)]

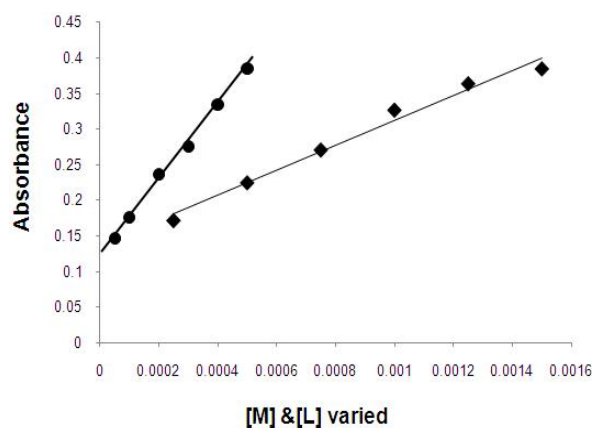


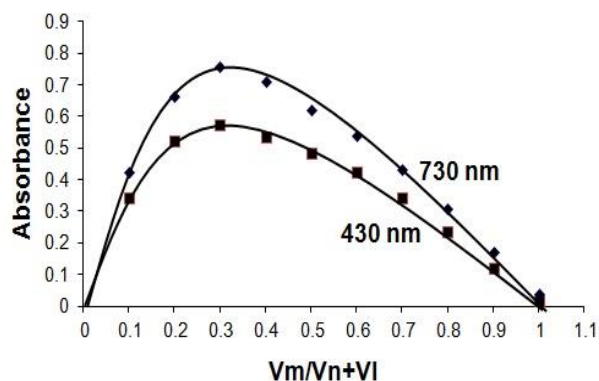
Figure 12. Plots of slope ratio method of Fe(II)-LD, in non-buffered medium; Absorbance vs. concentration of variable reagent, $T=25 \pm 1$ °C; $\lambda_{max}=730$ nm; Variable: ◆ [LD]; ● [Fe(II)]

Job's plot

Job's plot method also verified the stoichiometry ratio i.e. 1:3 in both the cases of Fe(II) and Fe(III) complexation with Levodopa (Fig.13). Overall formation constant of Fe(II)-LD at 430 and 730 nm were also evaluated (Table 5).

Table 5. Overall Formation constants by mole ratio and Job's plot method.

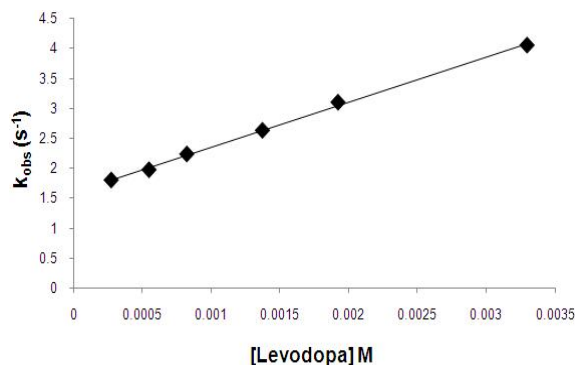
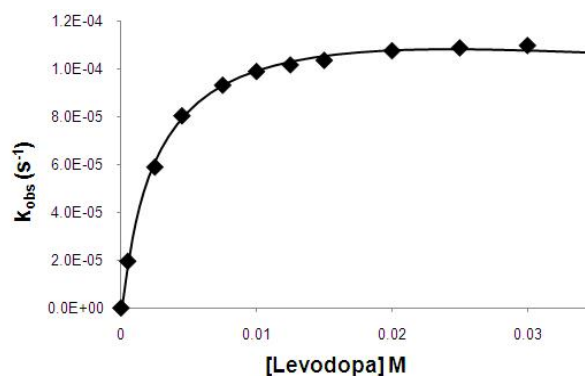
Metal complex	Wavelength (nm)	log K_f values	
		mole ratio	Job's method
Fe(III)-LD	730 nm	9.75	-----
Fe(II)-LD	430 nm	11.95	9.61
Fe(II)-LD	730 nm	11.45	10.31

**Figure 13.** Stoichiometry by Job's method of Fe(II)-LD, in non-buffered medium; [Fe(II)]= 5.0×10^{-4} M; $T=25 \pm 1$ °C; $\lambda_{\max}=430$ and 730 nm

The observations obtained by all of the three methods given above were consistent and suggested 1:3 stoichiometry for the complexes of Fe(II) and Fe(III) with Levodopa.

Kinetics

In the kinetic study, rate constant values were plotted against concentration of Levodopa. A direct relationship was found in the case of Fe(III)-LD complex, and that k_{obs} increases with the rise in the ligand concentration (Fig.14). Similar trend was observed in case of Fe(II)-LD complex at lower concentrations of the ligand. However at higher concentration the k_{obs} of complex become independent of ligand concentration (Fig.15). This demonstrates that Fe(II)-LD Kinetics goes through two pathways and it follows two step mechanism i.e. A ligand dependent along with a ligand independent pathway (Fig.2).

**Figure 14.** Graph of observed rate constant dependence of Fe(III)-LD complex in non-buffered medium; [Fe(III)]= 5.0×10^{-4} M; $T=25 \pm 1$ °C; $\lambda_{\max}=730$ nm**Figure 15.** Graph of observed rate constant dependence of Fe(II)-LD complex in non-buffered medium; [Fe(III)]= 5.0×10^{-4} M; $T=25 \pm 1$ °C; $\lambda_{\max}=730$ nm

CONCLUSION

Interaction of antiparkinsonian generic drug i.e. Levodopa, has been studied with +2 and +3 oxidation states of iron. Spectral analysis revealed that both the states of iron, form green color complex with Levodopa with the same spectral characteristics, whilst rate of reaction for the formation of Fe(III)-LD is higher as compared to Fe(II)-LD complex. Green colored complex with Levodopa is formed by +3 state of iron. This observation is substantiated by treating green complex solution with a reducing agent such as ascorbic acid, which resulted in disappearance of color.

LMCT bands were observed and molar absorptivities of the complexes were evaluated, which is comparatively high at 730 nm than 430 nm. pK were evaluated for Fe(II) and Fe(III) complex with LD by Potentiometric plots. At selected λ_{\max} , different methods explored ML_3 complex formation. Calculated log K_f showed comparative results of Fe(II)-LD complex.

Kinetic results for the complex formation tendencies of the two systems (Fig.13-14) revealed that formation of Fe(III)-LD complex is a fast single phase reaction while Fe(II)-LD complexation is relatively slow and two phase reaction. Observation leads us to conclude that Fe(II) is immediately converted to Fe^{+3} in the presence of Levodopa and it is +3 state of iron which is complexing with Levodopa. Figure 2 displays the suggested mechanism for this complex formation.

Variation in pH is instrumental in bringing such changes which influence the functioning of human body and its various organs. Hence kinetic behaviour of iron in its two oxidation states towards its complex formation with Levodopa may be controlled by the pH of the system. Therefore further study in this direction is desirable.

ACKNOWLEDGEMENT

The authors indebted to Dean Faculty of Science, University of Karachi, for their financial support. We are also very grateful to Prof. Dr. Iftikhar Imam Naqvi on his proficient guidance.

REFERENCES

- ¹Ben, S. B., Kahana, N., Kampel, V., Warshawsky, A., Youdim, M. B. H., *Neuropharmacol.*, **2004**, *46*, 254–263.
- ²Kaur, D., Yantiri, F., Rajagopalan, S., Kumar, J., Mo, J. Q., *Neuron*, **2003**, *37*, 899–909.
- ³Barron, A. B., Maleszka, R., Vander, Meer, R. K., Robinson, G. E., *Proc. Natl. Acad. Sci. USA.*, **2007**, *104*(5), 1703-7.
- ⁴Vanden H. D. M. A., Pasterkamp R. J., *Progr. Neurobiol.*, **2008**, *85*, 75-79.
- ⁵Arias-Carrión, O., Pöppel, E., *Acta Neurobiol Exp.*, **2007**, *67*(4), 481-488.
- ⁶Reaney, S. H., Smith, D. R., *Toxicol. Appl. Pharmacol.*, **2005**, *205*, 271–281.
- ⁷Recalcati, S., Invernizzi, P., Arosio, P., Cairo, G., *J. Autoimmun.*, **2008**, *30*(1-2), 84-9.
- ⁸Ross, B.M., Moszcynska, A., Ehrlich, J., Kish, S., *J. Neuroscience*, **1998**, *83*, 791-798.
- ⁹Blaschko, H., *J. Physiol. (London)*, **1939**, *96*, 50.
- ¹⁰Rodriguez, M. C., Obeso, J. A., Olanow, C. W., *Ann Neurol.*, **1998**, *44*(3), 175–188.
- ¹¹Wen-Xiong, W., Nicholas, S. F., *Sci. Total Environ.*, **1999**, *238*, 459–472.
- ¹²Atkins, P. W., Holker, J. S. E., Holiday, A. K., “*Metals and Minerals*”, Oxford Univ. Press, **1998**.
- ¹³Das, A. K., *A text book on Medicinal Aspects of Bioinorganic Chemistry*, CBS publishers Delhi, **1996**.
- ¹⁴Fiaz, T., Fatima, N., Zaidi, S. Z. A., *Pak. J. Chem.*, **2013**, *3*(2), 1.
- ¹⁵Fatima, N., Zaidi, S. Z. A., Nisar, S., Qadri, M., *Pak. J. Chem.*, **2013**, *3*(1), 23-28.
- ¹⁶Sawyer, D. T., Heineman, W. R., Beebe, J. M., “*Chemistry Experimental for Instrumental Methods*”, John Wiley and Sons, Inc., **1984**.
- ¹⁷Stadaert, D. G., Young, A. B., Goodman and Gilman's: *The Pharmacological Basis of Therapeutics*. Tenth edition. Edited by Alfred Goodman Gilman, Louis S. Goodman, Alfred Gilman. McGraw-Hill Publishing Co., Inc., New York, **2001**, 556.

Received: 31.03.2014.
Accepted: 14.05.2014.



STRUCTURE OF 2-AMINO-5-OXO-4-*p*-TOLYL-4,5-DIHYDRO-PYRANO[3,2-*c*]CHROMENE-3-CARBONITRILE

Suresh Sharma,^[a] Goutam Brahmachari,^[b] Bubun Banerjee,^[b] Rajni Kant^[a] and Vivek K. Gupta^[a] *

Keywords: 2-amino-5-oxo-4-*p*-tolyl-4,5-dihydropyrano[3,2-*c*]chromene-3-carbonitrile; scaffolds; hydrogen bond; crystal structure; direct methods.

The compound 2-amino-5-oxo-4-*p*-tolyl-4,5-dihydropyrano[3,2-*c*]chromene-3-carbonitrile, crystallizes in the monoclinic space group P121/c1 with the unit-cell parameters: $a = 9.1330(7)$, $b = 13.1343(9)$, $c = 13.1945(8)$ Å, $\beta = 91.746(4)^\circ$ and $Z = 4$. The crystal structure was solved by direct methods using single-crystal X-ray diffraction data collected at room temperature and refined by full-matrix least-squares procedures to a final R -value of 0.0537 for 1830 observed reflections. The molecules within the unit cell are stabilized by C-H...O, N-H...O N-H...N and C-H... π type of hydrogen bonding.

* Corresponding Authors

Mob: +91 9419102467

E-Mail: vivek_gupta2k2@hotmail.com

- [a] X-ray Crystallography Laboratory, Post-Graduate Department of Physics & Electronics, University of Jammu, Jammu Tawi - 180 006, India
 [b] Laboratory of Natural Products & Organic Synthesis, Department of Chemistry, Visva-Bharati (a Central University), Santiniketan – 731235, West Bengal, India.

Introduction

4*H*-Pyran-annulated heterocyclic scaffolds represent a “privileged” structural motif well distributed in naturally occurring compounds with a broad spectrum of significant biological activities.¹⁻² Recently, a series of synthetic 2-amino-3-cyano-4*H*-pyrans have been evaluated to possess potent anticancer, antibacterial and antifungal, and anti-rheumatic properties.³⁻⁴ In this communication, we wish to report the crystal structure of a 4*H*-pyran-annulated heterocyclic compound, namely 2-amino-5-oxo-4-(*p*-tolyl)-4,5-dihydropyrano[3,2-*c*] chromene -3-carbonitrile (**1**) which is synthesized *via* one-pot multi-component reaction (MCR) at room temperature using commercially available urea as inexpensive and environmentally benign organo-catalyst. The structure of the title compound **1** was elucidated by spectral methods and XRD studies.

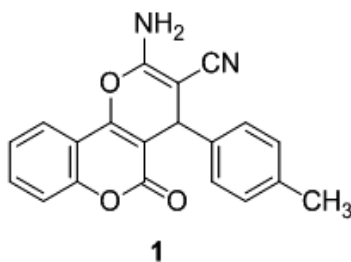


Figure 1. The chemical structure of the compound **1**.

Experimental

Synthesis

An oven-dried screw cap test tube was charged with a magnetic stir bar, 4-methylbenzaldehyde (0.120 gm, 1 mmol), malononitrile (0.066 gm, 1.1 mmol), urea (0.007 gm, 10 mol % as organo-catalyst), and EtOH:H₂O (1:1 *v/v*; 4 ml) in a sequential manner; the reaction mixture was then stirred vigorously at room temperature for about 20 min. After that, 4-hydroxycoumarin (0.162 gm, 1 mmol) was added to the stirred reaction mixture, and the stirring was continued for 10 hour.⁵ The progress of the reaction was monitored by TLC. On completion of the reaction, a solid mass precipitated out that was filtered off followed by washing with aqueous ethanol to obtain crude product which was purified just by recrystallization from ethanol without carrying out column chromatography. The structure of 2-amino-5-oxo-4-(*p*-tolyl)-4,5-dihydropyrano[3,2-*c*]chromene -3-carbonitrile (**1**) was confirmed by analytical as well as spectral studies including FT-IR, ¹H NMR, ¹³C NMR, and TOF-MS. Unit crystal was obtained from DMSO. For crystallization 50 mg of compound dissolved in 5 ml DMSO and left for several days at ambient temperature which yielded white block shaped crystals. The crystal structure of the title compound is given in Figure 2.

White solid. (0.301 gm, yield 91 %). m.p. 530-532 K. IR (KBr) ν_{\max} cm⁻¹: 3375, 3292, 3182, 3024, 2193, 1691, 1609, 1523, 1379, 1053, 916, 748, 490. ¹H NMR (400 MHz, DMSO-*d*₆) δ /ppm: 7.90 (1H, d, $J = 8.0$ Hz, aromatic H), 7.70 (1H, t, $J = 8.0$ & 7.6 Hz, aromatic H), 7.48 (1H, t, $J = 8.0$ & 7.6 Hz, aromatic H), 7.46 (1H, d, $J = 8.1$ Hz, aromatic H), 7.34 (2H, s, NH₂), 7.12 (4H, m, aromatic H), 4.40 (1H, s, CH), 2.26 (3H, s, CH₃). ¹³C NMR (100 MHz, DMSO-*d*₆) δ /ppm: 159.94, 158.33, 153.68, 152.51, 140.80, 136.71, 133.32, 129.48 (2C), 127.92 (2C), 125.09, 122.89, 119.67, 116.96, 113.37, 104.53, 58.52, 36.97, 21.03. TOF-MS: 353.0881 [M+Na]⁺. Elemental analysis: Calcd. (%) for C₂₀H₁₄N₂O₃: C, 72.72; H, 4.27; N, 8.48; found: C, 72.68; H, 4.29; N, 8.52.

X-Ray Structure determination

X-ray intensity data of 6510 reflections (of which 3100 unique) were collected on *X'calibur* CCD area-detector diffractometer equipped with graphite monochromated MoK α radiation ($\lambda = 0.71073$ Å). The crystal used for data collection was of dimensions 0.30 x 0.20 x 0.20 mm. The cell dimensions were determined by least-squares fit of angular settings of 1805 reflections in the θ range 3.75 to 28.42°. The intensities were measured by ω scan mode for θ ranges 3.8 to 26.00°. 1830 reflections were treated as observed ($I > 2\sigma(I)$). Data were corrected for Lorentz, polarization and absorption factors. The structure was solved by direct methods using SHELXS97.⁶ All non-hydrogen atoms of the molecule were located in the best E-map. Full-matrix least-squares refinement was carried out using SHELXL97.⁶ The final refinement cycles converged to an $R = 0.0537$ and $wR(F^2) = 0.1605$ for the observed data. Residual electron densities ranged from $-0.212 < \Delta\rho < 0.262$ eÅ⁻³. Atomic scattering factors were taken from International Tables for X-ray Crystallography (1992, Vol. C, Tables 4.2.6.8 and 6.1.1.4). The crystallographic data are summarized in Table 1.

Table 1. Crystal data and other experimental details

CCDC Number	994051
Crystal description	Block
Crystal size	0.30 x 0.20 x 0.20 mm
Empirical formula	C ₂₀ H ₁₄ N ₂ O ₃
Formula weight	330.33
Radiation,	Mo K α ,
Wavelength	0.71073 Å
Unit cell dimensions	$a = 9.1330(7)$ Å $b = 13.1343(9)$ Å $c = 13.1945(8)$ Å $\alpha = 90.0^\circ$ $\beta = 91.746(4)^\circ$ $\gamma = 90.0^\circ$
Crystal system,	monoclinic,
Space group	P2 ₁ /c ₁
Unit cell volume	1582.02(3) Å ³
No. of molecules per unit cell	4
Absorption coefficient	0.095 mm ⁻¹
F(000)	687.9
θ range for entire data collection	3.8 < θ < 26.00
Reflections collected / unique	6510 / 3100
Reflections observed $I > 2\sigma(I)$	1830
Range of indices	$h = -10$ to 11 $k = -16$ to 15 $l = -16$ to 15
No. of parameters refined	234
Final <i>R</i> -factor	0.0537
$wR(F^2)$	0.1605
R_{int}	0.0331
R_{sigma}	0.0659
Goodness-of-fit	1.042
(Δ/σ) _{max}	-0.001 for U22 O1
Final residual electron density	$-0.212 < \Delta\rho < 0.262$ eÅ ⁻³

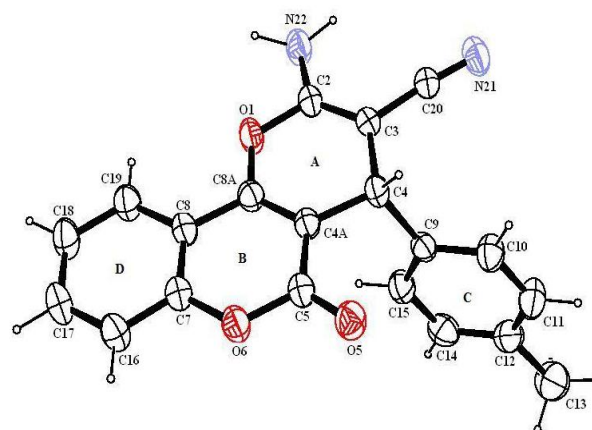


Figure 2. Ortep view of the molecule with displacement ellipsoids drawn at the 40% probability level. H-atoms are shown as small sphere of arbitrary radii.

Result and discussions

An ORTEP⁷ view of the compound with atomic labeling is shown in Figure 2. The geometry of the molecule was calculated using the WinGX⁸, PARST⁹ and PLATON¹⁰ softwares. Packing view of the molecules in the unit cell viewed down the *c*-axis is shown in Figure 3.

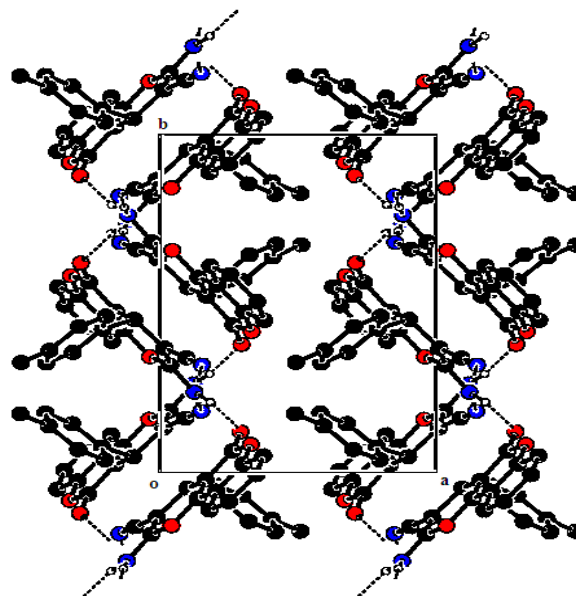


Figure 3. Packing diagram down to *c*-axis

The title compound comprises of four rings in which chromene moiety is fused with the pyran ring-A. Both the rings in chromene moiety (ring-B and ring-D) and pyran ring-A are almost coplanar as reflected from the small values of dihedral angle between these three rings i.e. dihedral angle between ring-A and ring-B, ring-A and ring-D and ring-B and ring-D are 1.99°(6), 1.54°(8) and 1.42°(7) respectively.

Table 2. Selected bond lengths (Å) and bond angles (°) for non hydrogen atoms (e.s.d.'s are given in parentheses)

Bond distances(Å)		Bond angles(°)		Torsion angles(°)	
C20-N21	1.147(3)	C11-C12-C13	120.6(3)	C4A-C4-C9-C15	-137.2(2)
C5-O5	1.208(3)	C14-C12-C13	122.0(2)	C19-C8-C8A-O1	1.4(4)
C12-C13	1.515(4)	N21-C20-C3	175.5(3)	C3-C4-C9-C10	-74.3(3)
C2-N22	1.338(3)	C3-C4-C9	110.67(19)		
C20-N21	1.047(3)	C10-C9-C4	121.6(2)		
O1-C8A	1.366(3)	O6-C7-C16	117.0(2)		
C5-O6	1.381(2)	C5-C4A-C4	117.65(19)		
		O1-C8A-C8	113.9(2)		

Table 3. Geometry of intermolecular hydrogen bonds

D-H...A	D-H (Å)	H...A (Å)	D...A (Å)	θ [D-H...A (°)]
N22 -- H16A.. N21 ⁱ	0.98	2.17	3.14	172(3)
N22 -- H16B.. O5 ⁱⁱ	0.99	2.00	2.98	168(3)
C10..H4..Cg1 ⁱⁱⁱ	0.93	2.86	3.18	101.7
C17..H24..Cg4 ^{iv}	0.93	3.36	4.20	151.1

Symmetry codes: i. x, 1/2-y, -1/2+z; ii. 2-x, -1/2+y, 1/2-z; iii. x, y, z; iv. 1-x, 1-y, -z

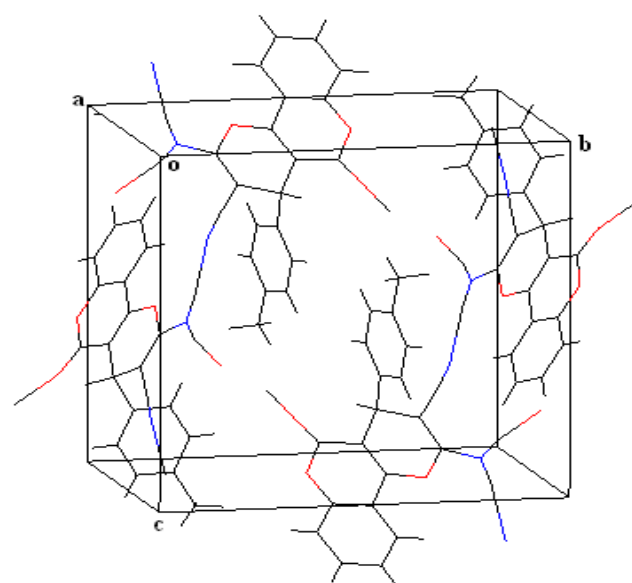
Table 4. Geometry of π - π interactions.

CgI-CgJ	CgI...CgJ(Å)	CgI...P(Å)	α (°)	β (°)	Δ (Å)
Cg1-Cg3 ⁱ	3.62	3.54	1.68	12.35	0.7568

Symmetry code: i. 2-x, 1-y, -z

The plane of phenyl ring-C is nearly perpendicular to the plane of the chromene and pyran ring moieties, as the dihedral angle of ring-C with ring-A, ring-B and ring-D are 85.90°(7), 87.66°(6) and 86.36°(7) respectively. Both the phenyl rings i.e. ring-C and ring-D are almost planar with maximum deviation from planarity is observed for atoms C14 and C18 by 0.009(3)Å for both in ring-C and ring-D respectively. The atoms C20 and N21 of cyanide group and atom N22 of amine group attached to ring-A have deviations of 0.059(2)Å, 0.047(2)Å and -0.010(2)Å respectively from the least square plane of ring-A. The bond length C20-N21 is 1.147(3) (Table 2) which is comparable with the typical C_{sp} -N bond length in most of the organic carbonitriles. The C5=O5 bond length is found to be 1.208(3) which is comparable with some similar structures.¹¹⁻¹² The C12-C13 bond length is 1.515(4) which is comparable to $C(sp_3)$ - C_{ar} bond length. The bond angles C11-C12-C13 and C14-C12-C13 are 120.6°(3) and 122.0°(2) respectively which are close to 120.0° as expected due to sp_2 hybridization of carbon atom C12. The bond angle C3-C20-N21 is 175.5(3)° which indicates that these three atoms are almost linear. The torsion angle C4A-C4-C9-C15 is found to be -137.2°(2). The other bond lengths and bond angles are within the expected values¹³ and are comparable to related structures.¹¹⁻¹²

Analysis of the crystal packing of title compound shows the presence of intermolecular N-H...N and N-H...O hydrogen bonds in the structure (Table 3). The hydrogen atom H16B of the amine group form N22-H16B...O5 interaction with the O5 of other molecule to form double helix like structure extended parallel to b-axis as shown in Figure 3.

**Figure 4.** Stereo plot of molecules within the unit cell linked with N-H...N hydrogen bonds

The other hydrogen atom H16A of amine group form N22-H16A...N21 interaction with the N21 of the neighboring molecule as represented in Figure 4. In addition to these the crystal packing is also stabilized by weak hydrogen bonds and π - π interactions (Table 4) shown in Figure 5.

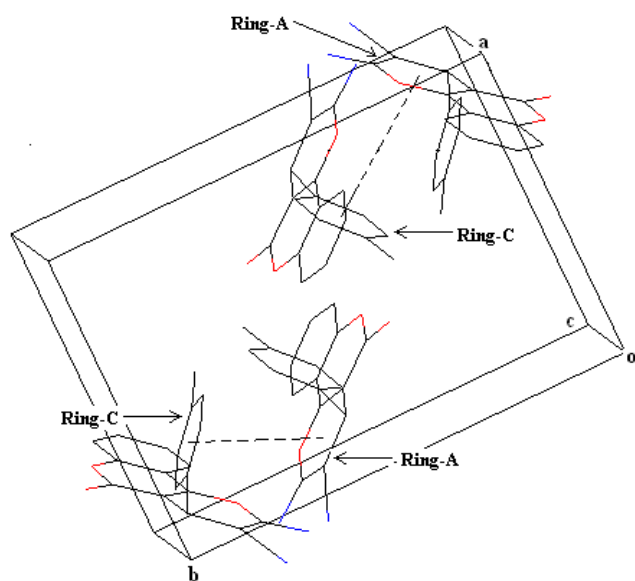


Figure 5. π - π interactions in the crystal structure

Acknowledgments

GB is thankful to the CSIR, New Delhi for financial support [Grant No. 02(0110)/12/EMR-II]. BB is grateful to the UGC, New Delhi for awarding him a Senior Research Fellowship.

References

- ¹Brahmachari, G., In: *Handbook of Pharmaceutical Natural Products*. Weinheim: Wiley-VCH Verlag GmbH & Co. **2010**.
- ²Morgan, L. R., Jursic, B. S., Hooper, C. L., Neumann, D. M., Thangaraj, K. and Leblance, B., *Bioorg. Med. Chem. Lett.* **2002**, *12*, 3407.
- ³Bhavanarushi, S., Kanakaiah, V., Yakaiah, E.; Saddanapu, V., Addlagatta, A. and Rani, V., *J. Med. Chem. Res.*, **2013**, *22*, 2446.
- ⁴Paliwal, P. K., Jetti, S. R. and Jain, S., *Med. Chem. Res.*, **2013**, *22*, 2984.
- ⁵Brahmachari, G. and Banerjee, B., *ACS Sustainable Chem. Eng.*, **2014**, *2*, 411.
- ⁶Sheldrick, G. M., *Acta Cryst.*, **2008**, *A64*, 112.
- ⁷Farrugia, L. J. *J Appl Cryst.*, **1997**, *30*, 565.
- ⁸Farrugia, L. J., *J Appl Cryst.*, **1999**, *32*, 837.
- ⁹Nardelli, M., *J Appl Cryst.*, **1995**, *28*, 659.
- ¹⁰Spek, A. L., *Acta Cryst.*, **2009**, *D65*, 148.
- ¹¹Shi, D., Wu, N., Zhuanga, Q. and Zhang, Y., *Acta Cryst.*, **2004**, *E60*, o2339.
- ¹²Shi, D., Wu, N., Zhuanga, Q. and Zhang, Y., *Acta Cryst.*, **2004**, *E60*, o2359.
- ¹³Allen, F. H., Kennard, O., Watson, D.G., Brammer, L., Orpen, A.G., and Taylor, R. *J. Chem. Soc., Perkin Trans. 2.*, **1987**, S1.

Received: 31.03.2014.

Accepted: 14.05.2014.



EFFECT OF PROTEINOUS AND NON-PROTEINOUS FRACTIONS ISOLATED FROM *PHASEOLUS VULGARIS* AND *VIGNA SINENSIS* FRUITS ON DIABETIC MICE

Nahida Saieed Hamoodi Al-Chalabi^{[a]*} and Shehab Ahmed Yousif Al-Bajari^[a]

Keywords: protein; aqueous extracts; *Phaseolus vulgaris*; *Vigna sinensis*; alloxan; diabetic mice.

This study is concerned with the preparation of cold and boiled aqueous extracts from the fruits of both *Phaseolus vulgaris* and *Vigna sinensis* plants, then isolating the proteinous compounds from these extracts by cold acetone precipitation method and therefore to separate the non-proteinous fraction. The work included the study of the effect of intraperitoneal administration of cold and boiled aqueous extracts, proteinous acetone precipitates, and non-proteinous materials isolated from these extracts on certain blood biochemical constituents (parameters) using a dose of 77 mg kg⁻¹ of body weight in normal and alloxan-induced diabetic mice. The results had been compared with those injected with insulin. The results showed that the boiled crude aqueous extract of *Vigna sinensis* plant and its isolated proteinous precipitate has a significant decrease effects for the level of the glucose and total lipids in the blood. On the other hand, the non-proteinous substance of cold aqueous extract of *Phaseolus vulgaris* fruit has a decrease effect for the level of glucose, cholesterol and total lipids in the blood serum of alloxan-induced diabetic mice, therefore may be used in the treatment of diabetes mellitus after make sure there is no side effects as well as we concluded that these materials mentioned above may be used in the treatment of diabetes mellitus .

Corresponding Authors*

E-Mail: nahida_alchalabi@yahoo.com

[a] Department of Chemistry, College of Education, University of Mosul, Mosul, Iraq

Introduction

It is well known that the incidence of diabetes mellitus is high all over the world, especially in Asia. Different types of oral hypoglycemic agents such as biguanides and sulphonylurea are available along with insulin for the treatment of diabetes mellitus,¹ but have side effects associated with their uses,^{2,3} therefore it is increasing interest in herbal remedies because of their effectiveness, minimal side effects and relatively low costs.

Herbal drugs or their extracts are prescribed widely, even when their biological active compounds are unknown. Even the world health organization (WHO) approves the use of plant drugs for different diseases, including diabetes mellitus. Therefore, studies with plant extracts are useful to know their efficacy and mechanism of action and safety. Medicinal plants useful in diabetes were reviewed recently.^{4,5}

The plant *Phaseolus vulgaris* is commonly called kidney-bean, French-bean in English. This plant and *Vigna sinensis* plant (cow-pea in English) belongs to *Fabacea* family.^{6,7} These plants is reputed to possess varied medicinal properties.^{7,8,9}

In the present study, an attempt has been made to study the hypoglycemic, hypocholesterolemic, hypolipidemic effect of *Phaseolus vulgaris* and *Vigna sinensis* fruits proteinous and non-proteinous aqueous extracts, also proteinous precipitate material on normal and alloxan-induced diabetic male mice.

Material and methods

Plants material

Fruits of *Phaseolus vulgaris* and *Vigna sinensis* plants were purchased from local of agriculture in Mosul city, cleaned and kept in nylon bags in a deep freeze till the day of experiment.

Preparation of crude extracts

The aqueous crude extract was prepared by freezing and thawing (500 g) of the fruits after cutting to small pieces with liquid nitrogen several times to rupture the cell membrane. Cold distilled water in a ratio of 1:3 w/v, was added and the mixture was then homogenized for 10 minute using a blender. The crude homogenate was stirred for additional two hours on ice bath , then filtered through several layers of shash . Finally the mixture was centrifuged using refrigerated centrifuge for 15 minutes at 33520xg. The filtrate of cold crude extracts after reduction its volume to about third ratio by lyophilization was kept for further investigation(precipitation of the protein) . Total protein concentration was determined for this filtrate of cold crude extract by modified Lowry method.¹⁰ This procedure was repeated using (400 g) of the fruits until after homogenized with a blender step, the mixture was boiled for 30 minutes and then leaved to cool, filtered through several layers of shash, centrifuged and lyophilized as indicated above this filtrate which was produced called boiled aqueous crude extract. At the second time, cold and boiled aqueous extract was prepared also using (300 g) fruits of each plants mentioned before were produced as indicated in all steps which was mentioned above till producing filtrate , then this filtrate were lyophilized until drying and produced a powdered materials, kept in a deep freeze at -20ú c in a tight sample tube until used for the next step, which is the

injection of animals experiment This powdered material called cold or boiled crude aqueous extract material (CCAEM) or (BCAEM) respectively.

Precipitation of the proteins

Proteinous materials were separated from cold, boiled aqueous extracts using cold acetone precipitation method.¹¹ This method was performed by adding cold acetone gradually to extract in a ratio (40:60, v/v) respectively with slow stirring at 0 °C. The mixture was left in a refrigerator for 24 hours and the precipitated protein was isolated by centrifugation for 20 minutes at 33520 x g at a refrigerated centrifuge. The proteinous precipitate material (PPM) was dried in a lyophilizer to remove trace amount of aqueous acetone, then kept in a tight sample tube in a freezer for the next step. At the same time, acetone was removed from the remained filtrate after precipitation of proteins by rotary evaporator (<40 °C), the remaining filtrate was dried in a lyophilizer till dryness. The powdered material which was produced called non-proteinous material (NPM). This materials was then kept in a tight sample tube in a freezer for the next step.

Experimental animals

Healthy adult male albino mice weighing 25-35 g were obtained from animal house of the Veterinary Medicine College, University of Mosul and housed under controlled conditions of light (14h light and 10 h dark) and temperature (25±2 °C commercial pelleted food and water were given *adlibitum*.

Determination of the effective dose

The animals were randomly divided to 5 groups (3 mice/group). The mice were fasted for 16 h before the experiment was started. *Group 1* (control , normal) injected intraperitoneal with 1 ml normal saline. *Groups (2-6 , normal)* were injected intraperitoneal with different doses (50 , 77, 100, 150) mg kg⁻¹ body weight (b.w.), respectively with each of solution in normal saline of the materials of cold crude aqueous extract material (CCAEM), proteinous precipitate material (PPM) of *Vigna sinensis* fruits plant. After two hours of injections blood samples were collected for analysis immediately (serum glucose level) by the orbital sinus puncture under ether anesthesia, using non-heparin zed micro-hematocrit capillary tubes. After determined the effective dose of these materials. This doses then it was used for the injection of normal and alloxan-induced diabetic mice.

Induction of diabetes in mice

Healthy adult male albino mice , weighing 25-35 g were selected and randomly divided into groups of 3 mice per group. They were fasted for 24 h before induction of diabetes. They were intraperitoneal injected with alloxan tetra hydrate which was dissolved in 1 ml sterile physiological saline solution immediately before use at a dose of 180 mg kg⁻¹ b.w.¹² The diabetic state was monitored by periodic tests for glucosuria (Tes-Tape-Eli Lilly and Co., USA) and hypoglycemia (colorimetric assay kit, Syrbio,

France), mice with blood glucose level more than 180 mg 100 ml⁻¹ were considered diabetic and used fore the study. At the end of the period, three alloxan diabetic animals were randomly divided for each group for the present study.

Intraperitoneal injection of the mice

The mice (25-35 g weight) were divided randomly into 28 groups (14 for normal and 14 for diabetic mice) each group containing three mice. *Group one* was kept as control. The *second group* was injected subcutaneously with insulin (10 IU kg⁻¹, neutral insulin injection Act rapid 100 IU ml⁻¹, Novo Nordisk, Denmark), while the other groups were injected intraperitoneal with 77 mg kg⁻¹ b.w. of crude (cold, boiled) aqueous extract material (CCAEM, BCAEM), non-proteinous materials (NPM) and proteinous precipitate materials (PPM) of *Phaseolus vulgaris* and *Vigna sinensis* fruits plants. The mice were fasted for 16 h before the experiment was started. After two hours of injection blood samples were collected from each mouse by the orbital sinus puncture under ether anesthesia using non-heparin zed microhematocrit capillary tubes.¹³ Blood serum glucose, total cholesterol levels were measured using colorimetric assay kits type (Syrbio, France).¹⁴ Total lipids was determined by colorimetric method.¹⁵

Statistical analysis

Statistical analysis was performed using one - way analysis of variance with a significance level of $p < 0.05$. Further specific group differences were determined using Duncan's test,¹⁶ the results were expressed as mean ± S.E.

Results and Discussion

Precipitation of the protein

Precipitation of total proteins from the crude aqueous extract was accomplished by cold acetone technique¹¹ but not by saturated ammonium sulphate technique.¹⁷ Since the former can be easily removed by evaporation, besides the fact that the precipitation power of both reagents were similar. Moreover , dialysis of the proteinous fraction to get rid of ammonium sulphate may remove some of the low molecular weight protein or peptides. The amount of total protein in crude aqueous extract was determined¹⁰ and the amount of the precipitated protein, efficiency of the precipitation method were shown in (Table 1). Higher amount of the protein was in the cold crude aqueous extract of *Vigna sinensis* fruits and found to be 1.868 %. Whereas, the lower amount was found in the boiled crude aqueous extract of *Phaseolus vulgaris* fruits which has efficiency of the precipitation of the protein is 86.11 % .

Determination of the effective doses for the plant extracts and proteins in normal mice :

The results in Tables 2 and 3 for crude cold aqueous extract material, proteinous precipitate of *Vigna sinensis* fruits plant shows that a dose 77 mg kg⁻¹ b.w. mice give a significant decrease in the level of blood serum glucose more than that for other doses.

Table 1. Amount of total proteins in the crude aqueous extract of *Vigna sinensis* plants, *Phaseolus vulgaris* fruits plants, their percentage and efficiency of acetone method precipitation

Extract name symbol	Protein concn., mg ml ⁻¹	Total volume in ml	Total protein in the extract, mg	Percent of the protein in plant, %	Weight of the plant, g	Total amount of the protein precipitated by acetone, mg	Efficiency of the precipitation method, %
CCAEM of <i>Vigna sinensis</i> fruits plant	5.75	1625	9343.75	1.868	500	5130	54.9
CCAEM of <i>Phaseolus vulgaris</i> fruits plant	4.30	1600	6880	1.376	500	4970	72.24
BCAEM of <i>Vigna sinensis</i> fruits plant	5.56	1000	5560	1.39	400	4710	84.7
BCAEM of <i>Phaseolus vulgaris</i> fruits plant	4.0	900	3600	0.9	400	3100	86.11

Table 2. Effective dose of cold crude aqueous extract of *Vigna sinensis* fruits plant on glucose level in normal mice.

*Conc. of serum glucose mmol L ⁻¹	Control	Dose of cold crude aqueous extract in mg kg ⁻¹ of body weight			
		50	77	100	150
	5.48±0.12	4.73±0.24	3.67±0.7	4.32±0.11	5.62±0.31
% Change	-	-13.69	-33.03	-21.17	2.55

*Values are mean ± S.E.

Table 3. Effective dose of proteinous precipitate material for cold crude aqueous extract of *Vigna sinensis* fruits plant on glucose level in normal mice.

*Conc. of serum glucose mmol L ⁻¹	Control	Dose of cold crude aqueous extract in mg kg ⁻¹ of body weight			
		50	77	100	150
	5.51±0.7	5.03±0.35	4.28±0.14	4.55±0.29	5.55±0.61
% Change	-	-8.7	-22.3	-17.4	0.7

*Values are Mean ± S.E.

Table 4. Effect of cold, boiled crude aqueous extracts, non-proteinous materials of *Vigna sinensis*, *Phaseolus vulgaris* fruits plants on serum glucose, cholesterol, total lipids levels in normal mice.

Treatment of groups	Glucose, mmol L ⁻¹	% Change	Cholesterol mmol L ⁻¹	% Change	Total lipids mg 100 mL ⁻¹	% Change
Normal (control)	5.68±0.21 d	-	2.38±0.65 e	-	384.56±8.25 b	-
Insulin	1.84±0.72 a	-67.6	1.85±0.461 abc	-22.26	213.16±3.95 a	-44.57
CCAEM of <i>Vigna sinensis</i> fruits plant	4.36±0.17 b	-23.2	1.69±0.345 a	-28.99	487±6.817 c	26.63
CCAEM of <i>Phaseolus vulgaris</i> fruits plant	6.97±0.21 f	22.71	2.08±0.608 d	-12.6	516.1±9.29 d	34.46
BCAEM of <i>Vigna sinensis</i> fruits plant	4.8±0.14 bc	-15.49	2.13±0.553 d	-10.5	484.4±8.78 c	25.96
BCAEM of <i>Phaseolus vulgaris</i> fruits plant	4.35±0.16 b	-23.41	1.86±0.461 abc	-21.84	489.1±8.21 c	27.18
CNPM of <i>Vigna sinensis</i> fruits plant	6.41±0.51 e	-12.85	1.99±0.216 cd	-16.38	523.26±4.73 de	36.07
CNPM of <i>Phaseolus vulgaris</i> fruits plant	5.22±0.20 cd	-8.09	1.68±0.336 a	-29.41	389.13±6.46 b	-1.18
BNPM of <i>Vigna sinensis</i> fruits plant	6.47±0.10 f	13.91	1.76±0.964 ab	-26.05	541.13±6.45 e	40.71
BNPM of <i>Phaseolus vulgaris</i> fruits plant	6.4±0.15 e	12.67	1.9±0.65 bc	-20.16	381.93±4.49 b	-0.68

*Values are mean ± S.E., different letters vertically mean significant at $p < 0.05$, each group include (3) mice, CCAEM, BCAEM, CNPM, BNPM symbols referred as in method

Table 5. Effect of cold, boiled crude aqueous extracts, non-proteinous materials of *Vigna sinensis*, *Phaseolus vulgaris* fruits plants on serum glucose, cholesterol, total lipids levels in alloxan-induced diabetic mice.

Treatment of groups	Glucose mmol L ⁻¹	% Change	Cholesterol mmol L ⁻¹	% Change	Total lipids mg 100 mL ⁻¹	% Change
Normal (control)	5.68±0.21 b	-	2.38±0.65 c	-	384.56±8.25 cd	-
Control (diabetic)	18.17±0.11 fg	219	2.86±0.1 d	20.1	552.9±13.5 f	43.7
Insulin	2.4±0.77 a	-87.15	2.18±0.78 bc	-23.4	352.26±4.07 b	-36.28
CCAEM of <i>Vigna sinensis</i> fruits plant	17.67±0.24 f	-5.48	1.65±0.29 a	-42.2	379.06±8.97 c	-10
CCAEM of <i>Phaseolus vulgaris</i> fruits plant	19.35±0.2 g	3.51	3.01±0.71 d	5.14	533.1±14.3 ef	-3.57
BCAEM of <i>Vigna sinensis</i> fruits plant	13.31±0.17 c	-28.79	3.14±0.12 d	9.47	365.53±8.21 bc	-33.88
BCAEM of <i>Phaseolus vulgaris</i> fruits plant	16.9±0.16 ef	-9.6	2.24±0.37 bc	-21.8	368.46±14.28 bc	-33.35
CNPM of <i>Vigna sinensis</i> fruits plant	15.14±0.35 d	-19.02	2.01±0.1 abc	-29.9	520.7±9.2 e	-5.8
CNPM of <i>Phaseolus vulgaris</i> fruits plant	12.6±0.14 c	-32.62	1.99±0.81 ab	-30.4	404.36±5.56 d	-26.86
BNPM of <i>Vigna sinensis</i> fruits plant	15.7±0.17 de	-15.88	2.01±0.53 bc	-27.1	633.26±5.17 g	14.55
BNPM of <i>Phaseolus vulgaris</i> fruits plant	14.8±0.24 ef	-9.42	2.16±0.57 bc	-24.6	298.8±11.05 a	-22.3

*Values are Mean ± S.E., different letters vertically mean significant at $p < 0.05$, each group include (3) mice, CCAEM, BCAEM, CNPM, BNPM symbols referred as in method

Table 6. Effect of proteinous precipitate materials isolated from cold, boiled crude aqueous extracts of *Vigna sinensis*, *Phaseolus vulgaris* fruits plants on serum glucose, cholesterol, total lipids levels in normal mice.

Treatment of groups	Glucose mmol L ⁻¹	% Change	Cholesterol mmol L ⁻¹	% Change	Total lipids mg 100 mL ⁻¹	% Change
Normal (control)	5.68±0.21 d	-	2.38±0.54 d	-	381.3±8.3 c	-
Insulin	1.83±0.97 a	-67.78	1.84±0.44 c	-22.68	2.13.1±3.8 a	-44.11
PPM of CCAE of <i>Vigna sinensis</i> fruits plant	4.95±0.17 c	-5.96	1.32±0.67 a	-44.53	223.6±6.2 a	-41.34
PPM of CCAE of <i>Phaseolus vulgaris</i> fruits plant	3.6±0.2 b	-36.61	1.77±0.69 c	-25.63	383.2±4.7 c	0.49
PPM of BCAE of <i>Vigna sinensis</i> fruits plant	3.95±0.95 b	-30.45	1.58±0.25 b	-33.61	336.8±6.5 b	-11.67
PPM of BCAE of <i>Phaseolus vulgaris</i> fruits plant	5.61±0.12 d	-1.23	1.6±0.53 b	-33.77	478.4±5.2 d	25.47

*Values are Mean ± S.E., different letters vertically mean significant at $p < 0.05$, each group include (3) mice, PPM of CCAE, PPM of BCAE, symbols referred as in method

Table 7. Effect of proteinous precipitate materials isolated from cold , boiled crude aqueous extracts of *Vigna sinensis*, *Phaseolus vulgaris* fruits plants on serum glucose , cholesterol , total lipids levels in alloxan-induced diabetic mice.

Treatment of groups	Glucose mmol L ⁻¹	% Change	Cholesterol mmol L ⁻¹	% Change	Total lipids mg 100 mL ⁻¹	% Change
Normal (control)	5.68±0.21 b	-	2.38±0.54 b	-	381.3±8.3 b	-
Control (diabetic)	18.18±0.13 g	22	2.86±0.92 c	22.1	555.13±13.7 d	45.6
Insulin	2.42±0.63 a	-87.03	2.29±0.5 ab	-19.19	353.23±3.17 a	36.1
PPM of CCAE of <i>Vigna sinensis</i> fruits plant	14.46±0.31 c	-22.63	2.39±0.56 b	-16.7	410.1±9.31 bc	-25.82
PPM of CCAE of <i>Phaseolus vulgaris</i> fruits plant	8.66±0.35 c	-53.67	2.55±0.43 b	-10.87	594.9±4.73 e	7.62
PPM of BCAE of <i>Vigna sinensis</i> fruits plant	11.27±0.29 d	-39.73	2.52±0.6 b	-12.07	342.36±6.51 a	-38.07
PPM of BCAE of <i>Phaseolus vulgaris</i> fruits plant	15.86±0.17 e	-15.15	2.12±0.48 a	-26	424.16±6.64 c	-23.27

*Values are mean ± S.E., different letters vertically mean significant at $p < 0.05$, each group include (3) mice , PPM of CCAE , PPM of BCAE, symbols referred as in method

This dose is more effective for decreasing the level of serum glucose in normal mice as an effective dose for normal and alloxan induced diabetic mice by intraperitoneal injection. The effective doses of this plant was also taken for *Phaseolus vulgaris* fruits plant.

Effect of aqueous extract , non-proteinous materials , proteins on some biochemical parameters on normal and alloxan-induced diabetic mice

The results of cold, boiled crude aqueous extracts, non-proteinous and proteinous precipitate materials for *Vigna sinensis*, *Phaseolus vulgaris* fruits plants on the level of glucose, cholesterol and total lipids blood serum in male normal and alloxan –induced diabetic mice were listed in Tables 4, 5, 6 and 7.

Effect of crude aqueous extract (cold, boiled) , non-proteinous materials of *Vigna sinensis*, *Phaseolus vulgaris* fruits plants on serum glucose level in normal and alloxan-induced diabetic mice.

Results depicted from Tables 4 and 5 indicated that treatment with cold, boiled crude aqueous extracts of *Vigna sinensis* fruits plant and boiled aqueous extract of *Phaseolus vulgaris* at a dose 77 mg kg⁻¹ of b.w. intraperitoneal a significant decrease in the level of serum glucose on normal mice compared to their control group. Also this dose injection with boiled aqueous extract, cold and boiled non-proteinous materials of *Vigna sinensis* produced a significant decrease which is (28.79 % , 19.02 % and 15.88 %) respectively in the level of serum glucose in alloxan-induced diabetic mice.

The decreasing effect of these extracts in agreement with other studies.^{18,19,20} This decrease may be due to these extracts may be contain an active materials which activate β -cells of pancreas to secretion insulin or may be containing materials acts as insulin to increase glycolysis in peripheral tissues or decrease gluconeogenesis.²¹

Effect of crude aqueous extract (cold, boiled) , non-proteinous materials of *Vigna sinensis* *Phaseolus vulgaris* fruits plant on serum cholesterol level in normal, and alloxan-induced diabetic mice

Treatment with extracts and non-proteinous (cold, boiled) for fruits of each plants *Vigna sinensis*, *Phaseolus vulgaris* which was indicated in Tables 4 and 5 at a dose 77 mg kg⁻¹ b.w. were give a significant decrease in the level of serum cholesterol on normal and diabetic mice compared to their control group, except the boiled crude aqueous extract of *Vigna sinensis* and cold for *Phaseolus vulgaris*. At the same time, boiled aqueous extract of *Phaseolus vulgaris* produce a significant decrease in cholesterol level in normal and diabetic mice and resembles the decrease of insulin and return the level of cholesterol for diabetic mice to their normal level compared to normal control mice group. This decrease may be due to the presence of saponin which lower blood cholesterol and increase rejecting of bile acids and neutral lipids out of the body²² or may be due to inhibit hydroxyl methyl glutaryl-CoA reductase enzyme which is responsible for the biosynthesis of cholesterol.²³

Effect of crude aqueous extract (cold, boiled) , non-proteinous materials of *Vigna sinensis*, *Phaseolus vulgaris* fruits plants on serum total lipids level in normal and alloxan-induced diabetic mice

Results for cold, boiled aqueous extracts of *Vigna sinensis*, *Phaseolus vulgaris*, non-proteinous (cold, boiled) for fruits of *Phaseolus vulgaris* and cold for *Vigna sinensis* showed a significant decrease in total lipids level when injected in diabetic mice. These results are in agreement with the results indicated for decreasing of total lipids level in alloxan-induced diabetic rats for cold and boiled aqueous extract of *Melia azedarach* and *Lactuca serriola* leaves.¹⁹ These extracts may be containing compounds which acts similar to the action of insulin, this insulin inhibit lipolysis of lipids during its effect on glucagon and catecholamine hormones which are increase lipolysis.²⁴

Effect of proteinous precipitate materials for *Vigna sinensis*, *Phaseolus vulgaris* fruits plants on serum glucose, cholesterol and total lipids level in normal and alloxan-induced diabetic mice

Treatment with the proteinous precipitate materials for cold, boiled crude aqueous extracts of *Vigna sinensis*, *Phaseolus vulgaris* fruits plants at a dose 77 mg kg⁻¹ b.w. intraperitoneal in male normal and diabetic mice were indicated in Tables 6 and 7. The results were showed a significant decrease in the level of serum glucose at different ratio, the proteinous precipitate material which was isolated from cold aqueous extract of *Phaseolus vulgaris* was showed a higher decrease percent (36.63 %) for normal mice and a decrease (53.6 %) for diabetic mice. These results in agreement with the results for cold and boiled aqueous extract of *Oleo europae* leaves for chickens.²⁵ This decrease may be due to activate beta cells of pancreas to secretion of insulin hormone or may be these proteinous precipitate act to increase biosynthesis of liver glycogen from glucose as the action of *Momordica charantica* fruit extract when given to mice, this extract showed a decrease of glucose level in normal and streptozotocin-induced diabetic mice.²⁶

The decrease effect of the proteinous precipitate materials of cold and boiled of each plants used in diabetic mice which is similar to a decrease of insulin and which are reached to normal level value of cholesterol may be due to occurrence changes in the flora of intestine who have the role to increase the excreted bile acids and then decreased serum cholesterol level.²⁷ On the other hand, a significant decrease effect were produced by cold, boiled proteinous materials of *Vigna sinensis* fruits plant, but the *Phaseolus vulgaris* proteinous (cold, boiled) material showed a significant increase for the level of serum total lipids on normal and diabetic mice. This increase may be due to possess these precipitate an effect similar to glucagon or epinephrine hormones in action which were activate lipolysis of lipids during the activation of lipase enzyme which increase lipolysis in adipose tissues²⁸. It was concluded that boiled crude aqueous extract material and its proteinous precipitate material which was isolated from it for *Vigna sinensis* fruits plant possess a decreasing effect for glucose and total lipids in blood, also cold non-proteinous material which due to *Phaseolus vulgaris* fruits plant possess a hypoglycemia, hypocholesterolemia and hypolipidemia effect which are used for the treatment of diabetes mellitus after sure there is no side effect.

References

- ¹Holman, R. R., Turner, R. C., *Oral agents and insulin in the treatment of diabetes*, Blackwell, Oxford, **1991**, 467-469.
- ²Kameshware, R., Giri, R., Kesavulu, M. M. and Apparao, C., *Manphar. Vaidhya. Patrica.*, **1997**, *1*, 33-35.
- ³Valiathan, M. S., *Curr. Sci.*, **1998**, *75*, 1122-1126.
- ⁴Shukla, R., Sharma, S. B., Puri, D., Pabhu, K. M. and Murth, P. S., *Indian J. Clin. Biochem.*, **2000**, *Suppl. 15*, 169-177.
- ⁵Grover, J. K., Yadav, S., and Vats, V., *J. Ethnopharmacol.*, **2002**, *81*, 81-100.
- ⁶Lawrence, H. M., *Taxonomy of Vascular Plants*, The MacMillan Company, **1951**, p. 82.
- ⁷Duke, J. A., *Handbook of Energy Crops*, CRC Press, Inc. **1983**.
- ⁸Walt, J. M., Breyer-Brandwijk, M. G., *The medicinal and poisonous plants of Southern and Eastern Africa*, E. and S. Livingstone Ltd., Edinborough, London, U.K. **1962**.
- ⁹Chakravarty, H. L., *Plant Wealth of Iraq*, Vol. 1, Atsrea Saraswaty Press Ltd., India, **1979**, p. 469.
- ¹⁰Schacterel, G. N., Pollack, K. L., *Anal. Biochem.*, **1973**, *51*, 654-655.
- ¹¹Robyt, J. F., White, B. J., *Biochemical Techniques, Theory and Practice*, Wedsworth Inc., Belmont, California, USA, **1987**, p.115-118.
- ¹²Al-Chalabi, N. S., Ahmad, T. Y. and Al-Jarah, I. A. *Nat. Chem. J.*, **2004**, *14*, 268-256.
- ¹³Tomoda, M., Shimizu, N., Gonda, R., Kanari, M., Yamada H. And Hikina, H., *Planta Med.*, **1990**, *56*, 168-170.
- ¹⁴Burtis, C. A., Ashwood, E., Tietz, R., *Textbook of Clinical Chemistry*, 3rd Ed., W. B. Saunders Company, London, **1999**, p. 840-841.
- ¹⁵Chabrol, E., Chardonnet, R. (**1937**) .Cited by Gelson Toro and Philip G. A., *In practical clinical chemistry*, Little Brown and Company, Boston, **1975**.
- ¹⁶Steel, R. G., Torrie, J. H., *Principles and Procedures of Statistics Biometrical Approach*, 2nd Ed., McGraw-Hill Inc., Singapore, **1984**, p.183.
- ¹⁷Dioxin, M., Weed, E. C., *Tools of Biochemistry*. Ed.: Copperol T. G., John Wiley and Sons Inc. **1977**, p.370.
- ¹⁸Ajabnoor, M. A., *J. Ethnopharmacol.*, **1990**, *28*, 215-220.
- ¹⁹Abdul Manna, K. S., M. Sc. Thesis, College of Education, University of Mosul, **2002**, (In Arabic).
- ²⁰Zakarya, M. M., M. Sc. Thesis, College of Science, University of Mosul, **2004**, (In Arabic).
- ²¹Ponnachan, P. T. Paulose, C. S. and Panikkar, K. R., *Ind. J. Exp. Biol.*, **1993**, *31*, 345-347.
- ²²Oakenfull, D. G., Fenwich, D. W., Hood, R. L., Topping, D. L., Iliman, R. L. and Stores, G. B., *Br. J. Nutr.*, **1979**, *42*, 204-216.
- ²³Ingebritsen, T. S., Geelen, M. J. H., Parker, R. A., Evenson, K. J. and Gibson, M. D., *J. Biol. Chem.*, **1979**, *254*(20), 9986-9989.
- ²⁴Goodman, L. S., Gillman, A., *The Pharmacological Basis of Therapeutics*, 7th Ed. Macmillan Co., New York, **1985**, p. 1490-1510.
- ²⁵Ahmad, T. Y., Al-Khayat, I., Mahmood, S., *J. Ed. Sci.*, **1994**, *15*, 54-61.
- ²⁶Kato, A., Miura, T., *Biol. Pharm. Bull.*, **1993**, *16*, 1118-1120.
- ²⁷Paolettle, R., Fumagalli, R., *Drugs Acting on Blood Lipids*, In: *Fundamentals of Biochemical Pharmacology*. Bacq, Z. M. (Ed.), Pergamon Press Ltd., Oxford, **1971**, p.557-570.
- ²⁸Al-Obaydee, S. O., M. Sc. Thesis, College of Science, University of Mosul, **1996**.

Received: 30.03.2014.
Accepted: 14.05.2014.



SYNTHESIS AND CRYSTALLOGRAPHIC CHARACTERIZATION OF MANGANESE(III) SCHIFF BASE COMPLEXES WITH AXIAL CARBOXYLATE LIGATION

H. Roseben,^[a] K. L. Sreebala^[a] and V. S. Thampidas^{[a]*}

Keywords: manganese(III); Schiff base; carboxylate; H-bond interactions; supramolecular assembly.

Two new complexes of manganese(III), [Mn(salen)(*p*-ClC₆H₄CO₂)H₂O] and [Mn(msalen)(C₆H₅CO₂)H₂O] have been synthesized from their manganese(II) carboxylate precursors [H₂salen=*N,N'*-bis(salicylidene)-1,2-diaminoethane and H₂msalen=*N,N'*-bis(3-methoxysalicylidene)-1,2-diaminoethane]. Single crystal X-ray diffraction studies show that the Jahn-Teller distorted octahedral complexes are stabilized by H-bonded chains in the solid state.

*Corresponding Authors

Phone: 0470-2602362

E-Mail: vstidas@gmail.com

[a] Department of Chemistry, Sree Narayana College, Varkala, Kerala, India-695 145

Introduction

Ligands such as aliphatic, cyclic Schiff bases, polypyridyl systems, carboxylic acids, alcohols, oximes and so on, have been extensively employed in the development of the coordination chemistry of high-valent manganese over the past few decades.¹⁻² Application and relevance of high-valent manganese complexes of these ligand systems in areas like bioinorganic modeling³⁻⁵, molecular magnetism⁶⁻⁸ and asymmetric catalysis^{9,10}, have been well-documented. Complexes where Schiff bases in combination with carboxylates stabilize higher oxidation states of manganese, have also been in focus in recent times.¹¹⁻¹⁸ Factors like the flexibility of the Schiff base ligand and the *pK_b* values of the carboxylates could bring about a great deal structural diversity in manganese(III) carboxylate complexes with Schiff base ligands, and these include mononuclear, dinuclear, and polymeric species.^{12,13} *N,N'*-bis(salicylidene)-1,2-diaminoethane (H₂salen) and its derivatives are among the most widely used Schiff base ligands in manganese(III) coordination chemistry.^{12-13,19-23} Our interest in exploring the chemistry of manganese(III) with *salen* ligands in conjunction with aryl carboxylates has led to the isolation of two new complexes, and herein we report structural characterization these two, mainly on the basis of a crystallographic analysis.

Experimental

All chemicals were purchased from E-Merck and used without further purification. The manganese(II) carboxylates were prepared as reported earlier or alternatively by mixing hot aqueous solutions of sodium carboxylate and manganese(II) chloride (2:1 molar ratio), which gave pale

pink crystals of the compounds in yields greater than 70 % in a day's time.¹²

Measurements

IR spectra were recorded on a Nicolet 6700 spectrophotometer (KBr pellets, 4000-400 cm⁻¹) while UV-Vis spectra were taken on a Cary 100 Bio UV-Vis spectrophotometer. Elemental analyses were performed using a Perkin-Elmer 2400 CHNS analyzer.

X-ray crystallography

Data were collected on a Bruker APEX II diffractometer, equipped with a CCD area detector [Mo *K* α radiation, $\lambda = 0.71073$ Å, graphite monochromator, at 296(2) K for complex **1**; (Cu-*K* α radiation, graphite monochromator, $\lambda = 1.54178$ Å, at 100(2) K for complex **2**]. The crystal structure was solved by direct methods and refined by full-matrix least squares methods based on *F*² values against all reflections including anisotropic displacement parameters for all non-H atoms, using SHELXS97 and SHELXL97.²⁴ All the non-hydrogen atoms were located from a Fourier map and refined anisotropically. Hydrogen site locations were inferred from neighbouring sites and were treated by a mixture of independent and constrained refinement. The molecular graphics were done with PLATON and MERCURY 2.0.²⁵⁻²⁶

Synthesis of [Mn(salen)(*p*-ClC₆H₄CO₂)H₂O] (**1**)

To a solution of Mn(*p*-ClC₆H₄CO₂)₂·2H₂O (1.00 g, 2.49 mmol) and salicylaldehyde (0.61 g, 4.98 mmol) in methanol (40 mL), 1,2-diaminoethane (0.15 g, 2.49 mmol) was added. The brown solution was stirred for 20 minutes, filtered and left to evaporation in an open conical flask. Greenish black crystals, deposited in 3-4 days were collected by filtration, washed with diethylether (10 mL) and dried in air. Yield: 0.91 g (74 %). *Anal.* Calc. for C₂₃H₂₀ClMnN₂O₅ (494.80): C, 55.8; H, 4.1; N, 5.6; Mn, 11.1 %. Found: C, 55.6; H, 4.0; N, 5.5, Mn, 10.9 %.

IR (KBr pellet): $\nu/\text{cm}^{-1} = 3064$ (*w,br*), 1622 (*s*), 1597 (*s*), 1537 (*s*), 1359 (*s*), 1274 (*m*), 1152 (*m*), 459 (*s*). UV-Vis (MeOH); $\lambda/\text{nm} = 216$ ($\epsilon_{\text{max}} = 9851 \text{ mol}^{-1} \text{ dm}^3 \text{ cm}^{-1}$), 250 ($\epsilon_{\text{max}} = 7811 \text{ mol}^{-1} \text{ dm}^3 \text{ cm}^{-1}$), 292 ($\epsilon_{\text{max}} = 3861 \text{ mol}^{-1} \text{ dm}^3 \text{ cm}^{-1}$), 322 ($\epsilon_{\text{max}} = 1985 \text{ mol}^{-1} \text{ dm}^3 \text{ cm}^{-1}$), 415 ($\epsilon_{\text{max}} = 985 \text{ mol}^{-1} \text{ dm}^3 \text{ cm}^{-1}$).

Synthesis of [Mn(msalen)(C₆H₅CO₂)H₂O] (**2**)

To a solution of Mn(C₆H₅CO₂)₂·2H₂O (1.00 g, 3.00 mmol) and 3-methoxysalicylaldehyde (0.87 g, 6.00 mmol) in methanol (40 mL), 1,2-diaminoethane (0.18 g, 3.00 mmol) was added. The brown solution was stirred for 20 minutes, filtered and left to evaporation in an open conical flask. Greenish brown crystals, deposited in 3-4 days were collected by filtration, washed with diethylether (10 mL) and dried in air. Yield: 1.19 g (77 %). *Anal. Calc.* for C₂₅H₂₅MnN₂O₇ (520.41): C, 57.7; H, 4.8, N, 5.4; Mn, 10.5 %. *Found:* C, 57.2; H, 4.7; N, 5.2; Mn, 10.1 %. IR (KBr pellet): $\nu/\text{cm}^{-1} = 3058$ (*w,br*), 1631 (*vs*), 1598 (*s*), 1538 (*s*), 1383 (*s*), 1259 (*m*), 1149 (*m*), 457 (*s*). UV-Vis (MeOH); $\lambda/\text{nm} = 215$ ($\epsilon_{\text{max}} = 11968 \text{ mol}^{-1} \text{ dm}^3 \text{ cm}^{-1}$), 233 ($\epsilon_{\text{max}} = 11864 \text{ mol}^{-1} \text{ dm}^3 \text{ cm}^{-1}$), 281 ($\epsilon_{\text{max}} = 4845 \text{ mol}^{-1} \text{ dm}^3 \text{ cm}^{-1}$), 314 ($\epsilon_{\text{max}} = 2984 \text{ mol}^{-1} \text{ dm}^3 \text{ cm}^{-1}$), 405 ($\epsilon_{\text{max}} = 1187 \text{ mol}^{-1} \text{ dm}^3 \text{ cm}^{-1}$).

Results and discussion

Molecular structures of **1** and **2**

A summary of crystallographic data collection and structure refinement for complexes **1** and **2** is furnished in table 1. In both complexes (Figures 1 and 2), the bis-deprotonated ligands with their N₂O₂ donor set define the equatorial planes consisting of two Mn–N_{imine} (1.97 and 1.99 Å) and two Mn–O_{phenol} (1.87–1.90 Å) bonds, in the overall distorted octahedral geometries around the manganese(III) ions. The *trans* positions are now open for carboxylate binding and previous reports are replete with examples of different structural patterns like monomers with chelating carboxylates, polymers with bridging carboxylates, μ -phenoxy dimers with unidentate carboxylates or a monomer with a unidentate carboxylate and a neutral ligand like water occupying axial positions.^{12–14}

The carboxylates adopt a unidentate coordination mode in **1** and **2**, accommodating the aqua ligands along the opposite axial directions. Jahn-Teller distortions which facilitate the removal of double degeneracy of the *e_g* electron at the metal centres are commonplace in high-spin manganese(III) complexes with polydentate Schiff-base ligands.

Both complexes typically undergo a Jahn-Teller distortion showing an elongation of the axial bonds [Mn–O_{aq} = 2.29–2.35 Å and Mn–O_{carb} = 2.11–2.14 Å]. The dihedral angles between the aromatic rings of the Schiff base ligands (5.87 and 12.03°) are indicative of substantial distortions around the Mn–N₂O₂ cores of the complexes. The deviation of the Mn(III) ion from the N,N',O,O' least-square planes along the Mn–O_{carb} directions in complex **1** is 0.048 Å, whereas the corresponding shift in complex **2** is more than twice at 0.101 Å.

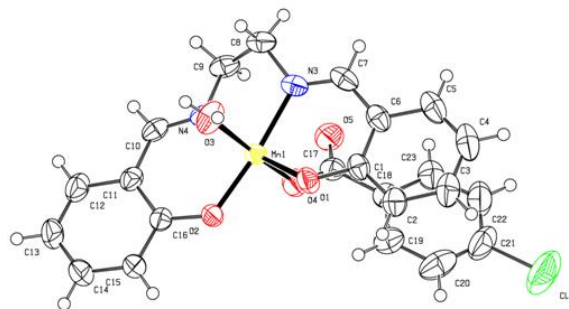


Figure 1. Molecular structure of **1**. Thermal ellipsoids are drawn at 50 % probability level.

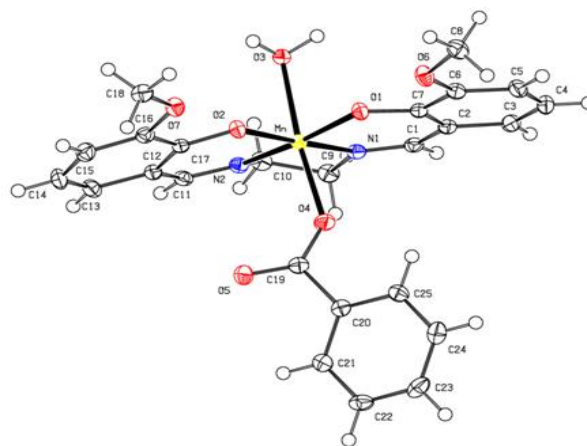


Figure 2. Molecular structure of **2**. Thermal ellipsoids are drawn at 50 % probability level.

Table 1. Crystal data and structure refinement for **1**, **2**.

Complex	1	2
Empirical formula	C ₂₃ H ₂₀ ClMnN ₂ O ₅	C ₂₅ H ₂₅ MnN ₂ O ₇
Formula weight	494.80	520.41
<i>T</i> (K)	296 (2)	100(2)
Wavelength (Å)	0.71073	1.54178
Crystal system	Monoclinic	Triclinic
Space group	<i>P</i> 21/ <i>n</i>	<i>P</i> -1
<i>a</i> (Å)	6.8060(4)	8.3366(1)
<i>b</i> (Å)	10.6760(6)	11.6426(2)
<i>c</i> (Å)	29.1458(16)	12.3893(2)
α (°)	90.00	100.064(1)
β (°)	90.451 (1)	97.230(1)
γ (°)	90.00	103.937(1)
<i>V</i> (Å ³)	2117.7 (2)	1131.26(3)
<i>Z</i>	4	2
ρ_{calc} (g cm ⁻³)	1.552	1.528
μ (mm ⁻¹)	0.79	5.187
<i>F</i> (000)	1016	540
$\theta_{\text{min/max}}$ (°)	1.4/28.1	3.68 /67.36
Total data	19400	9369
Unique data	5135	3694
<i>R</i> _{int}	0.023	0.016
Restraints/parameters	0/297	0/319
Goodness-of-fit (GOF)	1.12	1.085
Final <i>R</i> indices	<i>R</i> ₁ = 0.0520	<i>R</i> ₁ = 0.0286
[<i>I</i> > 2σ(<i>I</i>)]	<i>wR</i> ₂ = 0.0583	<i>wR</i> ₂ = 0.0299
<i>R</i> indices (all data)	<i>wR</i> ₂ = 0.1232	<i>R</i> ₁ = 0.0849
	<i>R</i> ₁ = 0.1283	<i>wR</i> ₂ = 0.086

$$R_1 = \Sigma(|F_o| - |F_c|) / \Sigma(|F_o|), wR_2 = \{ \Sigma[w(F^2 - F_c^2)^2] / \Sigma[w(F_o^2)^2] \}^{1/2}$$

$$w = 1 / [\sigma^2(F_o^2) + (0.0306P)^2 + 2.7747P], \text{ where } P = (F_o^2 + 2F_c^2) / 3$$

Solid state structures 1 and 2

Occupation of the *trans* coordination sites by carboxylate and water enable molecules of complexes **1** and **2** to recognize one another and spontaneously generate supramolecular architectures in the solid state through non-covalent interactions like hydrogen bonding. Carboxylate and water of adjacent [Mn(salen)(*p*-ClC₆H₄CO₂)H₂O] molecules meet in a nearly end on fashion along a screw (2₁) axis, in the crystal structure of complex **1**, resulting in hydrogen bonding interactions (O5---H1A = 1.95 Å; O3---O5 = 2.70 Å) that beget a helical chain parallel to the (001) plane (Figure 3). The intra-chain Mn---Mn distance is 6.49 Å.

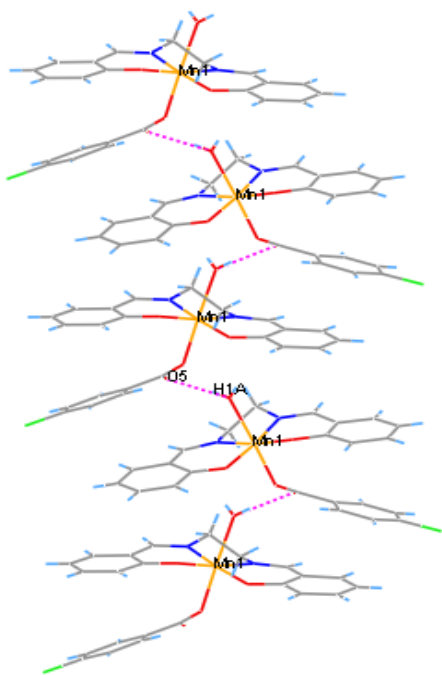


Figure 3. Helical chain of [Mn(salen)(*p*-ClC₆H₄CO₂)H₂O] (**1**) molecules parallel to the (001) plane; H-bonds (---).

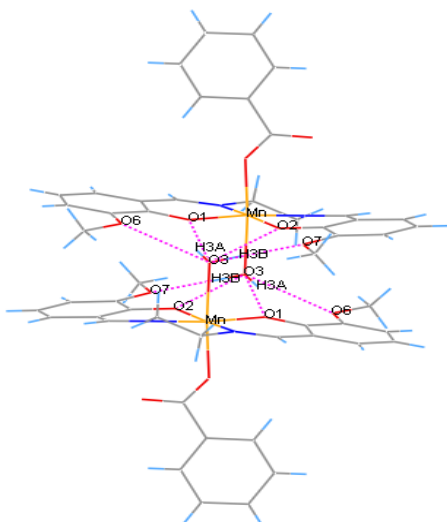


Figure 4. Section of the crystal structure of **2** showing the formation of a μ -aqua dimer; H-bonds (---)

The presence of extra methoxy groups on the Schiff base in complex **2**, afford four proximate recognition sites for each water molecule on the nearby asymmetric unit in the solid state structure. A face on approach of the coordinated water molecules in adjacent [Mn(msalen)(C₆H₅CO₂)H₂O] molecules help the aqua hydrogens, H3A (O3---O1 = 2.86 Å; O3---O6 = 3.03 Å) and H3B (O3---O2 = 2.66 Å; O3---O7 = 2.95 Å), to connect with the methoxy and phenoxy oxygens of the Schiff base through bifurcated hydrogen bonds generating a discrete supramolecular μ -aqua dimer with a Mn---Mn distance of 4.81 Å (Figures 4 and 5). The Schiff base aryl rings are involved in face-to-face (offset) π - π stacking interactions with a centroid to centroid distance of 3.99 Å and a dihedral angle (α) of 12.03°, that offer extra stabilization to the crystal structure. A survey of literature confirm that the formation of such dimers, stabilized by non-covalent interactions is not a rare feature in manganese(III)-Schiff base chemistry.^{14,27-28}

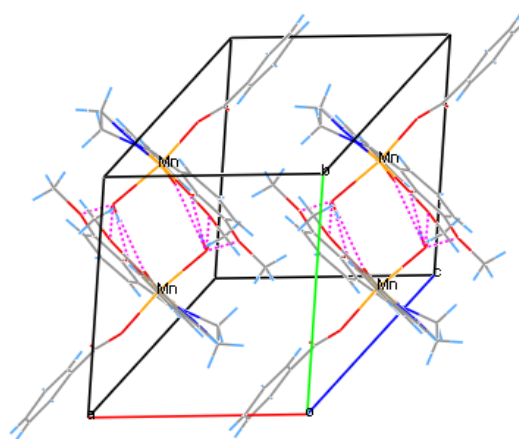


Figure 5. Crystal structure of **2** showing the close packing of μ -aqua dimers.

Conclusions

Manganese(II) carboxylate and Schiff bases generated *in situ* under aerobic conditions gave manganese(III) Schiff base complexes with supporting carboxylate ligands. The template reactions offer an easy route for the introduction of carboxylate and water as capping ligands in the octahedral complexes of manganese(III). Solid state structures reveal that the presence of these ligands at axial positions, leads to significant levels of non-covalent interactions in these complexes.

Acknowledgements

The authors are grateful to Prof. M. V. Rajasekharan, University of Hyderabad, India and Prof. R. Lalancette, Rutgers University, Newark, USA, for X-ray diffraction analysis.

Supplementary material

CCDC 914840 and CCDC 896929 contain the supplementary crystallographic data for this paper. These data can be obtained free of charge via <http://www.ccdc.cam.ac.uk/conts/retrieving.html> or from the Cambridge Crystallographic Data Centre (CCDC), 12, Union Road, Cambridge CB2 1EZ, UK; fax: +44 1223 336033; email: [http://deposit@ccdc.cam.ac.uk](mailto:deposit@ccdc.cam.ac.uk). Appendices A and B contain infra red and UV-Vis spectra of the complexes.

References

- ¹Weatherburn, D. C., Mandal, S., Mukhopadhyay, S., Bhaduri, S., Lindoy, L. F., *Comprehensive Coordination Chemistry II*, McCleverty, J. A., Meyer, T. J., Ed., 5, 1-125, Elsevier, Amsterdam, Netherlands, **2003**.
- ²Vites, J. C., Lynam, M. M., *Coord. Chem. Rev.*, **1998**, 169(1), 153-186.
- ³Wu, A. J., Penner-Hahn, J. E., Pecoraro, V. L., *Chem. Rev.*, **2004**, 104(2), 903-938.
- ⁴Brudvig, G. W., *Phil. Trans. B*, **2008**, 363, 1211-1218.
- ⁵Mullins, C. S., Pecoraro, V. L., *Coord. Chem. Rev.*, **2008**, 252(3-4), 416-443.
- ⁶Christou, G., *Polyhedron*, **2005**, 24, 2065-2075.
- ⁷Bagai, R., Christou, G., *Chem. Soc. Rev.*, **2009**, 38, 1011-1026.
- ⁸Aromi, G., Aguila, D., Gamez, P., Luis, F., Roubeauc, O., *Chem. Soc. Rev.*, **2012**, 41, 537-546.
- ⁹Jacobsen, E. N., *Catalytic Asymmetric Synthesis*, I. Ojima, Ed., 159-202, VCH, New York, USA, **1993**.
- ¹⁰Larrow, J. F., Jacobsen, E. N., *Topics Organomet. Chem.*, **2004**, 6, 123-152.
- ¹¹Aurangzeb, N., Hulme, C. E., McAuliffe, C. A., Pritchard, R. G., Watkinson, M., Garcia-Deibe, A., Bermejo, M. R., Sousa, A., *J. Chem. Soc. Chem. Comm.*, **1992**, 1524-1526.
- ¹²Hulme, C. E., Watkinson, M., Haynes, M., Pritchard, R. G., McAuliffe, C. A., Jaiboon, N., Beagley, B., Sousa, A., Bermejo, M. R., Fondo, M., *J. Chem. Soc., Dalton Trans.*, **1997**, 1805-1814.
- ¹³Watkinson, M., Fondo, M., Bermejo, M. R., Sousa, A., McAuliffe, C. A., Pritchard, R. G., Jaiboon, N., Aurangzeb, N., Naeem, M., *J. Chem. Soc. Dalton Trans.*, **1999**, 31-42.
- ¹⁴Bermejo, M. R., Fernández, M. I., González-Noya, A. M., Maneiro, M., Pedrido, R., Rodríguez, M. J., García-Monteagudo, J. C., Donnadiou, B., *J. Inorg. Biochem.*, **2006**, 100(9), 1470-1478.
- ¹⁵Biswas, S., Dutta, A. K., Mitra, K., Dul, M. -C., Dutta, S., Lucas, C. R., Adhikary, B., *Inorg. Chim. Acta*, **2011**, 37(1), 56-61.
- ¹⁶Vázquez-Fernández, Á., Bermejo, M. R., Fernández-García, M. I., González-Riopedre, G., Rodríguez-Doutón, M. J., Maneiro, M., *J. Inorg. Biochem.*, **2011**, 105(12), 1538-1547.
- ¹⁷Kar, P., Biswas, R., Drew, M. G. B., Ida, Y., Ishida, T., Ghosh, A., *Dalton Trans.*, **2011**, 3295-3304.
- ¹⁸Benetollo, F., Peruzzo, V., Tamburini, S., Vigato, P. A., *Inorg. Chem. Comm.*, **2012**, 84-87.
- ¹⁹Pecoraro V. L., Butler, W. M., *Acta Cryst. C*, **1986**, 42, 1151-1154.
- ²⁰Shyu, H. -L., Weib, H. -H., Wang, Y., *Inorg. Chim. Acta*, **1999**, 290(1), 8-13.
- ²¹Panja, A., Shaikh, N., Ali, M., Vojtišek, P., Banerjee, P., *Polyhedron*, **2003**, 22 (9), 1191-1198.
- ²²Darensbourg, D. J., Frantz, E. B., *Dalton Trans.*, **2008**, 37, 5031-5036.
- ²³Mukherjee, P., Kar, P., Ianelli, S., Ghosh, A., *Inorg. Chim. Acta*, **2011**, 365(1), 318-324.
- ²⁴Sheldrick, G. M., *SHELXS-97. Program for Crystal Structure Analysis*, University of Gottingen, Goettingen, Germany, **1997**.
- ²⁵Spek, A. L. *J. Appl. Cryst.*, **2003**, 36, 7-13.
- ²⁶Macrae, C. F., Edgington, P. R., McCabe, P., Pidcock, E., Shields, G. P., Taylor, R., Towler, M. van de Streek, J., *J. Appl. Cryst.*, **2006**, 39(3), 453-457.
- ²⁷Vázquez-Fernández, M. Á., Fernández-García, M. I., González-Noya, A. M., Maneiro, M., Bermejo, M. R., Rodríguez-Doutón, M. J. *Polyhedron*, **2012**, 31, 379-385.
- ²⁸Bhowmik, P., Nayek, H. P., Corbella, M., Aliaga-Alcalde, N., Chattopadhyay, S., *Dalton Trans.*, **2011**, 7916-7926.

Received: 30.03.2014.
Accepted: 17.04.2014.



EFFECT OF AGING ON THE RHEOLOGICAL PROPERTIES OF THE MODIFIED ASPHALT-RUBBER SYSTEM USING MICROWAVE TECHNIQUE

Khalid A. Owaid^{[a]*}

Keywords: asphalt; rheological properties; effect of aging; microwave treatment; anhydrous aluminium chloride

The present work aimed to study the effect of aging on asphalt-rubber system after 12 month of the preparation process. The rheological properties of Qaiyarah asphalt were improved with using reclaimed rubber tires treated with anhydrous aluminium chloride. The reclaimed rubber tire samples in 0.5 and 1.0 % of the total amount of the asphalt (the amount of used anhydrous aluminium chloride catalyst was 0.06, 0.12, 0.25, 0.5, 1 %, respectively) were added to Qaiyarah asphalt sample. The reaction components were introduced into a microwave oven operating at 360 W power for 5, 10 and 15 minutes, respectively. The rheological properties including ductility, penetration, softening point and penetration index were measured before and after aging experiments. It was found that the modified asphalt exposed to atmospheric conditions has lower damage in comparison with untreated one and the longer treatment time was used the less crack and the larger resistance were achieved.

*Corresponding author

E-Mail: k_owaid@yahoo.com

[a] Chemistry Department, Education College, Mosul University, Iraq

Introduction

Asphalt is an extremely complex mixture and contains a large number of hydrocarbons with variable molecular weight ranging between 400 and 5000 g mol⁻¹. Its viscosity increases very much with decreasing temperature. Asphalt components interact with each other by strong physical and chemical forces resulting in its homogeneous look.¹ The asphalt properties can be improved by different ways, e.g. by mixing with polymers additives which is one of the most common modification method.² Polymeric materials lead to hardening of the asphalt, improves its performance at low temperatures and resistance toward higher temperatures and improve its adhesion and cohesion properties as well.³

The rheological properties of asphalt change due to oxidation of hydrocarbons when it is exposed to the sunlight. The formation of free radicals leads to reactions that produce higher molecular weight components than those existed in the starting asphalt. This results in increasing the hardness and softening point and in reducing the values of ductility and penetration.⁴

The asphalt samples modified with rubber tires and styrene-butadiene rubbers after 12 months of aging time showed that prolonging the period of aging reduces the ductility, hardening and polymer breaking.⁴ Saleh studied the effect of asphaltene additives on the properties of Begi and Qaiyarah asphalts. The increase in homogeneity for both asphalt types and improvement in ageing specifications for Qaiyarah asphalt⁵ could be detected after 18 months of aging compared with untreated asphalt

Anjan and Veeragavan studied mixing of various additives with asphalt to improve its the mechanical properties.⁶ Alfi modified the properties of Begi and Qaiyarah asphalts by

using polymers such as polystyrene resins, melamine-formaldehyde and poly(methyl methacrylate) with or without aluminium chloride as the catalyst using microwave technique.

Changes in the rheological properties were proved to be advantageous, e.g. excellent values of flow and stability could be detected.⁷

Experimental

A Tokiwa 900 W microwave oven (500 MHz, Germany) was used for the ductility and penetration measurements according to the ASTM D5-83⁸ and the ASTM D36-70 standards.⁹ Softening point measurement were conducted in accordance with the specifications of ASTM D5-85 standrd.¹⁰

Qaiyarah crude asphalt was produced in Al-Qaiyarah refinery in Iraq. Reclaimed rubber tires, produced by Babylon Tyres Industry, were ground into ~1.0 mm granules (isoprene rubber content was ~40 %).¹¹ Anhydrous aluminum chloride was supplied by Fluka.

Thermal gravimetric analysis of rubber

One gram of reclaimed crushed rubber tyres granule, s (~1 mm in size) placed into a ceramic crucible and covered with aluminium foil, were heated between 50-600 °C (with 50 °C intervals). The results are given in the Table 1 and Fig 1.

Rubber preparation

Reclaimed rubber tires were thermally crushed before interaction with asphalt material in an electric oven at 350 °C for one hour and cooled at room temperature before crushing it in a mortar.

Table 1. Thermal analysis of reclaimed rubber tires.

Weight (g)	Temperature (°C)
1*	0
0.9996	50
0.9962	100
0.9852	150
0.9532	200
0.9223	250
0.8962	300
0.6493	350
0.6100	400
0.4640	450
0.1652	500
0.0523	550
0.0094	600

*Net weight

Modification of the rheological properties of asphalt by catalytic treatment

A 250 g of asphalt sample was heated up to 100 °C then crushed and mixed with either reclaimed rubber tyre granules (0.5 and 1.0 %) or anhydrous aluminium chloride (0.06, 0.12, 0.25, 0.5 and 1.0 %). The prepared samples were heated in the microwave oven for 5, 10 and 15 min. The ductility,⁸ penetration,⁹ softening point¹⁰ and penetration index¹² of the sample were measured.

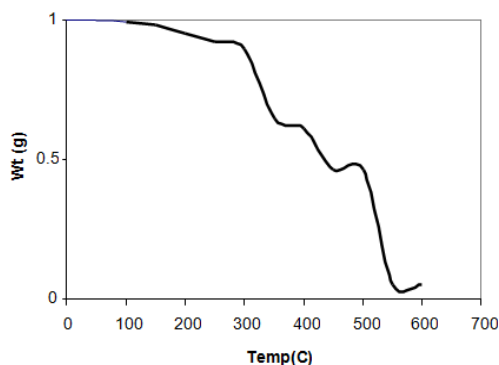
Effect of ageing time

The effect of ageing time under atmospheric condition was evaluated by measuring the ductility,⁸ penetration,⁹ softening point¹⁰ and penetration index¹² values. The measurements were repeated after 12 months.

Results and Discussion

Thermal treatment of reclaimed rubber tires

The reclaimed rubber tire granules were used as additive to modify the properties of asphalt which was thermally treated at 350 °C for 1 h. The weight loss of rubber sample at various temperatures is given in Table 1 and Fig.1.

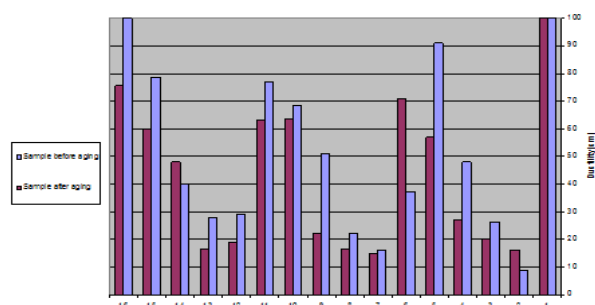
**Figure 1.** The weigh loss of reclaimed rubber tires at diffrenet temperatures

Modification of the rheological properties of asphalt

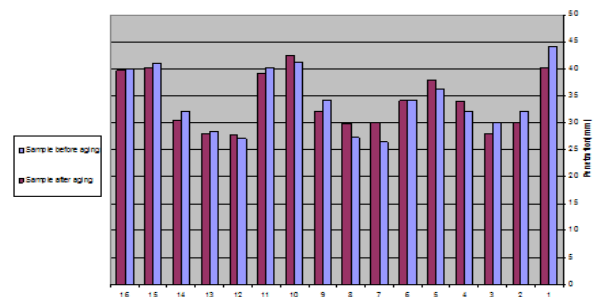
The properties of asphalt modified by reclaimed rubber tire granules in presence of catalytic amount of anhydrous aluminium chloride are given in Tables 2 and 3. The asphalt modified in this way has considerable resistance to ageing. Using more than 1 % of reclaimed rubber tires provides heterogeneity in the produced asphalt mixture. The 360 W power of microwave oven used was to be selected in order to ensure homogeneous dissolving of the components. The use of higher power caused hardening of the sample, decrease in ductility and penetration, and increase in the softening point.

The anhydrous aluminium chloride (AlCl_3) was selected as a Lewis acid catalyst in order to ensure appropriate conditions to react the appropriate components with each other.^{14,15}

(a)



(b)



(c)

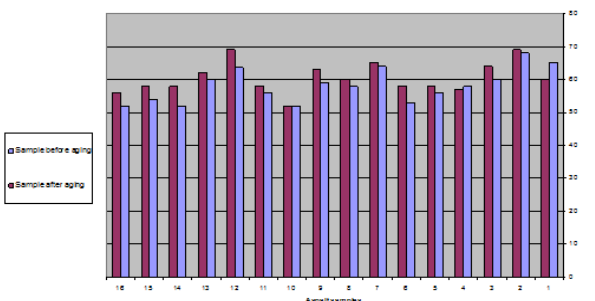
**Figure 2.** The rheological properties of reclaimed tires rubber before and after ageing of modified asphalt (0.5%) with different percentage of anhydrous aluminium chloride at (360) watt for different time intervals. (a) ductility of asphalt samples; (b) penetration of asphalt samples; (c) softening point of asphalt samples.

Table 1. Rheological properties of modified asphalt (0.5 % of reclaimed tires rubber with different percent of anhydrous aluminum chloride) samples heated at 360 W microwave power for different time intervals, before and after aging.

AlCl ₃ wt%	Time, min	Ductility at 25 °C, 5 cm min ⁻¹			Penetration at 25 °C, 100g, 5 s			Softening point, ring and ball			Penetration index, PI		
		Before	After	Δ	Before	After	Δ	Before	After	Δ	Before	After	Δ
0	0	+100	+100	0	44.2	40.2	4	65.0	60.0	5	1.662	0.506	1.156
1	5	9.0	16.3	-7.3	32.1	30.1	2	68.0	69.0	-1	1.434	1.456	-0.022
0.5	5	26.4	20.0	6.4	30.0	28.0	2	60.0	64.0	-4	-0.122	0.466	-0.588
0.25	5	48.0	27.3	20.7	32.2	34.0	-1.8	58.0	57.0	1	-0.365	-0.455	0.09
0.12	5	91.0	57.0	34	36.2	38.0	-1.8	56.0	58.0	-2	-0.529	-0.016	-0.513
0.06	5	37.3	71.0	-33.7	34.2	34.1	0.1	53.0	58.0	-5	-1.291	-0.248	-1.043
1	10	16.1	15.0	1.1	26.5	30.0	-3.5	64.0	65.0	-1	0.405	0.782	-0.377
0.5	10	22.0	16.5	5.5	27.2	29.8	-2.6	58.0	60.0	-2	-0.695	-0.135	-0.56
0.25	10	51.0	22.3	28.7	34.2	32.2	2	59.0	63.0	-4	0.044	0.579	-0.535
0.12	10	68.4	63.8	4.6	41.2	42.5	-1.3	52.0	52.0	0	-1.138	-1.073	-0.065
0.06	10	77.0	63.0	14	40.2	39.2	1	56.0	58.0	-2	-0.307	0.052	-0.359
1	15	29.0	19.2	9.8	27.0	27.8	0.8	63.5	69.0	-5.5	0.303	1.287	-0.984
0.5	15	28.0	16.4	11.6	28.4	28.0	0.4	60.0	62.0	-2	-0.231	0.109	-0.34
0.25	15	40.0	48.0	-8.0	32.2	30.5	1.7	52.0	58.0	-6	-1.629	-0.475	-1.154
0.12	15	78.5	60.0	18.5	41.0	40.2	1	54.0	58.0	-4	-0.696	0.108	-0.804
0.06	15	+100	75.6	24.4	40.0	39.7	0.3	52.0	56.0	-4	-1.201	-0.334	-0.867

Table 3. Rheological properties of modified asphalt (1.0 % of reclaimed tires rubber with different percent of anhydrous aluminium chloride) samples heated at 360 W microwave power for different time intervals, before and after aging.

AlCl ₃ wt%	Time, min	Ductility at 25 °C, 5 cm min ⁻¹			Penetration at 25 °C, 100g, 5 s			Softening point, ring and ball			Penetration index, PI		
		Before	After	Δ	Before	After	Δ	Before	After	Δ	Before	After	Δ
0	0	+100	+100	0	44.2	40.2	4	65.0	60.0	5	1.662	0.506	1.156
1	5	12.2	13.2	-1	26.2	30.0	-3.8	64.0	65.0	-1	0.331	0.782	-0.451
0.5	5	18.7	27.0	-8.3	32.0	30.2	1.8	56.0	60.0	-4	-0.783	-0.108	-0.675
0.25	5	23.3	35.4	-12.1	32.2	32.0	0.2	55.0	60.0	-5	-0.977	0.009	-0.986
0.12	5	31.5	56.2	-24.7	33.7	33.0	0.7	50.0	61.0	-11	-2.000	0.264	-2.264
0.06	5	56.0	50.0	6	34.4	32.0	2.4	57.0	57.0	0	-0.429	-0.579	0.15
1	10	12.0	15.7	-3.7	27.5	25.0	2.5	56.0	64.0	-8	-1.075	0.240	-1.315
0.5	10	19.0	17.3	1.7	33.2	30.5	2.7	58.0	62.0	-4	-0.304	0.284	-0.588
0.25	10	23.0	38.0	-15	31.6	33.7	-2.1	54.0	60.0	-6	-1.229	0.120	-1.349
0.12	10	53.0	33.0	20	34.2	32.0	2.2	57.0	60.0	-3	-0.443	0.009	-0.452
0.06	10	50.0	35.0	15	37.2	36.0	1.2	53.0	59.0	-6	-0.899	0.064	-0.963
1	15	13.0	12.5	0.5	31.2	28.5	2.7	58.0	62.0	-4	-0.430	0.146	-0.576
0.5	15	26.0	20.5	5.5	34.2	31.4	2.8	60.0	60.0	0	0.149	0.004	0.145
0.25	15	17.1	32.0	-14.9	30.5	31.9	-1.4	58.0	60	-2	-0.476	0.005	-0.481
0.12	15	52.0	44.0	8	29.2	30.0	-0.8	55.0	54.0	1	-1.168	-1.326	0.158
0.06	15	40.0	39.5	0.5	35.7	36.0	-0.3	54.0	57.0	-3	-0.985	-0.337	-0.648

It can be seen from the results in Tables 2 and 3 or Figures 2 and 3 that most of the modified asphalt samples that were subjected to ageing do not show substantial changes in their important properties. It is an advantageous result indicating that the samples of modified asphalts resisted large stresses and cracks. It ensures long operational life which does not alter importantly with aging. Using reclaimed rubber tires in this form as additives improves the mechanical properties via increasing the durability, reducing stresses and thermal cracking and increasing resistance towards forming grooves.^{16,17} This phenomenon might be the direct consequence of the presence of high amount of carbon black in reclaimed rubber which can increase the life and resistance of rubber materials against oxidation and sunlight.

The sulfur compounds, that exist as original components in the mixture of Qaiyarah crude asphalt in a relative high percentage (about 7 %), play an important role in the resistance of asphalt towards oxidation because these compounds act as free radical scavenger,^{1,18,19} and antioxidants thereby these can prevent the asphalt against free-radical accelerated oxidation processes.

Based on the results given in Tables 2 and 3 some samples were selected for engineering test for making paving asphalt. Some other samples characterized with high softening point and low values of penetration and ductility qualified in the production of moisture insulation material and some samples were tested as flattening asphalt.

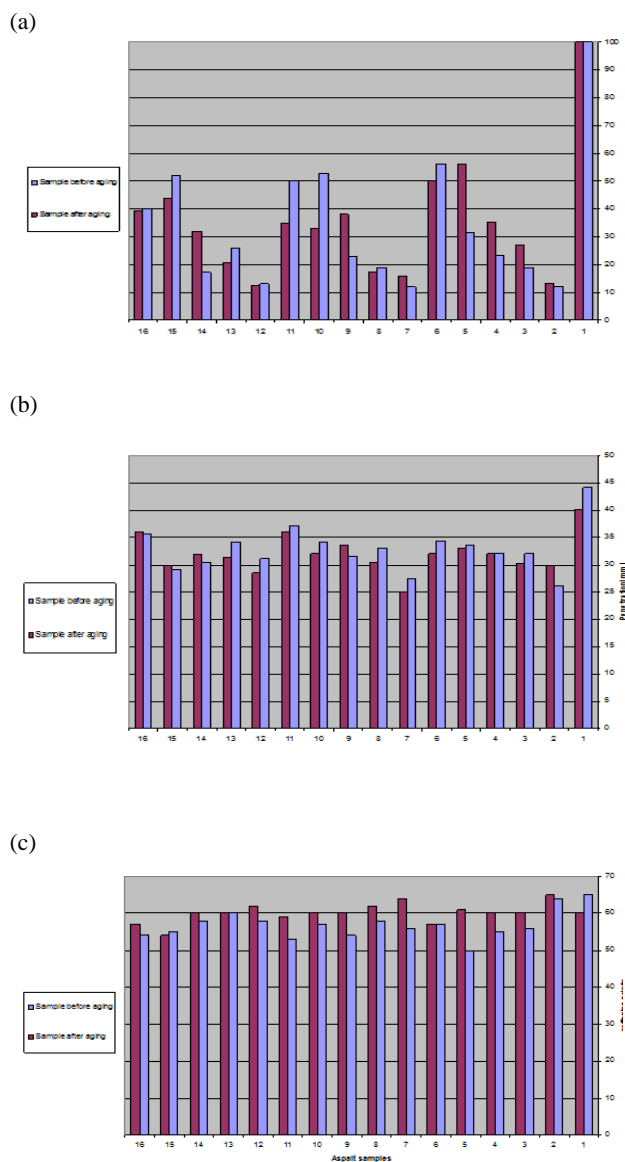


Figure 3. Rheological properties before and after ageing of modified asphalt (1 %) of reclaimed tires rubber with different percent of anhydrous aluminum chloride, at (360) watt for different time intervals. (a) ductility of asphalt samples; (b) penetration of asphalt samples; (c) softening point of asphalt samples.

The values of penetration, ductility and softening point of the asphalt which can be used for mastic insulator²⁰ to moisture, for flatness²¹ and for paving²² can be found in the appropriate American Standards (ASTM) descriptions.

Conclusion

The microwave energy is used to reduce the modification time from hours to minutes by making modified rubber asphalts in the presence of aluminium chloride or other Lewis acid catalysts. This microwave treatment decreased the amount of evolved pollutant gases during the treatment and thereby reduced the environmental pollution.

The thermal sensitivity was found to be correlated with the Penetration index (PI) values between +2 and -2. This shows the increasing thermal stability of the end products.

In addition, using of small amount of reclaimed rubber tyres into asphalt makes the system to be more homogenous and improves the asphalt resistance against weather conditions.

References

- ¹Aldboni, E. A. and Ali, H. A., *Petroleum Origin, Structure and Technology*, National Library for Printing and Publishing, University of Mosul, **1986**
- ²Shirkav, B. H., *Iranian Polym. J.*, **2010**, *19(5)*, 363-373.
- ³Awwad, M. T. and Shabeeb, L., *J. Appl. Sci.*, **2007**, *4*, 390-396.
- ⁴Yonghong, R. Richard, R. D. and Charles, J. G., *Fuel.*, **2003**, *82*, 1763-1773 .
- ⁵Saleh, I. A., *J. Sci. Raff.*, **1999**, *10(2)*, 16-25.
- ⁶Anjan, S. and Veeraragavan, A., *Construct. Build. Mater.*, **2010**, *24(11)*, 2041-2100 .
- ⁷Alfi, R. N., **2011** , Msc. Thesis, University of Mosul.
- ⁸ASTM, Part II, (D₃₆₋₇₀), **1972**, p.27.
- ⁹ASTM, Section 4, (D₅₋₈₃), **1986**, p .97.
- ¹⁰ASTM, Section 4, (D₅₋₈₅), **1986**, p.127.
- ¹¹Otaioa, S. D., Nema, A. E. and Abdul Karim, H. A., *The Ministry of Industry and Minerals, General Company for the Tire Industry, R & D (Iraq)*, **2009** .
- ¹²Traxler, R. N., "Asphalt, its Composition, Properties and Uses, Hall Ltd., London, **1961**, *3*, 72-73.
- ¹³Toohi, H. T., **2013**, MSc. Thesis, University of Mosul.
- ¹⁴Lylla, N. M., **1999**, MSc. Thesis, University of Mosul.
- ¹⁵Saleh, L. A., **1992** , MSc. Thesis, University of Mosul.
- ¹⁶Becker, Y., Menderz, M. P. and Rodriguez, Y., *Vision Technol.*, **2001**, *9(1)*, 39-50 .
- ¹⁷Navarro, F. J., Partal, P. and Martinez, B. F., *Fuel*, **2004**, *83*, 2041-2049 .
- ¹⁸Mahmoud, I. A., **2002**, Msc. Thesis, King Fahd of Petroleum and Minerals.
- ¹⁹"Introduction to Asphalt", The Asphalt Institute, **1967**, 6th ed., Manual series, *5*, 7-15 .
- ²⁰ASTM, Part II,(D₄₉₁₋₄₁), **1969**, 250-251.
- ²¹*Iraqi General Agency for Measurements and Quality Control*, **1988**, No. 1196
- ²²*Iraqi Specification of the Roads and Bridges the (S.O.R.B)*, Ministry of Housing and Reconstruction, Studies Department and Designs, **2001**, Baghdad.

Received: 27.03.2014.
Accepted: 28.05.2014.



NATURALLY OCCURRING CLAY, MONTMORILLONITE, AS A DRUG DELIVERY VEHICLE FOR IN VITRO EXTENDED RELEASE OF VENLAFAXINE HYDROCHLORIDE

Shilpa Jain^[a] and Monika Datta^{[a]*}

Keywords: Venlafaxine hydrochloride; montmorillonite; oral drug delivery

In the present work, a naturally occurring smectite group clay mineral, montmorillonite, (Mt) has been explored as a vehicle for delivery of an antidepressant drug Venlafaxine hydrochloride, VF. The effect of pH of the drug solution, time and initial drug concentration on drug loading capacity of Mt has been studied. The adsorption isotherm was fitted by the Langmuir model and follows the pseudo-second-order kinetics. The synthesized Mt-VF complexes were characterized by XRD, FTIR, TGA, DSC etc. VF was found to be intercalated in the Mt layers. The release profile of the VF and Mt-VF complex in simulated gastric and intestinal fluids has been discussed. The release behaviour of VF from Mt-VF complexes appears to be sustained/extended for a period of 12 h and reaches upto 52 % in simulated gastric fluid and is stable in intestinal fluid where as pure VF completely gets released in 5.5 h and 3.5 h in simulated gastric and intestinal fluid respectively. Out of all kinetic models used to elucidate the drug release mechanism, the best fitting was observed for first order model. On the basis of present studies it can be stated that the synthesized Mt-VF complexes have the potential for developing in to a sustained release formulation for oral drug delivery of an anti-depressant drug VF. This shows a path which can reduce doses substantially from 4 times in 24 h to twice in 24 h.

* Corresponding Authors

E-Mail: monikadatta_chem@yahoo.co.in

[a] Analytical Research Laboratory, Department of Chemistry, University of Delhi, Delhi 110007, India

It is a GRAS grade FDA approved clay and has attracted great interest from researchers. It belongs to the 2:1 smectite group of clay minerals.

INTRODUCTION

Clay minerals possessing layered structure are known to exhibit properties such as good water absorption, swelling and cation exchange ability which are considered beneficial for the synthesis of pharmaceutical products, both as inactive and active substances.¹⁻³ Clay minerals being natural cation exchanger can bind with cationic drugs via electrostatic interaction. These properties have encouraged the use of clay minerals for developing drug delivery vehicle for extended release of drugs.⁴⁻¹⁰ Pharmaceutical preparations, using minerals as carrier-releasers of active ingredients, can generally be administered orally to the patient there by making them a preferred choice for oral drug delivery vehicle.¹¹

Montmorillonite (Mt), also known as medical clay, is a potent detoxifier that can adsorb dietary and bacterial toxins.¹²⁻¹⁴

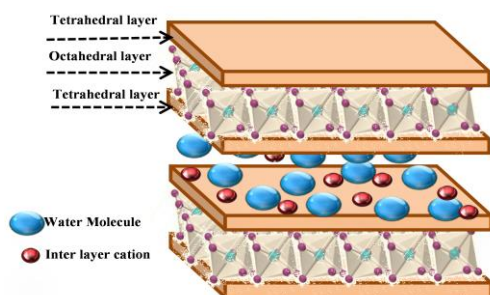


Figure 1. Structural representation of hydrated Mt general formula $M^{x+y}(Al_{2-x})(OH)_2(Si_{4-y}Al_y)O_{10}$

It has large specific surface area, good adsorption and cation exchange capacity. Mt is known to intercalate various protonated and hydrophilic organic molecules, which can be released in a controlled manner by replacement with other kind of cations in the release media.¹⁵⁻¹⁷ Drug intercalated Mt formulations offer a novel route to prepare organic and inorganic complexes that contain advantageous properties of both the inorganic host and organic guest in a single material.¹⁸⁻²⁰ (Fig. 1)

Belonging to the third generation antidepressant drugs Venlafaxine hydrochloride (Fig. 2) inhibits reuptake of serotonin, norepinephrine and, to a lesser extent, dopamine. It is a white crystalline solid which is highly soluble in water ($>500 \text{ mg mL}^{-1}$).²¹⁻²² Due to the short steady state elimination half-life (4-5 h) the drug has to be administered 2 to 3 times in 24 h so as to maintain required concentration of the drug in the blood plasma. The dose of VF ranges from 75 to 350 mg d^{-1} .²³ The available two formulations for this drug namely immediate and extended release formulations have various side effects and certain drawbacks such as, slow release characteristics, instability in high acidic conditions.²⁴ Therefore an effective oral drug delivery system is needed to overcome these drawbacks and to improve the clinical treatment process which is capable of maintaining the therapeutic concentration over a longer period of time. Therefore an oral drug delivery system with extended release characteristics can prove to be more patient compliant.²⁵⁻²⁶

The objective of the present work is to develop and characterize VF loaded Mt-VF complex as a controlled drug delivery system for oral administration of VF.

There is no report, to the best of our knowledge, on the preparation of VF intercalated Mt complexes for the oral extended delivery of VF.

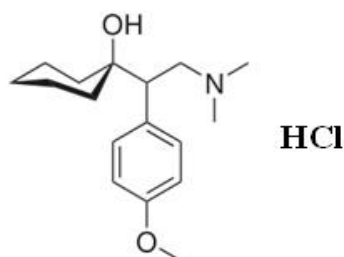


Figure 2. Structural representation of Venlafaxine hydrochloride (VF)

Therefore, the aim of our work was to undertake a systematic and detailed investigation on adsorption and optimization of conditions for preparing Mt-VF complexes for sustained release formulations. The effect of pH, time and initial drug concentration on drug intercalation capacity of Mt has been evaluated. Thus the developed Mt-VF complexes have the potential to be used as an oral extended delivery of VF for the patients requiring medicinal treatment around the clock.

EXPERIMENTAL

Materials

Montmorillonite (KSF) was procured from Sigma Aldrich (USA) and Venlafaxine hydrochloride (purity >98%) was gift from Ami life sciences Pvt. Limited, Maharashtra. Analytical grade sodium hydroxide, potassium dihydrogen phosphate, hydrochloric acid and potassium chloride for the preparation of drug release media were obtained from Merck Chemicals Ltd (India). Water used in the experiments was deionized and filtered (Milli-Q Academic, Millipore, France).

Effect of pH on absorption spectrum of VF

Initially the stability behaviour of VF was studied in the pH range 1-12 (Fig. 3).

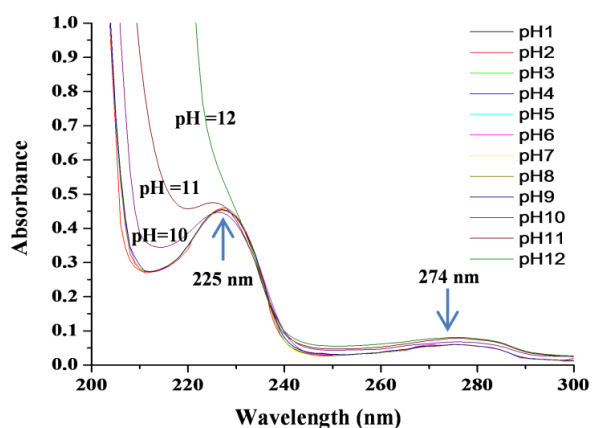


Figure 3. UV-Visible spectra of aqueous VF solution (10 ppm) showing effect of pH

Drug loading capacity of Mt for VF

In order to determine the conditions for maximum loading of VF on Mt, effect of various parameters such as contact time, pH and initial concentration of VF were investigated using batch extraction method. As the drug was not stable beyond pH 9 therefore the influence of pH on loading of VF on Mt was studied with in pH range of 1-9 at 25 °C. Initially a stock solution of the drug, 1000 $\mu\text{g mL}^{-1}$, was prepared. 5 mL of this solution containing 5000 μg of drug was taken in a 100 mL volumetric flask containing 100 mg of Mt. Then solution was maintained at various pH 1-9 and the volume was made upto 25 mL. The resulting dispersion was put on continuous mechanical shaking (Khera instruments).

The dispersion was centrifuged at 25,000 rpm for 30 min at room temperature (Sigma centrifuge). The free VF concentration in the supernatant was determined using UV-visible spectrophotometer (Analytic Jena) from the Lambert-Beer's plot and the percentage of the drug loaded was calculated using Equation (1)

$$\phi = \frac{C_i - C_e}{C_i} \quad (1)$$

where

C_i is the initial drug concentration (mg L^{-1}) and

C_e is the concentration of the drug (mg L^{-1}) in the supernatant at the equilibrium stage.

The amount of drug adsorbed q_e (mg g^{-1}) was calculated via the mass-balance relationship as per Equation (2)

$$q_e = (C_i - C_e) \frac{V}{m} \quad (2)$$

where

V (in L) is the volume of the reaction media and

m is the mass of Mt (in g) used for the studies.

The pH where the loading of drug on Mt was maximum was chosen to perform time dependent and adsorption kinetic studies in the time period of 0.25 h to 24 h, keeping all the other parameters constant.

Once the optimal time for highest uptake of drug was obtained, adsorption equilibrium studies of VF in the concentration range of 16 to 720 mg L^{-1} (400 μg -18000 μg) were carried out maintaining other obtained best pH and time.

Characterizations

The samples were analyzed and characterized using suitable analytical techniques discussed under appropriate headings.

UV- Visible spectrometry

UV-Visible absorbance of the supernatant solutions was measured at λ_{\max} = 225 nm (UV- Visible spectrophotometer Analytic Jena) equipped with a quartz cell having a path length of 1 cm.

X-ray Diffraction

Powder X-ray diffraction (PXRD) measurements of samples were performed on a powder X-ray diffractometer (D8 DISCOVER BRUKER AXS, Germany) the measurement conditions were Cu α radiation generated at 40 kV and 40 mA as X-ray source 2-40° (2 θ) and step angle 0.02° s⁻¹.

Thermal Analysis

The effect of Mt content on thermal stability of Mt-VF-complex was assessed by the thermogravimetric analyzer (TGA 2050 Thermal gravimetric Analyzer, Perkin Elmer).

The differential scanning calorimetric studies were conducted on DSC instrument (DSC Q200 V23.10 Build 79). The samples were purged with dry nitrogen at a flow rate of 10 mL min⁻¹, the temperature was raised at 5 °C min⁻¹.

Fourier-transformed infrared (FT-IR) spectrometry

FT-IR spectra was recorded with an FTIR spectrophotometer (Perkin Elmer, Spectrum BXFTIR Spectrometer) using the KBr (Merck, Germany) disc method.

Scanning electron microscopy (SEM) with EDS

Scanning Electron Microscopic (SEM) images were recorded to study the surface morphology of Mt and Mt-VF complex. Sample was mounted on carbon tape on a stub; sputter coated with gold in a vacuum evaporator and images were recorded using a scanning electron microscope (model, JEOL JSM-6610LV).

Behaviour of drug under in vitro conditions

Kinetics of drug release under in vitro conditions was performed using USP six stage dissolution rate test apparatus (DISSO 8000, Lab India, India) with the dialysis bag technique. Simulated gastric fluid was prepared by mixing 250 mL of 0.2 M HCl and 147 mL of 0.2 M KCl (buffer solution of pH 1.2). Simulated intestinal fluid was prepared by mixing 250 mL of 0.1 M KH₂PO₄ and 195.5 mL of 0.1 M NaOH (buffer solution of pH 7.4). Dialysis bags were equilibrated overnight with the dissolution media prior to experiments. A known amount of sample is placed in the dialysis bag containing 5 mL of dissolution medium. The drug loaded dialysis bag was placed into the receptor compartment containing 500 mL dissolution medium with constant stirring (80 rpm) maintained at 37±0.5 °C. An aliquot (5 mL) was withdrawn at regular interval of time followed by replenishment with equal volume of dissolution

medium to maintain same volume of dissolution medium. The extracted aliquots were analyzed for its drug content using UV spectrometer at 225 nm (calibration plot of standard drug solutions were prepared in the same releasing media). The above mentioned procedure is repeated for every sample (pure VF, Mt-VF complex) in simulated gastric fluid and simulated intestinal fluid.

To analyze the in vitro release data, various kinetic models including Zero order, First-order, Higuchi and Korsmeyer-Peppas model has been used to describe the release kinetics.²⁷⁻²⁹

RESULTS AND DISCUSSION

Interaction of VF at different pH values

Mt has the ability to swell on coming into contact with water and the exchangeable cations/drugs diffuse into the water phase [30]. To start with the experiment, effect of pH on the VF molecule was investigated in the range of 1-12. It was found that drug maintains its absorption maxima (Fig. 3) within the experimental pH range of 1-9. The UV absorption spectra of VF show two absorption peaks at 225 nm and 274 nm corresponding to different electronic transitions of the molecule.³¹⁻³³ In subsequent studies, wavelength of 225 nm has been selected for quantitative estimation of VF.

The pH of the solution has always played a crucial role in adsorption process.³⁰ The loading of VF in Mt was found to increase from 1750 μ g to 2400 μ g (35 % to 48 %) in the pH range of 1- 6 and then decrease to 1800 μ g (36 %) in the pH range of 7-9 (Fig. 4).

This could be explained on the basis that at lower pH loading of drug is less due to the competition between the cationic drug and H⁺ ions present as exchangeable ion in Mt where as in the slightly acidic medium around pH=6, VF will be positively charged because of the presence of tertiary amino groups in its molecular structure³⁴ therefore the amount of VF loaded on Mt increases slightly.

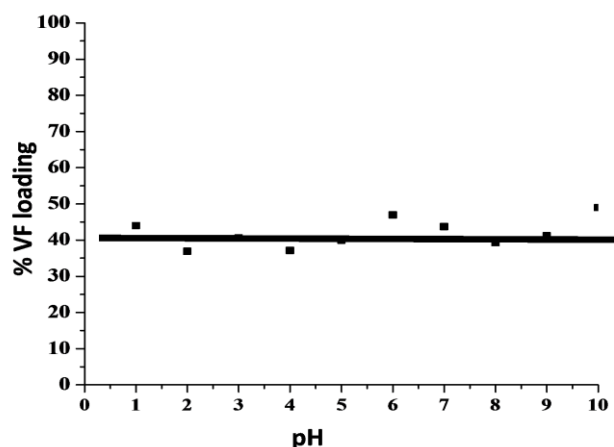


Figure 4. VF loading on Mt as a function of pH

The maximum drug loading was observed at pH=6 (48 %) which was also the natural pH of the drug solution used in the present work. Therefore, the subsequent studies were carried out at pH=6.

Effect of time on loading of VF on Mt

Intercalation of VF in Mt is a rapid process, due to occurrence of ion-exchange reaction between the interlayer Na^+ ions and cationic VF molecules at pH= 6 (Fig. 5).

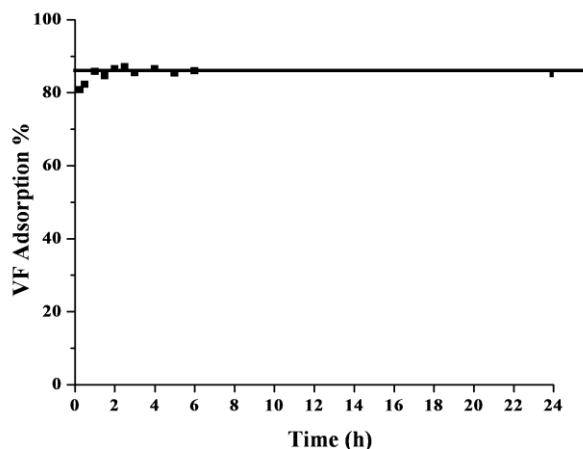


Figure 5. Effect of contact time on loading of VF on Mt.

Initially 4111 μg (80 % of 5000 μg) of VF was loaded within 0.5 h of interaction time, which increased to 4353 μg (87 % 5000 μg) in 2.5 h and remained almost constant 4300 μg (86 % of 5000 μg) up to 6 h and tends to decrease up to 4258 μg (85 % of 5000 μg) in further 18 h. Therefore, for further experiments in our studies, reaction time was set to 2.5 h in order to have maximum loading.

Effect of initial VF concentration on loading on Mt

The loading of VF in Mt layers is also affected by its initial amount present in the solution.

As the VF amount in the solution increases from 400 μg to 18000 μg (40 - 720 mg L^{-1}), the amount of VF loaded on Mt increases from 338 μg to 1758 μg (84.6 % to 94 %) (Fig. 6). Therefore, the optimal concentration was found to be 1800 μg of VF/100 mg of Mt for further studies and characterizations.

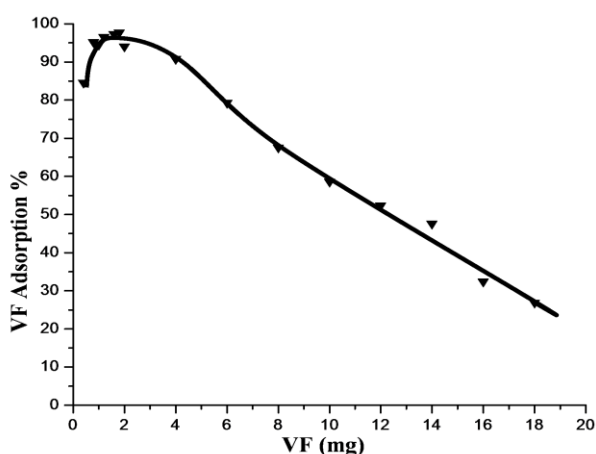


Figure 6. Effect of initial VF concentration on loading on Mt

Kinetics of VF Adsorption

In order to optimize the design of an adsorption system of VF on Mt, it is important to establish the most appropriate correlations for the equilibrium data for the system. In this respect two kinetic models including pseudo first order and pseudo-second order models have been applied to determine the adsorption mechanism.³⁵

Pseudo-first-order model

Pseudo-first-order equation can be expressed as below Equation (3): where k_1 is the pseudo-first-order rate constant (min^{-1}), q_t is the amount of drug adsorbed (mg g^{-1}) at different times t , q_1 is the maximum adsorption capacity (mg g^{-1}) for pseudo first-order adsorption. Plots of $1/q_t$ versus $1/t$ for the adsorption of VF on Mt surface were employed to generate the intercept values of $1/q_1$ and the slope of k_1/q_1 (Fig. 7). The values of k_1 , q_1 and the correlation coefficients are given in Table 1.

$$\frac{1}{q_t} = \frac{k_1}{q_1} \frac{1}{t} + \frac{1}{q_1} \quad (3)$$

Figure 7. Pseudo first order kinetic model for VF adsorption on Mt surface

Pseudo second order model

The pseudo-second-order kinetic equation can be represented as Equation (4): where k_2 is the pseudo-second order rate constant; q_2 is the maximum adsorption capacity (mg g^{-1}) for the second order adsorption process. The plots of t/q_t versus t for VF adsorption on Mt are given in Fig. 8. From the slope and intercept values, q_2 and k_2 values were calculated with results given in Table 1.

$$\frac{t}{q_t} = \frac{1}{k_2 q_2^2} + \frac{t}{q_2} \quad (4)$$

Figure 8. Pseudo second order kinetic model for VF adsorption on Mt

Table 1. Kinetic parameters for the adsorption of VF on Mt surface

Pseudo first order			Pseudo second order		
k_1 , min^{-1}	q_1 , mg g^{-1}	R_1^2	k_2 , g mg min^{-1}	q_2 mg g^{-1}	R_2^2
1.132	43.25	0.840	0.0428	43.04	0.999

Adsorption Isotherm for VF on Mt surface

The adsorption isotherm of VF on Mt surface obtained by plotting the amount of VF adsorbed by Mt (q_e , mg g^{-1}) vs equilibrium concentration of VF (C_e , mg L^{-1}) is shown in Fig. 9.

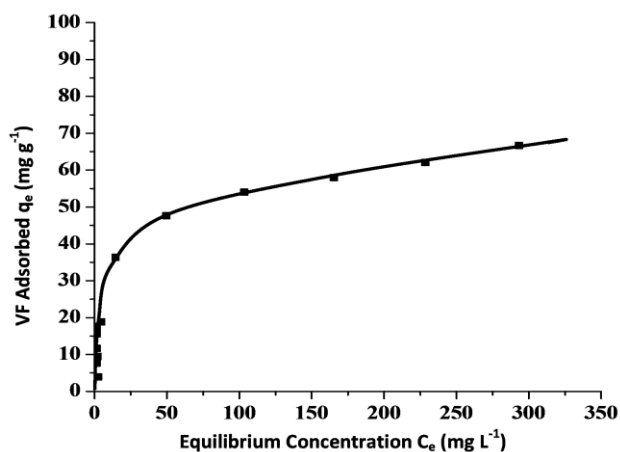


Figure 9. Adsorption isotherm of VF on Mt surface

The Langmuir (Equation-5) and Freundlich (Equation-6) adsorption isotherms were applied to evaluate the adsorption data which correspond to homogenous and heterogeneous adsorbent surfaces respectively.³⁰ The equations can be expressed as follows:

$$\frac{C_e}{q_e} = \frac{1}{q_m K_L} + \frac{C_e}{q_m} \quad (5)$$

$$\ln q_e = \ln K_f + n_f \ln C_e \quad (6)$$

where

q_e is the equilibrium VF concentration on the Mt surface (mg g^{-1}),

C_e is the equilibrium VF concentration in solution (mg L^{-1}),

q_m the monolayer adsorption capacity (mg g^{-1}), and

K_L is the Langmuir adsorption constant (L mg^{-1}).

In case of Freundlich adsorption isotherm,

K_f (mg g^{-1}) and n_f are considered as relative adsorption capacity and adsorption intensity respectively.

The values of q_m and K_L were computed from the slope and intercept of the linear plot of C_e/q_e versus C_e (Fig. 10) and are presented in Table 2.

Table 2. Isotherm constant for VF adsorption on Mt surface

Linear form of Langmuir		Linear form of Freundlich	
$q_m, \text{mg g}^{-1}$	67.11	$K_f, \text{mg g}^{-1}$	8.496
K_L	0.064	n_f	0.3873
R^2	0.989	R^2	0.7921

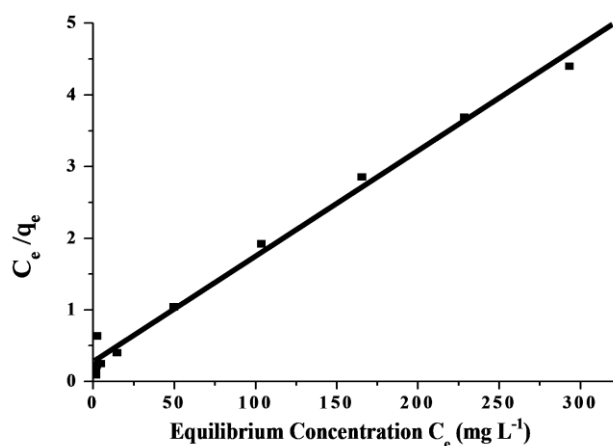


Figure 10. Linear form of Langmuir adsorption isotherm for VF on Mt

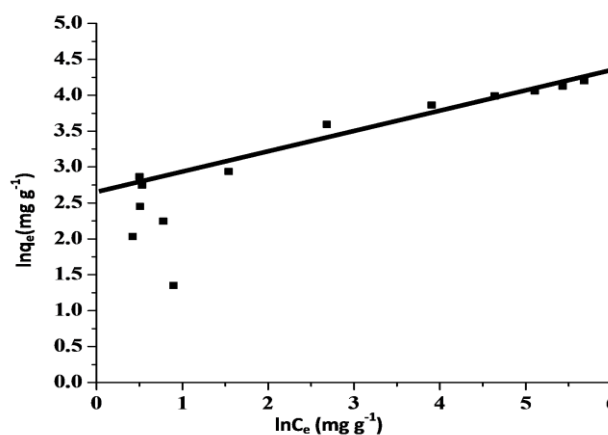


Figure 11. Linear form of Freundlich adsorption isotherm for VF on Mt

The linear form of Langmuir isotherms seems to produce a better fit in comparison with linear form of Freundlich isotherm (Fig. 11). The essential characteristics of the Langmuir equation can be expressed in terms of a dimensionless separation factor R_L as Equation-7:

$$R_L = \frac{1}{1 + K_L C_e} \quad (7)$$

The value of R_L indicates the shape of the isotherm to be either unfavorable ($R_L > 1$), linear ($R_L = 1$), favourable ($0 < R_L < 1$) or irreversible ($R_L = 0$) thereby indicates the nature of the favorability adsorption process and its feasibility. The results of R_L values were in the range of 0.494-0.023 indicate that the favourable adsorption of VF on Mt.³⁶

According to Freundlich equation, K_f value is 8.496 mg g^{-1} at 25°C . It can be said that the values of n_f equal to 0.3873 is smaller than 1, reflecting the favourable adsorption.

XRD Studies

The physical status of pure VF, Mt, Mt-VF complex has been compared with the help of XRD (Fig. 12). Pure VF shows strong diffraction peaks at $2\theta = 6.5^\circ, 8.5^\circ, 10.3^\circ, 12.8^\circ, 13.6^\circ, 15.6^\circ, 16.5^\circ, 19.1^\circ, 20.4^\circ, 21.2^\circ, 21.9^\circ, 25.1^\circ, 28.7^\circ, 31.2^\circ, 31.7^\circ, 35.3^\circ$ well supported by literature.³⁷

The XRD pattern of pristine Mt shows characteristic diffraction peak at 2θ value 6.4° corresponding to 001 plane with d value of 14.2 \AA .

In the case of Mt-VF complex an increase in intensity of 001 plane along with the shift in the 2θ value, from 6.02° to 5.5° , was observed. According to Bragg's law, shift in 2θ value from higher diffraction angle to lower diffraction angle is indicative of increase in d spacing i.e., from 14.2 \AA to 16 \AA ³⁸⁻⁴⁰ which can be related to the successful intercalation of VF in the Mt layers. Moreover the peaks at $8.5^\circ, 20.4^\circ, 21.8^\circ, 26.3^\circ$ indicates the presence of VF in the synthesized Mt-VF complex.

Subtracting the Mt layer thickness (9.6 \AA) from the d spacing (16 \AA) of the Mt-VF complex, the Mt layer thickness was estimated to be 6.4 \AA .³⁵ This data suggest the replacement of interlayer hydrated cations with monolayer the VF molecules parallel to the Mt layers is highly possible.⁴¹

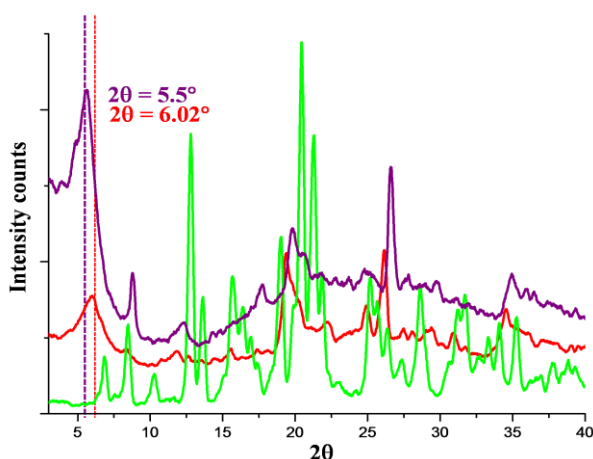


Figure 12. XRD patterns for Pure VF, Mt, Mt-VF complex.

FTIR Studies

In order to confirm the presence of VF within the interlayer region of the Mt, FTIR spectra were recorded in the region $400\text{-}4000 \text{ cm}^{-1}$.

In the FT-IR spectrum of Mt the band at 3436 cm^{-1} and 3641 cm^{-1} has been assigned to H-O-H stretching vibrations from interlayer water and Si-O-H stretching vibrations of the structural OH group. The broadness around $3496\text{-}3093 \text{ cm}^{-1}$ of the structural -OH band are mainly due to contributions of several structural -OH groups occurring in the Mt. The absorption band at 1645 cm^{-1} corresponds to H-O-H bending mode of adsorbed water.^{7,42}

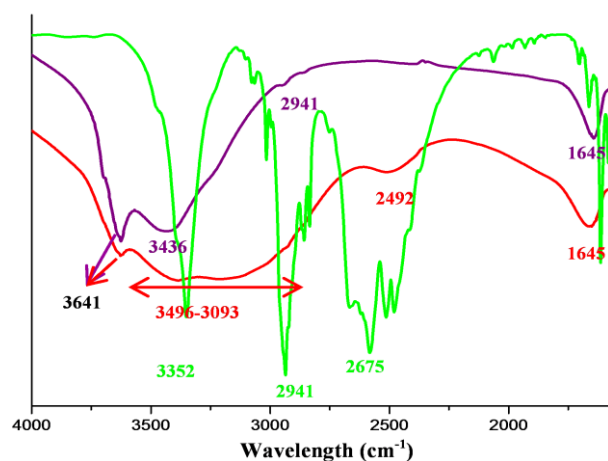


Figure 13. FTIR spectra of Pure VF, Mt, Mt-VF complex.

In the FTIR spectrum of the pure VF, appearance of absorption band at 3352 cm^{-1} corresponds to the stretching vibrations of hydroxyl group and band at 2941 cm^{-1} correspond to the stretching vibrations of aromatic CH present in VF.³⁴ However few characteristic bands around $2675\text{-}2480 \text{ cm}^{-1}$ have been observed but no vibrational mode have been assigned in literature as well.^{7,34}

In case of Mt-VF complex the vibrational bands 3436 cm^{-1} and 3641 cm^{-1} has been assigned to H-O-H stretching vibrations from interlayer water and Si-O-H stretching vibrations of the structural OH group but the broadness of this peak decreases as compared to Mt therefore decreasing the number of -OH stretching vibrations contributing to this peak indicating the intercalation of the VF (as confirmed by XRD) into the interlayer region has displaced the water molecules. The presence of functional groups of VF in the Mt-VF complex on the surface of Mt is also suggested by peak about 2941 cm^{-1} characteristic of the aliphatic C-H symmetric stretch of aromatic group of VF.

TGA Studies

Pristine Mt, pure VF and Mt-VF complex were characterized by TGA to evaluate their thermal behavior.

Pure Mt shows mass loss of 18 % from $30 \text{ }^\circ\text{C}$ to $140 \text{ }^\circ\text{C}$ and is attributed to the loss of adsorbed and interlayer water, with an endothermic peak in the DTA curve around $80 \text{ }^\circ\text{C}$. Mass loss in the temperature range from $600\text{-}750 \text{ }^\circ\text{C}$ is due to the loss of hydroxyl groups in the aluminosilicate structure and the structure of the Mt layers collapses, also indicated by a broad endothermic peak in DTA curve of Mt at $600 \text{ }^\circ\text{C}$.⁴³⁻⁴⁴

The pure VF shows two thermal decomposition stages. In the DTA curve for pure VF, a sharp endothermic peak at $218 \text{ }^\circ\text{C}$ was observed without any weight loss in TGA which corresponded to the melting point of VF. The drug show a sharp weight loss ($\sim 99 \%$) at around $230\text{-}320 \text{ }^\circ\text{C}$ resulting in a strong endothermic peak in DTA curve at $297 \text{ }^\circ\text{C}$ followed by a broad exotherm at $600 \text{ }^\circ\text{C}$ corresponding to decomposition of VF.⁴⁵

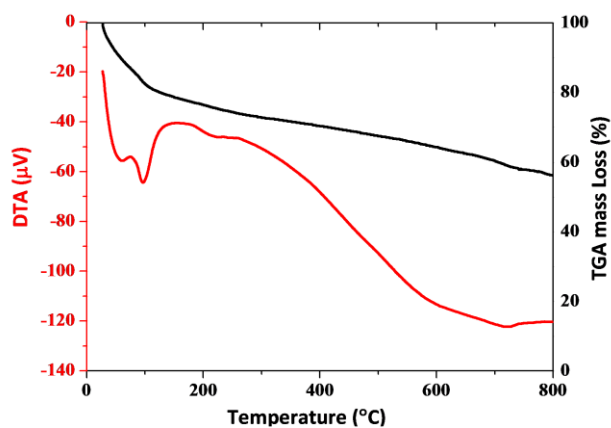


Figure 14a. TGA-DTA curves of Montmorillonite

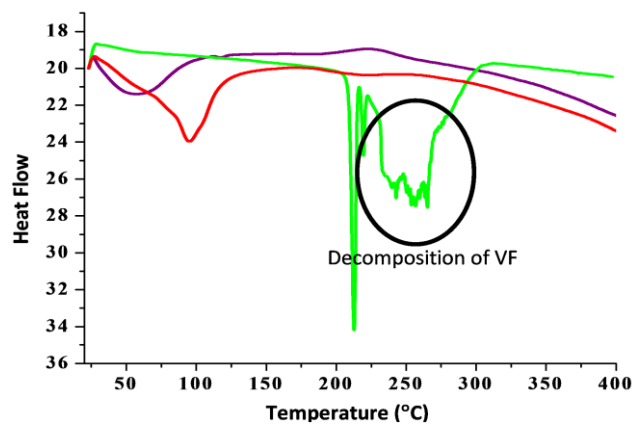


Figure 15. DSC curves of Pure VF, Montmorillonite and Mt-VF complex

Mt shows an exothermic peak around 90 °C suggesting the dehydration of adsorbed water from the surface of Mt.

In case of Mt-VF complex a broad endotherm was appeared in the region of 60 °C to 100 °C which might corresponds to dehydration of surface water. In the temperature region of 200 °C to 300 °C, an exotherm might be related to the decomposition of VF within Mt layers was observed. (Fig. 15).

Scanning Electron Microscopy with Energy dispersive X-Ray Analysis

To analyze the surface morphology of Mt-VF complex Scanning Electron Microscopic with Energy dispersive X-Ray Analysis was performed. The surface of Mt has a layered smooth surface whereas the Mt-VF complex has layered but rough surface indicating the presence of VF molecule on the surface.

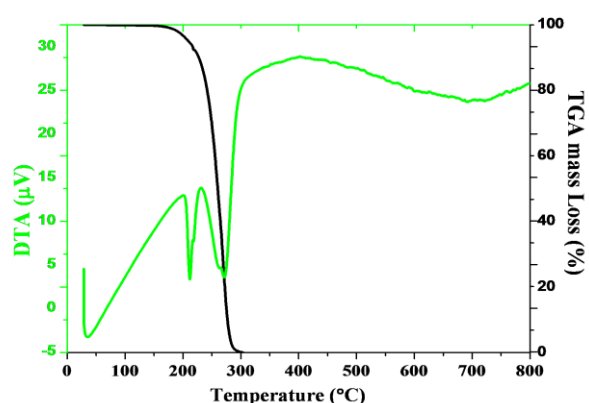


Figure 14b. TGA-DTA curves of Pure VF

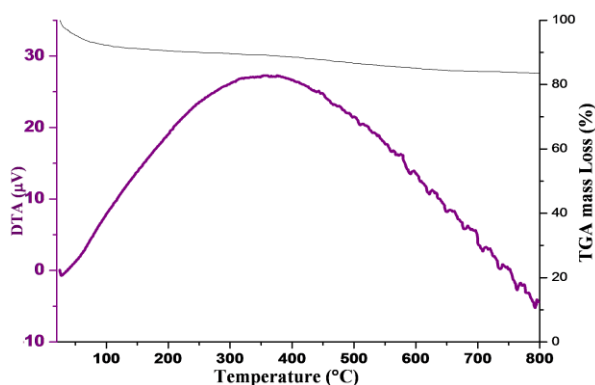


Figure 14c. TGA-DTA curves of Mt-VF complex.

In case of Mt- VF complex the single step mass loss of 18 % in the range from 205 °C to 700 °C suggests the decomposition of intercalated VF.

DSC Studies

The physical state and crystallinity of the drug in case of Mt-VF complex have been investigated and compared to pure VF and Mt. Sharp endotherm at 212 °C and 250 °C has been observed for VF corresponding to the melting and decomposition of the pure compound.^{45,46}

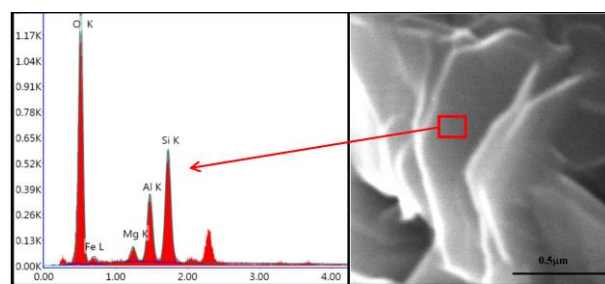


Figure 16a. SEM image and EDX graph of montmorillonite

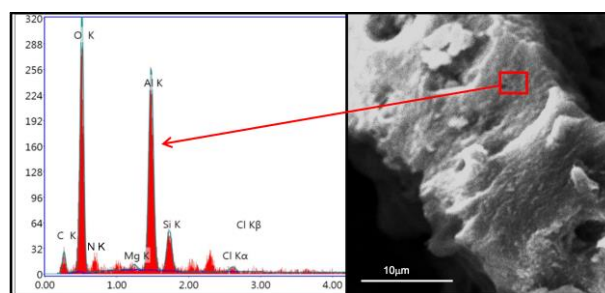


Figure 16b. SEM image and EDX graph of Mt-VF complex

High % content of oxygen, silicon and aluminum is observed in case of Mt where as in Mt-VF complex additional peaks of carbon nitrogen and chlorine are present along with oxygen, silicon and aluminum EDX analysis (Figs. 16a and 16b and Table 3). Since, the drug contains chlorine, nitrogen and carbon therefore it can be taken as an evidence for the presence of drug on the Mt-VF complex.

Table 3. Elemental analysis of Mt and Mt-VF complex

Element	Mt		Mt-VF complex	
	Weight%	Atomic%	Weight %	Atomic %
Fe	05.68	01.99	00.00	00.00
Mg	02.39	01.93	00.00	00.00
C	00.00	00.00	15.25	21.98
O	60.3	73.73	54.30	58.74
N	00.00	00.00	00.57	00.41
Al	11.40	08.26	23.20	14.88
Si	20.23	14.09	05.72	03.52
Cl	0.00	0.00	00.95	00.46
Total	100.00	100.00	100.00	100.00

Drug Release Profile

VF is well absorbed and extensively metabolized in the liver.⁴⁷ Therefore it is necessary to study the release profile of the selected Mt-VF-complex in simulated gastric and intestinal fluid, in comparison with the release profile of pure drug under identical experimental conditions.

In stimulated gastric fluid the pure VF shows a rapid burst (releasing 35 % of the drug) in the initial 0.5 h followed by 100 % release of the drug over a period of 5.5 h. In case of Mt-VF complex a sustained release of VF in the gastric fluid (HCl,pH 1.2) was observed. Within initial 2 h, only 7.3 % of VF was released which approaches to 48 % in 7 hours and 53 % over a period of 10 h (Fig.17). The release in acidic media may be due to cation exchange with H⁺ ions from the media, being smaller in size, they can penetrate deep into the Mt layers and results in high ion exchange process (Fig. 17).

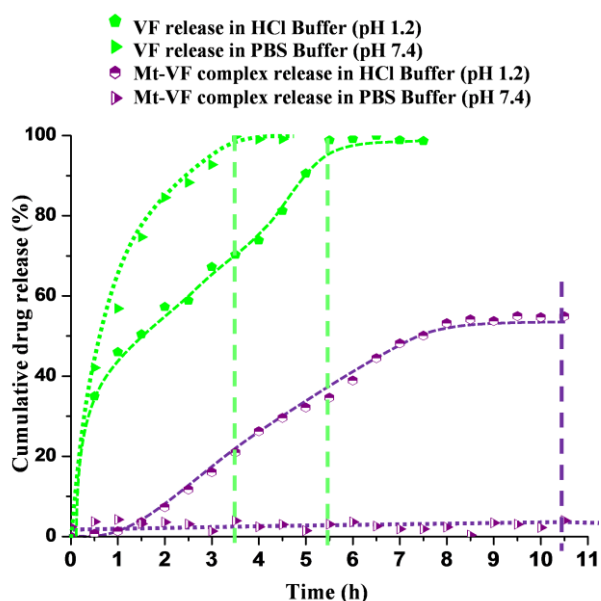


Figure 17. Release profile of pure VF and Mt-VF complex in HCl buffer pH 1.2 and PBS pH 7.4

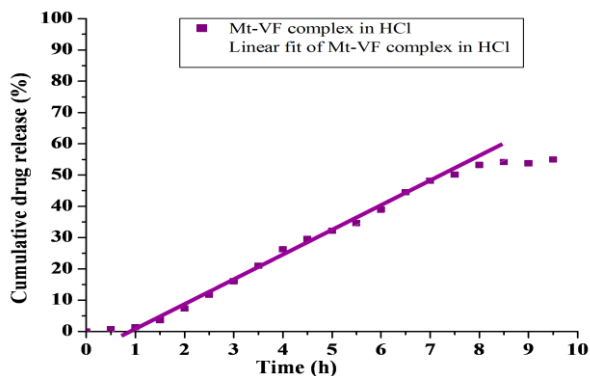


Figure 17a. Zero order kinetic model of Mt-VF complex in simulated gastric fluid

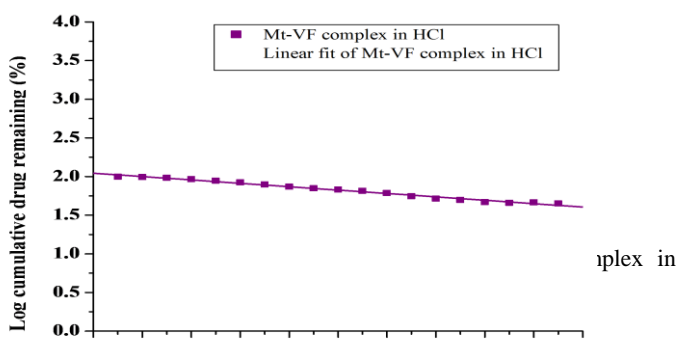


Figure 17b. Higuchi kinetic model of Mt-VF complex in simulated gastric fluid

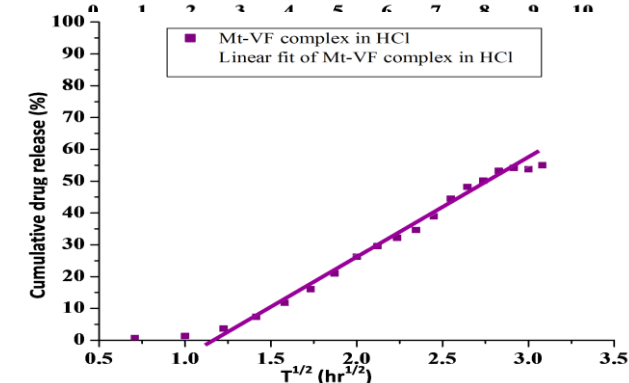


Figure 17c. Hignuchi kinetic model of Mt-VF complex in simulated gastric fluid

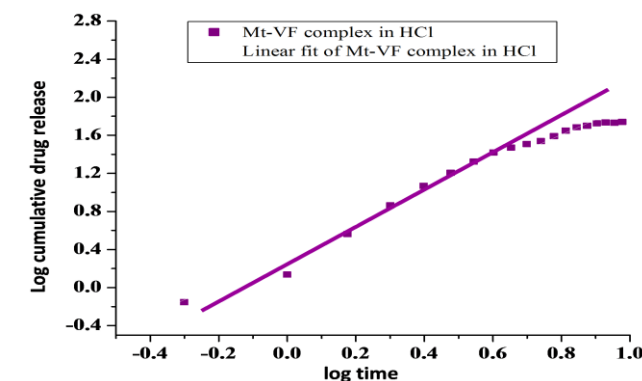


Figure 17d. Korsmeyer-Peppas kinetic model of Mt-VF complex in simulated gastric fluid

Table 4. Release kinetics of Mt-VF complex in simulated gastric fluid (HCl, pH 1.2)

Release media	Zero order, $C=K_0t$		First order, $\log C = \log C_0 - k_1t/2.303$		Higuchi, $Q = K_H t^{1/2}$		Korsmeyer-Peppas, $M_t/M_\infty = kt^n$		
	R^2	K_0, h^{-1}	R^2	K_1, h^{-1}	R^2	$K_H^{(-1/2)}$	R^2	n	K_{kp}, h^{-n}
HCl pH 1.2	0.979	6.871	0.985	0.101	0.972	27.36	0.971	1.5	2.215

In stimulated intestinal fluid, PBS (pH 7.4) the pure VF shows a rapid burst (releasing 42 % of the drug) in the initial 0.5 h followed by 100 % release of the drug over a period of 3.5 h. In case of Mt-VF complex no release of VF was observed up to 10.5 h. This indicates that VF release was greatly influenced by the pH of the releasing media.³⁵

In vitro drug release data suggest that the synthesized Mt-VF complex are able to extend the release of VF in gastric fluid (acidic media, pH 1.2) beyond 8 h. As a result more amounts is expected to reach liver for its complete absorption.⁴⁸

The release data of VF form Mt-VF complex were fitted by zero order (Fig. 17a), first-order kinetics (Fig. 17b), Higuchi (Fig. 17c) and Korsmeyer-Peppas models (Fig. 17d) and the values of release kinetics constants in simulated gastric (HCl, pH 1.2) fluid are summarized in Table 4. In (HCl, pH 1.2) the first order equation gave the best representation of the release data.⁴⁹

CONCLUSIONS

VF sustained release formulation was prepared successfully using natural clay mineral Mt as a host to retard the drug release. Intercalation of VF in Mt layers was indicated by XRD. The adsorption isotherms of VF on Mt were best fitted by the Langmuir model and the adsorption kinetics followed the pseudo second-order kinetic model. Drug release kinetics of this formulation corresponds best to first order model in gastric media (pH 1.2). In vitro drug release data suggest that the synthesized Mt-VF complex is capable of gradual drug release over a longer period of time in gastric media (pH 1.2) as compared to pure drug thereby increasing the availability of the drug for absorption in liver. Thus the obtained results are proposing a possibility of new formulation suitable as an extended delivery carrier of venlafaxine hydrochloride.

ACKNOWLEDGEMENT

Authors are thankful to the USIC, University of Delhi for providing instrumentation facilities and CSIR for providing financial assistance to one of the authors, Shilpa Jain.

REFERENCES

- Yuan, Q., Shah, J., Hein, S., Misra, R.D.K., *Acta Biomater.*, **2010**, *6*, 1140.
- Ricka, J., Tanaka, T., *Macromolecules*, **1984**, *17*, 2916.
- Hirokawa, Y., Tanaka, T., *J. Chem. Phys.*, **1984**, *81*, 6379.
- Sorby, D.L., *J. Pharm. Sci.*, **1965**, *54*, 677.

- Sorby, D.L., Liu, G., *J. Pharm. Sci.*, **1966**, *55*, 504.
- Aguzzi, C., Cerezo, P., Viseras, C., Caramella, C., *Appl. Clay Sci.*, **2007**, *36*, 22.
- Peppas, N.A., *Int. J. Pharm.*, **2004**, *277*, 11.
- Nair, L.S., Laurencin, C.T., *Prog Polym Sci.*, **2007**, *32*, 762.
- Coviello, T., Matricardi, P., Marianecchi, C., Alhaique, F., *J. Control. Release.*, **2007**, *119*, 5.
- Wai, K.N., Banker, G.S., *J. Pharm. Sci.*, **1966**, *55*, 1215.
- Carretero, M. I., Pozo, M., *Appl. Clay Sci.*, **2009**, *46*, 73.
- Lee, Y.H., Kuo, T.F., Chen, B.Y., Feng, Y.K., Wen, Y.R., Lin, W. C., Lin, F.H., *Biomed. Eng. Appl., Basis Commun.*, **2005**, *17*, 72.
- Feng, S.S., Mei, L., Anitha, P., Gan, C.W., Zhou, W., *Biomaterials*, **2009**, *30*, 3297.
- Dong, Y., Feng, S.S., *Biomaterials*, **2005**, *26*, 6068.
- Chen, Y.M., Zhou, A.N., Liu, B., Liang, J., *Appl. Clay Sci.*, **2010**, *49*, 108.
- Joshi, G.V., Kevadiya, B.D., Patel, H.A., Bajaj, H.C., Jasra, R.V., *Int. J. Pharm.*, **2009**, *374*, 53.
- Meng, N., Zhou, N.L., Zhang, S. Q., Shen, J., *Int. J. Pharm.*, **2009**, *382*, 45.
- Joshi, G.V., Patel, H.A., Bajaj, H.C., Jasra, R.V., *Coll. Polym. Sci.*, **2009**, *287*, 1071.
- Joshi, G.V., Kevadiya, B.D., Bajaj, H.C., *Micropor. Mesopor. Mater.*, **2010**, *132*, 526.
- Chen, B.Y., Lee Y.H., Lin W.C., Lin F.H., Lin K.F., *Biomed. Eng. Appl., Basis Commun.*, **2006**, *18*, 30.
- Entsuah, R., Chitra, R., *Psychopharmacol. Bull.*, **1997**, *33*, 671.
- Klamerus, K.J., Maloney, K., Rudolph, R.L., Sisenwine, S.F., Jusko, W.J., Chiang, S.T., *J. Clin. Pharmacol.*, **1992**, *32*, 716.
- Haskins, J.T., Moyer, J.A., Muth, E.A., Sigg, E.B., *Eur. J. Pharmacol.*, **1985**, *115*, 139–146.
- Olver, J.S., Burrows, G.D., Norman, T.R., *CNS Drugs*, **2001**, *15*(12), 941.
- Patel, H. A., Shah, S., Shah, D.O., Joshi, P.A., *Appl. Clay Sci.*, **2011**, *51*, 126.
- Rx list, the internet drug index, <http://www.rxlist.com/effexor-xr-side-effects-drug-center.htm>
- Dash, S., Murthy, P.N., Nath, L., Chowdhury, P., *Acta Pol. Pharm. Drug. Res.*, **2010**, *67*, 217.
- Singhvi, G., Singh, M., *Int. J. Pharm. Stud. Res.*, **2011**, *January-March*, 77.
- Costa, P., Lobo, J.M.S., *Eur. J. Pharm. Sci.*, **2001**, *13*, 123.
- Raghvendra, R. S., *Int. J. Pharm. Sci. Rev. Res.*, **2012**, *17*, 51.
- Lavanya, K., Sunitha, P., Kumar, A., Ramana, K.V., *Int. J. Pharm. Qual. Ass.*, **2013**, *14*, 1.
- Rao, K.S., Jadhav, S., Patil, P., Dattatraya, B.U., *Int. Res. J. Pharm.*, **2011**, *2*, 261.
- Patel, B., Patel, J., Banwait, H., Darji, N., Patel, D., Gabhawala, A., Patel, B., Patel, M., *Int. J. Inst. Pharm. Life Sci.*, **2011**, *1*.

- ³⁴Shah, S., Pal, A., Kaushik, V. K., Devi, S., *J. Appl. Polym. Sci.*, **2009**,112, 2876.
- ³⁵Seema, Datta, M., *Eur. Chem. Bull.*, **2013**, 2, 942.
- ³⁶Alzaydien, A.S., *Am. J. Environ. Sci.*, **2009**, 5, 197.
- ³⁷Aronhime, J., Dolitzky, B.Z., Nisnevish, G., Wizel, S., US patents US20020143211 A1 Oct 3, **2002**.
- ³⁸Das, P.R., Nanda, R.M., Behara, A., Nayak, P.L., *Int. Res. J. Biochem. Bioinform.*, **2011**,1,35.
- ³⁹Olad, A., Advances in Diverse Industrial Applications of Nanocomposites, Chapter 7, 1st edition, India: Intech, **2011**,113. ISBN: 978-953-307-202-9,
- ⁴⁰Zampori, L., Stampino, P.G., Cristiani, C., Cazzola, P., Dotelli, G., *Appl. Clay Sci.*, **2010**, 50, 266.
- ⁴¹Sivalakshmi, A., Vyas, K., Rao, S.M., Reddy, G.O., *Acta Cryst. Sect. E*. **2002**, 58, 1072-1074
- ⁴²Abdeen, R., Salahuddin, N., *J. Chem.*, **2013**, 1-9.
- ⁴³Entsuah, R., Chitra, R., *Psychopharmacol. Bull.*, **1997**, 33, 671.
- ⁴⁴He, H., Ding, Z., Zhu, J., Yuan, P., Xi, Y., Yang, D., Frost, R.L., *Clays Clay Miner.*, **2005**, 53, 287.
- ⁴⁵Roy, S., Aitipamula, S., Nangia, A. *Cryst. Growth Design*, **2005**, 5, 2268.
- ⁴⁶Bernardi, L.S., Oliveira, P.R., Murakami, F.S., Silva, M.A.S., Borgmann, S.H.M., Cardoso, S.G., *J. Therm. Anal. Calorim.*, **2009**,97, 729.
- ⁴⁷<http://www.healthcentral.com/druglibrary/408/effexor> xr-clinical_pharmacology.html
- ⁴⁸Singh, G., Ghosh, B., Kaushalkumar, D., Somsekhar, V., *AAPS PharmSciTech*, **2008**, 9(3), 791.
- ⁴⁹Ajit, I., Senthil, A., Rahul, B., Narayanaswamy, V.B., *Int. J. Pharm.*, **2012**, 3, 226.

Received: 31.03.2014.

Accepted: 28.05.2014.



ADSORPTION STUDIES OF ZINC(II) IONS ON BIOPOLYMER COMPOSITE BEADS OF ALGINATE-FLY ASH

Uzma Nadeem^[a] and Monika Datta^{[a]*}

Keywords: biopolymer beads; sodium alginate; adsorption; isotherm models; wastewater

The gelling and metal-chelating properties of alginate were combined to develop an adsorbent for heavy metal removal. Biopolymer beads composed of fly ash and sodium alginate proved to be an effective adsorbent for removal of Zn(II) ions from aqueous solutions. The effect of initial pH (2–10), bead dose (10–80), agitation time (1–24 h), beads composition (0.1 g–0.7 g fly ash) and Zn(II) ions initial concentration (5–30 mg L⁻¹) on the adsorption process, as well as to what extent the adsorption data obey Langmuir and Freundlich adsorption isotherms were investigated. The maximum adsorption was found 84.20 % within 8 h and after that reaches equilibrium. The adsorption of Zn(II) ions is quite sensitive to pH of the suspension and shows an optimum uptake value at pH 6.0. Maximum adsorption occurred for 40 beads and in case of composition, beads composed of 0.5 g fly ash has shown good results. It is clear from the experimental results that the pH plays an important role in adsorption of zinc ions. The average size, bulk density and swelling ratio of beads calculated are; 0.12 cm, 0.34 g mL⁻¹ and 28.65 respectively. The synthesized beads were also characterized by FTIR, XRD, SEM, TGA/DTA and other methods.

*Corresponding Authors

E-Mail: monikadatta_chem@yahoo.co.in

[a] Department of Chemistry, University of Delhi, Delhi, 110007, India.

[a] E-Mail: uzmanadeem3@gmail.com

Department of Chemistry, University of Delhi, Delhi, 110007, India.

Introduction

Environmental pollution by heavy metals which are released into the environment through various anthropogenic activities such as mining, energy and fuel production¹, electroplating, wastewater sludge treatment and agriculture are one of the world's major environmental problems. This is probably due to rapid industrialization^{2,3}, population growth and complete disregard for the environmental health. Initially, heavy metals are naturally present in soils as natural components but as of now, the presence of heavy metals in the environment has accelerated due to human activities. Even though zinc is an essential requirement for a healthy body⁴, excess zinc can be harmful, and cause zinc toxicity.⁵⁻⁸ The free zinc ions in solution is highly toxic to plants, invertebrates, and even vertebrate fish. Stomach acid contains hydrochloric acid, in which metallic zinc dissolves readily to give corrosive zinc chloride, which can cause damage to the stomach lining due to the high solubility of the zinc ion in the acidic stomach.

Fly ash is a significant waste that is released of thermal power plants and defined as very fine particles that are drifted upward with up taken by the flue gases due to the burning of used coal.⁹ Fly ash, a finely divided and powdered by-product, from coal fired power plants or biomass combustion facilities requires ultimate disposal. Studies on the country and the world of fly ash usage has increased in the last two decades and as a result of these studies have been identified fly ash as a suitable adsorbent for the adsorption of heavy metals from waste water.¹⁰ The major constituents of fly ash are silica, alumina, and iron

oxide, which are ideal metal adsorbents. In recent years, fly ash has been employed as a low-cost adsorbent for gas and water cleaning¹¹ and much effort have been focused on heavy metal and dye adsorption on fly ash particles.¹²

Recently numerous approaches have been studied for the development of cheaper and more effective adsorbents containing natural polymers. The use of naturally occurring biopolymer seems to be a preferred alternative to the use of expensive chemical adsorbents for the removal of heavy metal ions. Adsorption onto polysaccharide derivatives can be a low-cost procedure of choice in water decontamination. Among the industrially attractive polysaccharide biopolymers, alginate is known to have high complex formation ability with various heavy metals.¹³

Sodium alginate was chosen as the material for preparation of the carrier matrix because it is a natural, biodegradable, biocompatible, non toxic orally and hydrophilic polymer suitable for the entrapment of water soluble toxicants. They produce thermally irreversible gels by association with most divalent cations. Alginates are polysaccharides found in brown seaweeds and are composed mainly of linear polymers of β -(1 \rightarrow 4)-D-mannuronic (M) and α -L-guluronic (G) acids differing in terms of their proportions and linear arrangements. Different species of algae contain different percentages of mannuronic acid (M) and guluronic acid (G). Because of the differences in conformation of the two different residues, gelation with divalent cations can be attributed mainly to the G residue (especially to the pure polyguluronic (GG) chains), while the M residue contributes mainly to the cation exchange capacity of this naturally occurring polymer. Hydroxyl groups have been found to play an important role not only in cation exchange capacity but also in the affinity of the material towards different metal ions.¹⁴

The mechanisms of biosorption are not fully understood, but it is well known that alginates of algal cell walls play an important role in metal binding.¹⁵

In the present work the gelling and metal-chelating properties of alginate were combined with fly ash to develop composite adsorbents for heavy metal removal.

Experimental

Reagents

Sodium alginate was obtained from Thomas Baker Pvt. Limited. The fly ash obtained from National Thermal Power Corporation was grounded and sieved to a particle size of 200–400 micron. The sieved fly ash was washed 2–3 times by distilled water to remove the impurities and preserved in glass bottles. Analytical grade of $\text{ZnSO}_4 \cdot 7\text{H}_2\text{O}$ was used for metal sorption experiments. The stock solution was diluted by serial dilution method as per requirement. The initial pH of the solution was adjusted by using either 0.1 M NaOH or 0.1 M HCl. All the chemicals used for the study were of analytical grade.

Beads preparation

Alginate-fly ash composite beads employed as an adsorbent were prepared in two steps. In the first step, sodium alginate (1 % w/v) in 100 mL distilled water was dissolved followed by addition of known amount of fly ash and agitated for 30 minutes. In the second step the solution of alginate-fly ash was added into a 100 mL solution of 0.1 M CaCl_2 solution drop wise with the help of a syringe with constant stirring. The schematic diagram of bead preparation and the process of turning of sodium alginate into a gel is described in Figure 1.

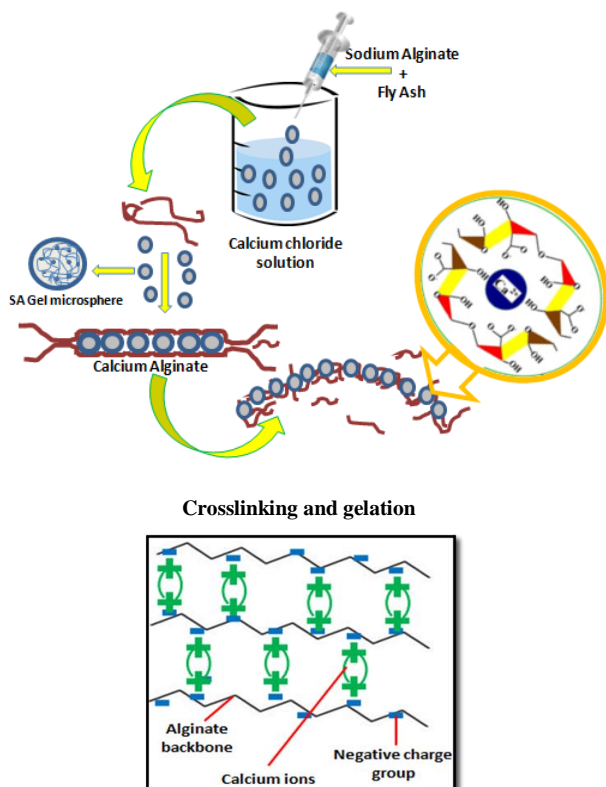


Figure 1. The process of turning a sodium alginate solution into a gel

The produced beads were allowed to harden by leaving them in CaCl_2 solution for 24 h and thereafter filtered and washed thrice with double distilled water. These biopolymeric beads were stored at room temperature in double distilled water and the swollen beads (Figure 2) were used for the adsorption of Zn(II) ions. Immediately before use, the calcium alginate beads were washed again three times with distilled water.

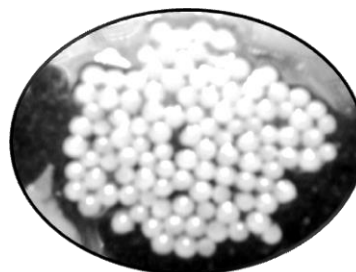


Figure 2. The swollen alginate-fly ash composite beads

FT-IR spectroscopy

FTIR spectra of the composite beads was recorded with an FTIR spectrophotometer (Perkin Elmer, Spectrum BXFTIR Spectrometer) using the KBr (Merck, Germany) disc method.

X-Ray Diffraction (XRD) studies

Powder X-ray diffraction (PXRD) measurements of composite beads was performed on a powder X-ray diffractometer (XPRT PRO Pananalytical, model PW3040160, Netherland) the measurement conditions were Cu K α radiation generated at 40 kV and 30 mA as X-ray source 2– 40° (2θ) and step angle 0.01 ° second⁻¹.

Scanning electron microscopy (SEM) studies

The surface morphology and EDAX analysis of the synthesized beads were examined with the Scanning Electron Microscope (Zeiss EVO 40). A few samples of beads were taken on a copper stub and sputtered with gold for 2 minutes. These gold-coated microspheres were mounted on the SEM instrument and photographs were taken at different magnifications.

Thermal analysis

The thermal stability of the alginate-fly ash composite beads was assessed by the thermogravimetric analyzer. Thermogravimetric analysis was carried out within 30 – 800 °C at 10 °C min⁻¹, in nitrogen flow (TGA 2050 Thermal gravimetric Analyzer).

Beads size

The size of 100 beads was measured by a calibrated scale and their average size was calculated.

Bulk Density

For the determination of bulk density of beads accurately weighed amount of the beads and transferred into 50 mL measuring cylinder. It was subjected to tapping for 3 times and the volume occupied by the beads was noted. Bulk density was estimated by using the following formula.¹⁶

$$\text{Bulk density} = \frac{\text{weight of the beads}}{\text{bulk volume of the beads}}$$

Swelling index

100 mg of dry beads were soaked in pH 7.4 phosphate buffer and the beads were reweighed at regular intervals of time, carefully wiping off the excess liquid with a tissue paper.¹⁷ The under given expression was used for swelling index determination:¹⁸

$$\text{Swelling Index} = \frac{W_t - W_0}{W_0}$$

where

W_t and W_0 are the weight of the beads at time 't' and under dry state, respectively.

Batch adsorption experiments

A stock solution of Zn(II) ions was prepared by dissolving accurate weight of zinc in definite volume of distilled water. Proper concentrations of the adsorbate were prepared from the stock solution through proper dilution. The required concentration for the adsorption experiments were prepared by serial dilution. The initial pH of the solution was adjusted by using either 0.1 M NaOH or 0.1 M HCl. The batch adsorption experiments were performed on an orbital shaker (Khera Lab Instruments). At the end of a predetermined time interval, the adsorbent was removed by filtration and the residual Zn(II) ions was estimated in the filtrate by atomic absorption spectrophotometer (Analytic Jena; ZEE nit 700 P). The effect of initial pH (2–10), agitation time (1–24 h), bead dose (10–80), bead composition (0.1–0.7 g fly ash), and initial metal concentration (5–30 mg L⁻¹) on the adsorption process, as well as to what extent the adsorption data obey Langmuir and Freundlich adsorption isotherms were investigated.

Calculations

The percent removal of metal ions was calculated by using the Eqn. 1.

$$R(\%) = \frac{C_i - C_f}{C_i} \times 100 \quad (1)$$

where,

R is the removal,

C_i is the initial metal concentration and

C_f is the final concentration of the metal ion in mg L⁻¹.

The sorption capacity was calculated from Eqn. 2

$$Q_e = \frac{V(C_i - C_e)}{1000W} \quad (2)$$

where,

Q_e is the adsorption capacity (mg g⁻¹),

C_i is the initial metal concentration (mg L⁻¹),

C_e is the equilibrium concentration of metal (mg L⁻¹),

W is the adsorbent dose (g) and V is the solution volume (mL).

Results and discussion

FTIR Analysis

The infrared spectra for the fly ash (FA), sodium alginate (SA) and composite beads of alginate-fly ash (Alg-F) in the wavelength range of 4000–500 cm⁻¹ is shown in Figure 3.

The IR spectrum of FA, SA and composite beads of Alg-F exhibiting bands at 3435.15 cm⁻¹, 3316.00 cm⁻¹ and 3430 cm⁻¹ which correspond to OH stretching mode in molecular water.¹⁹ In the FTIR spectrum of fly ash, the band at 3435 cm⁻¹ has been assigned to H-O-H stretching vibrations from interlayer water and Si-O-H stretching vibrations of the structural -OH group. The bands at 2924 cm⁻¹ (CH stretching) in FA were also detected.¹⁹ The characteristic band at 1099 cm⁻¹ has been assigned to Si-O stretching vibration. The absorption bands at 797.20 assigned as Si-O vibrations in SiO₂. The absorption bands at 553.84 cm⁻¹ are strong bending vibrations corresponding to Al-O-Si.²⁰⁻²²

In the spectra of SA the characteristic peak of sodium alginate appeared at 820.68 cm⁻¹.²³ The IR spectrum of the pure sodium alginate displayed characteristic peaks at 3316 cm⁻¹, 2944.46 cm⁻¹ and 1610 cm⁻¹ due to O-H, N-H and C=O groups, respectively.²⁴ The adsorption peak of 1610 cm⁻¹ assigned to the asymmetrical stretching vibration of -COO- groups. Small peaks observed at 1610.79-1420.21 cm⁻¹ were attributed to carboxylate groups.²⁵

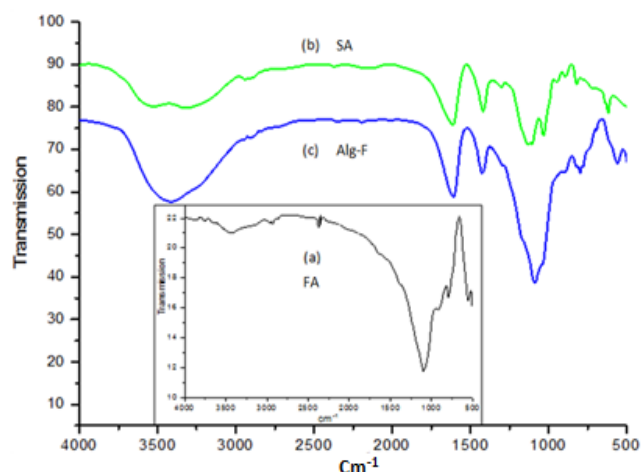


Figure 3. IR Patterns of (a)-Fly ash (FA), (b)- Sodium alginate (SA) (c)- Composite beads, (Alg-F)

In the spectra of Alg-F the characteristic peak of sodium alginate appeared at 819 cm^{-1} was observed. The presence of functional groups of sodium alginate on the surface of beads is verified by peaks at about 3417 cm^{-1} and 2940 cm^{-1} and 1608.06 cm^{-1} due to O-H, N-H and C=O groups, respectively. The peak 3417.97 cm^{-1} has been assigned to the H-O-H stretching vibrations of the interlayer water. The bands at 1608.06 cm^{-1} and 1424.04 cm^{-1} assigned to be bending vibrations of NH and NH_2 and the characteristics peaks of Si-O-Si vibration and SiO_2 was observed at 462.10 cm^{-1} and 798.11 cm^{-1} respectively. However, after the formation of Alg-F beads the absorption peaks in pure sodium alginate at 1026.35 cm^{-1} assigned to the asymmetrical stretching vibration of -COO- groups coupled with the peaks at 1032.22 cm^{-1} and shifted to 1688.08 cm^{-1} . The absorption bands at 560.53 cm^{-1} are strong bending vibrations corresponding to Al-O-Si. The presence of these bands in Alg-F complex indicates the presence of fly ash in the alginate matrix but the intensity of this peak is increased compared to fly ash and sodium alginate. Furthermore, the bands at about 3441.80 cm^{-1} and 3316 cm^{-1} , which were the stretching vibration of groups involved in both inter and intramolecular hydrogen bonds, broadened and coupled with -OH band of sodium alginate at 3400 cm^{-1} , induced by the addition of sodium alginate to fly ash implying that the occurrence of hydrogen bonds between -OH groups of sodium alginate and fly ash molecules. Small peaks observed at $1614.98\text{--}1423.42\text{ cm}^{-1}$ were attributed to carboxylate groups.²⁵

All the spectra show presence of several -OH and -COOH groups. Hydrogen of these groups is capable of ion exchange with metal cation.

XRD Analysis

The XRD patterns of fly ash (FA), composite beads before adsorption (Alg-F) and after adsorption (Alg-FM) are shown in Figure 4. Sodium alginate is usually crystalline due to strong interaction between the alginate chains through intermolecular hydrogen bonding.²⁶

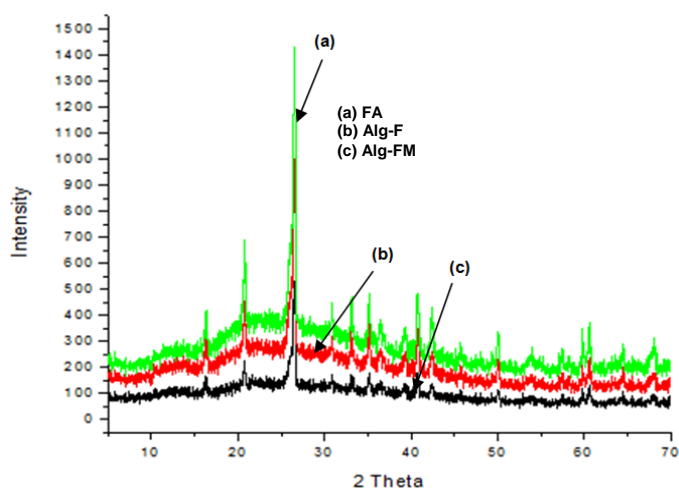


Figure 4. XRD Patterns of (a)-Fly ash (FA), (b)- Alginate-fly ash composite beads (Alg-F), (c)-Composite beads after metal adsorption, (Alg-FM)

It was observed that the fly ash consisted of crystalline minerals mullite, quartz, hematite and small amounts of calcium oxide with large characteristic peaks of quartz (SiO_2). This result is similar to that reported for a fly ash investigated.²⁷ It can be observed that there are no significant differences for all XRD profiles but the large characteristic peaks of quartz (SiO_2) in the Alg-F than those for Alg-F and Alg-FM are indicative of large SiO_2 concentrations. The intensity of quartz is very strong, with mullite forming a chemically stable and dense layer. The FA is of lower activity and at this state its glassy surface layer particles is dense, chemically stable and also protected the more active inner constituents of the fly ash comprises of porous, spongy and amorphous particles. Three diffraction peaks at 2θ values 16° , 21° and 41° were observed for sodium alginate.

In case of Alg-F, the intensity of diffraction peaks of alginate decreased notably which indicates that the nucleation and growth of semiconductor or metal particles affected the crystalline nature of sodium alginate. The pattern of fly ash has sharp peaks showing the crystalline nature of the fly ash. After the formulation of beads the XRD patterns show very weak, unoriented, hump like shape indicating Alg-F is an amorphous material.²⁸

The low degree of crystallinity shows that *in-situ* nucleation leads to the formation of very small nuclei and interaction with the polymer prevent any further crystallization of fly ash. If sodium alginate and fly ash have low compatibility, each polymer would have its own crystal region, so X-ray diffraction patterns are expressed as simply mixed patterns of sodium alginate and fly ash with the same ratio. However, in comparison to fly ash the patterns of the Alg-F show that the intensity of diffraction peak between 2θ values $12^\circ\text{--}36^\circ$ decreased. This means intermolecular hydrogen bonds between sodium alginate and fly ash and was introduced, which destroyed the original molecular structure of sodium alginate, resulting in the changes of diffraction patterns.

Same pattern was observed after the adsorption of metal on alginate-fly ash beads (Alg-FM), the XRD patterns show decrease in the intensity of diffraction peaks than Alg-F. This means intermolecular hydrogen bonds between Alg-F and metal were introduced, which destroyed the original molecular structure of Alg-F, resulting in the changes of diffraction patterns.

SEM Studies

SEM images of Alginate-fly ash (Alg-F) beads taken at different magnification are shown in Figure 5. The beads are found to be around $100\text{ }\mu\text{m}$ and the SEM images reveal the presence of pores on the surface and the beads were almost spherical in shape with networked and smooth surfaces. The SEM of the microbeads prepared with sodium alginate are spherical in shape exhibits a sandy appearance. The image portrays layers of crosslinked polymers that are formed inside the bead. At magnification 1.1 KX bridging and dense nature of beads is due to coalescence and fusion to the colloidal aqueous polymer dispersions in the alginate-fly ash matrix.

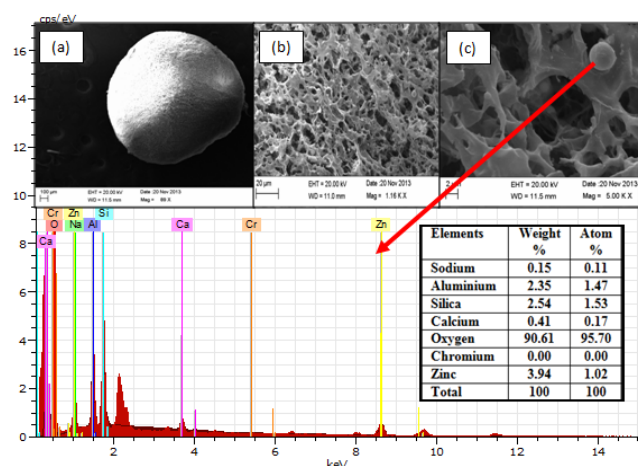


Figure 5. Scanning electron micrographs and EDAX of alginate-fly ash beads

The EDAX analysis of the bead surface disclosed the beads composition. EDAX is the microanalysis technique that could provide information of the bulk composition.²⁹ Evidently, EDAX peaks of metals and each element used for the synthesis along with notable amount of oxygen from alginate backbone on the surface of the beads.

Thermal Studies

The TGA/DTA thermogram of alginate-fly ash beads (Alg-F) shows (Figure 6) high thermal stability in the temperature region of 30-900 °C. The Alg-F shows three zones of weight loss. TGA shows the onset of decomposition near 30 °C which is due to the loss of water molecules trapped in the samples.

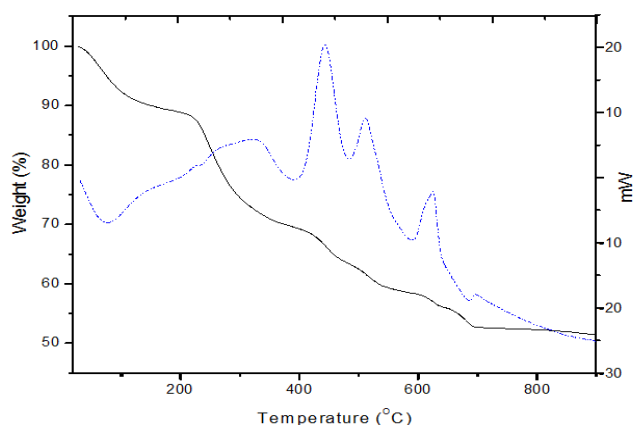


Figure 6. The TGA/DTA thermogram of alginate-fly ash beads (Alg-F)

DTA curves shows an endothermic peak at 75.85 °C attributed to the loss of water absorbed in the beads, the exothermic peak at 442.12, 513.02 and 625.77 °C means the taking place of thermal degradation of intermolecular side chain. Second weight loss was observed in the temperature range from 29-214 °C, implying that the occurrence of different extent thermal degradation of sodium alginate, rupture of alginate chains. Third weight loss was observed approximately 35 % from 409-902 °C indicates the rupture of chains, fragments, and monomers

resulting in 51 % residual. Weight loss in the temperature range from 600-750 °C is due to the loss of hydroxyl groups in the aluminosilicate structure. Significant changes of DTA curves of the beads suggest that a strong interaction established between sodium alginate and fly ash molecules.

TGA curve of beads after metal adsorption (Alg-FM) shows three thermal decomposition stages (Figure 7). The first weight loss of 12 % from 32-200 °C corresponds to the evaporation of free water. DTA curves show an endothermic peak at 68.63 °C due to the loss of water bound to the cations present within the interlayer.

Second weight loss of 60 % was observed 200-286 °C indicates which resulted from the greatest thermal degradation of the thermal degradation of sodium alginate along with decomposition of metal adsorbed on beads.

DTA curves shows a sharp exothermic peak at 247.06 °C which resulted from the greatest thermal degradation of the zinc. Third major weight loss was observed approximately 60% from 300-700 °C indicates the rupture of chains, fragments, and monomers resulting in 19% residual.

The starting temperature of the greatest thermal degradation increased in the sequence of Alg-F (214.78) > Alg-FM (188.60 °C), which is the same as that of their crystallinity, implying thermal stability of the beads were improved by their crystalline domains and hydrogen bonding interactions.³⁰

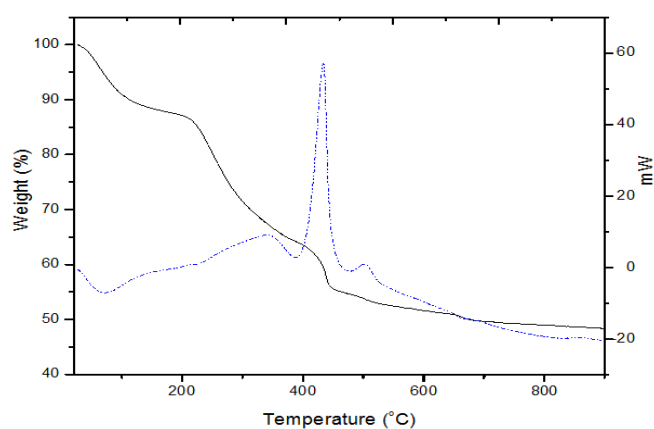


Figure 7. The TGA/DTA thermogram of alginate-fly ash beads after metal adsorption (Alg-FM)

Apart from this the average size, bulk density and swelling ratio of beads calculated are; 0.12 cm, 0.34 g mL⁻¹ and 28.65 respectively.

Batch Adsorption Studies

Effect of pH

The adsorptive behavior of Zn(II) ions was studied from the aqueous solution at different pH values are the principle factor influencing the adsorptive capacities of Zn(II) ions on alginate-fly ash beads. The pH of the aqueous solution is an important controlling parameter in the adsorption process. As the solution pH increase, the onset of the metal hydrolysis and precipitation began at pH >7 and the onset of

adsorption therefore occurs before the beginning of hydrolysis.³¹ When the pH of the adsorbing medium was increased from 2-6, there was a corresponding increase in de-protonation of the adsorbent surface, leading to decrease in H^+ ion on the adsorbent surface, which favours adsorption of positively charge species and the positive sites on the adsorbent surface.^{32,33} The results obtained are shown in Figure 8, which shows the effect of pH on the adsorption of Zn(II) ions from the aqueous solution on fly ash composite beads.

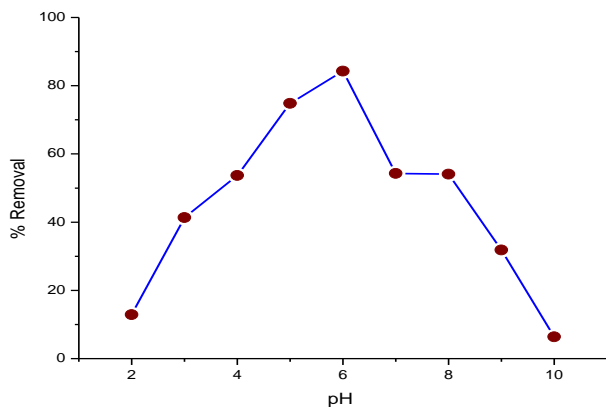


Figure 8. Effect of pH on removal of Zn(II) ions

It is clear that Zn(II) ions was effectively adsorbed in the pH range of 4-6 and the maximum adsorption of ion fly ash beads occurred at pH 6 thus, pH 6 is chosen for all experiments. The decrease in adsorption at pH greater than 6 is probably due to the formation of hydroxide. This is in agreements with the results obtained by Khalid *et al.*³⁴ for adsorption of lead on rice husk. The hydrolysis of cations occurs by the replacement of metal ligands in the inner coordination sphere with the hydroxyl groups.³⁵ This replacement occurs after the removal of the outer hydration sphere of metal cations. Adsorption may not be related directly to the hydrolysis of the metal ion, but instead of the outer hydration sphere that precede hydrolysis.

Most probably, the removal of Zn(II) ions from the aqueous solution by alginate-fly ash beads involves a complex mechanism which is partly controlled by adsorption and partly by the chemical precipitation at the solid solution interface and also partly by the pore filling mechanism.³⁶

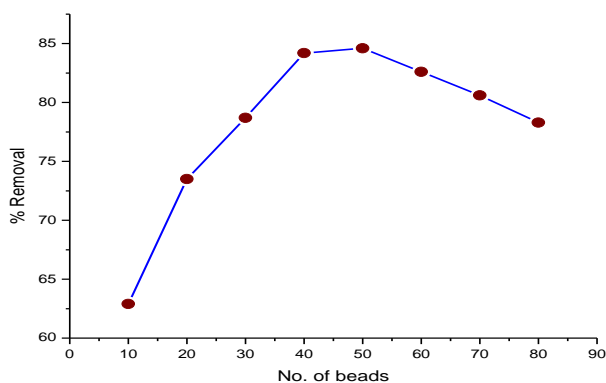


Figure 9. Effect of beads dose on removal of Zn(II) ions

Effect of adsorbent dose

The effect of adsorbent dose on the adsorption of these metal ions by varying amount of bead dose is shown in Figure 9. It was observed that the dose of beads (10–80) definitely influences the amount of adsorbed metal ions. It was observed that percentage removal of zinc was increased with the increase of no. of beads up to 40 beads. Further, the increase in beads reduces the percentage removal of Zn(II) ions to some extent.

The adsorption of metal ions on alginate-fly ash beads may involve metal interaction.³⁷ and co-ordination to functional. According to Shukla *et al.*,³⁸ the decrease in adsorption with increase in adsorbent dose is due to the high number of unsaturated sites.

Effect of bead composition

The effect of fly ash composition in the beads on the adsorption of the Zn(II) ions is shown in Figure 10. It was observed that the amount of adsorbent dose in the range (0.1–0.7 g) definitely influences the amount of adsorbed metal ions.

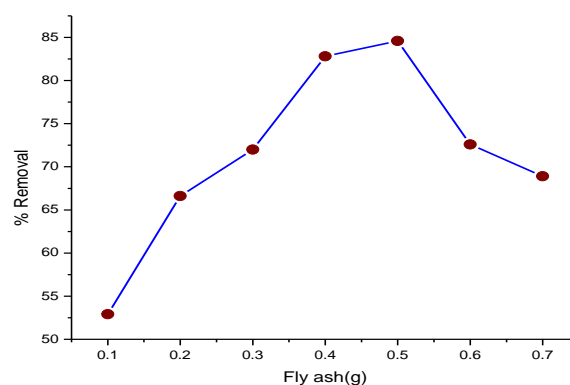


Figure 10. Effect of bead composition on removal of Zn(II) ions

It was observed that percentage removal increased with the increasing the concentration of fly ash up to 0.5 g, where it was maximum. Further, the increase in fly ash amount in the beads composition reduces the percentage removal of Zn(II) ions due to high number of unsaturated sites.³⁸

Effect of contact time

The effect of contact time on the adsorption of Zn(II) ions is shown in Figure 11. The results indicated that increase in the contact time increased the metal uptake but remained constant after an equilibrium time.

The uptake of Zn(II) ions was rapid and the equilibrium was attained in 8 hours of contact between the adsorbent and metal solution. According to Bhattacharya and Gupta³⁹ the initial high rate of metal uptake may be attributed to the existence of the base surface. However, the number of available adsorption sites decreased as the number of metal ions adsorbed increases.

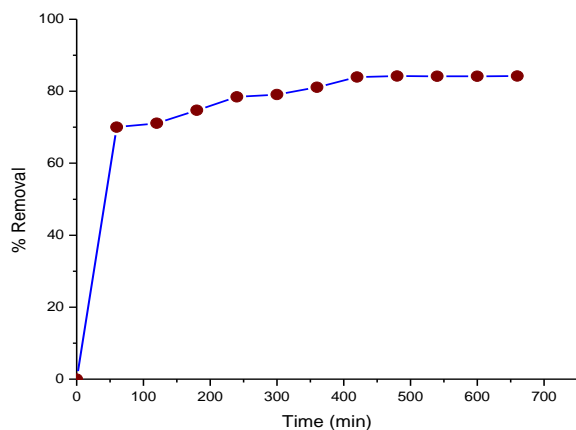


Figure 11. Effect of contact time on removal of Zn(II) ions

The enhanced adsorption of metal ions with in agitation time may also in boundary resistance to mass transfer in the bulk solution and an increase in the kinetic energy of hydrated ion.⁴⁰ By increasing the agitation time, the boundary layer resistance will be reduced and there will be an increase in the mobility of ions in the solution.

Adsorption models

Since, the adsorption isotherm is important to describe how adsorbate will interact with adsorbents and so is critical for design purpose, therefore, data using an equation is essential adsorption operation.⁴¹ Modelling of equilibrium data is fundamental for the industrial application of adsorption since it gives information for comparison among different adsorbent under different operational conditions, designing and optimizing operation procedure.⁴²

The result of batch equilibrium was used to characterize the equilibrium between the amount of adsorbate that accumulated on the adsorbate and the concentration of dissolve adsorbate. The experimental isotherm data set obtained was fitted using adsorption models including the Langmuir and Freundlich isotherm.^{43, 44}

The isotherm constants of Langmuir and Freundlich were calculated using normal linearization method.

Freundlich model

The adsorption data have been fitted to the Freundlich isotherm. Its linearised form is represented by Eqn. 3.

$$\lg Q_e = \lg K + \frac{1}{n} \lg C_e \quad (3)$$

where,

C_e is the equilibrium concentration (mg L^{-1}),

Q_e is the amount adsorbed (mg g^{-1})

K is adsorption capacity and

$1/n$ is adsorption intensity.

A plot of $\log Q_e$ versus $\log C_e$ gives a straight line of slope $1/n$ and intercept K is shown in Figure 12.

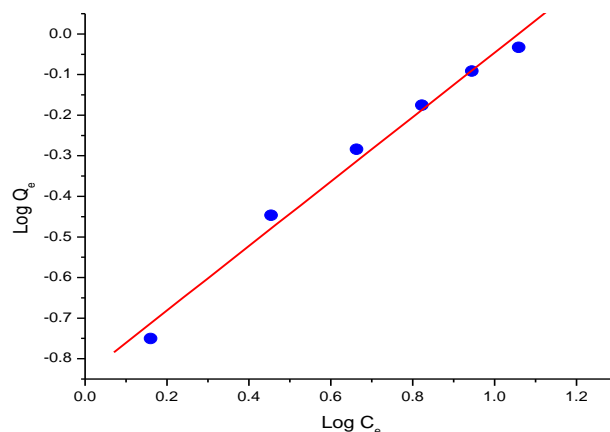


Figure 12. The linearized plot for the Freundlich adsorption isotherm of Zn(II) ions using biopolymer composite beads of alginate-fly ash

Langmuir model

The capacity of metal binding was determined by plotting C_e/Q_e against C_e , using the Langmuir equation. The plot of the specific sorption C_e/Q_e against equilibrium concentration C_e gave the linear isotherm parameters Q_{\max} , b and the coefficient of determination (R^2). The linear equation of Langmuir represented as Eqn. - 4.

$$\frac{C_e}{Q_e} = \frac{1}{Q_{\max}b} + \frac{C_e}{Q_{\max}} \quad (4)$$

where,

C_e is the metal concentration in the solution at equilibrium (mg L^{-1}),

Q_{\max} (adsorption capacity) and

b (energy of adsorption) are the Langmuir constants.

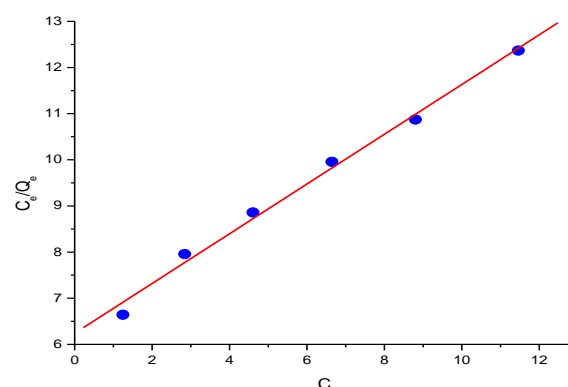


Figure 13. The linearized plot for the Langmuir adsorption isotherm of Zn(II) ions using biopolymer composite beads of alginate-fly ash

The Langmuir isotherm model effectively describes the sorption with R^2 values. The sorption capacity, Q_{\max} which is a measure of maximum adsorption capacity corresponding to complete monolayer coverage showed that composite beads of alginate-fly ash beads had a mass capacity for Zn(II) ions is 1.8554 mg g^{-1} .

The adsorption coefficient b which is related to the apparent energy of adsorption Zn(II) ions is 0.0860. The plots of C_e/Q_e against C_e for adsorption of Zn(II) ions gave a straight line are shown in Figure 13. It has seen that the linear fit is fairly good and enables the applicability of the Langmuir model to the Zn(II) ions adsorption on the alginate-fly ash composite beads.

The essential characteristics of Langmuir equation can be described by dimensionless equilibrium parameter,⁴⁵ R_L which is defined as;

$$R_L = \frac{1}{1+bC_0} \quad (5)$$

where,

b is the Langmuir constant

C_0 is the initial metal concentration of Zn(II) ions.

In the present study the R_L for Zn(II) ions were found between 0 and 1 as shown in Figure 14, for the initial concentration of Zn(II) ions of 5-30 mg L⁻¹ indicating that the adsorption of Zn(II) ions is favorable. The R_L values indicate the shape of isotherm as shown in Table 1. The R_L values between 0 and 1 indicate favorable adsorption.⁴⁶

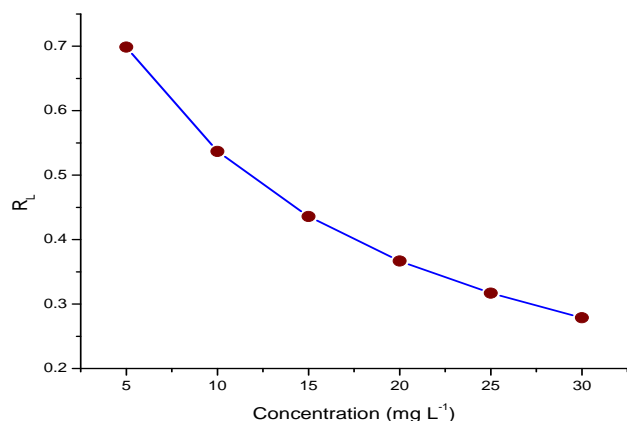


Figure 14. R_L vs initial concentration of metal ions

Table 1. Relationship between R_L and type of isotherm

R_L	Type of isotherm
$R_L > 1$	Unfavourable
$R_L = 1$	Linear
$R_L < 1$	Favourable
$R_L = 0$	Irreversible

Examination of correlation coefficient suggests that both the isotherms models fitted well for the sorption of Zn(II) ions. This isotherm does not predict any saturation of the sorbent by the sorbate; thus infinite surface coverage is predicted mathematically, indicating multilayer adsorption on the surface.⁴⁷ The correlation coefficient of data for Langmuir and Freundlich plot give a value which is > 0.9 although this value for Freundlich isotherm is slightly higher

than that of Langmuir isotherm since, the correlation coefficient for both are high, it reveals that besides monolayer adsorption there is multilayered adsorption and also suggests that adsorption reaction is physico-chemical type.

The values of both Langmuir and Freundlich isotherm parameters were given in Table 2. Examination of data suggests that Freundlich isotherm is a good model for the sorption of Zn(II) ions. The values of $1/n$ that vary between 0.1 and 1.0 indicate the favorable adsorption of heavy metals.⁴⁸

Table 2. Langmuir and Freundlich adsorption parameters for the adsorption of Zn(II) ions at 30 °C.

Langmuir Parameters		Freundlich Parameters	
Q_{max} , (mg g ⁻¹)	1.8554	K	1.2610
b (L, mg ⁻¹)	0.0860	$1/n$	0.1449
R^2	0.9700	R^2	0.9860

The Langmuir model deals with monolayer coverage and constant adsorption energy while Freundlich equation deals with physicochemical adsorption on heterogeneous surfaces.⁴⁹ The applicability of both these isotherms to the alginate-fly ash composite beads, in the present study, implies that monolayer adsorption and heterogeneous surfaces conditions exist under the experimental conditions used. The adsorption properties of the adsorbent are thus likely to be complex, involve more than one mechanism.

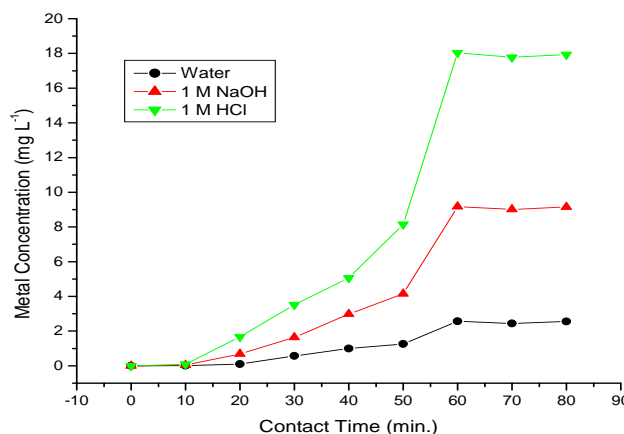


Figure 15. Desorption profile for Zn(II) ions

Desorption studies

In order to desorb the metal ions, the beads loaded with Zn(II) ions were exposed to 20 mL of distilled water, 0.1 M HCl and 0.1 M NaOH separately for 15 minutes and washed with double distilled water. It was found that 0.1 M HCl is the better eluent for desorption of metal from the beads (Figure 15). The beads were then again exposed to distilled water, followed by 0.1 M HCl, to strip any remaining Zn(II) ions. The desorbed beads were reused in next adsorption experiments. In order to show the multiple reuse of adsorbent beads, an adsorption-desorption cycle of metal ions was repeated three times using the same preparations.

Conclusions

This work indicates that alginate-flyash composite beads can be used for removal of Zn(II) ions from wastewater. Both Langmuir and Freundlich isotherm models can be used to estimate maximum metals uptake and the affinity parameter. It was found that the adsorption equilibrium data was better fitted by both the Freundlich and the Langmuir isotherm in the concentration range studied. The removal of Zn(II) ions was found to depend on adsorbent dosage, composition of beads, solution pH and contact time. Solution pH is an important parameter affecting adsorption of ions and maximum removal for Zn(II) ions at pH value 6.0. The adsorption mechanism of Zn(II) ions on alginate-fly ash composite beads involves either cation exchange or complexation between the metal cation and the hydroxide ion in the solution. This study shows a new trend for using alginate-fly ash composite beads for the benefit of environmental pollution control.

Acknowledgements

Authors are thankful to the Head, Department of Chemistry, Director, USIC, University of Delhi, and Director of AIRF-Jawaharlal Nehru University for providing instrumentation facilities and UGC [F.15-76/12 (SA-II)] for providing financial assistance.

References

- ¹Ayoub, G. M., Semerjian, L., Acra, A., El Fadel, M. and Koopman, B., *J. Env. Eng.*, **2001**, 27, 196- 207.
- ²Ho, Y. S. M., *Water Res.*, **2003**, 37, 2323-2330.
- ³Inbaraj, B. S., Selvarani, K. and Sulochana, N., *J. Sci. & Ind. Res.*, **2002**, 61, 971-978.
- ⁴Lo, W. H., Chua, H., Lam, K. H. and Bi, S. P., *Chemosphere*, **1999**, 39, 2723-2736.
- ⁵Mellah, A. and Chegrouche, S., *Water Res.*, **1997**, 31, 621- 629.
- ⁶Undaybeytia, T., Morillo, E. and Maqueda, C., *Clays Clay Min.*, 1996, 31, 485-490.
- ⁷Mangale Sapana, M., Chonde Sonal G. and Raut, P. D., *Res. J. Recent Sci.*, **2012**, 1(3), 31-40.
- ⁸Vaishnav, V., Kailash, D., Suresh C. and Madan, L., *Res. J. Recent Sci*, **2012**, 1, 160-165.
- ⁹Bilodeau, A. and Malhotra, V. M., *ACI Mater. J.*, **2000**, 97, 4-49.
- ¹⁰Ahmaruzzaman, M., *Adv. Colloid Interface Sci.*, **2008**, 143, 48-67.
- ¹¹Wang, S. and Wu, H., *J. Hazard. Mater.* **2006**, 136, 482-501.
- ¹²Wang, S. B., Soudi, M., Li, L. And Zhu, Z. H., *J. Hazard. Mater.*, **2006**, 133, 243-251.
- ¹³Aravindhnan, R., Fathima, N. N., Rao, J. R. and Nair, B. U., *Colloids and Surfaces A: Physicochemical and Engineering Aspects*, **2007**, 299, 232-238.
- ¹⁴Davis, T. A., Volesky B. and Mucci, A., *Water Research*, **2003**, 37, 4311-4330.
- ¹⁵Kuyucak, N., and Volesky, B., *Biotechnol. Bioeng.*, **1989**, 33, 823-831.
- ¹⁶Ashok Kumar, A., Rajesh Kumar, P., Anil Kumar, A., Lokeswara Reddy, K., Murthy, T. E. G. K. and Venkateswara Rao, T., *Journal of Applied Pharmaceutical Science*, **2011**, 01 (06), 127-132.
- ¹⁷Kanaka Durga Devi, N., Chandana, M., Sindhura, A., Ratnavali, G. and Kavitha, R., *Pharmacophore*, **2010**, 1(3), 196-213.
- ¹⁸Sonone, S. B., Kokane, S. P., Shirote, P. J. And Naikawade, N. S., *Inter. Jour. of Pharm. Tech. Res.*, **2011**, 3(1), 225-230.
- ¹⁹Freddi, G., Tsukada, M. and Beretta, S., *J. Appl. Polym. Sci.*, **1999**, 71, 1563-1571.
- ²⁰Meng, M., Zhou, N. L., Zhang, S, Q. and Shen, J., *Int. J. Pharm.*, **2009**, 382, 45-49.
- ²¹Joshi, G. V., Patel, H. A., Bajaj, H. C. and Jasra, R. V., *Colloid. Polym. Sci.*, **2009**, 287, 1071-1076.
- ²²Chen, B. Y., Lee, Y. H., Lin, W. C., Lin, F. H. and Lin, K. F., *Biomed. Eng. Appl. Basis Commun.*, **2006**, 18(1), 30-36.
- ²³Zhang, L., Zhou, D., Wang, H., and Sheng, S., *J. Membrane Sci.*, **1997**, 124, 195-201.
- ²⁴Nikolic, C. V., Nikolic, L. J., Stankovic, M., Kapor, A., Popsavin, M. and Cvetkovic, D., *J. Serb. Chem. Soc.*, **2007**, 72, 737-746.
- ²⁵Stuart, B., *Modern Infrared Spectroscopy*, Wiley, Chister, U.K., **1996**.
- ²⁶Fang, D., Liu, Y., Jiang, S., Nie, J. and Ma, G., *Carbohydr. Polym.*, **2011**, 85, 276-279.
- ²⁷Sarkar, A., Bassu, A. K., Udaybhanu, G. and Rano, R., *Fuel*, **2006**, 87, 259-277.
- ²⁸Yan, F., Zheng, C. R., Zhai, X. D. and Zhao, D. J., *J. Appl. Polym. Sci.*, **1998**, 67, 747-754.
- ²⁹Velásquez, P., Leinen, D., Pascual, J., Ramos-Barradoa, J. R., Cordova, R. and Gómez, H., *J Electroanal Chem.*, **2001**, 510, 20-28.
- ³⁰Liang, C. X. and Hirabayashi, K., *J. Appl. Polym. Sci.*, **1992**, 45, 1937-1943.
- ³¹Baes, G. B. and Mesmer, R. E., "Hydrolysis of Cations", John Wiley and Sons, New York, **1976**.
- ³²Kadirvelu, K. and Namasivayam, C., *Adv. Environ. Res.*, **2003**, 7, 471- 478.
- ³³Abdus-Salam, N. and Adekola, F. A., *Afr. J. Sci. Technol.*, **2005**, 6, 55-66.
- ³⁴Khalid, N., Ahmad, S., Naseer Kiani, S. and Ahmed, J., *Sep. Sci. Technol.*, **1998**, 33, 2349-2362.
- ³⁵Badmus, M. A. O., Audu, T. O. K. and Anyata, B. U., *Turkish J. Eng. Env. Sci.*, **2007**, 31, 251 – 263.
- ³⁶Knocke, W. R. and Hemphill, L. M., *Water Res.*, **1981**, 15, 275-282.
- ³⁷Sengupta, A. K. and Clofford, D., *Environ. Sci. Technol.*, **1986**, 20, 149-155.
- ³⁸Shukla, A., Zhang, Y. H., Dubey, P., Margrave, J. L. and Shukla, S. S., *J. Hazar. Mater*, **2002**, B95, 137-152.
- ³⁹Bhattacharya, K. G. and Gupta, S. S., *Colloid Surf. A: Physiochem. Eng. Asp.*, **2006**, 277, 191-200.
- ⁴⁰Horsfall, M. and Abia, A. A., *Water Res.*, **2003**, 37, 4913-4923.
- ⁴¹Hashem, M. A., Abdelmonem, R. M. and Farrag, T. E., *Alexandria Eng. J.*, **2007**, 1, 1-9.
- ⁴²Benguella, B. and Benaissa, H., *Water Res.*, **2002**, 36, 2463-2474.
- ⁴³Langmuir, I., *J. Am. Chem. Soc.*, **1918**, 40, 1361-1402.
- ⁴⁴Freundlich, H., *Z. Phys. Chem.*, **1907**, 57, 385- 470.

⁴⁵Hall, K. R., Eagleton, I. C., Acrivos, A. and Vermeulen, T., *Ind. Eng. Chem. Fund.*, **1966**, 5, 212-223.

⁴⁶Ahalya, N., Kanamadi, R. D. and Ramachandra, T. V., *Indian J. Chem. Technol.*, **2006**, 13, 122-127.

⁴⁷Hasany, S.M., Saeed, M. M. and Ahmed, M., *J. Radioanal. Nucl. Chem.*, **2002**, 252, 477-484.

⁴⁸Unnithan, M. R. and Anirudhan, T. S., *Indian Eng. Chem. Res.*, **2001**, 40, 2693-2701.

⁴⁹Singh, K. K., Singh, A. K. and Hasan, S. H., *Bioresour. Technol.*, **2006**, 97, 994-1001.

Received: 31.03.2014.

Accepted: 28.05.2014.



ADSORPTION OF ARSENIC(V) ONTO METAL LOADED CELLULOSE NANOCOMPOSITE BEAD (MCNB)-ISOTHERM AND THERMODYNAMIC STUDY

Dhiman Santra,^[a] Rubi Ghosh,^[a] Mridula Das,^[b] Parshati Majumdar,^[a] Mitali Sarkar*^[a]

Keywords: Metal loaded cellulose nanocomposite bead; batch study; arsenic adsorption; isotherm; water analysis.

Cellulose nanocomposite bead modified with metal (MCNB) such as Ce, Al and Fe is synthesized for selective adsorption of arsenate anions As(V) from drinking water in batch system. The adsorbent was characterized by FTIR, FESEM, EDS and EPR studies. In the present report arsenic(V) adsorption performance on cerium modified cellulose bead was described. The maximum adsorption of As(V) is near about 100 percent up to an initial arsenic load of 5.0 mg L⁻¹ at the acidic pH of 3.0 and the equilibrium is reached in 5 h. The much higher adsorption extent and quick equilibrium time compared to the other reported adsorbents makes the present adsorbent as efficient one. Among the three adsorption isotherm models used, Langmuir model fitted the experimental data best. The adsorption is found to be exothermic, spontaneous and random in nature. The process was applied for removal of arsenic from some real sample.

Corresponding Authors

Tel: 091 033 2582 8750

Fax: 091 033 2582 8282

E-Mail: mitaliku@gmail.com; msarkar@klyuniv.ac.in

[a] Department of Chemistry, University of Kalyani, Kalyani 741 235, INDIA

[b] Kalna College, Kalna, Burdwan, 713409, INDIA

Various treatment technologies have been used to remove arsenic from water such as oxidation,⁵ coagulation,⁶ ion exchange,⁷ chemical precipitation,⁸ membrane separation,⁹ etc. However, adsorption is recognized as an effective technique due to availability of wide range of adsorbents including natural and synthetic materials. The high concentration efficiency, simple operation, and environmental friendly behavior¹⁰ of certain adsorbents make the process quite popular. Cellulose, the most widely available and renewable biopolymer in nature, is a very promising raw material available at low cost for the preparation of various functional materials. Due to the presence of hydroxyl groups, cellulose may undergo surface modification.^{10,11} Cellulose beads show good adsorption ability due to their unique hydrophilic and porous nature as well as high surface area. Beads made from cellulose and its derivative are commonly used as ion exchangers, packing materials for chromatography, adsorbents for heavy metal ions, and proteins, cosmetic additives, and carriers for immobilization of biocatalysts.¹²⁻¹⁴ However, studies on cellulose beads as arsenic scavenger are still scarce. Adsorbents modified with metals such as Fe,^{15,16} Ce,¹⁷ Ti,^{18,19} Al,²⁰ La,^{21,22} etc are found to have potential ability to absorb arsenic from water under optimized condition. In the present investigation cerium loaded nanocomposite cellulose bead (CCNB) for As(V) adsorption is reported as a representative of the metal loaded nanocomposite cellulose bead.

The synthesized bead was characterized by Fourier transformed infrared spectroscopy (FTIR), field emission scanning electron microscopy (FESEM), energy dispersive spectroscopy (EDS) and electron paramagnetic resonance (EPR) study. The feasibility of equilibrium adsorption was interpreted by adsorption isotherms such as Langmuir, Freundlich, and Temkin model as well as the thermodynamic parameters such as change in free energy, enthalpy, and entropy.

Introduction

Arsenic (As) contamination in ground water is one of the most critical environmental problems today. Arsenic (atomic number 33) is ubiquitous and ranks 20th in natural abundance, comprising about 0.00005 % of the earth's crust, 14th in the seawater, and 12th in the human body.¹ Arsenic, due to its toxic and carcinogenic effect, has been recorded by the World Health Organization as a first priority pollutant.^{2,3} Acute and chronic arsenic poisoning via drinking water has been reported in many countries, especially Argentina, Bangladesh, India, Mexico, Mongolia, Thailand, and Taiwan, as a result of in groundwater⁴ arsenic load at levels from 100 to over 2000 µg L⁻¹.

Millions of people worldwide are exposed to naturally occurring arsenic contaminated groundwater, which they use as their sole source of drinking water. Increased use of groundwater as a source for drinking water has caused serious health problems such as neurological, dermatological, gastrointestinal, cardiac, and renal diseases. Factors such as anthropogenic activities, biological actions, and geochemical reactions accelerate arsenic mobilization into groundwater.¹ Arsenic compounds are stable in the environment, have a tendency to bioaccumulate in the food chain, and can undergo biotransformation with an increase in toxicity. It is necessary to control the arsenic concentration in environmental samples, industrial wastes, biological materials, and foods.

Experimental

Materials

All the chemicals used are of analytical grade (Merck, India). The cellulose powder used was procured from Loba Chemie, Mumbai, India

Preparation of CCNB

Cerium loaded cellulose nanocomposite bead was synthesized by the method described elsewhere²³ following sol gel techniques.

1 g of cellulose is esterified with carbon disulfide with shaking in alkaline medium and stirred for 3 h.²⁴ The sol was allowed for ageing (syneresis) at room temperature for 72 h and the gel probably formed by condensation of the sol, was purged drop by drop into de-aerated methanol through a needle. A faint red colored beads initially formed were filtered and immediately washed several times with double distilled water. The cellulose beads appeared as snow white, were stored under de-ionized water.

The cellulose nanocomposite beads were next poured into a solution of 0.10 M cerium ammonium nitrate at pH 1.6 and shaken at a speed of 100 spm at room temperature for 2 h. A faint orange yellow colored cerium loaded cellulose nanocomposite bead, (CCNB) was formed, washed with distilled water, and stored under de-ionized water.

Characterization of CCNB

Field emission scanning electron microscope (FESEM) with a JEOL, JSM 6700F microscope was used to study surface morphology and energy dispersive spectroscopy (EDS, model FEI QUANTA FEG 250) was used for element detection. Electron paramagnetic resonance (EPR) study to identify the binding pattern of cerium in the bead was recorded in a Varian X-band EPR spectrometer (Model E-109). The Fourier transformed infrared (FTIR) spectral study was recorded in a Perkin Elmer L120-000A spectrophotometer.

Batch adsorption study

Batch adsorption experiment was performed using As(V) solution of known concentration, shaken with a specific amount of CCNB, and agitated at a constant shaking rate of 120 spm in a temperature controlled shaker. The initial solution pH was adjusted using 0.1 M HCl/NaOH. The As(V) concentration in solution was determined using atomic absorption spectroscopy (AAS, Varian AA240 model). Adsorption efficiency (ϕ , in %), expressed as percent adsorption, was calculated using the following equation:

$$\phi = 100 \frac{C_0 - C_e}{C_0} \quad (1)$$

where,

C_0 and C_e are the initial and equilibrium As(V) concentration (mg L^{-1}), respectively in solution.

Result discussion

Characterization of CCNB

Physicochemical parameters such as bulk and material density were found to be 0.902 and 0.410 g cm^{-3} respectively. The degree of swelling was found to be 22 while the water content and porosity were found to be 95.120 and 89 % respectively.

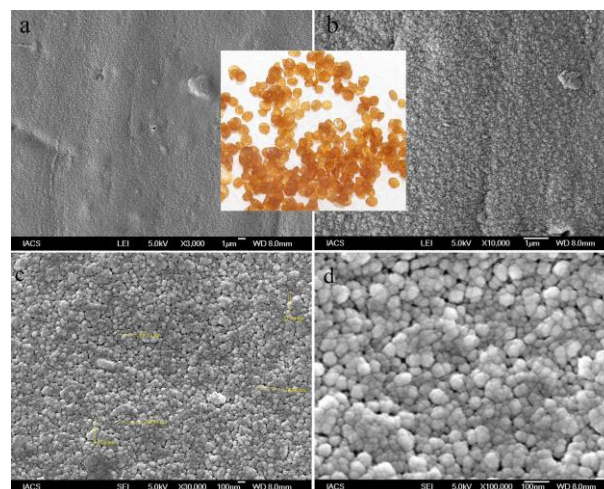


Figure 1. FESEM at different magnification and physical image (inset)

The surface structure of CCNB, as revealed from FESEM analysis, indicates the spherical nature of the bead with an average size in the range 28 to 61 nm (Fig. 1). The EDS shows peaks corresponding to the presence of 'C', 'O' and 'Ce' in the CCNB (Fig. 2).

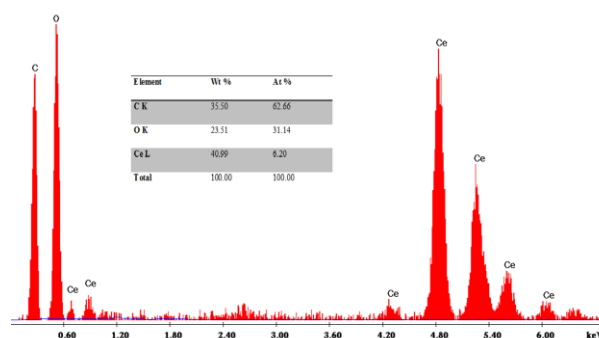


Figure 2. EDS of CCNB with table of weight percentage of element

The EPR study conducted at room temperature (303 K) and lower temperature (77 K) shows similar signals having characteristics g values attributed to $g_e=2.03$, $g_{\perp}=1.98$, $g_{\parallel}=1.93$, ($g_e > g_{\perp} > g_{\parallel}$)²³ corresponding to Ce^{3+} . The FTIR spectral analysis of CCNB showing the characteristic bands of cellulose moiety with characteristic linkages²⁵⁻²⁷ is presented in Table 1.

Table 1. FTIR spectral analysis of CCNB

Position, cm^{-1}	Assignment
3402	O–H stretching
2918	C–H stretching
1642	molecular water bending
1424	C–O–H and C–C–H deformations
1375–1317	C–H flexure (symmetric)
1161, 1060	C–O stretching
898	C–H bending (β -anomeric link of cellulose)
769	C–C stretching
535	Ce–O linkage

Effect of pH on As(V) adsorption

The effect of pH on As(V) adsorption by the CCNB is shown in Fig. 3 for the pH ranging between 2 and 12. It is observed that maximum adsorption of As(V) occurs at pH 3.0. pH dependent adsorption is significantly due to the specific arsenic species and the adsorbent surface charge. Speciation study indicates that the dominant species of arsenate are H_3AsO_4 (pH < 2), $H_2AsO_4^-$ (pH = 2–6.1), $HAsO_4^{2-}$ (pH = 6.1–11.5), and AsO_4^{3-} (pH > 11.5). It is probable that $H_2AsO_4^-$ is the most suitable species of arsenic for adsorption on CCNB.

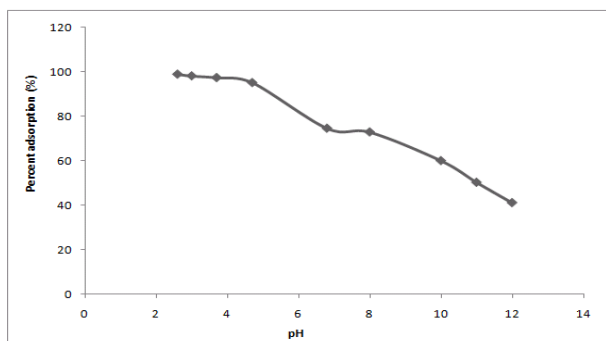


Figure 3. Effect of pH on As(V) adsorption

Effect of contact time on As(V) adsorption

Fig. 4 illustrates the effect of time on the percent adsorption as well as the attainment of equilibrium. It is found that with increase of time the percent adsorption corresponding to each concentration of As(V) increases. After a certain time it reaches a maxima forming a plateau. The time corresponding to maximum adsorption is known as the equilibrium time. It is observed that equilibrium is reached at 5 h for all the concentrations studied.

Effect of initial concentration on As(V) adsorption

The decrease in the percentage of As(V) adsorbed due to the increase in initial As(V) concentration at fixed adsorbent dosage is presented in Fig. 5. The increase in arsenic

adsorption capacity with the decrease in initial concentration was due to the availability of more adsorption sites. However, as the initial arsenic concentration increases, the ratio of the number of arsenic ions to the available active sites on the adsorbent becomes high and the arsenic ions are difficult to get adsorbed, leading to a decrease in the removal percentage.

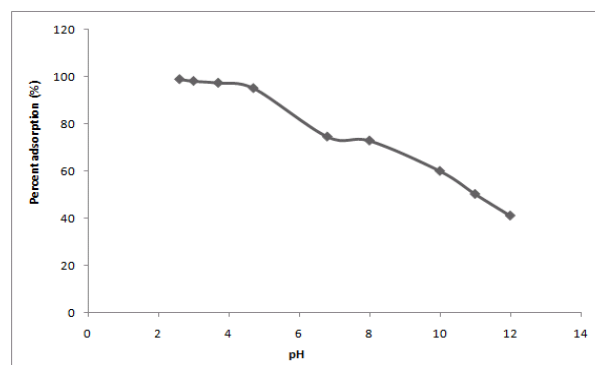


Figure 3. Effect of pH on As(V) adsorption

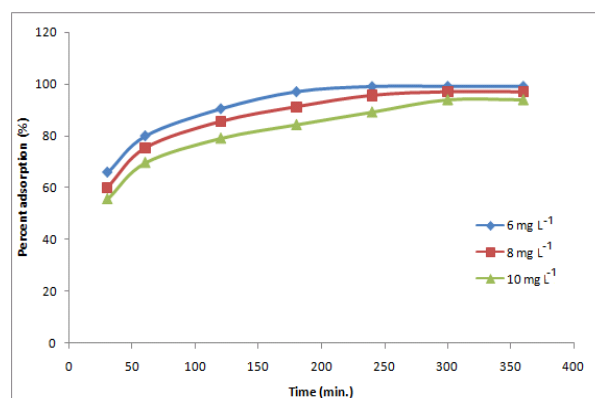


Figure 4. Effect of contact time on As(V) adsorption

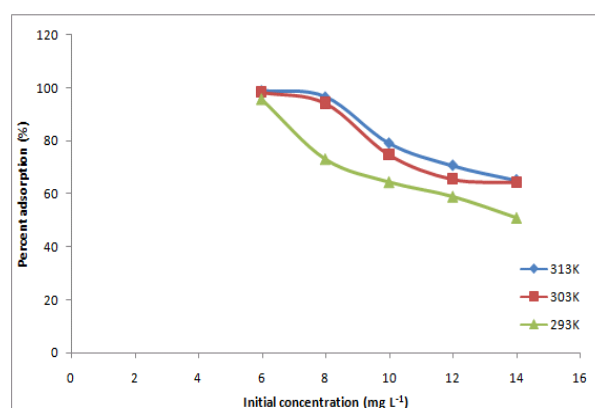


Figure 5. Effect of initial concentration on As(V) adsorption

Effect of adsorbent dose on As(V) adsorption

Fig. 6 showed that the increased adsorbent dose led to an increase in As(V) removal. The increase in percent adsorption with adsorbent dosage can be attributed to the increased adsorbent surface active sites.

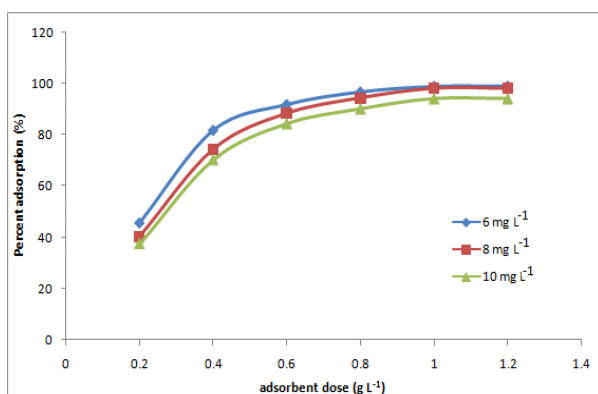


Figure 6. Effect of adsorbent dose on As(V) adsorption

Adsorption isotherm

In an aim to describe the equilibrium adsorption for As(V) ions from aqueous solution on CCNB, three most popular isotherm models viz. Langmuir, Freundlich, and Temkin are tested.

The Langmuir isotherm, (Fig. 7a) applicable for the monolayer adsorption²⁸ is expressed in its linear form as,

$$\frac{C_e}{q_e} = \frac{1}{Qb} + \frac{1}{Q}C_e \quad (2)$$

where,

Q (mg g^{-1}) and b (L mg^{-1}) are Langmuir isotherm constants signifying the adsorption capacity and the energy of adsorption respectively.

The Freundlich isotherm, (Fig. 7b) assuming an exponentially decaying adsorption site energy distribution and applicable to non-ideal adsorption on heterogeneous surfaces showing multi-layer adsorption,²⁹ is expressed by the following linear equation:

$$\ln q_e = \ln K_F + \frac{1}{nF} \ln C_e \quad (3)$$

where,

K_F is the constant indicative of the relative adsorption capacity of the adsorbent (mg g^{-1}), and

$1/n_F$ is the constant indicative of the intensity of the adsorption.

The Temkin isotherm,³⁰ (Fig. 7c) that considers solute/adsorbent interactions based on decaying heat of adsorption of the solute linearly with adsorbent surface coverage, is represented in linear form as,

$$q_e = \frac{RT}{b_{TM}} \ln k_{TM} + \frac{RT}{b_{TM}} \ln C_e \quad (4)$$

where,

k_{TM} is the isotherm constant and

b_{TM} is related to heat of adsorption.

The adsorption equilibrium data for As(V) adsorption at three different temperatures were determined and fitted to the above three isotherm equations. The quality of data fit was judged from the R^2 values. High R^2 value describes the most preferred situation. From Table 2 it is found that both the Q and b values increase with increase of temperature. This indicates that adsorption (Q) capacity increases with temperature. It is also supported by the fact that with higher temperature percent adsorption increase for each initial concentration of arsenic (Fig. 5). Among the three different isotherm models R^2 value corresponding to Langmuir is of higher magnitude than the Freundlich and Temkin model. Thus, Langmuir isotherm model most suitably describe the As(V) adsorption on CCNB.

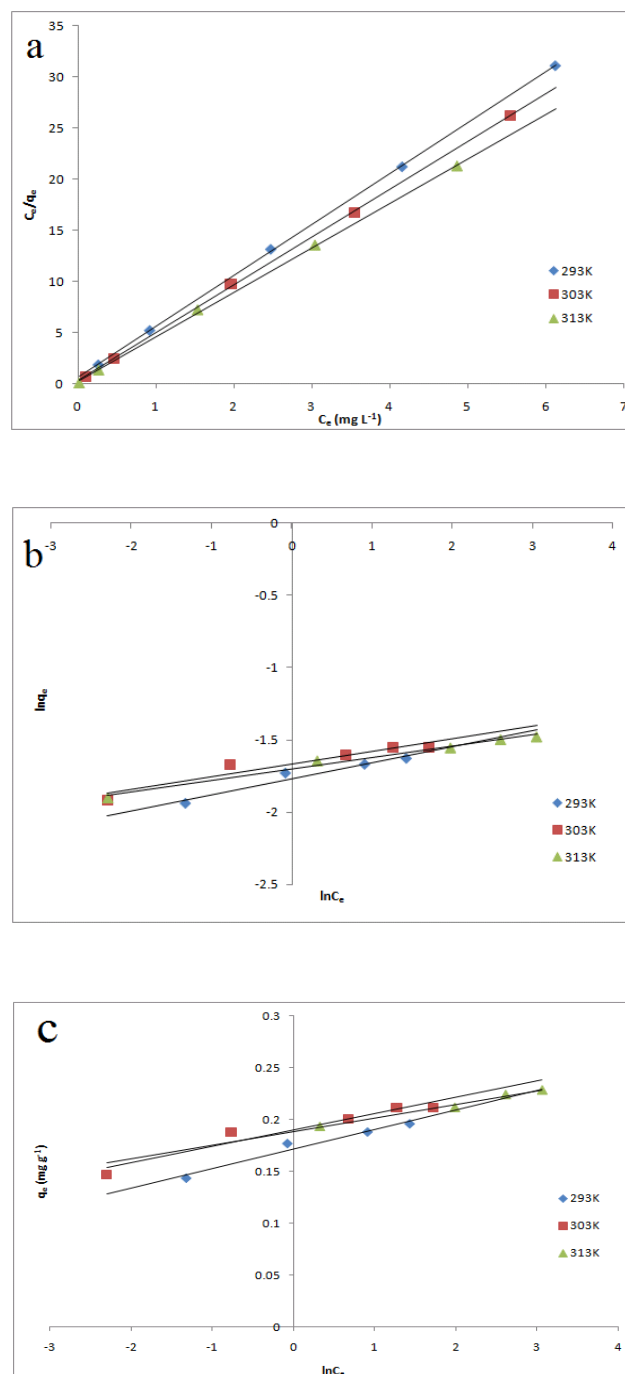


Figure 7. Isotherm data plots at different temperatures (a) Langmuir (b) Freundlich (c) Temkin

The applicability of Langmuir isotherm model was further tested by evaluating sf , the separation factor,³¹ a dimensionless quantity as expressed by

$$sf = \frac{1}{1 + bC_0} \quad (5)$$

where,

b is the Langmuir constant and

C_0 is the initial concentration of As(V).

The parameter ' sf ' indicates the nature of the isotherm as it is given in Table 3.

Table 2. Isotherm parameters

Langmuir isotherm	T , (K)	Q , (mg g ⁻¹)	b , (L mg ⁻¹)	R^2
	293	0.200	8.005	0.999
	303	0.214	14.590	0.999
	313	0.229	17.497	0.999
Freundlich Isotherm	T , (K)	K_F , mg g ⁻¹ (L mg ⁻¹) ^{1/n}	$1/n_F$	R^2
	293	0.170	0.111	0.945
	303	0.188	0.087	0.915
	313	0.182	0.078	0.985
Temkin isotherm	T , (K)	K_{TM} , (L mg ⁻¹)	b_{TM} , (kJ mol ⁻¹)	R^2
	293	1.330 x 10 ⁴	135.330	0.960
	303	3.148 x 10 ⁵	167.942	0.936
	313	1.901 x 10 ⁶	200.000	0.986

Table 3. Feasibility and nature of isotherm study

sf	Nature
$sf > 1$	Unfavorable
$sf = 1$	Linear
$0 < sf < 1$	Favorable
$sf = 0$	Irreversible

The sf value at each temperature corresponding to each concentration of As(V) is calculated (Table 4).

Table 4. Temperature dependent separation factor

T (K)	Sf , C_0 (mg L ⁻¹)		
	6.0	8.0	10.0
293	0.020	0.015	0.012
303	0.011	0.008	0.006
313	0.009	0.007	0.005

It is found that the sf values lie within 0.012 to 0.020 at 293 K, 0.006 to 0.011 at 303 K and 0.005 to 0.009 at 313 K. As all values lie between 0 to 1, the adsorption of As(V) on CCNB indicates a favorable case of adsorption.

Thermodynamic study

The knowledge of thermodynamic parameters is of fundamental importance to test the spontaneous occurrence of a given process as well as the feasibility of operation at a given temperature. Thermodynamic parameters associated with the adsorption process, viz., standard free energy change (ΔG^0), standard enthalpy change (ΔH^0), and standard entropy change (ΔS^0) were calculated using the following Eqs. 6 and 7.

$$\Delta G^0 = -RT \ln K_c \quad (6)$$

$$\Delta G^0 = \Delta H^0 - T\Delta S^0 \quad (7)$$

where,

T is the absolute temperature (K) and

R is the gas universal constant.

The equilibrium constant K_c for the adsorption was evaluated from the slope and intercept of the Langmuir plot³² (Fig. 7a).

The magnitude and sign of ΔG^0 depends on the value of K_c . When the rates of the adsorption and desorption processes are equal in magnitude, K_c becomes unity and $\Delta G^0 = 0$. The value of ΔG^0 is negative for $K_c > 1$ and positive for $K_c < 1$. If adsorption occurs spontaneously, the rate of adsorption being higher than desorption, ΔG^0 will always be a negative quantity.³³ Spontaneity of the adsorption process is also affected by the thermodynamic parameters ΔH^0 , and ΔS^0 .

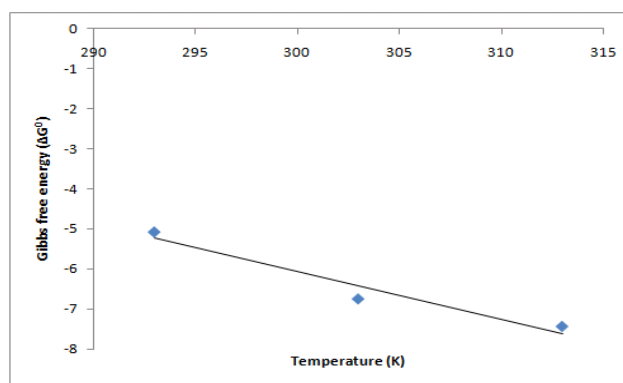


Figure 8. Plot of ΔG^0 versus temperature, T

A plot of ΔG^0 versus temperature, T , will be linear following equation (7) and the values of ΔH^0 , and ΔS^0 are determined from the slope and intercept of the plot Fig. 8. The values of K_c , ΔG^0 , ΔH^0 , and ΔS^0 are presented in Table 5.

Table 5. Thermodynamic parameters

T , (K)	K_c	ΔG^0 , (kJ mol ⁻¹)	ΔH^0 , (kJ mol ⁻¹)	ΔS^0 , (kJ mol ⁻¹ K ⁻¹)
293	8.005	-5.06705	29.63	0.119
303	14.59	-6.75215		
313	17.49	-7.44677		

Application

The efficiency of the present adsorbent is tested with the spiked samples. The results are shown in Table 6.

Table 6. Efficiency study with spiked sample

Sl. no.	As(V) concentration, (mg L ⁻¹)			Adsorption, (%)
	Mean	Spiked	Found	
1	0.5	0.0	0.51 ± 0.02	100
2	0.5	2.5	2.99 ± 0.02	100
3	0.5	5.0	5.44 ± 0.03	99
4	0.5	7.5	7.76 ± 0.04	97
5	0.5	10.0	8.56 ± 0.04	84

The applicability of the present method was judged with the field sample. The water sample was collected from some arsenic affected area of Deganga, North 24 Paragana, West Bengal, India. The composition of the field sample was presented in Table 7.

Table 7. Physicochemical parameters of the studied field sample

Parameter	Load, (mg L ⁻¹)
Hardness	142
pH	6.7
SO ₄ ²⁻	5.0
NO ₃ ⁻	Nil
Ca ²⁺	22.0
Mg ²⁺	5.0
Na ⁺	17.0
Iron	5.3
Arsenic	0.227

The load of the arsenic after treatment with CCNB was found to reach below the detection limit.

Conclusion

Metal loaded cellulose nanocomposite bead is found to be effective for adsorptive removal of arsenic from water. The process is dependent significantly on the pH of the solution. At acidic pH range quantitative adsorption occurs. The process is found to follow the Langmuir isotherm than the Freundlich and Temkin model. The process is thermodynamically feasible as shown by negative free energy change and positive entropy change. The process is effective for removing arsenic from real sample.

Acknowledgement

One of the authors (D.S) is thankful to University of Kalyani for providing a research fellowship. Authors sincerely acknowledge the support and facilities provided under UGC-SAP, DST-FIST, and DST-PURSE program.

References

- Mohan, D. and Pittman, C. U. Jr., *J. Hazard. Mater.*, **2007**, 142, 1–53.
- EPA. *Arsenic in drinking water: health effects research*. www.epa.gov/OGWDW/ars/ars10.html, **1999**.
- WHO. *Toxic effects of arsenic in humans*. www.who.int/peh-super/Oth.lec/Arsenic/series4/002.htm, **1999**.
- Smedley, P. L. and Kinniburgh, D. G., *Appl. Geochem.*, **2002**, 17, 517–568.
- Martin, D. F., O'Donnell, L., Martin, B. B. and Alldredge, R., *J. Environ. Sci. Health A Tox. Hazard. Subst. Environ. Eng.*, **2007**, 42, 97–102.
- Moreno-Casillas, H. A., Cocke, D. L., Gomes, J. A. G., Morkovsky, P., Parga, J. R. and Peterson, E., *Sep. Purif. Technol.*, **2007**, 56, 204–211.
- Anirudhan, T. S. and Unnithan, M. R., *Chemosphere*, **2007**, 66, 60–66.
- Mercer, K. L. and Tobiason, J. E., *Environ. Sci. Technol.*, **2008**, 42, 3797–3802.
- Iqbal, J., Kim, H. J., Yang, J. S., Baek, K. and Yang, J. W. *Chemosphere*, **2007**, 66, 970–976.
- Yu, X., Tong, S., Ge, M., Wu, L., Zuo, J., Cao, C. and Song, W., *Carbohydr. Polym.*, **2013**, 92, 380–387.
- Habibi, Y., Lucia, L. A. and Rojas, O. J., *Chem. Rev.*, **2010**, 110, 3479–3500.
- Stamberg, J. and Peska, J., *React. Polym.*, **1983**, 1, 145–147.
- Boeden, H. F., Pommerening, K., Becker, M., Rupprich, C. and Holtzhauser, M., *J. Chromatogr.*, **1991**, 552, 389–414.
- Wolf, B. *Int. J. Pharm.*, **1997**, 156, 97–107.
- Guo, X., Du, Yonghua F. C., Park, H. and Xiev, Y., *J. Colloid Interface Sci.*, **2007**, 314, 427–433.
- Ciftci, T. D., Yayayuruk, O. and Henden, E., *Environ. Technol.*, **2011**, 32, 341–351.
- Sun, W., Li, Q., Gao, S. and Shang, J. K., *Chem. Eng. J.*, **2012**, 185–186, 136–143.
- Pena, M. E., Korfiatis, G. P., Patel, M., Lippincott, L. and Meng, X. G., *Water Res.*, **2005**, 39, 2327–2337.
- Yabing, X., Jie, L., Shahua, Q. and Anqing L., *Water Environ. Res.*, **2007**, 79, 1015.
- Masue, Y., Loepfert, R. H. and Kramer, T. A., *Environ. Sci. Technol.*, **2007**, 41, 837–842.
- Wasay, S. A., Haran, Md. J. and Tokunaga, S., *Water Environ. Res.*, **1996**, 68, 295–300.
- Jang, M., Park, J. K. and Shin E. W., *Microporous Mesoporous Mater.*, **2004**, 75, 159–168.
- Santra, D., Joarder, R. and Sarkar, M., *Carbohydr. Polym.*, (accepted for publication) CARBPOL-D-13-02852.
- Wang, D. M., Hao, G., Shi, Q. H. and Sun, Y., *J. Chromatogr. A*, **2007**, 1146, 32–40.
- Jagtap, S., Thakre, D., Wanjari, S., Kamble, S., Labhsetwar, N. and Rayalu, S., *J. Colloid Interface Sci.*, **2009**, 332, 280–290.
- Li, Z., Deng, S., Zhang, X., Zhou, W., Huang, J. and Yu, G., *Front Environ. Sci. Eng. China*, **2010**, 4, 414–420.
- Rocha, R. A. and Muccillo, E. N. S., *Mater. Res. Bull.*, **2003**, 38, 1979–1986.
- Ho, Y. S., Huang, C. T. and Huang, H.W., *Process Biochem.*, **2002**, 37 1421–1430.

²⁹Al Duri, B. and McKay, G., *The Chem. Eng. J.*, **1988**, 38, 23–31.

³²Khan, A. S. A., *Turk. J. Chem.*, **2012**, 36, 437–443.

³⁰Allen, S. J., McKay, G. and Porter, J. F., *J. Colloid Interface Sci.*, **2004**, 280, 322–333.

³³Munoz, J. A., Gonzalo, A. and Valiente, M., *Environ. Sci. Technol.*, **2002**, 36, 3405–3411.

³¹Weber, T. W. and Chakrabarty, R. K., *Am. Inst. Chem. Eng. J.*, **1974**, 20, 228–232.

Received: 31.03.2014.

Accepted: 29.05.2014.



SYNTHESIS AND CRYSTAL STRUCTURE OF ETHYL 1-(4-METHYLPHENYL)-4-(4-METHYLPHENYLAMINO)-2,6-BIS(4-NITROPHENYL)-1,2,5,6-TETRAHYDROPYRIDINE-3-CARBOXYLATE

Sumati Anthal^[a], D. R. Patil^[b], M. B. Deshmukh^[b], Vivek K. Gupta^[a] and Rajni Kant^{[a]*}

Keywords: Tetrahydropyridine ring; crystal structure; direct methods; intermolecular hydrogen bonding.

The title compound was synthesized by standard routes of synthesis and its structure was established by spectral and X-ray diffraction studies. The compound crystallizes in the triclinic space group P-1 with unit cell parameters $a=10.4395(6)$, $b=11.9493(6)$, $c=13.8651(7)$, $\alpha=108.958(5)$, $\beta=103.089(5)$, $\gamma=97.885(4)$, $Z=2$. The crystal structure was solved by direct methods using single-crystal X-ray diffraction data collected at room temperature and refined by full-matrix least squares procedures to a final R -value of 0.0664 for 3330 observed reflections. In the title molecule, the tetrahydropyridine ring adopts a distorted boat conformation and both 4-nitro-phenyl substituents are in axial positions. The dihedral angle between the planes of the nitro-substituted rings is $45.5(1)^\circ$. The amino group and carbonyl O atom are involved in intramolecular hydrogen bonding and this interaction leads to the formation of a virtual-six membered ring. In the crystal, C-H...O intermolecular interactions stabilizes the crystal packing.

* Corresponding Authors

Fax: +91 191 243 2051

E-Mail: rkvk.paper11@gmail.com

- [a] X-ray Crystallography Laboratory, Post-Graduate Department of Physics & Electronics, University of Jammu, Jammu Tawi - 180 006, India
- [b] Department of Chemistry, Shivaji University, Kolhapur - 416 004 (Maharashtra State), India

Hence, investigation of the structural features of biologically relevant piperidine derivatives is demanding. In continuation of our structural studies of densely functionalized piperidines,^{13,14} we present the crystal structure of ethyl 1-(4-methylphenyl)-4-(4-methylphenylamino)-2,6-bis(4-nitrophenyl)-1,2,5,6-tetrahydropyridine-3-carboxylate, determined by X-ray diffraction.

Introduction

Functionalized piperidines are found to constitute a very important core in numerous natural products,^{1,2} synthetic pharmaceuticals,^{3,4} and a wide variety of biologically active compounds. In particular, 1,4-disubstituted piperidine scaffolds find useful applications as established drugs,^{5,6} and they exhibit a wide range of pharmacological activities including antibacterial,⁷ antimalarial,⁸ anticonvulsant, anti-inflammatory⁹ and enzyme inhibitory activity.^{10,11} Moreover a large number of compounds bearing piperidine scaffold have entered into preclinical and clinical trials over the last few years.¹²

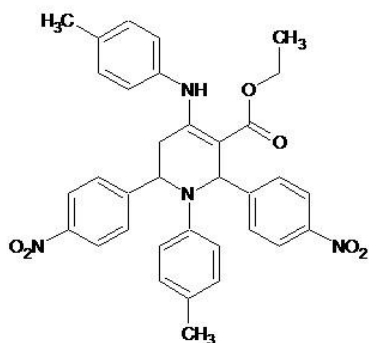


Figure 1. Chemical structure of the title compound

Experimental Methods

Synthesis

A mixture of ethyl acetoacetate (1 mmole), 4-methylaniline (2 mmole) and sulfamic acid (15 mol %) in 5 ml ethanol was stirred at RT for 15 min, then 4-nitro benzaldehyde (2 mmole) was added and stirring was continued at 78 °C till the completion of TLC. Then reaction mass gradually cools to RT, a solid precipitated out. The solid was filtered and washed with cold ethanol.

M.P.: 210-211 °C, Yield: 79 %. ¹H NMR (300 MHz, CDCl₃): δ = 1.45-1.50(t, 3H), 2.18(s, 3H), 2.29(s, 3H), 2.84-2.85(d, 2H), 4.31-4.53(m, 2H), 5.24(s, 1H), 6.30-6.33(d, 4H), 6.44(s, 1H), 6.90-6.98 (dd, $J=8.1$ Hz, 4H), 7.29-7.32(d, 2H), 7.51-7.53(d, 2H), 8.13-8.18(m, 4H), 10.25(s, 1H);

X-ray Data Collection, Crystal Structure Determination and Refinement

X-ray intensity data of 11409 reflections (of which 6077 unique) were collected on *X'calibur* CCD area-detector diffractometer equipped with graphite monochromated MoK α radiation ($\lambda = 0.71073$ Å).¹² The crystal used for data collection was of dimensions 0.30 x 0.20 x 0.20 mm.

The cell dimensions were determined by least-squares fit of angular settings of 2828 reflections in the θ range 3.90 to 27.83°. The intensities were measured by ω scan mode for θ ranges 3.70 to 26.00°. 3330 reflections were treated as observed ($I > 2\sigma(I)$). Data were corrected for Lorentz, polarisation and absorption factors. The structure was solved by direct methods using SHELXS97.¹³ All non-hydrogen atoms of the molecule were located in the best E-map. All the hydrogen atoms (except N2 H atoms) were geometrically fixed and allowed to ride on the corresponding non-hydrogen atoms with C-H = 0.93-0.98 Å, and $U_{\text{iso}} = 1.5U_{\text{eq}}$ of the attached C atom for methyl H atoms and $1.2U_{\text{eq}}$ for other H atoms. Full-matrix least-squares refinement was carried out using SHELXL97.¹³ The final refinement cycles converged to an $R=0.0663$ and $wR(F^2)=0.1723$ for the observed data. Residual electron densities ranged from -0.435 to $0.520 \text{ e}\text{\AA}^{-3}$. Atomic scattering factors were taken from International Tables for X-ray Crystallography (1992, Vol. C, Tables 4.2.6.8 and 6.1.1.4).

Table 1. Crystallographic data and other experimental details of (I).

CCDC deposition no.	990129
Crystal description	White block
Chemical Formula	C ₃₄ H ₃₂ N ₄ O ₆
Molecular weight(g mol ⁻¹)	592.64
Cell parameters	
<i>a</i> , Å	10.4395(6)
<i>b</i> , Å	11.9493(6)
<i>c</i> , Å	13.8651(7)
α , deg	108.958(5)
β , deg	103.089(5)
γ , deg	97.885(4)
Unit cell volume(Å ³)	1551.02(14)
Crystal system	Triclinic
Space group	P-1
Temperature (K)	293(2)
Number of molecules per unit cell	2
Radiation	MoK α
Wavelength (Å)	0.71073
F(000)	624
θ range for entire data collection	3.70< θ <26.00
Range of indices	-12 ≤ <i>h</i> ≤ 12, -12 ≤ <i>k</i> ≤ 14, -17 ≤ <i>l</i> ≤ 16
Number of measured reflections	11409
Number of unique reflections	6077
Number of observed reflections	3330
Number of parameters refined	404
Restraints	0
Refinement method	Full-matrix least squares on F^2
Final <i>R</i> -factor	0.0663
$wR^2(F^2)$	0.1723
Weight	$1/[\sigma^2(F_o^2)+(0.0932P)^2 + 0.3988]$, where $P=[F_o^2+2F_c^2]/3$
Goof(<i>S</i>) on (F^2)	1.029
Final residual electron density, Å ³	-0.435 < $\Delta\rho$ < 0.520
(Δ/σ) _{max} in the final cycle	0.001 (for tors H34A)

Scan mode	ω
-----------	----------

The crystallographic data are summarized in Table 1. CCDC - 990129 contains the supplementary crystallographic data for this paper. These data can be obtained free of charge from The Cambridge Crystallographic Data Centre via www.ccdc.cam.ac.uk/data_request/cif.

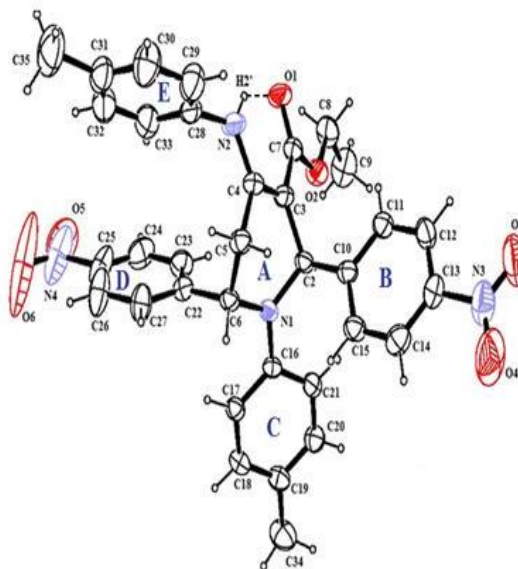


Figure 2. ORTEP view of the molecule with displacement ellipsoids drawn at the 50 % probability. H atoms are shown as small spheres of arbitrary radii

Results and Discussion

An ORTEP view of the title compound with atomic labeling is shown in Figure 2.¹⁴ The geometry of the molecule was calculated using the PLATON¹⁵ and PARST¹⁶ software. Crystal data, along with data collection and structure refinement details are summarized in Table 1. Selected bond lengths and angles are given in Table 2, while hydrogen bonds are presented in Table 3. In (I) (Fig.1), all bond lengths and angles are normal and correspond to those observed in related structures.¹⁷⁻²⁰

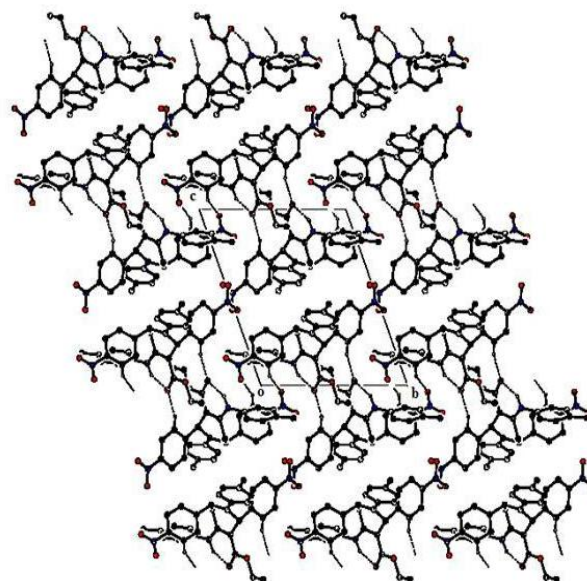


Figure 3. The crystal packing viewed down the a-axis is shown

Table 2. Selected bond lengths (Å) and angles (°) for (I).

Bond lengths, Å		Bond angles, °		Bond angles, °	
N1-C16	1.392(3)	C16-N1-C6	120.2(2)	C33-C28-N2	120.2(3)
N1-C6	1.453(3)	C16-N1-C2	120.5(2)	C29-C28-N2	121.2(3)
N1-C2	1.459(3)	C6-N1-C2	119.1(2)	C12-C13-N3	118.9(3)
O2-C7	1.344(3)	N1-C16-C21	122.0(2)	C14-C13-N3	119.5(3)
O2-C8	1.449(3)	N1-C16-C17	121.2(2)	O2-C8-C9	107.7(3)
O1-C7	1.215(3)	C7-O2-C8	117.6(2)	O3-N3-O4	123.1(4)
N2-C4	1.353(4)	N1-C2-C3	110.6(2)	O3-N3-C13	119.4(4)
N2-C28	1.433(4)	N1-C2-C10	113.6(2)	O4-N3-C13	117.5(4)
C13-N3	1.470(5)	C4-N2-C28	125.8(3)	C24-C25-N4	118.6(5)
N3-O3	1.193(4)	N1-C6-C22	114.8(2)	C26-C25-N4	119.0(5)
N3-O4	1.205(5)	N1-C6-C5	110.2(2)	O6-N4-O5	124.0(5)
O5-N4	1.214(6)	N2-C4-C3	124.4(2)	O6-N4-C25	118.1(6)
C25-N4	1.486(6)	N2-C4-C5	119.6(3)	O5-N4-C25	117.6(5)
N4-O6	1.155(7)	O1-C7-O2	122.1(3)	O2-C7-C3	112.5(2)
		O1-C7-C3	125.3(3)		

Table 3. Hydrogen bonding parameters (Å, °) for (I).

D-H	H...A	D...A	D-H...A	Symmetry Code
N2-H2'-O1	0.91(4)	1.92(4)	2.688(3)	141(4)
C11-H11...O1	0.93	2.44	3.255(3)	147
C24-H24...O5	0.93	2.56	3.340(7)	142
				-x+2,-y+2,-z+1
				-x+1,-y,-z

In the title molecule, the tetrahydropyridine ring (A) adopts distorted boat conformation with best mirror plane passing through the atoms C2 and C5 and bisecting the bonds C3-C4 and N1-C6 with asymmetry parameters [$\Delta C_s(C2)=9.53$] and [$\Delta C_s(C3-C4)=13.58$].²¹ The two nitrophenyl rings (B and D) are attached to the tetrahydropyridine ring in a *trans* orientation. Both the nitrophenyl rings are inclined to one another by 45.5(1)°, while for the 4-tolyl rings the dihedral angle is 46.2(1)°. The dihedral angle between nitrophenyl ring B and 4-tolyl ring C (B/C) is 69.7(1)°, ring B/E is 82.3(1)°, ring C/D is 85.6(1)° and ring D/E is 42.4(1)°. The amino group and carbonyl O atom are involved in an intramolecular N-H...O hydrogen bonding. This interaction leads to the formation of S(6) motif comprising atoms O1, C7, C3, C4, N2 and H2'. The double bond C7=O1 is confirmed by its respective distance of 1.215(3) Å. The length of the double bond C7=O1 is larger than the standard value for carbonyl group (1.192 Å) and lengthening of the C7=O1 double bond is due to strong intramolecular hydrogen bond between N2 and O1.

Packing view of the molecules in the unit cell viewed down the a-axis is shown (see Figure 2). The title molecule is stabilized by N-H...O intramolecular interactions and C-H...O intermolecular interactions are responsible for the stability of crystal structure (see Table 3).

Acknowledgements

One of the authors (Rajni Kant) acknowledges the Department of Science & Technology for single crystal X-

ray diffractometer as a National Facility under Project No. SR/S2/CMP-47/2003.

References

- Desai, M. C., Lefkowitz, S. L., Thadeio, P. F., Longo, K. P., Sridar, R. M., *J. Med. Chem.*, **1992**, *35*, 4911–4913.
- Pinder, A. R., *Nat. Prod. Rep.*, **1992**, *9*, 491–504.
- Breman, J. G., Egan, A. and Keusch, G. T., *Am. J. Trop. Med. Hyg.*, **2001**, *64*, iv–vii.
- Watson, P. S., Jiang, B. and Scott, B., *Org. Lett.*, **2000**, *2*, 3679–3681.
- Targum, S., Zboroaski, J., Henry, M., Schmitz, P., Sebree, T., Wallin, B., *Eur. Neuropsychopharmacol.*, **1995**, *5*, 4–71.
- Schotte, A., Janssen, P. F. M., Gommeren, W., Luyten, W. H. M. L., van Gompel, P., Lasage, A. S., De Loore, K. and Leysen, J. E., *Psychopharmacol.*, **1996**, *124*, 57–73.
- Zhou, Y., Gregor, V. E., Ayida, B. K., Winters, G. C., Sun, Z., Murphy, D., Haley, G., Bailey, D., Froelich, J. M., Fish, S., Webber, S. E., Hermann, T., Wall, D., *Bioorg. Med. Chem. Lett.*, **2007**, *17*, 1206–1210.
- Misra, M., Pandey, S. K., Pandey, V. P., Pandey, J., Tripathi, R., Tripathi, R. P., *Bioorg. Med. Chem.*, **2009**, *17*, 625–633.
- Bin, H., Crider, A. M. & Stables, J. P., *Eur. J. Med. Chem.*, **2001**, *36*, 265–286.
- Agrawal, A. G., Somani, R. R., *Mini Rev. Med. Chem.*, **2009**, *9*, 638–52.
- Dekus, J. A., Epperson, J. R., Charles, P. S., Joseph, A., C., Deextraze, P., Qian- Cutrone, J., Gao, Q., Ma, B., Beno, B. R., Mattson, G. K., Molski, T. F., Krause, R. G., Taber, M. T., Lodge, N. J., Mattson, R., *Bioorg. Med., Chem. Lett.*, **2007**, *17*, 3099–3104.

- ¹²Kamei, K., Maeda, N., Katswagi-Ogino, R., Koyamaa, M., Nakajima, M., Tatsuoka, T., Ohno, T., Inoue, T., *Bioorg. Med. Chem. Lett.*, **15**, 2990–2993.
- ¹³Sambyal, A., Bamezai, R. K., Razdan, T. K., Gupta, V. K., *J. Chem. Crystallogr.*, **2011**, *41*, 868–873.
- ¹⁴Brahmachari, G., Das, S., *Tetrahedron Lett.*, **2012**, *53*, 1479–1484.
- ¹²Oxford Diffraction **2010**, CrysAlis PRO. Oxford Diffraction Ltd, Yarnton, Oxfordshire, England.
- ¹³Sheldrick, G. M., *Acta Cryst.* **2008**, *A64*, 112.
- ¹⁴Farrugia, L. J., *J. Appl. Cryst.* **2012**, *45*, 849.
- ¹⁵Spek, A. L., *Acta Cryst.* **2009**, *D65*, 148.
- ¹⁶Nardelli, M., *J. Appl. Cryst.*, **1995**, *28*, 659.
- ¹⁷ Anthal, S., Brahmachari, G., Das, S., Kant, R., Gupta, V. K., *Acta Cryst.* **2013b**, *E69*, o299-300.
- ¹⁸Anthal, S., Brahmachari, G., Das, S., Kant, R., Gupta, V. K., *Acta Cryst.*, **2013c**, *E69*, o373-374.
- ¹⁹Anthal, S., Brahmachari, G., Das, S., Kant, R., Gupta, V. K., *Acta Cryst.*, **2013d**, *E69*, o454-455.
- ²⁰Anthal, S., Brahmachari, G., Das, S., Kant, R., Gupta, V. K., *Acta Cryst.*, **2013a**, *E69*, o506-507.
- ²¹Duax, W. L., Norton, D. A., *In Atlas of Steroid Structures*, Vol. 1. New York: Plenum Press, **1975**.

Received: 31.03.2014.

Accepted: 29.05.2014.



MOLECULAR INTERACTIONS OF BUTYL ETHANOATE + ETHER BINARY MIXTURES

M. V. Rathnam,^{[a]*} D. R. Ambavadekar^[a] and M. S. S. Kumar^[b]

Keywords: density; viscosity; speed of sound; excess volume; butyl ethanoate; interaction parameters

As part of a study on the molecular interactions between esters and ethers; density, viscosity and speed of sound data were measured for butyl ethanoate + ether mixed solvents. From these data, excess volumes V^E , deviation in viscosity $\Delta\eta$, isentropic compressibility K_s , deviation in isentropic compressibility ΔK_s , intermolecular free length L_f , internal pressure π_i , and the excess intermolecular free length L_f^E , excess internal pressure π_i^E , were deduced. These excess or deviation properties were fitted to the Redlich-Kister type equation. Further the experimental mixture viscosities were correlated using Frenkel, Heric, and McAllister (four-body) models. The studied excess or deviation properties were found to be both positive and negative. These results were interpreted in terms of intermolecular interactions and structural effects.

Corresponding Authors

Tel: Tel.: +91 – 8976545095,

Fax: Fax: 022 - 25337672

E-Mail: myrathnam58@rediffmail.com

[a] Physical Chemistry Research Laboratory, B.N.Bandodkar
College of Science, Thane, 40060, India

[b] Zulal Bhilajirao Patil College, Deopur, Dhule, 424002, India

Introduction

Intermolecular interactions play an important role in the development of molecular science.

The study of physicochemical properties of liquid mixtures finds extensive applications in chemical, pharmaceutical, and bio-chemical industries. Direct measurement of the characteristic excess or deviation properties of binary non-electrolyte solutions has gained much importance in the recent years.

Butyl ethanoate is often employed in combination with n-butanol in paints, because it enhances resistance to blushing and increase solvency in many cases. Likewise ethers are important industrial solvents. They can be used as scrubbing in cleaning of exhaust air and gas streams from industrial production plants, because of their favorable properties such as low vapor pressure, low viscosity, low toxicity, and high chemical stability. Ethers are increasingly used as additives to gasoline, due to their octane enhancing and pollution reducing properties.

Over the last several years there have been a number of studies on thermophysical properties of liquid mixtures containing butyl ethanoate in various organic solvents.¹⁻¹⁰ Oswal et.al^{11,12} have measured viscosity, speed of sound, isentropic compressibilities and excess molar volumes of binary mixtures containing p-dioxane with butyl acetate at 303.15K. Recently Roy et.al¹³ have determined excess molar volumes and viscosity deviations of binary mixtures of 1, 3-dioxane and 1, 4-dioxane with butyl acetate at 298.15 K. In order to understand further the molecular interactions of butyl ethanoate mixed with ether binary mixtures and as follow-up of our earlier work¹⁴⁻¹⁶ on thermophysical properties of various types ester containing mixtures, we report here the density, viscosity, and speed of sound for

binary mixtures of butyl ethanoate with tetrahydrofuran, 1, 4-dioxane, anisole, and butyl vinyl ether at $T=303.15$, 308.15, and 313.15 K over the entire range of composition and under atmospheric pressure. Experimental results have been used to calculate the excess molar volumes V^E , deviation in viscosity $\Delta\eta$, isentropic compressibility K_s , deviation in isentropic compressibility ΔK_s , excess intermolecular free length L_f^E , and excess internal pressure π_i^E . The calculated results have been fit to the Redlich-Kister polynomial¹⁷ equation to derive the binary coefficients and standard deviations. Further the experimental (kinematic or dynamic) viscosities were used to test the applicability of the equations proposed by Frankel,¹⁸ Heric,¹⁹ and McAllister (four-body interaction)²⁰ at the studied temperatures.

Experimental

Chemicals

All the chemicals used in the present study were of analytical grade (Fluka) obtained from S. D. Fine Chemical Ltd. Mumbai, India. The final mass fraction purities as determined by gas chromatography (HP 8610) using FID are shown in Table 1. Prior to the use all liquids were stored over 0.4 nm molecular sieves for 72 h to reduce water content if any and were degassed at low pressure.

Apparatus and procedure

The binary mixtures were prepared by weighing appropriate amounts of butyl ethanoate and ether on an electronic balance (Mettler AE-240, Switzerland) with precision of ± 0.01 mg, by syringing each liquid into airtight stopper bottles in order to minimize evaporation losses. The resulting uncertainty in mole fraction was estimated to be less than ± 0.0001 . Each mixture was immediately used after it was well mixed by shaking.

The density of pure liquids and their binary mixtures were determined with density meter (DMA 4500 Anton Paar) with precision of ± 0.00001 g.cm⁻³. The uncertainty in the density measurements was found to be ± 0.0002 g.cm⁻³.

Table 1. Chemical specification with purity estimation.

Chemical Name	Source	Initial mole fraction (purity)	Purification method	Final mole fraction (purity)	Analysis Method
Butyl ethanoate	Sigma-Aldrich	0.99	none	0.998	GC ^a (HP-8610)
Tetrahydrofuran	E.Merk	0.98	distillation	0.996	GC (HP-8610)
1,4-Dioxane	E.Merk	0.99	none	0.997	GC (HP-8610)
Anisole	Fluka	0.99	none	0.998	GC (HP-8610)
Butyl vinyl ether	Sigma-Aldrich	0.99	distillation	0.996	GC (HP-8610)

^a Gas-liquid chromatography

The dynamic viscosities of the pure liquids and their binary mixtures were measured at the required temperature using an Ubbelohde viscometer. The uncertainty in the viscosity measurement was estimated to be ± 0.005 mPa s. In viscosity measurements the temperature of the samples was controlled by using a viscometer bath equipped with a thermostat of accuracy ± 0.01 K.

Speed of sound of pure liquids and their mixtures were determined using a single-crystal variable path interferometer (model F-81, Mittal Enterprises, New Delhi, India), at a frequency of 2 MHz. The uncertainty in speed of sound was estimated to be ± 1 m s⁻¹.

Results and Discussion

The experimental results of density ρ , excess molar volume V^E , viscosity η , speed of sound u , isentropic compressibility K_s , intermolecular free length L_f , and internal pressure π_i for the binary mixtures of (butyl ethanoate + tetrahydrofuran), (butyl ethanoate + 1,4-dioxane), (butyl ethanoate + anisole), and (butyl ethanoate + butyl vinyl ether) at $T = 303.15, 308.15, \text{ and } 313.15$ K and at the atmospheric pressure are reported in Table 2.

The excess molar volumes V^E are calculated from the density data using the following relation.

$$V^E = \sum_{i=1}^2 x_i M_i (\rho^{-1} - \rho_i^{-1}) \quad (1)$$

where M_i , ρ_i and ρ are the molar mass, density of the i^{th} component and density of the mixture respectively.

Isentropic compressibility, K_s are calculated from the relation

$$K_s = \frac{1}{u^2 \rho} \quad (2)$$

Where u is the speed of sound.

The intermolecular free length L_f was calculated as

$$L_f = K(K_s)^{1/2} \quad (3)$$

Where

K is the temperature dependent Jacobson constant,
 K_s is the isentropic compressibility

The internal pressure π_i was calculated from the following relation

$$\pi_i = bRT \left(\frac{K\eta}{u} \right)^{1/2} \left(\frac{\rho^2}{M_{\text{eff}}^{1/6}} \right) \quad (4)$$

where

b is the cubical packing fraction taken as 2 for all the liquids,

R is the universal gas constant,

T is the experimental temperature,

$M_{\text{eff}} = \sum x_i M_i$ (x is the mole fraction and M is the molecular weight of i^{th} component) and η is the viscosity.

Excess or deviation values (V^E , $\Delta\eta$, ΔK_s , L_f^E and π_i^E) of all the studied parameters were computed using the general equation

$$Y^E = Y_{\text{exp}} - (x_1 Y_1 + x_2 Y_2) \quad (5)$$

where

Y represents any parameter,

Y^E its value Y_1 and

Y_2 denote values of parameters for pure liquids, and

Y_{exp} represents the corresponding experimental value for the mixture.

Table 2. Values of density (ρ), excess molar volume (V^E), viscosity (η), speed of sound (u), isentropic compressibility (K_s), intermolecular free length (L_f), internal pressure (π) for the binary liquid mixture

x_1	$P, \text{g.cm}^{-3}$	$V^E, \text{cm}^3\text{mol}^{-1}$	$\eta, \text{mPa.s}$	$u, \text{m.s}^{-1}$	K_s, TPa^{-1}	$L_f \times 10^8, \text{cm}$	$\pi \times 10^6, \text{Nm}^{-2}$
Butyl ethanoate (1) + tetrahydrofuran(2)							
$T/\text{K}=303.15$							
0.0000	0.8778		0.4388	1248	731	0.561	3.857
0.0653	0.8769	0.017	0.4564	1228	756	0.571	3.793
0.1123	0.8763	0.029	0.4692	1212	777	0.579	3.748
0.2099	0.8751	0.059	0.4965	1200	794	0.585	3.627
0.2911	0.8743	0.073	0.5129	1188	810	0.591	3.527
0.3800	0.8735	0.088	0.5310	1176	828	0.597	3.420
0.4798	0.8728	0.091	0.5473	1172	834	0.599	3.280
0.5882	0.8722	0.082	0.5656	1168	840	0.602	3.150
0.7096	0.8717	0.058	0.5857	1164	847	0.604	3.017
0.8439	0.8712	0.033	0.6077	1164	847	0.604	2.878
1.0000	0.8707		0.6333	1160	854	0.606	2.740
$T/\text{K}=308.15$							
0.0000	0.8725		0.4276	1228	760	0.577	3.877
0.0653	0.8715	0.034	0.4456	1212	781	0.585	3.812
0.1123	0.8709	0.052	0.4604	1196	803	0.593	3.769
0.2099	0.8697	0.094	0.4805	1184	820	0.600	3.643
0.2911	0.8689	0.117	0.4951	1172	838	0.606	3.533
0.3800	0.8682	0.131	0.5116	1164	850	0.611	3.417
0.4798	0.8676	0.132	0.5263	1160	857	0.613	3.274
0.5882	0.8671	0.121	0.5411	1156	863	0.615	3.135
0.7096	0.8667	0.095	0.5558	1152	869	0.618	2.991
0.8439	0.8664	0.052	0.5688	1152	870	0.618	2.835
1.0000	0.8661		0.5883	1148	876	0.620	2.683
$T/\text{K}=313.15$							
0.0000	0.8670		0.3903	1212	785	0.592	3.781
0.0653	0.8659	0.050	0.4118	1200	802	0.598	3.726
0.1123	0.8652	0.082	0.4263	1188	819	0.605	3.689
0.2099	0.8639	0.144	0.4478	1176	837	0.611	3.571
0.2911	0.8631	0.175	0.4641	1168	849	0.616	3.467
0.3800	0.8624	0.198	0.4803	1158	865	0.621	3.352
0.4798	0.8619	0.196	0.4948	1154	871	0.624	3.220
0.5882	0.8615	0.182	0.5093	1148	881	0.627	3.089
0.7096	0.8613	0.138	0.5203	1144	887	0.629	2.939
0.8439	0.8612	0.074	0.5331	1140	893	0.632	2.793
1.0000	0.8611		0.5480	1136	900	0.634	2.641
Butyl ethanoate(1) +1, 4-dioxane(2)							
$T/\text{K}=303.15$							
0.0000	1.0227		1.0896	1320	561	0.492	5.179
0.0557	1.0097	0.024	1.0388	1304	582	0.501	4.930
0.1159	0.9966	0.041	0.9800	1284	609	0.512	4.692
0.1841	0.9827	0.062	0.9244	1268	633	0.522	4.434
0.2595	0.9684	0.085	0.8779	1252	659	0.533	4.195
0.3452	0.9535	0.106	0.8318	1236	687	0.544	3.951
0.4401	0.9384	0.098	0.7927	1224	711	0.554	3.717
0.5502	0.9225	0.075	0.7517	1208	743	0.566	3.477
0.6703	0.9068	0.057	0.7157	1196	771	0.576	3.247
0.8230	0.8890	0.033	0.6751	1180	808	0.590	2.993
1.0000	0.8707		0.6333	1160	854	0.606	2.740
$T/\text{K}=308.15$							
0.0000	1.0174		0.9988	1312	571	0.500	5.026
0.0557	1.0043	0.039	0.9509	1292	597	0.512	4.811
0.1159	0.9912	0.062	0.9041	1272	624	0.523	4.586

0.1841	0.9773	0.080	0.8533	1248	657	0.537	4.349
0.2595	0.9631	0.110	0.8117	1230	686	0.549	4.122
0.3452	0.9483	0.119	0.7684	1208	723	0.563	3.891
0.4401	0.9333	0.119	0.7320	1196	749	0.573	3.659
0.5502	0.9175	0.095	0.6957	1184	777	0.584	3.422
0.6703	0.9019	0.075	0.6644	1172	807	0.595	3.201
0.8230	0.8842	0.050	0.6283	1160	840	0.607	2.950
1.0000	0.8661		0.5883	1148	876	0.620	2.683
x₁	T/K=313.15						
0.0000	1.0111		0.9458	1304	582	0.510	4.977
0.0557	0.9980	0.058	0.9000	1280	612	0.523	4.759
0.1159	0.9848	0.094	0.8565	1260	640	0.534	4.538
0.1841	0.9711	0.116	0.8134	1236	674	0.549	4.318
0.2595	0.9570	0.130	0.7728	1216	707	0.562	4.093
0.3452	0.9423	0.142	0.7307	1116	742	0.576	3.858
0.4401	0.9275	0.136	0.6954	1184	769	0.586	3.628
0.5502	0.9118	0.117	0.6582	1172	798	0.597	3.386
0.6703	0.8964	0.102	0.6260	1160	829	0.608	3.161
0.8230	0.8789	0.072	0.5893	1148	863	0.621	2.906
1.0000	0.8611		0.5480	1136	900	0.634	2.641
Butyl ethanoate (1) + anisole(2)							
x₁	T/K=303.15						
0.0000	0.9854		0.9225	1388	527	0.476	3.568
0.0829	0.9746	-0.064	0.8794	1380	539	0.482	3.450
0.1685	0.9640	-0.150	0.8431	1372	551	0.487	3.342
0.2588	0.9531	-0.228	0.8112	1360	567	0.494	3.241
0.3527	0.9421	-0.301	0.7797	1342	589	0.504	3.149
0.4499	0.9309	-0.347	0.7486	1324	613	0.514	3.049
0.5499	0.9196	-0.353	0.7218	1300	644	0.527	2.978
0.6545	0.9077	-0.314	0.6951	1272	681	0.542	2.911
0.7642	0.8955	-0.226	0.6724	1244	722	0.558	2.842
0.8786	0.8832	-0.117	0.6499	1204	781	0.580	2.786
1.0000	0.8707		0.6333	1160	854	0.606	2.740
x₁	T/K=308.15						
0.0000	0.9793		0.8495	1368	546	0.489	3.526
0.0829	0.9690	-0.104	0.8083	1360	558	0.495	3.409
0.1685	0.9586	-0.198	0.7705	1348	674	0.502	3.293
0.2588	0.9479	-0.284	0.7373	1336	591	0.509	3.186
0.3527	0.9370	-0.352	0.7085	1320	613	0.518	3.092
0.4499	0.9259	-0.394	0.6800	1300	639	0.529	2.972
0.5499	0.9146	-0.395	0.6579	1276	672	0.543	2.921
0.6545	0.9030	-0.363	0.6358	1250	709	0.558	2.846
0.7642	0.9108	-0.284	0.6158	1224	749	0.573	2.775
0.8786	0.8788	-0.170	0.5998	1188	806	0.595	2.731
1.0000	0.8661		0.5883	1148	876	0.620	2.683
x₁	T/K=313.15						
0.0000	0.9729		0.7636	1348	566	0.503	3.478
0.0829	0.9630	-0.135	0.7220	1336	582	0.510	3.367
0.1685	0.9529	-0.250	0.6879	1324	599	0.517	3.259
0.2588	0.9424	-0.345	0.6581	1312	616	0.525	3.159
0.3527	0.9316	-0.411	0.6326	1294	641	0.535	3.066
0.4499	0.9206	-0.449	0.6094	1276	667	0.546	2.874
0.5499	0.9095	-0.460	0.5923	1252	701	0.560	2.900
0.6545	0.8980	-0.425	0.5752	1228	739	0.574	2.831
0.7642	0.8861	-0.341	0.5599	1220	784	0.592	2.756
0.8786	0.8739	-0.207	0.5504	1170	836	0.611	2.697
1.0000	0.8611		0.5480	1136	900	0.634	2.641

Butyl ethanoate(1) + butyl vinyl ether(2)							
x_1	T/K=303.15						
0.0000	0.7734		0.3865	1084	1100	0.689	2.432
0.0969	0.7841	-0.168	0.3997	1100	1054	0.674	2.434
0.1944	0.7944	-0.267	0.4135	1116	1011	0.660	2.436
0.2931	0.8046	-0.338	0.4308	1128	977	0.649	2.450
0.3929	0.8146	-0.383	0.4466	1136	951	0.640	2.463
0.4941	0.8247	-0.399	0.4679	1148	920	0.630	2.484
0.5934	0.8344	-0.406	0.5001	1152	903	0.624	2.531
0.6942	0.8440	-0.383	0.5275	1156	887	0.618	2.580
0.7960	0.8534	-0.324	0.5625	1160	871	0.612	2.630
0.8981	0.8624	-0.209	0.5962	1164	856	0.607	2.685
1.0000	0.8707		0.6333	1160	854	0.606	2.740
x_1	T/K=308.15						
0.0000	0.7682		0.3647	1072	1132	0.705	2.399
0.0969	0.7788	-0.146	0.3797	1084	1093	0.692	2.418
0.1944	0.7891	-0.238	0.3966	1100	1047	0.678	2.432
0.2931	0.7993	-0.301	0.4139	1112	1012	0.666	2.448
0.3929	0.8094	-0.338	0.4314	1120	985	0.657	2.467
0.4941	0.8195	-0.361	0.4510	1132	952	0.646	2.486
0.5934	0.8292	-0.358	0.4761	1136	935	0.640	2.517
0.6942	0.8389	-0.341	0.5016	1140	917	0.634	2.560
0.7960	0.8484	-0.287	0.5294	1144	901	0.629	2.601
0.8981	0.8575	-0.176	0.5574	1148	885	0.623	2.643
1.0000	0.8661		0.5883	1148	876	0.620	2.683
x_1	T/K=313.15						
0.0000	0.7633		0.3541	1060	1166	0.721	2.411
0.0969	0.7738	-0.133	0.3680	1072	1125	0.709	2.422
0.1944	0.7840	-0.212	0.3829	1084	1085	0.696	2.435
0.2931	0.7941	-0.262	0.3980	1096	1048	0.684	2.447
0.3929	0.8041	-0.285	0.4151	1104	1020	0.675	2.467
0.4941	0.8141	-0.294	0.4325	1116	986	0.664	2.481
0.5934	0.8238	-0.294	0.4500	1120	968	0.657	2.503
0.6942	0.8335	-0.279	0.4731	1124	950	0.651	2.538
0.7960	0.8430	-0.225	0.4966	1128	932	0.645	2.572
0.8981	0.8523	-0.145	0.5222	1132	916	0.639	2.608
1.0000	0.8611		0.5480	1136	900	0.634	2.641

For each binary mixture, the composition dependence of V^E , $\Delta\eta$, ΔK_s , L_r^E and π_i^E versus mole fraction x_1 can be expressed by using Redlich-Kister polynomial¹⁷ equation.

$$Y = x_1 x_2 \sum_{k=0}^m A_k (x_1 - x_2)^{k-1} \quad (6)$$

Where m is the number of estimated parameters. The coefficients A_k of equation (6) along with the standard deviation σ (Y^E) are given in Table 3. These coefficients are adjustable parameters to get best fit value of Y^E . The standard deviation σ (Y^E) was calculated by using the relation

$$\sigma(Y^E) = \left[\sum \frac{(Y_{\text{exp}} - Y_{\text{cal}})^2}{(n-m)} \right]^{1/2} \quad (7)$$

where n and m represent the number of experimental data points and that of estimated parameters used in the equation (6)

Semi empirical models for analyzing mixture viscosities

In this paper we have selected some of the semi empirical relations to represent the dependence of viscosity on concentration of the component in the mixtures, which are suited for practical engineering use. The methods were chosen because they are well known and accepted or appear potentially promising. The methods are categorized according to the number of adjustable parameters. An attempt has been made to check the suitability of equations for the present experimental data fits by taking into account the number of empirical adjustment coefficients.

The applicability and average relative deviations for each method are discussed with the recommended method identified.

The equations discussed are:

Frankel¹⁸

$$\log \eta = x_1^2 \log \eta_1 + x_2^2 \log \eta_2 + 2x_1 x_2 \log \eta_{12} \quad (8)$$

Where η is the viscosity coefficient and η_{12} is the interaction parameter.

Heric¹⁹

Heric proposed a two parameter model of the form

$$\ln(\eta_{\text{mix}}) = x_1 \ln(\eta_1) + x_2 \ln(\eta_2) + x_1 \ln(M_1) + x_2 \ln(M_2) - \ln(x_1 M_1 + x_2 M_2) + x_1 x_2 [\gamma_{12} + \gamma_{21}(x_1 - x_2)] \quad (9)$$

Where

M_1 and M_2 are the molecular weights of pure components,

γ_{12} and γ_{21} are the adjustable parameters.

McAllister (four-body)²⁰

McAllister four-body interaction model is a three parameter equation

$$\begin{aligned} \ln v = & x_1^4 \ln v_1 + 4x_1^3 x_2 \ln v_{1112} \\ & + 6x_1^2 x_2^2 \ln v_{1122} + 4x_1 x_2^3 \ln v_{2221} \\ & + x_2^4 \ln v_2 - \ln \left[x_1 + \left(\frac{x_2 M_2}{M_1} \right) \right] \\ & + 4x_1^3 x_2 \ln \left[\frac{3 + (M_2/M_1)}{4} \right] \\ & + 6x_1^2 x_2^2 \ln \left[\frac{1 + (M_2/M_1)}{2} \right] \\ & + 4x_1 x_2^3 \ln \left[\frac{1 + (3M_2/M_1)}{4} \right] \\ & + x_2^4 \ln (M_2/M_1) \end{aligned} \quad (10)$$

These three adjustable parameters v_{1112} , v_{1122} , and v_{2221} are determined from the kinematic viscosity-composition data. The correlating ability of equations (8-10) was tested by calculating the average relative deviation (ARD) between the experimental and the calculated viscosities as obtained by relation

$$\sigma(\%) = \left[\left(\frac{1}{n-k} \frac{\sum \{100(\eta_{\text{exp}} - \eta_{\text{cal}})\}^2}{\eta_{\text{exp}}} \right)^{1/2} \right] \quad (11)$$

where,

n , represents the number of data points in each set and, k , is the number of adjustable parameters in Eqs. (8-10).

The values of parameters of equations (8-10) and the ARD values of equation (11) are given in the Table 4. Comparison of ARD values in Table 3 reveals that these values lie in the range (0.011-0.129) for the one-parameter model of Frankel, (0.012–0.034) for two-parameter model of Heric, and (0.004–0.008) for three-parameter model of McAllister (4-body). From this it is apparent that McAllister model with more number of adjustable parameters has the good predictive ability as compared to one, and two parameter models; however McAllister model is a correlative in nature, severely limits its predictability and usefulness. This is mainly because costly and time consuming data are required for the determination of the adjustable parameters contained in the model. Figure 1 shows the variation of V^E of binary mixtures at $T= 303.15, 308.15,$ and 313.15 K

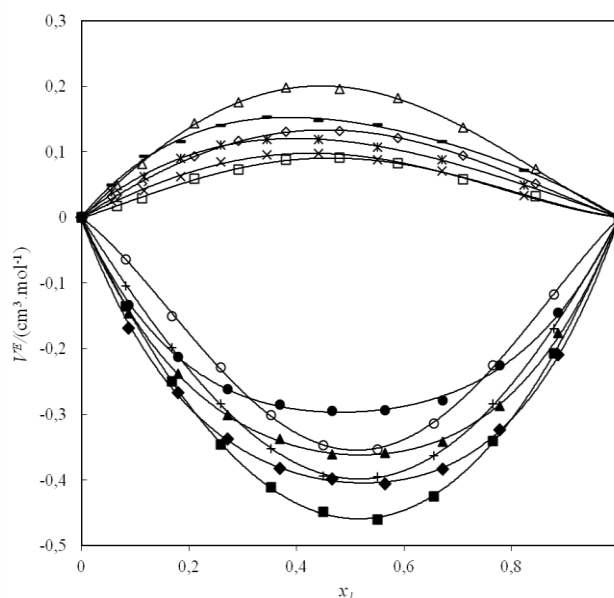


Figure 1. Curves of excess molar volume V^E versus mole fraction X_1 for the binary mixtures butyl ethanoate + tetrahydrofuran at (\square , 303.15; \diamond , 308.15; Δ , 313.15) K, butyl ethanoate + 1,4-dioxane at (\times , 303.15; \times , 308.15; \times , 313.15) K, butyl ethanoate + anisole at (\circ , 303.15; $+$, 308.15; \blacksquare , 313.15) K, butyl ethanoate + butyl vinyl ether (\blacklozenge , 303.15; \blacktriangle , 308.15; \bullet , 313.15) K.

In the present study the values of V^E were found to be positive for (butyl ethanoate + tetrahydrofuran) and (butyl ethanoate + 1, 4-dioxane) systems, where as in case of (butyl ethanoate + anisole) and (butyl ethanoate + butyl vinyl ether) systems V^E is negative over the entire range of composition at all the temperatures studied. The effect of temperature is noteworthy as the magnitude of V^E either increase or decrease with increase in temperature. The positive V^E values indicate the dispersive interactions between unlike molecules are weaker than those between like molecules.²¹ While the negative V^E values may be attributed to charge transfer complex, dipole-dipole interactions and structural effects that arise from proper interstitial accommodation leading to more compact structure and greater packing in the mixture due to higher molar volume²² of the solvent butyl ethanoate.

Table 3. Derived parameters of excess functions and standard deviation of binary liquid mixtures

Function	T/K	A ₀	A ₁	A ₂	σ
	Butyl ethanoate (1) + tetrahydrofuran(2)				
V ^E	303.15	0.3590	-0.0738	-0.1730	0.002
	308.15	0.5294	-0.1215	-0.1159	0.002
	313.15	0.7909	-0.2128	-0.1816	0.002
Δη	303.15	0.6309	-0.0552	0.0156	0.001
	308.15	0.8929	-0.0582	-0.0020	0.001
	313.15	0.1129	-0.6219	0.1673	0.001
ΔK _s	303.15	17.360	-10.763	1.7488	0.306
	308.15	16.390	-10.627	1.5757	0.257
	313.15	12.645	-6.658	1.1139	0.187
L _r ^E	303.15	0.0657	-0.0401	0.0097	0.001
	308.15	0.0606	-0.0392	0.0032	0.001
	313.15	0.0479	-0.0260	0.0056	0.001
π _r ^E	303.15	-0.1563	-0.2709	0.151	0.004
	308.15	-0.1175	-0.2851	0.176	0.004
	313.15	-0.0638	-0.3059	0.198	0.004
Butyl ethanoate (1) + 1, 4-dioxane(2)					
V ^E	303.15	0.3812	-0.1567	-0.1322	0.002
	308.15	0.4578	-0.2025	0.0421	0.002
	313.15	0.5823	-0.2327	0.1739	0.004
Δη	303.15	-0.3698	0.2043	-0.0679	0.001
	308.15	-0.3304	0.1817	-0.0161	0.001
	313.15	-0.2905	0.1527	-0.0189	0.001
ΔK _s	303.15	8.6603	-6.1010	-1.5477	0.118
	308.15	12.1419	-6.5438	-2.2169	0.268
	313.15	13.2142	-8.3458	0.2736	0.229
L _r ^E	303.15	0.0456	-0.0265	-0.0025	0.001
	308.15	0.0794	-0.0299	-0.0179	0.001
	313.15	0.0846	-0.0397	-0.0075	0.001
π _r ^E	303.15	-1.5226	0.5562	-0.1563	0.003
	308.15	-1.3132	0.4867	-0.0006	0.004
	313.15	-1.2596	0.3885	-0.0864	0.004
Butyl ethanoate (1) + anisole(2)					
V ^E	303.15	-1.4168	-0.0985	0.7042	0.003
	308.15	-1.5918	-0.1146	0.2101	0.003
	313.15	-1.8355	-0.1081	-0.0391	0.002
Δη	303.15	-0.1704	0.0338	-0.0465	0.001
	308.15	-0.2009	0.0466	-0.0393	0.001
	313.15	-0.2203	0.0493	-0.0698	0.001
ΔK _s	303.15	-24.9284	-6.5334	-2.8797	0.147
	308.15	-22.4828	-5.1904	-2.8797	0.151
	313.15	-19.6285	-2.8968	-2.9539	0.103
L _r ^E	303.15	-0.0846	-0.0168	-0.0106	0.001
	308.15	-0.0753	-0.0114	-0.0040	0.001
	313.15	-0.0626	-0.0018	0.0053	0.001

π_r^E	303.15	-0.5720	0.0831	-0.1326	0.002
	308.15	-0.5908	0.0863	-0.0434	0.003
	313.15	-0.6607	0.0958	-0.1189	0.003
Butyl ethanoate (1) + butyl vinyl ether(2)					
V^E	303.15	-1.6076	-0.2401	-0.7241	0.003
	308.15	-1.4378	-0.1988	-0.5664	0.002
	313.15	-1.1857	-0.0542	-0.5552	0.003
$\Delta\eta$	303.15	-0.1536	-0.0041	0.0700	0.001
	308.15	-0.1058	0.0036	-3.97E-04	0.001
	313.15	-0.0721	-0.0030	0.0288	0.001
ΔK_S	303.15	-21.874	3.9882	-4.3763	0.261
	308.15	-20.190	3.4373	2.2346	0.287
	313.15	-17.867	4.1050	5.1867	0.205
L_r^E	303.15	-0.1050	0.0011	-0.0224	0.001
	308.15	-0.1004	0.0014	-0.0028	0.001
	313.15	-0.0937	0.0024	0.0137	0.001
π_r^E	303.15	-0.3728	0.0554	0.1508	0.004
	308.15	-0.2018	-0.0116	0.1639	0.002
	313.15	-0.1714	-0.0066	0.1008	0.003

Table 4. Adjustable parameters and average relative deviations of viscosity models for binary mixtures

T/K	Frenkel		Heric			McAllister-4-body			
	η_{12}	$\sigma\%$	γ_{12}	γ_{21}	$\sigma\%$	v_{1112}	v_{1122}	v_{2221}	$\sigma\%$
Butyl ethanoate (1) + tetrahydrofuran(2)									
303.15	-0.540	0.011	0.3041	-0.1582	0.022	4.802	4.6988	4.5752	0.007
308.15	-0.573	0.011	0.3370	-0.1633	0.018	4.808	4.7048	4.5816	0.007
313.15	-0.615	0.014	0.4138	-0.2032	0.037	4.814	4.7116	4.5886	0.007
Butyl ethanoate (1) +1, 4-dioxane(2)									
303.15	-0.349	0.119	-0.2739	0.1555	0.017	4.810	4.708	4.599	0.005
308.15	-0.421	0.113	-0.2577	0.1458	0.022	4.816	4.712	4.605	0.005
313.15	-0.464	0.097	-0.2206	0.1265	0.013	4.822	4.718	4.612	0.005
Butyl ethanoate (1) + anisole(2)									
303.15	-0.3502	0.024	-0.1602	0.0820	0.025	4.849	4.795	4.750	0.004
308.15	-0.4611	0.023	-0.2256	0.0189	0.018	4.853	4.802	4.755	0.004
313.15	-0.5907	0.037	-0.3069	0.0252	0.034	4.858	4.808	4.760	0.004
Butyl ethanoate (1) + butyl vinyl ether(2)									
303.15	-0.793	0.061	-0.1707	0.051	0.051	4.881	4.879	4.867	0.009
308.15	-0.811	0.030	-0.1341	-0.012	0.049	4.887	4.885	4.8740	0.009
313.15	-0.850	0.025	-0.0509	-0.013	0.022	4.894	4.892	4.8806	0.009

Figure 2 depicts the variation of $\Delta\eta$ with mole fraction of butyl ethanoate. The $\Delta\eta$ values for all the studied systems except for (butyl ethanoate + tetrahydrofuran) are negative at all the studied temperatures. For the mixtures of tetrahydrofuran the $\Delta\eta$ values are positive. The minima of the ($\Delta\eta - x_1$) curves occur at about $x_1 \sim 0.375$. Like V^E the magnitude of $\Delta\eta$ values also vary with temperature indicating the effect of temperature on $\Delta\eta$. In our present case the components have different molecular structure, the molar volume of the solvent butyl ethanoate ($133.32 \text{ cm}^3 \text{ mol}^{-1}$) being large, the inclusion of smaller molecules of

solute in the structure of larger molecules causes the $\Delta\eta$ values negative.

It was observed that the speed of sound values (Table 2) for (butyl ethanoate + tetrahydrofuran) and (butyl ethanoate +1, 4-dioxane) and (butyl ethanoate + anisole) decrease with increase in temperature at any given concentration of ester, while for (butyl ethanoate + butyl vinyl ether) these values increase with increase in temperature. The decreasing trend with increase in temperature indicates breaking of hetero and homo molecular clusters at high temperature.²³

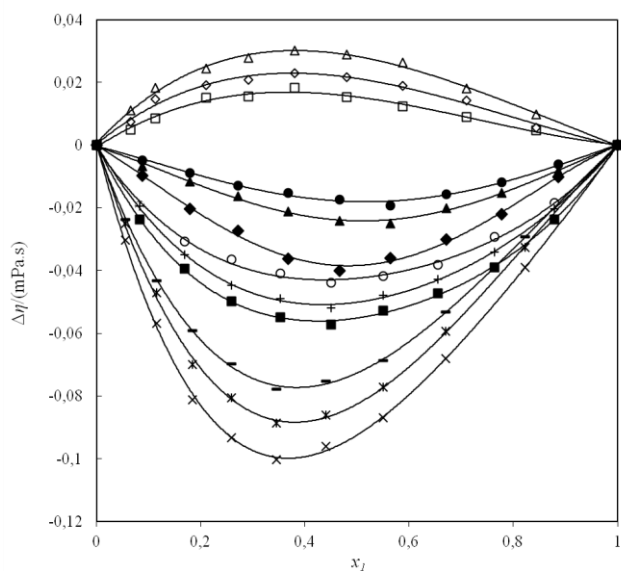


Figure 2. Curves of deviation in viscosity $\Delta\eta$ Vs mole fraction for the binary mixtures. Butyl ethanoate+ tetrahydrofuran at (\square , 303.15 ; \diamond , 308.15 ; Δ , 313.15) K, butyl ethanoate + 1,4-dioxane at (\times , 303.15 ; κ , 308.15 ; — , 313.15) K, butyl ethanoate + anisole at (\circ , 303.15 ; $+$, 308.15 ; \blacksquare , 313.15) K, butyl ethanoate + butyl vinyl ether at (\blacklozenge , 303.15 ; \blacktriangle , 308.15 ; \bullet , 313.15) K

The speed of sound will decrease if the intermolecular free length increases with temperature and vice – versa. This phenomenon of interdependence of intermolecular free length and speed of sound was explained by Kincaid and Eyring²⁴

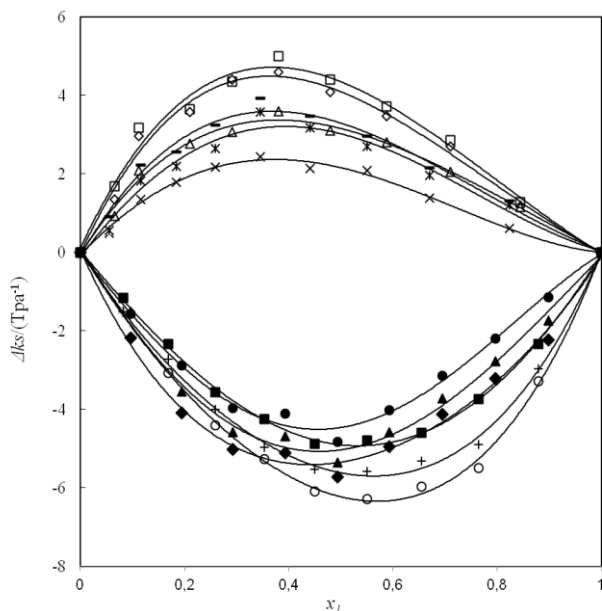


Figure 3. Curves of deviations in isentropic compressibility ΔK_S vs mole fraction for the binary mixture butyl ethanoate + tetrahydrofuran at (\square , 303.15 ; \diamond , 308.15 ; δ , 313.15) K, butyl ethanoate + 1, 4-dioxane at (\times , 303.15 ; κ , 308.15 ; — , 313.15) K, butyl ethanoate + anisole at (\circ , 303.15 ; $+$, 308.15 ; \blacksquare , 313.15) K, butyl ethanoate + butyl vinyl ether (\blacklozenge , 303.15 ; \blacktriangle , 308.15 ; \bullet , 313.15) K.

Figure 3 represents the variation of ΔK_S values with mole the fraction of butyl ethanoate. The ΔK_S values show positive deviations for tetrahydrofuran and 1, 4-dioxane

systems, while for anisole and butyl vinyl ether ΔK_S values show negative deviations. The magnitude of ΔK_S values change with rise in temperature. The negative ΔK_S for anisole and butyl vinyl ether systems in our present study may be attributed to the dipole – dipole interactions.

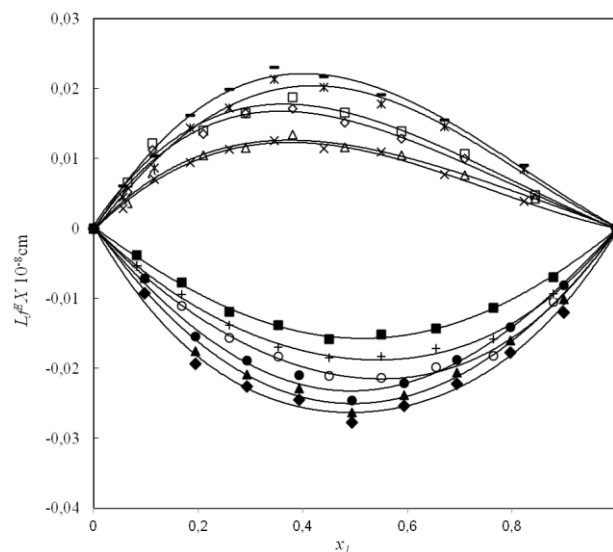


Figure 4. Curves of excess intermolecular free length L_f^E vs mole fraction for the binary mixtures butyl ethanoate + tetrahydrofuran at (\square , 303.15 ; \diamond , 308.15 ; δ , 313.15) K, butyl ethanoate + 1,4-dioxane at (\times , 303.15 ; κ , 308.15 ; — , 313.15) K, butyl ethanoate + anisole at (\circ , 303.15 ; $+$, 308.15 ; \blacksquare , 313.15) K, butyl ethanoate + butyl vinyl ether (\blacklozenge , 303.15 ; \blacktriangle , 308.15 ; \bullet , 313.15) K.

Figure 4 shows the variation of L_f^E with x_1 . Like ΔK_S the L_f^E values for tetrahydrofuran and 1, 4-dioxane systems are positive, while for anisole and butyl vinyl ether the L_f^E values are negative over the entire composition range of butyl ethanoate. According to Ramamurthy and Sastry²⁵ the negative values of L_f^E indicate that sound wave has to travel a larger distance due to the dominant nature of interactions between unlike molecules.

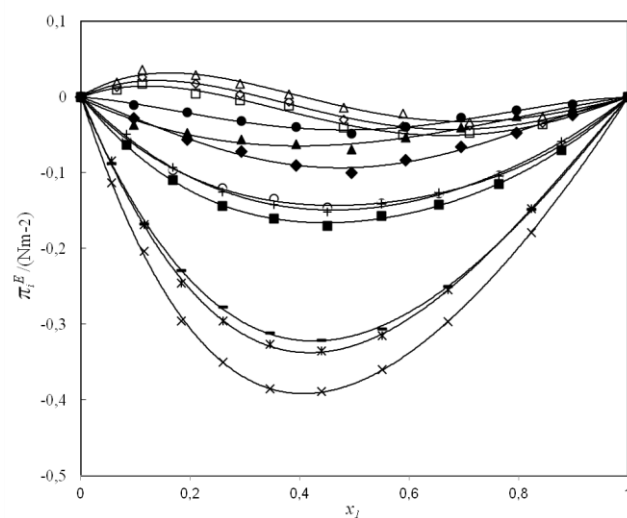


Figure 5. Plots of excess internal pressure π_i^E Vs mole fraction for the binary mixture butyl ethanoate + tetrahydrofuran at (\square , 303.15 ; \diamond , 308.15 ; δ , 313.15) K, butyl ethanoate+ 1,4-dioxane at (\times , 303.15 ; κ , 308.15 ; — , 313.15) K, butyl ethanoate + anisole at (\circ , 303.15 ; $+$, 308.15 ; \blacksquare , 313.15) K, butyl ethanoate + butyl vinyl ether (\blacklozenge , 303.15 ; \blacktriangle , 308.15 ; \bullet , 313.15) K.

Figure 5 shows the variation of π_i^E versus mole fraction of butyl ethanoate, wherein it is observed that the π_i^E values except for (butyl ethanoate + tetrahydrofuran) system, exhibit negative deviation over the entire range of composition at all the studied temperatures. For the mixtures of tetrahydrofuran inversion of sign of π_i^E from positive to negative occurs at about $x_1 \sim 0.275$. It is also observed that the values of π (Table 2) except for (butyl ethanoate + butyl vinyl ether) decrease with increase in concentration of butyl ethanoate. The decrease in internal pressure with increase in concentration of ester may be explained as the addition of monomer (solute) decreases the cohesive forces of the solvent. Whereas for butyl vinyl ether the π values increase with increase in concentration of ester. Similar behavior has been noticed in the earlier studies.^{26, 27}

Conclusions

Density, viscosity and speed of sound for the binary mixtures of butyl ethanoate with tetrahydrofuran, 1, 4-dioxane, anisole, and butyl vinyl ether were determined over the entire range of composition at $T=303.15$, 308.15 , and 313.15 K. The various excess or deviation parameters (V^E , $\Delta\eta$, ΔK_S , L_r^E and π_i^E) were evaluated from the measured data. All these parameters were correlated by the Redlich-Kister polynomial equation to derive the coefficients and standard errors. These properties exhibit either positive or negative deviations from ideality. The results were interpreted in terms of intermolecular interactions and structural effects. It is observed that the interactions involved in the present study are mostly of dipolar-dipolar type. Finally we have employed some of the available semi-empirical equations to correlate the experimental viscosity data and compared their predictive abilities. From the analysis it was concluded that McAllister equation with three adjustable parameters has a good predictive ability as compared to one, and two adjustable parameter models.

References

- ¹Resa, J. M., Gonzalez, C., Moradillo, B., Lanz, J., *J. Chem. Thermodyn.*, **1998**, *30*, 1207.
- ²Aminabhavi, T. M., Banerjee, K., *J. Chem. Eng. Data.*, **1998**, *43*(4), 514.
- ³Li-Chia, F., Chou, C. H., Tang, M., Chen, Y. P., *J. Chem. Eng. Data.*, **1998**, *43*(4), 658.
- ⁴Qin, A., Hoffman, D. E., Munk, P., *J. Chem. Eng. Data.*, **1992**, *37*, 66.
- ⁵Aralaguppi, M. I., Jadar, C. V., Aminabhavi, T. M., *J. Chem. Eng. Data.*, **1999**, *44*, 441.
- ⁶Chandrasekhar, G., Venkatesu, P., Rao, M.V.P., *J. Chem. Eng. Data.*, **2000**, *45*, 590.
- ⁷Sastry, N.V., Patel, M.C., *J. Chem. Eng. Data.*, **2003**, *48*, 1019.
- ⁸Reddy, G. S., Subbaiah M. V., Boddu, V. M., Krishnaiah, A., *J. Mol. Liq.*, **2008**, *141*, 94.
- ⁹Patwari, M. K., Bachu, R. K., Boodida, S., Nallani, S., *J. Chem. Eng. Data.*, **2009**, *54*, 1069.
- ¹⁰Rathnam, M.V., Reema, S.T., Kavita, R.B., Kumar M.S.S., *J. Chem. Eng. Data.*, **2012**, *57*, 1721.
- ¹¹Oswal, S.L., Oswal, P., Phalak, R. P., *Int. J. Thermophys.*, **1996**, *17*(6), 1255
- ¹²Oswal, S. L., Oswal, P., Phalak, R. P., *J. Soln. Chem.*, **1998**, *27*(6), 507
- ¹³Roy, M.N., Sinha, B., Dakua, V. K., *J. Chem. Eng. Data.*, **2006**, *51*, 590
- ¹⁴Rathnam, M.V., Ambavadekar, D.R., Nandini, M., *J. Chem. Eng. Data.*, **2013**, *58*, 3370.
- ¹⁵Rathnam, M.V., Ambavadekar, D.R., Nandini, M., *J. Mol. Liq.*, **2013**, *187*, 58.
- ¹⁶Rathnam, M.V., Ambavadekar, D.R., Nandini, M., *Eur. Chem. Bull.*, **2013**, *2*(9), 642.
- ¹⁷Redlich, O., Kister, A. T., *Ind. Eng. Chem.*, **1948**, *40*, 345.
- ¹⁸Frenkel, Y. I., *Theory of the Viscosity of liq. mixtures, petroleum, (London)*, **1946**, *9*(1), 27
- ¹⁹Heric, E. L., *J. Chem. Eng. Data.*, **1966**, *11*, 66.
- ²⁰McAllister, R. A., *AIChE J.*, **1960**, *6*(3), 427.
- ²¹Alvarez, E., Cancelli, A., Maceiras, R., Navaza, J.M., Taboas, R., *J. Chem. Eng. Data.*, **2006**, *51*, 940.
- ²²Peralta, R.D., Infante, R., Cortez, G., Ratriquez, O., Wisniak, J., *J. Soln. Chem.*, **2002**, *31*(3), 175.
- ²³Nikam, P.S., Jagdale, B.S., Sawant, A.B., Hassan, M., *J. Pure Appl. Ultrasonic.*, **2000**, *22*, 115.
- ²⁴Kincaid, J.F., Eyring, H., *J. Chem. Phys.*, **1938**, *6*(10), 620.
- ²⁵Ramamurthy, M., Sastry, O. S., *Indian. J. Pure Appl. Phys.*, **1983**, *21*, 579.
- ²⁶Anil, G., Palaniappan, L., *Indian. J. Pure Appl. Phys.*, **2001**, *39*, 561.
- ²⁷Srinivasulu, I.J., Naidu, P.R., *Indian J. Pure Appl. Ultrasonic.*, **1995**, *17*, 23.

Received: 17.04.2014.

Accepted: 04.06.2014.



SYNTHESIS OF THIENO[3,2-*d*]PYRIMIDIN-4-ONES AND ALKYLATION THEREOF

Alexander S. Shestakov,^{[a]*} Mikhail A. Prezent,^[b] Victor G. Kartsev,^[c] Khidmet S. Shikhaliev^[a]

Keywords: thiophenes, thienopyrimidinones, 3-*R*-thieno[3,2-*d*]pyrimidine-2,4(1*H*,3*H*)-dione, 3-*R*-2-thioxo-2,3-dihydrothieno[3,2-*d*]pyrimidin-4(1*H*)-one, 2-aminothieno[3,2-*d*]pyrimidin-4(3*H*)-one, alkylation.

The 3-*R*-thieno[3,2-*d*]pyrimidine-2,4(1*H*,3*H*)-diones (**5a-c**) and 3-*R*-2-thioxo-2,3-dihydrothieno[3,2-*d*]pyrimidine-4(1*H*)-ones (**5d-g**) were synthesized using methyl 3-aminothiophene-2-carboxylate and alkyl-, arylisocyanates and isothiocyanates respectively, which in turn converted into its *N*- or *S*-alkyl derivatives (**8a-e**, **9a-g**). 2-Aminothieno[3,2-*d*]pyrimidin-4(3*H*)-one (**14a-c**, **16**) were received as a result the interaction the methyl 3-aminothiophene-2-carboxylate with benzoyl- and pyrimidin-2-yl cyanamides.

* Corresponding Authors

Phone: +7-473-2208956

E-Mail: schas@vmail.ru

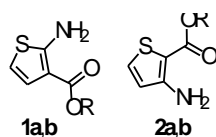
- [a] Department of Chemistry, Voronezh State University, Universitetskaya pl. 1, Voronezh, 394006, Russian Federation
- [b] N.D. Zelinsky Institute of Organic Chemistry, RAS, Leninsky prosp. 47, Moscow, 119991, Russian Federation
- [c] InterBioScreen Ltd., Institutsky prosp. 7a, Chernogolovka, 142432, Russian Federation

Introduction

The interest for thieno[2,3-*d*]pyrimidines is caused by a wide spectrum of biological activity of these compounds, and half of these reports are revealed in the last decade.¹

Synthesis of the thieno[2,3-*d*]pyrimidines, which include substituents in position 2, more often realised through the interaction of methyl 2-aminothiophene-3-carboxylates **1** with nitrile compounds²⁻⁴ or cyanamides⁵⁻⁷ in conditions of acid catalysis. With the isocyanates⁸⁻¹² and the isothiocyanates^{11,13} in the absence of a catalyst formed compounds with the substituent in position 3. Far less reports about the synthesis of regioisomeric thieno[3,2-*d*]pyrimidines.^{7,12} Anyway, 3-aminothiophene-2-carboxylate **2**, that are necessary for it, could be obtained through the condensation esters of mercaptoacetic acid with halogenated propionitriles^{14,15} and now are commercially available.

It makes us hope that the synthetic approaches, realized for the 2-aminothiophene-3-carboxylate, could be used in the case of their regioisomers too.



1, 2 R=Me (a), Et (b)

Experimental

Instrumentation

Melting points were determined in an open capillary tube and are uncorrected. ¹H NMR spectra were recorded on a Bruker AC-300 instrument in DMSO-*d*₆ as solvent and TMS as an internal standard. Elemental analyses were performed on a Carlo Erba NA-1500 CHNS Elemental Analyzer. Reaction progress monitored on TLC 0.2 mm silica gel 60 F-254 (Merck) plates using chlorophorm/methanol (20:1) combination as the mobile phase and U.V. light (254 nm) for visualization.

Density functional theory (DFT) calculations were performed using Gaussian 03 program with the B3LYP exchange-correlation functional. The basis (6-311++G*) was used for all atoms. Geometry optimizations were performed with full relaxation of all atoms. Calculations were performed in gas phase without solvent effects. Vibrational frequency calculations were performed to check that the stable structures had no imaginary frequency.

General Procedure for the synthesis of 3-*R*-thieno[3,2-*d*]pyrimidine-2,4(1*H*,3*H*)-diones (**5a-c**) and 3-*R*-2-thioxo-2,3-dihydrothieno[3,2-*d*]pyrimidine-4(1*H*)-ones. (**5d-g**)

0.01 mole of isocyanate or isothiocyanate was added to solution of 1.57 g (0.01 mol) methyl 3-aminothiophene-2-carboxylate **2a** in anhydrous dioxane. The reaction mixture was heated to 60 °C during 6 h. The solvent was removed in a rotary evaporator, 10 ml of 1M solution MeONa in methanol was added and was heated to 60 °C during 6 h. The solvent was removed in a rotary evaporator, the residue was dissolved in 40 ml of water and treated with hydrochloric acid to weak acid reaction. The formed solid product was filtered and washed with water.

Synthesis of methyl 3-(3-(2-chloroethyl)ureido)thiophene-2-carboxylate. (6)

1.05 g (0.01 mol) 2-chloroethylisocyanate was added to solution of 1.57 g (0.01 mol) methyl 3-aminothiophene-2-carboxylate **2a** in anhydrous dioxane. The reaction mixture was heated to 70 °C during 6 h. The cooled reaction mixture was poured onto water (500 ml). The separated white solid product was filtered, dried and recrystallized from dioxane, (2.26 g, 86%), m.p. 146-148 °C [139-142 °C]¹². ¹H NMR (DMSO-*d*₆): δ = 3.78 (s, 3H, OCH₃), 4.06 (t, 2H, *J* = 8.2 Hz, CH₂), 4.47 (t, 2H, *J* = 8.2 Hz, CH₂), 6.32 (s, 1H, NH), 7.11 (d, 1H, *J* = 5.2 Hz, thiophene ring), 7.83 (d, 1H, *J* = 5.2 Hz, thiophene ring), 10.54 (s, 1H, NH). Anal. Calcd. for C₉H₁₁ClN₂O₃S: C, 41.15; H, 4.22; N, 10.66. Found: C, 41.08; H, 4.25; N, 10.66.

Synthesis of 6,7-dihydro-oxazolo[3,2-*a*]thieno[3,2-*d*]pyrimidine-9-one. (7)

2.63 g (0.01 mol) compound **6** was dissolved in 10 ml dioxane, was added 5 ml strong ammonia and was boiled the resulting solution within 8 hours. The reaction mass was poured in 100 ml water, treated with hydrochloric acid to weak acid reaction and the separated white solid product was filtered, dried and recrystallized from *i*-PrOH:DMF (1:1), (1.44 g, 74 %), m.p. 182-184 °C. ¹H NMR (DMSO-*d*₆): δ = 4.29 (t, 2H, *J* = 8.3, CH₂), 4.79 (t, 2H, *J* = 8.3, CH₂), 7.09 (d, 1H, *J* = 5.2, H-4 thiophene ring), 7.86 (d, 1H, *J* = 5.2, H-5 thiophene ring). Anal. Calcd. for C₈H₆N₂O₂S: C, 49.47; H, 3.11; N, 14.42. Found: C, 49.58; H, 3.20; N, 14.52.

General procedure for the synthesis of alkylated 3-*R*-thieno[3,2-*d*]pyrimidine-2,4(1*H*,3*H*)-diones (8a-e) and 3-*R*-2-thioxo-2,3-dihydrothieno[3,2-*d*]pyrimidin-4(1*H*)-ones. (9a-g)

0.005 mol compound **5a-g** was dissolved in 5 ml 1M solution MeONa in metanol. The solvent was removed in a rotary evaporator, the residue was dissolved in anhydrous DMF and 0.005 mol alkylhalogenide was added. The reaction mixture was heated to 100 °C during 5 min and after 15 min was poured in 100 ml water. The separated solid product was filtered, dried and recrystallized from *i*-PrOH:DMF (1:1).

General procedure for the synthesis of 2-(pyrimidine-2-ylamino)thieno[3,2-*d*]pyrimidin-4(3*H*)-ones. (14a-c)

0.01 mol corresponding *N*-(pyrimidin-2-yl)cyanamide and 0.01 mol strong hydrochloric acid were added to solution of 1.57 g (0.01 mol) methyl 3-aminothiophene-2-carboxylate **2a** in 25 ml *i*-PrOH, was boiled the resulting solution within 3 hours and after cooling to room temperature was poured in 100 ml water. The solution NaOH (0.6 g in 15 ml water) was added. The separated solid product was filtered, dried and recrystallized from *i*-PrOH:DMF (1:1).

Synthesis of *N*-(4-oxo-3,4-dihydrothieno[3,2-*d*]pyrimidine-2-yl)benzamide. (16)

The solution of 0.785 g (0.005 mol) methyl 3-aminothiophene-2-carboxylate **2a** and 0.67 g (0.005 mol) benzoylcyanamide in 20 ml dioxane was heated to 60 °C during 2 h. The separated solid product was filtered, dried and recrystallized from dioxane, (0.80 g, 59%), m.p. 241-242 °C. ¹H NMR (DMSO-*d*₆): δ = 7.21 (d, 1H, *J* = 5.2 Hz, thiophene ring), 7.51 (t, 2H, *J* = 7.5 Hz, ArH), 7.62 (t, 1H, *J* = 7.3 Hz, ArH), 8.03 (d, 1H, *J* = 5.2 Hz, thiophene ring), 8.12 (d, 2H, *J* = 7.9 Hz, ArH), 11.79 (br s, 1H, NH), 12.42 (br s, 1H, NH). Anal. Calcd. for C₁₃H₉N₃O₂S: C, 57.55; H, 3.34; N, 15.49. Found: C, 57.57; H, 3.29; N, 15.52.

Spectral data of newly prepared compounds.**3-(4-Chlorophenyl)thieno[3,2-*d*]pyrimidine-2,4(1*H*,3*H*)-dione. (5a)**

Yield: 95 %, m.p. 345-346 °C. ¹H NMR (300 MHz, DMSO-*d*₆+CCl₄) δ: 6.93 (d, 1H, *J* = 5.2, H-4 thiophene ring), 7.29 (d, 2H, *J* = 7.5, ArH), 7.50 (d, 2H, *J* = 7.5, ArH), 8.01 (d, 1H, *J* = 5.2, H-5 thiophene ring), 11.98 (s, 1H, NH). Anal. Calcd. for C₁₂H₇ClN₂O₂S: C, 51.71; H, 2.53; N, 10.05. Found: C, 51.68; H, 2.54; N, 10.07.

3-(2,4-Difluorophenyl)thieno[3,2-*d*]pyrimidine-2,4(1*H*,3*H*)-dione. (5b)

Yield: 82 %, m.p. 344 °C. ¹H NMR (300 MHz, DMSO-*d*₆+CCl₄) δ: 7.05 (d, 1H, *J* = 5.3 Hz, H-4 thiophene ring), 7.15-7.32 (m, 2H, ArH), 7.40-7.49 (m, 1H, ArH), 8.12 (d, 1H, *J* = 5.3 Hz, H-5 thiophene ring), 11.88 (s, 1H, NH). Anal. Calcd. for C₁₂H₆FN₂O₂S: C, 51.43; H, 2.16; N, 10.00. Found: C, 51.38; H, 2.24; N, 9.93.

3-Isopropylthieno[3,2-*d*]pyrimidine-2,4(1*H*,3*H*)-dione. (5c)

Yield: 62 %, m.p. 235-236 °C. ¹H NMR (300 MHz, DMSO-*d*₆+CCl₄) δ: 1.45 (d, 6H, *J* = 6.8 Hz, 2CH₃), 5.12 (sept, 1H, CH), 7.24 (d, 3H, *J* = 5.3 Hz, H-4 thiophene ring), 8.05 (d, 1H, *J* = 5.3 Hz, H-5 thiophene ring) 12.11 (s, 1H, NH). Anal. Calcd. for C₉H₁₀N₂O₂S: C, 51.41; H, 4.79; N, 13.32. Found: C, 51.48; H, 4.84; N, 13.37.

3-Methyl-2-thioxo-2,3-dihydrothieno[3,2-*d*]pyrimidine-4(1*H*)-one. (5d)

Yield: 62 %, m.p. 327-328 °C. ¹H NMR (300 MHz, DMSO-*d*₆+CCl₄) δ: 2.58 (s, 3H, SCH₃), 7.17 (d, 1H, *J* = 5.2 Hz, H-4 thiophene ring), 7.86 (d, 1H, *J* = 5.2 Hz, H-5 thiophene ring), 12.04 (s, 1H, NH). Anal. Calcd. for C₇H₆N₂OS₂: C, 42.41; H, 3.05; N, 14.13. Found: C, 42.37; H, 3.04; N, 14.06.

3-Phenyl-2-thioxo-2,3-dihydrothieno[3,2-*d*]pyrimidine-4(1*H*)-one. (5e)

Yield: 94 %, m.p. 347 °C (destr.). ¹H NMR (300 MHz, DMSO-*d*₆+CCl₄) δ: 7.19-7.30 (m, 3H, ArH, H-4 thiophene ring), 7.48-7.57 (m, 3H, ArH), 8.08 (d, 1H, *J* = 5.3 Hz, H-5 thiophene ring), 11.97 (s, 1H, NH). Anal. Calcd. for C₁₂H₈N₂OS₂: C, 55.36; H, 3.10; N, 10.76. Found: C, 55.36; H, 3.18; N, 10.67.

3-(2-Fluorophenyl)-2-thioxo-2,3-dihydrothieno[3,2-*d*]pyrimidine-4(1*H*)-one. (5f)

Yield: 70 %, m.p. 295-297 °C. ¹H NMR (300 MHz, DMSO-*d*₆+CCl₄) δ: 7.22 (d, 3H, *J* = 5.2 Hz, H-4 thiophene ring), 7.38-7.49 (m, 3H, ArH), 7.63-7.73 (m, 1H, ArH), 8.00 (d, 1H, *J* = 5.2 Hz, H-5 thiophene ring), 11.92 (s, 1H, NH). Anal. Calcd. for C₁₂H₇FN₂O₂S₂: C, 51.78; H, 2.54; N, 10.06. Found: C, 51.84; H, 2.49; N, 9.98.

3-(4-Methoxyphenyl)-2-thioxo-2,3-dihydrothieno[3,2-*d*]pyrimidine-4(1*H*)-one. (5g)

Yield: 35 %, m.p. 278-280 °C. ¹H NMR (300 MHz, DMSO-*d*₆+CCl₄) δ: 3.87 (s, 3H, OCH₃), 7.11 (d, 2H, *J* = 7.8 Hz, ArH), 7.25 (d, 1H, *J* = 5.3 Hz, H-4 thiophene ring), 7.29 (d, 2H, *J* = 7.8 Hz, ArH), 8.12 (d, 1H, *J* = 5.3 Hz, H-5 thiophene ring), 12.06 (s, 1H, NH). Anal. Calcd. for C₁₃H₁₀N₂O₂S₂: C, 53.77; H, 3.47; N, 9.65. Found: C, 53.84; H, 3.42; N, 9.66.

2-(3-(4-Chlorophenyl)-2,4-dioxo-3,4-dihydrothieno[3,2-*d*]pyrimidine-1(2*H*)-yl)acetonitrile. (8a)

Yield: 64 %, m.p. 189 °C. ¹H NMR (300 MHz, DMSO-*d*₆+CCl₄) δ: 5.22 (s, 2H, CH₂), 7.30 (d, 2H, *J* = 7.3 Hz, ArH), 7.44-7.51 (m, 3H, ArH, H-4 thiophene ring), 8.12 (d, 1H, *J* = 5.3 Hz, H-5 thiophene ring). Anal. Calcd. for C₁₄H₈ClN₃O₂S₂: C, 52.92; H, 2.54; N, 13.22. Found: C, 52.84; H, 2.43; N, 13.16.

3-(2,4-Difluorophenyl)-1-methylthieno[3,2-*d*]pyrimidine-2,4(1*H*,3*H*)-dione. (8b)

Yield: 72 %, m.p. 262 °C. ¹H NMR (300 MHz, DMSO-*d*₆+CCl₄) δ: 3.61 (s, 3H, CH₃), 7.04-7.20 (m, 2H, ArH), 7.29 (d, 1H, *J* = 5.3 Hz, H-4 thiophene ring), 7.30-7.45 (m, 1H, ArH), 8.06 (d, 1H, *J* = 5.3 Hz, H-5 thiophene ring). Anal. Calcd. for C₁₃H₈F₂N₂O₂S₂: C, 53.06; H, 2.74; N, 9.52. Found: C, 53.17; H, 2.62; N, 9.44.

3-(2,4-Difluorophenyl)-1-(2-oxopropyl)thieno[3,2-*d*]pyrimidine-2,4(1*H*,3*H*)-dione. (8c)

Yield: 48 %, m.p. 166-168 °C. ¹H NMR (300 MHz, DMSO-*d*₆+CCl₄) δ: 2.29 (s, 3H, CH₃), 5.02 (s, 2H, CH₂), 7.05-7.19 (m, 2H, ArH), 7.22 (d, 1H, *J* = 5.3 Hz, H-4 thiophene ring), 7.30-7.41 (m, 1H, ArH), 8.05 (d, 1H, *J* = 5.3 Hz, H-5 thiophene ring). Anal. Calcd. for C₁₅H₁₀F₂N₂O₃S₂: C, 53.57; H, 3.00; N, 8.33. Found: C, 53.47; H, 2.99; N, 8.26.

3-Isopropyl-1-methylthieno[3,2-*d*]pyrimidine-2,4(1*H*,3*H*)-dione. (8d)

Yield: 68 %, m.p. 115-116 °C. ¹H NMR (300 MHz, DMSO-*d*₆+CCl₄) δ: 1.41 (d, 6H, *J* = 6.8 Hz, 2CH₃), 3.50 (s, 3H, CH₃), 5.17 (sept, 1H, CH), 7.18 (d, 3H, *J* = 5.3 Hz, H-4 thiophene ring), 7.97 (d, 1H, *J* = 5.3 Hz, H-5 thiophene ring). Anal. Calcd. for C₁₀H₁₂N₂O₂S₂: C, 53.55; H, 5.39; N, 12.49. Found: C, 53.42; H, 5.34; N, 12.35.

4-((3-Isopropyl-2,4-dioxo-3,4-dihydrothieno[3,2-*d*]pyrimidine-1(2*H*)-yl)methyl)benzotrile. (8e)

Yield: 77 %, m.p. 204-205 °C. ¹H NMR (300 MHz, DMSO-*d*₆+CCl₄) δ: 1.50 (d, 6H, *J* = 6.8 Hz, 2CH₃), 5.21 (sept, 1H, CH), 5.32 (s, 2H, CH₂), 7.10 (d, 3H, *J* = 5.3 Hz, H-4 thiophene ring), 7.51 (d, 2H, *J* = 7.4 Hz, ArH), 7.70 (d, 2H, *J* = 7.4 Hz, ArH), 7.90 (d, 1H, *J* = 5.3 Hz, H-5 thiophene ring). Anal. Calcd. for C₁₇H₁₅N₃O₂S₂: C, 62.75; H, 4.65; N, 12.91. Found: C, 62.87; H, 4.77; N, 13.01.

3-Methyl-2-(methylthio)thieno[3,2-*d*]pyrimidine-4(3*H*)-one. (9a)

Yield: 64 %, m.p. 196-197 °C. ¹H NMR (300 MHz, DMSO-*d*₆+CCl₄) δ: 2.62 (s, 3H, SCH₃), 3.54 (s, 3H, NCH₃), 7.21 (d, 1H, *J* = 5.2 Hz, H-4 thiophene ring), 7.99 (d, 1H, *J* = 5.2 Hz, H-5 thiophene ring). Anal. Calcd. for C₈H₈N₂O₂S₂: C, 45.26; H, 3.80; N, 13.20. Found: C, 45.30; H, 3.80; N, 13.27.

2-(Methylthio)-3-phenylthieno[3,2-*d*]pyrimidine-4(3*H*)-one. (9b)

Yield: 54 %, m.p. 182-183 °C. ¹H NMR (300 MHz, DMSO-*d*₆+CCl₄) δ: 2.47 (s, 3H, SCH₃), 7.23-7.34 (m, 3H, ArH, H-4 thiophene ring), 7.52-7.61 (m, 3H, ArH), 7.97 (d, 1H, *J* = 5.3 Hz, H-5 thiophene ring). Anal. Calcd. for C₁₃H₁₀N₂O₂S₂: C, 56.91; H, 3.67; N, 10.21. Found: C, 56.86; H, 3.63; N, 10.25.

2-(4-Oxo-3-phenyl-3,4-dihydrothieno[3,2-*d*]pyrimidine-2-ylthio)acetonitrile. (9c)

Yield: 52 %, m.p. 194-195 °C. ¹H NMR (300 MHz, DMSO-*d*₆+CCl₄) δ: 4.09 (s, 2H, CH₂), 7.31-7.43 (m, 3H, ArH, H-4 thiophene ring), 7.55-7.63 (m, 3H, ArH), 8.08 (d, 1H, *J* = 5.3 Hz, H-5 thiophene ring). Anal. Calcd. for C₁₄H₉N₃O₂S₂: C, 56.17; H, 3.03; N, 14.04. Found: C, 56.11; H, 3.11; N, 13.97.

3-(2-Fluorophenyl)-2-(methylthio)thieno[3,2-*d*]pyrimidine-4(3*H*)-one. (9d)

Yield: 54 %, m.p. 137-139 °C. ¹H NMR (300 MHz, DMSO-*d*₆+CCl₄) δ: 2.52 (s, 3H, SCH₃), 7.30 (d, 3H, *J* = 5.2 Hz, H-4 thiophene ring), 7.35-7.47 (m, 3H, ArH), 7.57-7.65 (m, 1H, ArH), 8.08 (d, 1H, *J* = 5.2 Hz, H-5 thiophene ring). Anal. Calcd. for C₁₃H₉FN₂O₂S₂: C, 53.41; H, 3.10; N, 9.58. Found: C, 53.35; H, 3.15; N, 9.64.

2-(3-(2-Fluorophenyl)-4-oxo-3,4-dihydrothieno[3,2-*d*]pyrimidin-2-ylthio)acetonitrile. (9e)

Yield: 20 %, m.p. 117-118 °C. ¹H NMR (300 MHz, DMSO-*d*₆+CCl₄) δ: 4.15 (s, 2H, CH₂), 7.36-7.47 (m, 3H, ArH, H-4 thiophene ring), 7.54 (t, 1H, *J* = 7.8 Hz, ArH), 7.63-7.71 (m, 1H, ArH), 8.11 (d, 1H, *J* = 5.2 Hz, H-5 thiophene ring). Anal. Calcd. for C₁₄H₈FN₃OS₂: C, 52.98; H, 2.54; N, 13.24. Found: C, 53.06; H, 2.50; N, 13.32.

Methyl 2-(3-(2-fluorophenyl)-4-oxo-3,4-dihydrothieno[3,2-*d*]pyrimidin-2-ylthio)acetate. (9f)

Yield: 64 %, m.p. 177-178 °C. ¹H NMR (300 MHz, DMSO-*d*₆+CCl₄) δ: 3.71 (s, 3H, OCH₃), 3.96 (s, 2H, CH₂), 7.25 (d, 1H, *J* = 5.2 Hz, H-4 thiophene ring), 7.36-7.44 (m, 2H, ArH), 7.48 (t, 1H, *J* = 7.8 Hz, ArH), 7.60-7.68 (m, 1H, ArH), 8.06 (d, 1H, *J* = 5.2 Hz, H-5 thiophene ring). Anal. Calcd. for C₁₅H₁₁FN₂O₃S₂: C, 51.42; H, 3.16; N, 7.99. Found: C, 51.36; H, 3.09; N, 8.09.

3-(4-Methoxyphenyl)-2-(2-oxopropylthio)thieno[3,2-*d*]pyrimidin-4(3*H*)-one. (9g)

Yield: 66 %, m.p. 161-163 °C. ¹H NMR (300 MHz, DMSO-*d*₆+CCl₄) δ: 2.29 (s, 3H, CH₃), 3.89 (s, 3H, OCH₃), 3.96 (s, 2H, CH₂), 7.09 (d, 2H, *J* = 7.8 Hz, ArH), 7.20 (d, 1H, *J* = 5.3 Hz, H-4 thiophene ring), 7.25 (d, 2H, *J* = 7.8 Hz, ArH), 7.99 (d, 1H, *J* = 5.3 Hz, H-5 thiophene ring). Anal. Calcd. for C₁₆H₁₄N₂O₃S₂: C, 55.47; H, 4.07; N, 8.09. Found: C, 55.39; H, 4.10; N, 8.13.

2-(Pyrimidin-2-ylamino)thieno[3,2-*d*]pyrimidin-4(3*H*)-one. (14a)

Yield: 37 %, m.p. 278-279 °C. ¹H NMR (300 MHz, DMSO-*d*₆) δ: 7.10-7.15 (m, 2H, H-5 pyrimidine ring, H-4 thiophene ring), 7.92 (d, 1H, *J* = 5.2 Hz, H-5 thiophene ring), 8.71 (d, 2H, *J* = 5.2 Hz, H-4, H-6 pyrimidine ring), 10.98 (br s, 1H, NH), 13.11 (br s, 1H, NH). Anal. Calcd. for C₁₀H₇N₅OS: C, 48.97; H, 2.88; N, 28.55. Found: C, 49.07; H, 2.86; N, 28.55.

2-(4,6-Dimethylpyrimidin-2-ylamino)thieno[3,2-*d*]pyrimidin-4(3*H*)-one. (14b)

Yield: 42 %, m.p. 271-272 °C. ¹H NMR (300 MHz, DMSO-*d*₆) δ: 2.47 (s, 6H, CH₃), 6.81 (s, 1H, H-5 pyrimidine ring), 7.12 (d, 1H, *J* = 5.2 Hz, thiophene ring), 7.85 (d, 1H, *J* = 5.2 Hz, thiophene ring), 10.51 (br s, 1H, NH), 13.39 (br s, 1H, NH). Anal. Calcd. for C₁₂H₁₁N₅OS: C, 52.73; H, 4.06; N, 25.62. Found: C, 52.81; H, 4.10; N, 25.70.

2-(4-Phenylpyrimidin-2-ylamino)thieno[3,2-*d*]pyrimidin-4(3*H*)-one. (14c)

Yield: 88 %, m.p. 256-258 °C. ¹H NMR (300 MHz, DMSO-*d*₆) δ: 7.20 (d, 1H, *J* = 5.2 Hz, thiophene ring), 7.56-7.62 (m, 3H, ArH), 7.68 (d, 1H, *J* = 5.3 Hz, H-5 pyrimidine ring), 7.20 (d, 1H, *J* = 5.2 Hz, thiophene ring), 8.04 (d, 1H, *J* = 5.2 Hz, thiophene ring), 8.16-8.22 (m, 2H, ArH), 8.74 (d,

1H, *J* = 5.3 Hz, H-6 pyrimidine ring), 11.04 (br s, 1H, NH), 13.35 (br s, 1H, NH). Anal. Calcd. for C₁₆H₁₁N₅OS: C, 59.80; H, 3.45; N, 21.79. Found: C, 59.87; H, 3.47; N, 21.87.

Results and Discussion

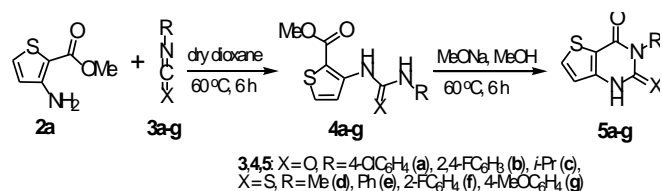
Reaction of isocyanates and isothiocyanates with aminoester **1** as well as their isomers with **2** begins with the formation of the corresponding urea or thiourea, which is the product of nucleophilic attack on the carbon atom of the isocyanate or isothiocyanate groups of the amino nitrogen atom. Further in basic catalysis conditions the interaction resulting urea nitrogen or thiourea with a carbonyl group carbon atom of the ester group and the pyrimidine ring closure of an annelated. Under the conditions of acid catalysis generated thiourea result thieno[1,3]thiazin-4-one.^{16,17} Thus the cyclization involves an amino group and the carbonyl carbon of the ester group. However their reactivity apparently depends on the position of the thiophene ring. In fact, p*K*_a for thiophene-2-carboxylic acid (3.53) is 0.57 lower than for thiophene-3-carboxylic acid (4.10),¹⁸ in other words carboxyl group position 2 has more acid than in position 3. In the same way the protonation of the oxygen atom in thiophene-3-carboxamide is easier,¹⁹ so it is more basic than in amide group in position 2.

The same result is shown by our quantum-chemical calculations with the GAUSSIAN 03 program.²⁰ Payment of charges made by the method of Merz-Singh-Kollman,²¹ which, in our opinion, the most adequately reflects the reactivity of the atoms in the processes occurring under the charge control. Thus, the data in Table 1 demonstrate that the amino compound **2a** more nucleophilic and electrophilic carbonyl group is more than the compound **1a**.

Table 1. The charge on the amino nitrogen atom and the carbonyl group of compounds **1a**, **2a**, and methyl anthranilate.

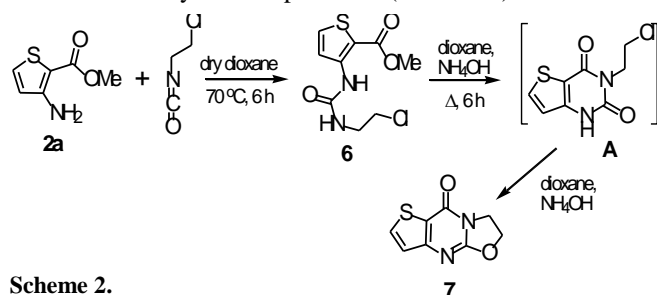
Functional group	1a	2a	methyl anthranilate
-NH ₂	-0.703	-0.776	-0.776
-C(O)OMe	0.614	0.785	0.601

Furthermore, the optimal conformation aminoester **1a** formed in the intramolecular hydrogen bond between the hydrogen atom of the amino group and the carbonyl oxygen stabilizing the initial state. In the methyl 3-aminothiophene-2-carboxylate the formation of such a connection **2a** is difficult as the ester group undergoes steric hindrance by volume of sulfur, which leads to the formation of weak hydrogen bond between the hydrogen atom of the amino group and the bridging nitrogen atom of the ester group, a carbonyl atom and not oxygen, as in the case **1a**. Thus, in aminoester **2a** aminogroup is a more nucleophilic and carbonyl more electrophilic than methyl 2-aminothiophene-3-carboxylate **1a**. The interaction of compound **2a** with isocyanates and isothiocyanates **3a-g** also initially leads to carbamides or thiocarbamides **4a-g**, alkaline treatment of which leads to pyrimidinediones **5a-c** or 2-thioxopyrimidin-4-ones **5d-g** (Scheme 1).



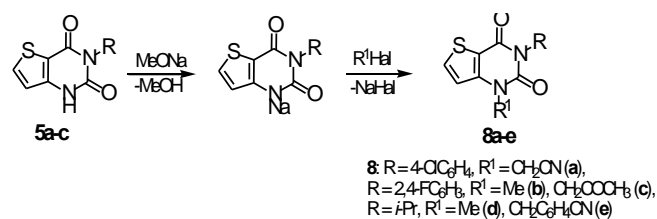
Scheme 1.

Due to interaction of compound **2a** with 2-chloroethylisocyanates methyl 3-(3-(2-chloroethyl)ureido)thiophene-2-carboxylate **6** was received with potential antihypertensive activity.¹² Our attempt to obtain 3-(2-chloroethyl)thieno[3,2-*d*]pyrimidine-2,4(1*H*,3*H*)-dione **A** in the conditions similar to the conditions of getting 3-(2-chloroethyl)quinazolin-2,4(1*H*,3*H*)-dione,²² shows that the reaction proceeds very slowly. In more complicated conditions (two-day boiling ammonia-dioxane solution) leads to the tricyclic compounds **7** (Scheme 2).



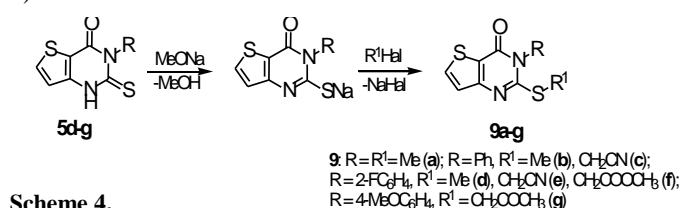
Scheme 2.

Pyrimidinediones **5a-c**, due to a movable hydrogen atom at position 1, are able to join the reaction of alkylation, just as 3-*R*-quinazolin-2,4(1*H*,3*H*)-diones²³ and thieno[2,3-*d*]pyrimidine-2,4(1*H*,3*H*)-diones.²⁴ Treatment of a solution of 1M sodium methoxide in methanol solution was transferred to their corresponding sodium salts. After removal of methanol on a rotary evaporator, the salt was dissolved in dimethylacetamide and treated with a solution of the alkyl halide. The brief heating leads to the forming of alkyl derivatives **8a-e** (Scheme 3).



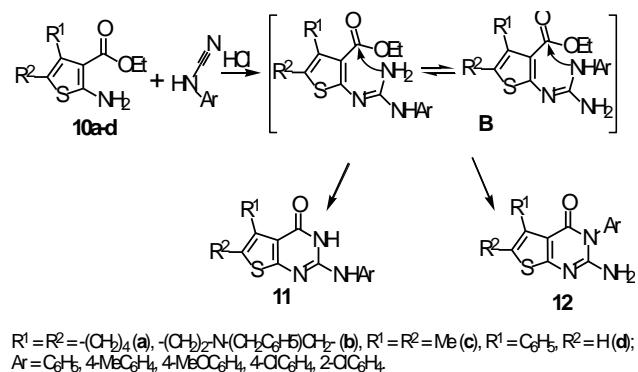
Scheme 3.

2-Thioxopyrimidin-4-ones **5d-g**, is like the isomeric 2-thioxo-2,3-dihydrothieno[2,3-*d*]pyrimidin-4(1*H*)-ones^{13,25-26} alkylated at the sulfur atom. In this case, the compound **5d-g** are also converted into its sodium salt, which under mild conditions with good yields subjected to alkylation (Scheme 4).



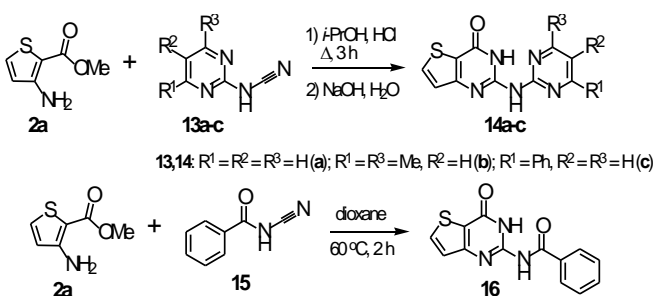
Scheme 4.

Structural analog of isocyanates and isothiocyanates are cyanamides. Describes the reaction of substituted ethyl 2-aminothiophene-3-carboxylates **10a-d** and a dialkyl- and diarylcyanamides, catalyzed anhydrous HCl (Scheme 5).⁶ Dialkyl cyanamides yield 2-dialkylaminothieno[2,3-*d*]pyrimidin-4(3*H*)-ones under these reaction conditions. However, when *N*-monoarylcyanamides were used two isomeric thienopyrimidin-4-ones **11** and **12** have been obtained as the condensation products of their dry HCl catalyzed reaction with thiophene *o*-aminoesters **10a-d**. The reaction proceeds via the transient guanidine intermediate **B**, which cyclizes through two alternate pathways to afford the isomeric 2-aminothieno[2,3-*d*]pyrimidin-4 (3*H*)-ones.



Scheme 5.

We used the *N*-pyrimidin-2-ylcyanamides **13a-c** and benzoylcyanamide **15**. Previously, we have shown²⁷⁻²⁹ that these cyanamides reacted with esters of anthranilic acid to form quinazolin-4(3*H*)-ones similar to compound **11**. Structure of the reaction product of methyl anthranilate with cyanamide **13b** is confirmed RSA.³⁰ Quantum-chemical calculation results given above indicate that 3-aminothiophene-2-carboxylates **2** largely similar anthranilate than 2-aminothiophene-3-carboxylates **1**. This suggests that the main product cyclization are just compounds **14a-c** and **16** (Scheme 6). Indeed, in the ¹H NMR spectrum of compounds **14a-c** singlets observed in the 10.5-11.0 ppm and 13.1-13.5 ppm, which corresponds to sufficiently "sour" magnetically nonequivalent protons of NH groups. In the case of a structure similar to the structure of the compounds **12**, in the spectrum of protons expected signal group NH₂. In the ¹H NMR spectrum of compound **16** are also present singlets 11.79 and 12.45 ppm



Scheme 6.

Conclusion

The interaction of methyl 3-aminothiophene-2-carboxylate with isocyanates, isothiocyanates and the cyanamides leads to 2- and 3-substituted thieno[3,2-*d*]pyrimidine-4(1*H*)-ones (**5a-g**, **14a-c**, **16**). The 3-*R*-thieno[3,2-*d*]pyrimidine-2,4(1*H*,3*H*)-diones (**5a-c**) and 3-*R*-2-thioxo-2,3-dihydrothieno[3,2-*d*]pyrimidine-4(1*H*)-ones (**5d-g**) are suitable scaffolds for getting various *N*- or *S*-alkyl derivatives. Use of 2-chloroethyl isocyanate allows to obtain tricyclic 6,7-dihydro-oxazolo[3,2-*a*]thieno[3,2-*d*]pyrimidin-9-one (**7**). The interaction of methyl 3-aminothiophene-2-carboxylate with cyanamides is a regioselective process and it leads to *N*-2-substituted 2-aminothieno[3,2-*d*]pyrimidine-4(3*H*)-ones (**14a-c**).

Acknowledgement

This article is supported by The Ministry of education and science of the Russian Federation (the state contract No 02.G25.31.0007).

References

- Aly, A. A., Ishak, E. A., Ramadan, M., Germoush, M. O., El-Emary T. I., Al-Muaiikel, N. S., *J. Heterocyclic Chem.*, **2013**, *50*, 451.
- Bogolubsky, A. V., Ryabukhin, S. V., Stetsenko, S. V., Chupryna, A. A., Volochnyuk, D. M., Tolmachev, A. A., *J. Comb. Chem.*, **2007**, *9*, 661.
- Bogolubsky, A. V., Ryabukhin, S. V., Plaskon, A. S., Stetsenko, S. V., Volochnyuk, D. M., Tolmachev, A. A., *J. Comb. Chem.*, **2008**, *10*, 858.
- Kucherenko, T. T., Zadorozhny, A. V., Kovtunenkov, V. A., *Chem. Heterocycl. Comp.*, **2008**, *44*, 750.
- Shishoo, Ch., Ananthan, S., Bhadti, V., Ullas, G., Chhabria, M., Bariwal, J., Venkatesh, L., Nargund, G., Jain, K., *Heterocycles*, **2009**, *78*, 1627.
- Shishoo, C. J., Devani, M. B., Bhadti, V. S., Ullas, G. V., Ananthan, S., Pathak, U. S., Jain, K. S., Rathod, I. S., Talati, D. S., Doshi, N. H., *J. Heterocyclic Chem.*, **1984**, *21*, 375.
- Shishoo, C. J., Pathak, U. S., Jain, K. S., Devani, I. T., Chhabria, M. T., *Indian J. Chem.*, **1994**, *33B*, 436.
- El-Emary, T. I., Khodairy, A., *Phosphorus Sulfur Silicon Relat. Elem.*, **2006**, *181*, 1073.
- Prasad, M. R., Rao, A. R., Rao, P. S., Rajan, K. S., *Synthesis*, **2001**, *14*, 2119.
- Sasakir, S., Cho, N., Nara, Y., Harada, M., Endo, S., Suzuki, N., Furuya, S., Fujinori, M., *J. Med. Chem.*, **2003**, *46*, 123.
- Al-Taisan, Kh. M., Al-Hazimi, H. M. A., Al-Shihry, Sh. S., *Molecules*, **2010**, *15*, 3932.
- Russell, R. K., Press, J. B., Pampulla, R. A., McNally, J. J., Falotico, R., Keiser, J. A., Bright, D. A., Tabia, A., *J. Med. Chem.*, **1988**, *31*, 1786.
- El-Kashef, H., Farghaly, A.-R., Al-Hazmi, A., Terme, Th., Vanelle, P., *Molecules*, **2010**, *15*, 2651.
- Huddleston, P. R., Barker, J. M., *Synth. Commun.*, **1979**, *9*, 731.
- GB Patent 837086*, Hoechst AG, 1960.
- Gütschow, M., *J. Heterocyclic Chem.*, **1996**, *33*, 355.
- Sreekumar, R., Rugmini, P., Raghavakaimal Padmakumar, *Tetr. Lett.*, **1997**, *38*, 3179.
- Fringuelli, F., Marino, G., Taticchi, A., *J. Chem. Soc., Perkin Trans. 2*, **1972**, 1738.
- Alberghina, G., Fisichella, S., Musumarra, G., *J. Chem. Soc., Perkin Trans. 2*, **1979**, 1700.
- Frisch, M. J., Trucks, G. W., Schlegel, H. B., Scuseria, G. E., Robb, M. A., Cheeseman, J. R., Montgomery, J. A., Vreven, Jr. T., Burant, J. C., Millam, J. M., Iyengar, S. S., Tomasi, J., Barone, V., Mennucci, B., Cossi, M., Scalmani, G., Rega, N., Petersson, G. A., Nakatsuji, H., Hada, M., Ehara, M., Toyota, K., Fukuda, R., Hasegawa, J., Ishida, M., Nakajima, T., Honda, Y., Kitao, O., Nakai, H., Klene, M., Li, X., Knox, J.E., Hratchian, H. P., Cros, J. B., Adamo, C., Jaramillo, J., Gomperts, R., Stratmann, R.E., Yazyev, O., Austin, A. J., Cammi, R., Pomelli, C., Ochterski, J. W., Ayala, P. Y., Morokuma, K., Voth, G. A., Salvador, P., Dannenberg, J. J., Zakrzewski, V.G., Dapprich, S., Daniels, A. D., Strain, M. C., Farkas, O., Malick, D. K., Rabuck, A. D., Paghavachari, K., Foresman, J.B., Ortiz, J. V., Cui, Q., Baboul, A. G., Clifford, S., Cioslowski, J., Stefanov, B. B., Liu, G., Liashenko, A., Piskorz, P., Komaromi, I., Martin, R. L., Fox, D. J., Keith, T., Al-Laham, M. A., Peng, C. Y., Faanayakkara, A., Challacombe, M., Gill, P. M. W., Johnson, B., Chen, W., Wong, M. W., Gonzalez, C., Pople, J. A., *Gaussian 03, Revision C.02*, Gaussian, Inc., Wallingford CT, **2004**.
- Singh, U. C., Kollman, P. A., *J. Comp. Chem.*, **1984**, *5*, 129.
- Papadopoulos, E. P., *J. Heterocyclic Chem.*, **1980**, *17*, 1553.
- Shestakov, A. S., Sidorenko, O. E., Bushmarinov, I. S., Shikhaliev, Kh. S., Antipin, M. Yu., *Russ. J. Org. Chem.*, **2009**, *45*, 1691.
- Sasaki, S., Cho, N., Nara, Y., Harada, M., Endo, S., Suzuki, N., Furuya, Sh., Fujino, M., *J. Med. Chem.*, **2003**, *46*, 113.
- Ahmed, E. K., Sensfuss, U., Habicher, W. D., *J. Heterocyclic Chem.* **1999**, *36*, 1119.
- Panico, A. M., Cardile, V., Santagati, A., Gentile, B., *Farmaco*, **2001**, *56*, 959.
- Shikhaliev, Kh. S., Shestakov, A. S., Medvedeva, S. M., Gusakova N. V., *Russ. Chem. Bull.*, **2008**, *57*, 170.
- Shestakov, A. S., Kvasova, I. P., Potapov, A. Yu., Didenko, V. V., Ledenyova, I. V., Shikhaliev, Kh. S., *Proc. Voronezh State Univ.*, **2011**, *No. 1*, 69.
- Shestakov, A. S., Moustafa, A. H., Bushmarinov, I. S., Sidorenko, O. E., Shikhaliev, Kh. S., *Butlerov Comm.*, **2012**, *31*, 1.
- Shestakov, A. S., Bushmarinov, I. S., Sidorenko, O. E., Potapov, A. Yu., Shikhaliev, Kh. S., Antipin, M. Yu., *Chem. Heterocycl. Comp.*, **2011**, *47*, 316.

Received: 09.05.2014.

Accepted: 05.06.2014.



SYNTHESIS OF 2-THIOXOQUINAZOLIN-4(1H)-ONES IN WATER AT ROOM TEMPERATURE

Farhad Hatamjafari,^{[a]*} and Kurosh Rad-Moghadam^[b]

Keywords: 2-thioxoquinazolin-4(1H)-ones; potassium carbonate catalyst; room temperature three-component reaction; isatoic anhydride; isocyanates

Potassium carbonate was found to be an efficient catalyst for synthesis of novel 2-thioxoquinazolin-4(1H)-one derivatives via a one-pot condensation of isatoic anhydride with primary amines and phenyl isothiocyanate in water at room temperature

Corresponding Authors*

E-Mail: hatamjafari@yahoo.com

[a] Department of Chemistry, Faculty of Science, Islamic Azad University-Tonekabon Branch, Tonekabon 46841-61167, Iran

[b] Department of Chemistry, University of Guilan, 41335-19141, Rasht, Iran

INTRODUCTION

Quinazolinones are very important structural units found as the main constituents of several bioactive molecules displaying a wide range of biological and pharmacological activities.¹ Owing to the promised properties of quinazolinones such as anti-inflammatory,² antimalarial,³ antihypertensive,⁴ anticonvulsant,⁵ anti-HIV,⁶ and anti-cancer⁷ activities, a plethora of research efforts were rewarded to their synthesis. As a consequence, there are a number of synthetic methods available for preparation of quinazolinones.⁸⁻¹⁸

The most common route resorted for synthesis of 4(3H)-quinazolinones involves the amidation of 2-aminobenzoic acid or its derivatives, followed by a oxidative ring closure.¹⁹⁻²² Other synthetic methods include the cyclization of anthranil amides with aldehydes²³ or ketones or even with acid chlorides under acidic or basic conditions.²⁴⁻²⁵ However, most of the reported methods involve multistep processes requiring prolong experimental procedures or toxic reagents for giving poor yields.

Moreover, very few methods are available for the synthesis of 2-thioxoquinazolin-4-ones whilst most of the reported methods were developed for synthesis of quinazolin-2,4(1H,3H)-diones.²⁶

Recently, a base-catalyzed intramolecular nucleophilic cyclization of substituted thioureas in DMF for synthesis of 2-thioxoquinazolin-4-ones was reported.²⁷ In addition, solid-phase syntheses were developed for preparation of many libraries of 2-thioxoquinazolin-4-one derivatives.²⁸⁻³⁰

EXPERIMENTAL SECTION

Materials, methods and instruments

All the chemicals were obtained from Merck or Fluka without further purifications. Melting points were determined on an Electrothermal 9100 melting point apparatus. Silica gel 60F₂₅₄ plates were used for TLC. IR spectra were measured on a Shimadzu IR-470 spectrometer. ¹H NMR and ¹³C NMR spectra were determined on Bruker 500 DRX AVANCE instrument at 500 and 125 MHz, respectively. The elemental analyses (C, H, N) were obtained from a Carlo ERBA Model EA 1108 analyzer carried out on Perkin-Elmer 240c analyzer. Mass spectra were recorded on a FINNIGAN-MAT 8430 Mass spectrometer operating at an ionization potential of 70 eV.

Typical synthesis of compounds (4a-h)

To a magnetically stirred mixture of isatoic anhydride (2 mmol) in 10 mL of water was added a proper primary amine (2 mmol). When the addition was complete, the mixture retained stirring for additional 2 hours at room temperature. After that time, the mixture became milky and phenyl isothiocyanate (2 mmol) and potassium carbonate (0.1 g) were added to it. The mixture was stirred further for nearly 1 hour at room temperature to complete the reaction. Each time the progress of the reaction was monitored by TLC. At the end of reaction, the mixture was diluted with CH₂Cl₂ and washed with water and the organic layer was dried over MgSO₄. Evaporation of the solvent under reduced pressure provided a residue which was purified by column chromatography (using n-hexane:ethylacetate in the ratio of 8:2 as eluents) to afford the desired 2-thioxoquinazolin-4(1H)-one products (4a-h).

2,3-Dihydro-3-phenyl-2-thioxoquinazolin-4(1H)-one (4a).

White powder, m.p. 307-309 °C; IR: (ν_{max}/cm⁻¹): 3247 (N-H), 3068 (C-H), 1664 (C=O), 1197 (C=S); ¹H NMR (500 MHz, DMSO): δ= 7.27-7.96 (m, 9H, Ar), 13.03 (s, 1H, NH); ¹³C NMR (125 MHz, DMSO): 115.6, 116.1, 124.3,

127.3, 128.0, 128.8, 128.9, 135.5, 139.2, 139.6, 159.7, 176.0 ppm. MS (m/z, %): 254 (M⁺). Anal. Calcd. For C₁₄H₁₀N₂O₃S: C, 66.12; H, 3.96; N, 11.02. Found: C, 65.92; H, 3.90; N, 11.13.

3-(4-Chlorobenzyl)-2,3-dihydro-2-thioxoquinazolin-4(1H)-one (4b).

White powder, m.p. 317-319 °C; IR: ($\nu_{\max/\text{cm}^{-1}}$): 3054 (N-H), 2932 (C-H), 1664 (C=O), 1224 (C=S); ¹H NMR (500 MHz, DMSO): δ = 5.06 (s, 2H), 7.16-7.59 (m, 8H, Ar), 12.03 (s, 1H, NH); ¹³C NMR (125 MHz, DMSO): 43.2, 114.6, 125.3, 127.0, 127.4, 128.2, 133.9, 134.7, 137.2, 142.0, 149.6, 159.7 ppm. MS (m/z, %): 302 (M⁺). Anal. Calcd. For C₁₅H₁₁ClN₂O₃S: C, 59.50; H, 3.66; N, 9.25. Found: C, 59.41; H, 3.72; N, 9.19.

7-Chloro-2,3-dihydro-3-phenyl-2-thioxoquinazolin-4(1H)-one, (4c).

White powder, m.p. 324-326 °C; IR: ($\nu_{\max/\text{cm}^{-1}}$): 3159 (N-H), 3005 (C-H), 1717 (C=O), 1180 (C=S); ¹H NMR (500 MHz, DMSO): δ = 7.29-7.90 (m, 8H, Ar), 13.06 (s, 1H, NH); ¹³C NMR (125 MHz, DMSO): 14.9, 56.6, 115.5, 116.4, 124.5, 125.6, 126.3, 126.9, 127.9, 135.4, 138.8, 140.3, 158.3, 176.5 ppm. MS (m/z, %): 288 (M⁺). Anal. Calcd. For C₁₄H₉ClN₂O₃S: C, 58.23; H, 3.14; N, 9.70. Found: C, 58.34; H, 3.17; N, 9.58.

2,3-Dihydro-3-(1-phenylethyl)-2-thioxoquinazolin-4(1H)-one (4d).

White powder, m.p. 264-266 °C; IR: ($\nu_{\max/\text{cm}^{-1}}$): 3310 (N-H), 3025 (C-H_{arom}), 1666 (C=O), 1198 (C=S); ¹H NMR (500 MHz, DMSO): δ =1.85 (d, *J* = 7.1 Hz, 3H), 2.08 (q, *J* = 7.1 Hz, H), 7.18-7.80 (m, 9H, Ar), 12.96 (s, 1H, NH); ¹³C NMR (125 MHz, DMSO): 31.8, 47.0, 55.5, 112.0, 112.3, 115.5, 115.6, 120.4, 124.5, 127.2, 130.8, 135.4, 139.0, 147.4, 148.7, 159.1, 174.9, ppm. MS (m/z, %): 282 (M⁺). Anal. Calcd. For C₁₆H₁₄N₂O₃S: C, 68.06; H, 5.00; N, 9.92. Found: C, 68.12; H, 5.04; N, 9.80.

3-(3,4-Dimethoxyphenethyl)-2,3-dihydro-2-thioxoquinazolin-4(1H)-one (4e).

White powder, m.p. 302-305 °C; IR: ($\nu_{\max/\text{cm}^{-1}}$): 3180 (N-H), 3040 (C-H), 1686 (C=O), 1145 (C=S); ¹H NMR (500 MHz, DMSO): δ = 2.51 (t, *J* = 7.5 Hz, 2H), 3.74 (s, 6H), 4.57 (t, *J* = 7.5 Hz, 2H), 7.79-7.97 (m, 7H, Ar), 13.03 (s, 1H, NH); ¹³C NMR (125 MHz, DMSO): 158.5, 152.3, 145.4, 138.3, 135.6, 131.4, 128.3, 126.5, 125.5, 124.8, 118.5, 21.0, 13.1, 9.0 ppm. MS (m/z, %): 342 (M⁺). Anal. Calcd. For C₁₈H₁₈N₂O₃S: C, 63.14; H, 5.30; N, 8.18. Found: C, 63.21; H, 5.36; N, 8.03.

2,3-Dihydro-3-((pyridin-2-yl)methyl)-2-thioxoquinazolin-4(1H)-one, (4f)

White powder, m.p. 294-297 °C; IR: ($\nu_{\max/\text{cm}^{-1}}$): 3268 (N-H), 3071(C-H), 1664 (C=O), 1171 (C=S); ¹H NMR (500 MHz, DMSO): δ = 5.77 (s, 2H), 7.22-8.41 (m, 8H, Ar),

13.04 (s, 1H, NH); ¹³C NMR (125 MHz, DMSO): 50.0, 115.4, 115.7, 120.6, 121.9, 124.5, 127.3, 135.5, 136.5, 139.2, 148.8, 155.3, 159.4, 175.6 ppm. MS (m/z, %): 269 (M⁺). Anal. Calcd. For C₁₄H₁₁N₃O₃S: C, 62.43; H, 4.12; N, 15.60. Found: C, 62.48; H, 4.08; N, 15.56.

3-((Furan-3-yl)methyl)-2,3-dihydro-2-thioxoquinazolin-4(1H)-one, (4g)

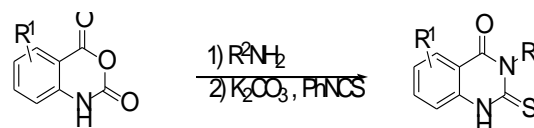
White powder, m.p. 278-280 °C; IR: ($\nu_{\max/\text{cm}^{-1}}$): 3246 (N-H), 3044 (C-H), 1658 (C=O), 1162 (C=S); ¹H NMR (500 MHz, DMSO): δ = 5.65 (s, 2H), 7.35-7.98 (m, 8H, Ar), 13.03 (s, 1H, NH); ¹³C NMR (125 MHz, DMSO): 42.2, 108.3, 110.5, 115.3, 115.7, 124.6, 127.3, 135.7, 139.0, 142.0, 149.6, 159.0, 175.0 ppm. MS (m/z, %): 258 (M⁺). Anal. Calcd. For C₁₃H₁₀N₂O₂S: C, 60.45; H, 3.90; N, 10.85. Found: C, 60.39; H, 3.81; N, 10.93.

3-Benzyl-2,3-dihydro-2-thioxoquinazolin-4(1H)-one, (4h)

White powder, m.p. 253-256 °C; IR: ($\nu_{\max/\text{cm}^{-1}}$): 3200 (N-H), 3073(C-H), 1688 (C=O), 1177 (C=S); ¹H NMR (500 MHz, DMSO): δ = 5.67 (s, 2H), 7.23-7.96 (m, 8H, CH), 13.06 (s, 1H, NH); ¹³C NMR (125 MHz, DMSO): 48.7, 115.4, 115.7, 124.6, 126.9, 127.1, 127.3, 128.2, 135.6, 136.5, 139.1, 159.3, 175.5 ppm. MS (m/z, %): 268 (M⁺). Anal. Calcd. For C₁₅H₁₂N₂O₃S: C, 67.14; H, 4.51; N, 10.44. Found: C, 67.23; H, 4.47; N, 10.38.

RESULTS AND DISCUSSION

As mentioned above, synthesis of quinazolines have long been the subject of numerous studies and over the years of study several methods have been proposed for their synthesis. However, despite of this vast investigation there is scarce methods on synthesis of quinazolines in water using environmental friendly reagents. Organic reactions in watery solutions or without the use of harmful organic solvents have long been attracting much attention, because water is a very cheap, safe, and environmentally benign solvent. We describe here our findings regarding the synthesis of 2-thioxoquinazolin-4(1H)-one derivatives via condensation of isatoic anhydride, primary amines and phenylisothiocyanate in water by using potassium carbonate as catalyst at room temperature (Scheme 1).



Scheme 1. Synthesis of 2-thioxoquinazolin-4(1H)-ones via reaction of isatoic anhydride, primary amine and phenylisothiocyanate

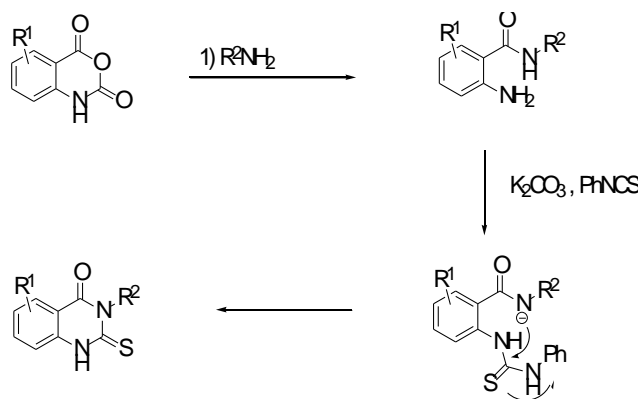
The synthesis was simply commenced by the reaction of isatoic anhydride and a primary amine in water to give the intermediate 2-aminobenzanilide, which subsequently subjected to reaction with phenylisothiocyanate to yield the

Table 1. Synthesis of various 2-thioxoquinazolin-4(1H)-ones from reaction of isatoic anhydride with different primary amines and isothiocyanates at room temperature in water.

Entry	R ¹	R ²	MP (°C)	Yields (%)	Reaction Time (h)
4a	H	phenyl	307-309	75	3
4b	H	4-chlorobenzyl	317-319	71	3
4c	meta-Cl	phenyl	324-325	70	3.5
4d	H	C ₆ H ₅ CH(CH ₃)	264-266	68	4
4e	H	3,4-(MeO) ₂ C ₆ H ₃ CH ₂	302-305	72	5
4f	H	2-pyridylmethyl	294-297	69	4.5
4g	H	3-furylmethyl	278-280	66	4
4h	H	benzyl	253-256	74	4

expected intermediate 2-[(anilinothioyl)amino]-N-phenylbenzamide (Scheme 2). Removal of a proton from the later intermediate by K₂CO₃ promotes the intramolecular transimidation in this compound and accompanies with liberation of aniline to afford the 2-thioxoquinazolin-4(1H)-one products. All these processes were completed within nearly 3 hours under nitrogen at room temperature in water.

The IR spectrum of **4a**, for example, shows the characteristic vibration of N-H bond at 3247 cm⁻¹, the absorption band corresponding to vibration of aromatic C-H bonds at around 3067 cm⁻¹, and an strong band originating from C=O bond at 1664 cm⁻¹. The vibration of C=S bond appeared at 1197 cm⁻¹, which is relatively at higher wave number compared to the parent thiourea. ¹H NMR spectrum of this product shows a characteristic broad singlet for N-H at δ 13.03 in addition to the signals due to aromatic protons at δ 7.27–7.96 ppm. In ¹³C NMR spectrum of compound **4a** the characteristic peak for C=S carbon appears downfield compared to that of C=O, in contrast to the trend in thioureas and ureas where the C=O carbon resonates at relatively lower field respect to the C=S carbon, hence for this product the resonance of C=S appeared at δ 176.0 and that of C=O appeared at δ 159.7 ppm.

**Scheme 2.** The reaction of isatoic anhydride, primary amine and phenyl isothiocyanate

Application of other ordinary bases such as NaOH and KOH to this reaction instead of K₂CO₃ in water led to lower yields, perhaps due to their advanced side reaction with phenylisothiocyanate. Various substituted isothiocyanates were condensed with isatoic anhydride, a primary amine and phenylisothiocyanate in water by using potassium carbonate to give the desired 2-thioxoquinazolin-4(1H)-one derivatives in 66-75% yields completing within 3-5 hours (Table 1).

CONCLUSION

In summary, we have developed a facile and efficient method for synthesis of 2-thioxoquinazolin-4(1H)-one derivatives through reaction of isatoic anhydride, a primary amine and an isothiocyanate in water with the aid of K₂CO₃ as an available and cheap catalyst to afford excellent yields of the products.

This method also has the advantage to employ a homogeneous and environment friendly catalyst and therefore is ideal for industrial applications.

ACKNOWLEDGEMENTS

We gratefully acknowledge the financial support from the Research Council of Tonekabon Branch of Islamic Azad University.

REFERENCES

- (a) Armarego, W. L. F., Brown, D. J., *Quinazolines*, John Wiley., Sons, Ltd, London, **1967**. (b) Ellis, G. P., *Synthesis of Fused Heterocycles*, John Wiley., Sons, Ltd, Chichester, **1987**.
- Gueyrard, D., Gurnel, V., Leoni, O., Palmieri, S., Rollin, P., *Heterocycles*, **2000**, 52, 827-843.
- Liverton, N. J., Armstrong, D. J., Claremon, D. A., Remy, D. C., Baldwin, J. J., Lynch, R. J., Zhang, G., Gould, R., *Bioorg. Med. Chem. Lett.*, **1998**, 39, 483-486.
- Kurogi, Y., Inoue, Y., Tsutsumi, K., Nakamura, S., Nagao, K., Yohsitsug, H., Tsuda, Y., *J. Med. Chem.*, **1996**, 39, 1443-1448.
- Pandeya, S. N., Sriram, D., Nath, G., Declercq, E., *Pharmaceutica Acta Helvetica*, **1999**, 74(1), 11-17.
- Wolfe, J. F., Rathman, T. L., Sleevi, M. C., Campbell, J. S. A., Greenwood, T. D., *J. Med. Chem.*, **1990**, 33, 161-166.
- Jiarong, L., Xian, C., Daxin, S., Shuling, M., Qing, L., Qi, Z., Jianhong, T., *Org. Lett.*, **2009**, 11, 1193-1196.
- Li, Z., Huang, H., Sun, H., Jiang, H., Liu, H., *J. Comb. Chem.*, **2008**, 10(3), 484-486.
- Barker, A. J., *Eur. Pat.*, **1995**, 635498.
- Bekhit, A. A., Khalil, M. A., *Pharmazie*, **1998**, 53, 539-543.
- Gursoy, A., Karali, N., *Farmaco*, **1995**, 50, 857.
- Nawrocka W., Zimecki M., *Arch. Pharm.*, **1997**, 330, 399-405.
- Shiba, S. A., El-Khamry, A. A., Shaban, M. E., Atia, K. S., *Pharmazie*, **1997**, 52, 189-194.

- ¹⁴Abdel-Hamid, S. G., *J. Ind. Chem. Soc.*, **1997**, 74, 613-618.
- ¹⁵Raffa, D., Dailone, G., Maggio, B., Sehillaci, D., Plescia F., *Arch. Pharm.*, **1999**, 332, 317-320.
- ¹⁶Baek, D. J., Park, Y. K., Heo, H. I., Lee, M. H., Yang, Z. Y., Chio, M. H., *Bioorg. Med. Chem. Lett.*, **1998**, 8, 3287-3290.
- ¹⁷Hamel, E., Lin, C. M., Plowman, J., Wang, H. K., Lee, K. H., Paull, K. D., *Bioorg. Pharm.*, **1996**, 51, 53-59.
- ¹⁸Patil, Y. P., Tambade, P. J., Parghi, K. D., Jayaram, R. V., Bhanage, B. M., *Catal. Lett.*, **2009**, 133, 201-208.
- ¹⁹Couture, A., Cornet, H., Grandclaoudon, P., *Synthesis*, **1991**, 1009-1010.
- ²⁰Kotsuki, H., Sakai, H., Morimoto, H., Suenaga, H., *Synlett.*, **1999**, 1993-1995.
- ²¹Abdel-Jalil, R. L., Voelter, W., Saeed, M., *Tetrahedron Lett.*, **2004**, 45, 3475-3476.
- ²²Feldman, J. R., Wagner, E. C., *J. Org. Chem.*, **1942**, 7, 31-47.
- ²³Yale, H. L., *J. Heterocycl. Chem.*, **1977**, 14, 1357-1359.
- ²⁴Mhaske, S. B., Argade, N. P., *J. Org. Chem.*, **2004**, 69, 4563-4566.
- ²⁵Nimalini, D. M., Warjeet, S. L., *Beilstein J. Org. Chem.*, **2010**, 6, 1056-1060.
- ²⁶Saeed, A., Flörke, U., *Crystals*, **2011**, 1, 254-259.
- ²⁷Saeed, A., Shaheen, U., Bolte, M., *J. Chin. Chem. Soc.*, **2010**, 57, 82-88.
- ²⁸Makino, S., Suzuki, N., Nakanishi, E., Tsuji, T., *Tetrahedron Lett.*, **2000**, 41, 8333-8337.
- ²⁹Makino, S., Nakanishi, E., Tsuji, T., *Tetrahedron Lett.*, **2001**, 42, 1749-1752.
- ³⁰Makino, S., Nakanishi, E., Tsuji, T., *Bull. Korean Chem. Soc.*, **2003**, 24, 389-392.

Received: 04. 05. 2014.

Accepted: 07. 06. 2014.



NOVEL FUSED AND SPIRO HETEROCYCLIC COMPOUNDS DERIVED FROM 4-(4-AMINO-5-MERCAPTO-4H-1,2,4- TRIAZOL-3-YL)PHTHALAZIN-1(2H)-ONE

M. R. Mahmoud,^[a] W. S. I. Abou-Elmagd,^[a] M. M. El-Shahawi^[a] and M. H. Hekal^{[a]*}

Keywords: triazolothiadiazole; triazolothiadiazine; spiro thiadiazole derivatives; phthalazin-1(2H)-ones; 4-amino-5-mercapto-1,2,4-triazoles.

Some new fused heterocyclic systems such as 1,2,4-triazolo[3,4-b]1,3,4-thiadiazoles and 1,3,4-thiadiazines were synthesized through the reaction of the starting material 4-(4-amino-5-mercapto-4H-1,2,4-triazol-3-yl)phthalazin-1(2H)-one with triethyl orthoformate, furyl chloride, thiophene-2-aldehyde, phenylisothiocyanate, chloroacetonitrile, and p-nitro-2-bromoacetophenone. Also spiro systems were achieved from reaction of the starting compound with isatine, and fluorenone. The newly synthesized 1,3,4-thiadiazoles and 1,3,4-thiadiazines were obtained in good yields and their structures were elucidated by spectral data and elemental analysis.

* Corresponding Authors

E-Mail: mohahekal2007@yahoo.com

[a] Chemistry Department, Faculty of Science, Ain Shams University, Abbassia, Cairo, Egypt, post code 11566

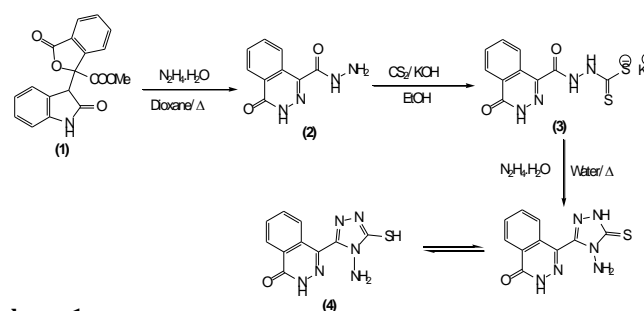
Introduction

A survey of the literature revealed that compounds bearing 1,2,4-triazole ring are well known as antimicrobial, anticonvulsant, antidepressant, antihypertensive, antitumoral and analgesic agents.¹⁻³ Moreover, some 1,2,4-triazolo[3,4-b]1,3,4-thiadiazoles and triazolo-1,3,4-thiadiazines derived from 4-amino-3-mercapto-1,2,4-triazoles are associated with diverse pharmacological activities.⁴⁻⁶ On the other hand, phthalazines and phthalazinones are *N*-heterocycles with a wide range of biological activities.⁷⁻¹³

Continuing our efforts directed toward the synthesis of new heterocyclic compounds with anticipated biological activities.¹⁴⁻²⁰ Much attention has been directed in our laboratory for synthesis of heterocycles containing the phthalazine and triazolothiadiazole or triazolothiadiazine rings.

Results and discussions

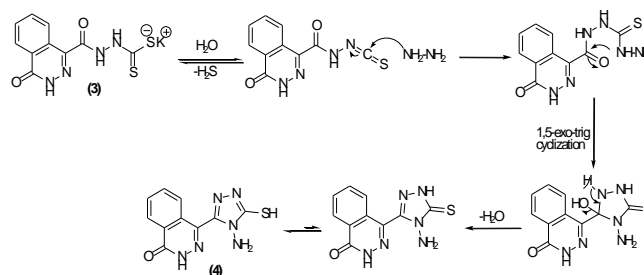
We previously reported¹⁹ that hydrazinolysis of the lactone **1** with hydrazine hydrate afforded the hydrazide **2** (unexpected product) which when treated with carbon disulphide in ethanol containing potassium hydroxide gave the corresponding potassium dithiocarbazate **3**, finally treatment of compound **3** with hydrazine hydrate in refluxing water afforded 4-(4-amino-5-mercapto-4H-1,2,4-triazol-3-yl)phthalazin-1(2H)-one **4**. (Scheme 1)



Scheme 1

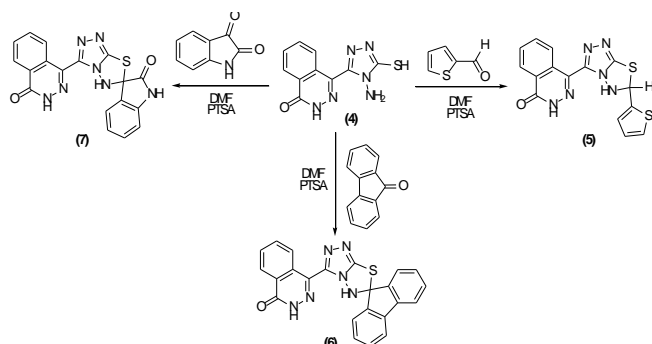
The structure of **4** was deduced from the spectroscopic and analytical data. Thus, IR spectrum of compound **4** displayed $\nu_{\text{NH}_2, \text{NH}}$ at 3245, 3162, 3108 cm^{-1} , $\nu_{\text{C=O}}$ at 1665 cm^{-1} . Moreover $^1\text{H-NMR}$ spectrum of compound **4** exhibited signals at δ (ppm) 14.2 (s, 1H, SH, exchangeable with D_2O), 13.27 (s, 1H, NH, exchangeable with D_2O), 8.33 (d, 1H_{arom.}, $J = 1.5$ Hz), 7.95 (dd, 2H_{arom.}, $J = 10.8$ Hz), 7.82 (d, 1H_{arom.}, $J = 3.6$ Hz) and 5.74 (brs, 2H, NH_2 , exchangeable with D_2O). Furthermore, the mass spectrum show the correct molecular ion peak at $m/z = 260$ (100 %) which represent the base peak.

A plausible mechanism for the formation of compound **4** is shown in Scheme 2.



Scheme 2

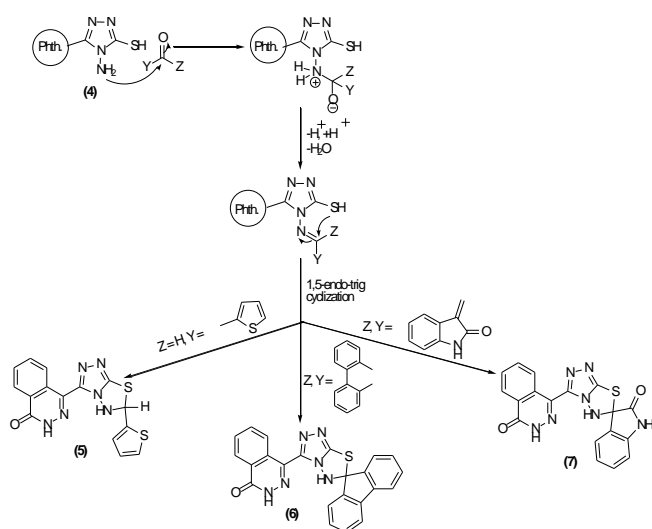
The functionalities in 4-amino-5-mercapto-3-substituted-1,2,4-triazoles made them valuable key precursors for the formation of fused heterocyclic compounds containing 1,2,4-triazolo[3,4-b], 1,3,4-thiadiazoles and 1,3,4-thiadiazines.^{20, 21} Treatment of **4** with thiophene-2-aldehyde in refluxing DMF yielded 4-[6-(thiophen-2-yl)-5,6-dihydro[1,2,4]triazolo[3,4-b][1,3,4-thiadiazol-3-yl] phthalazin-1(2*H*)-one **5**. (Scheme 3)



Scheme 3

Treatment of compound **4** with cyclic ketone and isatin was found to give spiro thiadiazole derivatives. Thus, the reaction of 4-amino-5-mercapto-3-substituted-1,2,4-triazole **4** with fluorenone and/or isatin in refluxing DMF in the presence of the catalytic amount of *p*-toluene sulphonic acid [PTSA] resulted in the formation of 4-(5*H*-spiro-1,2,4-triazolo[3,4-b][1,3,4-thiadiazole-6,9'-fluorene-3-yl] phthalazin-1(2*H*)-one **6** and 3-(4-oxo-3,4-dihydro-phthalazin-1-yl)-5*H*-spiro-1,2,4-triazolo[3,4-b][1,3,4-thiadiazole-6,3'-indolin-2'-one **7**, respectively. (Scheme 3)

The conversion of **4** to compounds **5**, **6** and **7** could be explained on the basis of nucleophilic addition by the nitrogen nucleophile of the amino group on the carbonyl group to give the corresponding Schiff's bases followed by cyclization process via the nucleophilic addition for the thiol group on the azomethine to give **5** and spiro compounds **6** and **7**. (Scheme 4)

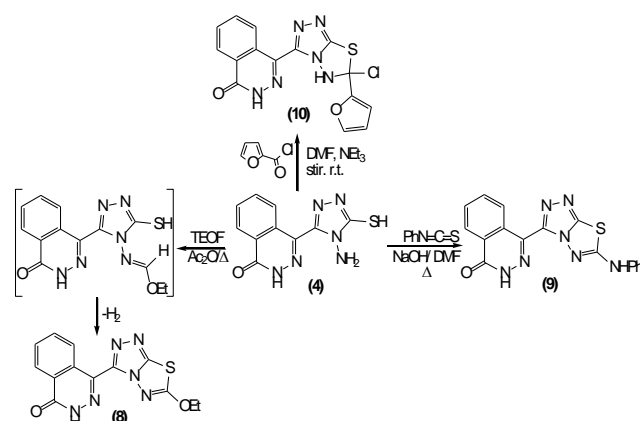


Scheme 4

The reaction of compound **4** with one carbon donors such as TEOF (triethyl orthoformate) and phenylisothiocyanate has been investigated. Thus, treatment of compound **4** with TEOF in freshly distilled acetic anhydride yielded the unexpected product which identified as 4-(6-ethoxy-[1,2,4]triazolo[3,4-b][1,3,4]thiadiazol-3-yl)phthalazin-1(2*H*)-one **8**.²² (Scheme 5)

The structure **8** was confirmed using the analytical and spectroscopic data (IR and ¹H-NMR). The IR spectrum of **8** displayed ν_{NH} at 3214, 3159 cm^{-1} and $\nu_{\text{C=O}}$ at 1667 cm^{-1} . The ¹H-NMR of this unexpected product confirmed the structure **8**, a result of possible formation of **8** indicated the presence of quartet and triplet of ethoxy protons and the absence of a signal corresponding to the thiol and formyl protons. The ¹H-NMR exhibited signals at δ (ppm) 13.3 (s, 1H, NH, exchangeable with D₂O), 8.96 (d, 1H_{arom.}, J = 7.8 Hz), 8.35 (d, 1H_{arom.}, J = 6.9 Hz), 8.06 (dd, 1H_{arom.}), 7.9 (dd, 1H_{arom.}), 3.38 (q, 2H, CH₂, J = 7.5 Hz) and 1.4 (t, 3H, CH₃, J = 7.5 Hz).

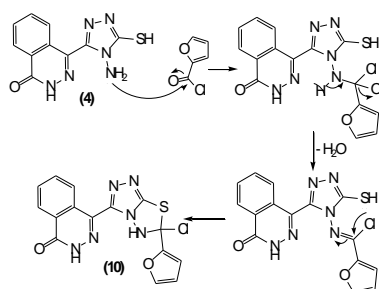
Refluxing compound **4** with phenylisothiocyanate in the presence of sodium hydroxide in DMF afforded 4-(6-(phenylamino)-[1,2,4]triazolo[3,4-b][1,3,4]thiadiazol-3-yl)phthalazin-1(2*H*)-one **9**. (Scheme 5)



Scheme 5

Stirring compound **4** with furoyl chloride in dry dimethylformamide in the presence of triethyl amine at room temperature followed by acidification yielded the triazolothiadiazole derivative **10**. (Scheme 5).

The formation of compound **10** could be formulated as shown in Scheme 6.



Scheme 6

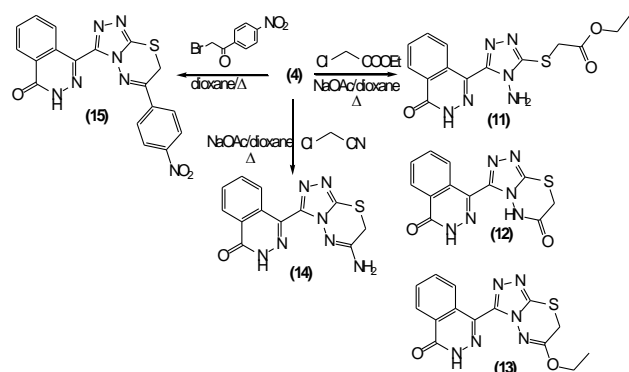
Carboethoxymethylation of **4** with ethyl chloroacetate in boiling dioxane in the presence of fused sodium acetate for 2 hrs resulted in the *S*-alkylation and afforded the uncyclized product **11** rather than the cyclized product **12** or **13**. (Scheme 7)

The uncyclized nature of **11** was confirmed from its elemental analysis which was consistent with the molecular formula $C_{14}H_{14}N_6O_3S$ and the existence of $\nu_{NH_2, NH}$ at 3315, 3217, 3160, 3106 cm^{-1} , $\nu_{C=O(ester)}$ at 1734 cm^{-1} in the IR spectrum. Moreover, the presence of one singlet in 1H -NMR spectrum at δ 6.108 ppm integrated for two protons disappeared in D_2O corresponding to the NH_2 protons which ruled out the existence of the cyclized compound **12** and **13**.

Furthermore, the recorded peaks in the mass spectrum at $m/z = 346$ (20.4 %) and $m/z = 273$ (100%) represent the molecular ion peak and the base peak $[M-C_2H_4, -CO_2]$ which completely in accord with the assigned structure.

Cyanomethylation of **4** with chloroacetonitrile in boiling dioxane in the presence of fused sodium acetate for 10 hrs yielded the cyclized product 4-[6-amino-6,7-dihydro-5*H*-1,2,4-triazolo[3,4-*b*]1,3,4-thiadiazin-3-yl]phthalazin-1(2*H*)-one **14**. (Scheme 7)

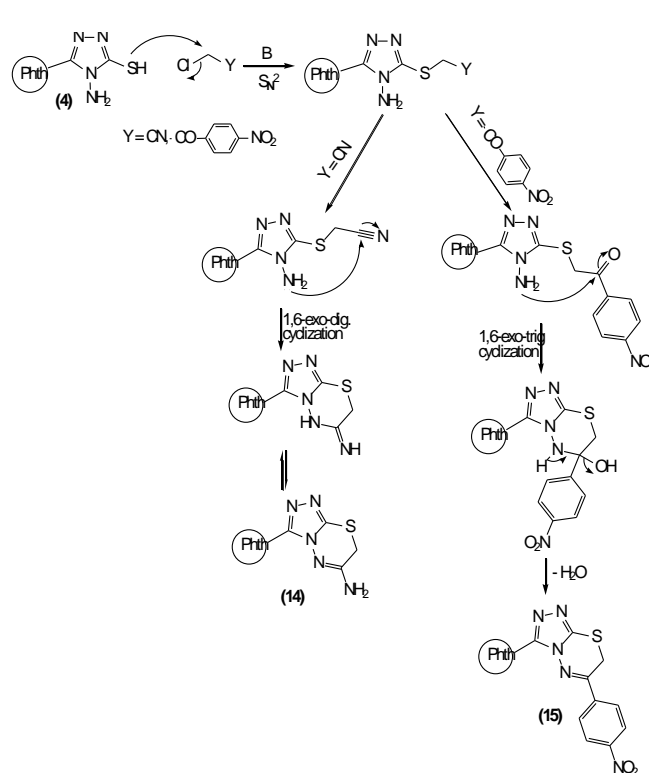
The absence of the stretching absorption band for the nitrile group in the IR spectrum ruled out the uncyclized product.



Scheme 7

4-[6-(4-Nitrophenyl)-7*H*-1,2,4-triazolo[3,4-*b*]1,3,4-thiadiazin-3-yl]phthalazin-1(2*H*)-one **15** was prepared in quantitative yield upon treatment of compound **4** with *p*-nitro-2-bromoacetophenone in refluxing dioxane. (Scheme 7)

The absence of the stretching absorption bands for NH_2 in the IR and 1H -NMR confirm the cyclized structure **15**. The IR spectrum of **15** displayed one absorption band for NH group at 3301 cm^{-1} and one absorption band for carbonyl group (phthalazinone) at 1674 cm^{-1} . The formation of compound **14** and **15** may proceed via nucleophilic substitution reaction (S_N2) followed by 1,6-*exo*-dig and *exo*-trig cyclization, respectively. (Scheme 8)



Scheme 8

Antimicrobial evaluation

The antibiotic resistance is a growing problem; this is due to the overuse of antibiotics in human, and the use of antibiotics as growth promoters in food of animals, so there is a growing demand for new antibiotics. Some selected examples were evaluated for their *in vitro* antimicrobial activity against two strains of bacteria and two fungus strains; tetracycline was used as standard drug for bacteria and amphotericin was used as standard drug for fungi. Preliminary screening of the synthetic derivatives and standard drugs were performed at fixed concentration 20 mg/ml, inhibition was recorded by measuring the diameter of the inhibition zone at the end of 18hrs for bacteria.

Based on the results of the inhibition zone, data in table 1 revealed that compounds **4**, **5**, **9**, **10** and **11** exhibited moderate antibacterial and antifungal activities compared with the standard drugs. Compounds **6**, **7**, **8** and **14** exhibited no antimicrobial activity.

Experimental

All melting points were taken on Griffin and Geory melting point apparatus and are uncorrected. IR spectra were recorded on Pye Unicam SP1200 spectrophotometer using KBr Wafer technique. 1H -NMR spectra were determined on a Varian Gemini 300 MHz using TMS as internal standard (chemical shifts in δ -scale). EI-MS were measured on a Shimadzu-GC-MS operating at 70 eV. Elemental analyses were carried out on a Perkin-Elmer 2400 CHN elemental analyzer and satisfactory analytical data (± 0.4) were obtained for all compounds.

Biological activities were carried out at microanalytical center, Faculty of Science, Cairo University. The homogeneity of the synthesized compounds was controlled by TLC [Using TLC aluminum sheets silica gel F₂₅₄ (Merck)].

Table 1. Antimicrobial screening results of the tested compounds against *Escherichia coli* (G+), *Staphylococcus aureus* (G-), *Aspergillus flavus* and *Candida albicans*

Sample	Inhibition zone diameter (mm mg ⁻¹)			
	<i>E. coli</i>	<i>S. aureus</i>	<i>A. flavus</i>	<i>C. albicans</i>
Control(DMSO)	0.0	0.0	0.0	0.0
4	9	9	0.0	9
5	10	0.0	0.0	0.0
6	0.0	0.0	0.0	0.0
7	0.0	0.0	0.0	0.0
8	0.0	0.0	0.0	0.0
9	10	12	0.0	9
10	12	0.0	0.0	0.0
11	11	12	33	12
14	0.0	0.0	0.0	0.0
Tetracycline	32	30	0.0	0.0
Amphotericin B	0.0	0.0	18	20

G: Gram reaction; Solvent: DMSO; 0.0: no activity (inhibition zone less than 7 mm); 7-10 mm - weak activity; 11-15 mm - moderate activity; more than 15 mm - strong activity

Synthesis of 4-(4-amino-5-mercapto-4H-1,2,4-triazol-3-yl)-phthalazin-1(2H)-one, 4

To a stirred solution of 4-oxo-3,4-dihydrophthalazine-1-carbohydrazide **2** (2 g, 10 mmol) and potassium hydroxide (0.84 g, 15 mmol) in absolute ethanol (30 mL), carbon disulfide (0.88 mL, 15 mmol) was added dropwise and the mixture was stirred at room temperature for 6 h. The precipitated potassium dithiocarbamate salt **3** was collected by filtration, washed with dry ether, and dried under vacuum.

This salt was obtained in quantitative yield and was used in the next step without further purification. To a suspension of the potassium salt **3** (1 g, 2.8 mmol) in water (10 mL), hydrazine hydrate (0.28 mL, 5.7 mmol) was added and the whole mixture then heated under reflux until all hydrogen sulfide evolved. The reaction mixture was cooled then acidified with cold dilute hydrochloric acid and the precipitated product was filtered off, dried, and then recrystallized from EtOH/dioxane to give **4** as beige crystals; mp: 240-2 °C, yield: 65 %. IR (ν/cm⁻¹): 3245, 3162, 3108 (NH₂, NH), 1665 (C=O). MS m/z (%): 260 (M⁺; 100), 172 (38.7), 145 (4.5), 115 (18), 102 (15.2), 89 (11.4). ¹H-NMR (DMSO-d₆) δ (ppm): 14.2 (s, 1H, SH, exchangeable with D₂O), 13.27 (s, 1H, NH, exchangeable with D₂O), 8.33 (d, 1H_{arom.}, J = 1.5 Hz), 7.95 (dd, 2H_{arom.}, J = 10.8 Hz), 7.82 (d, 1H_{arom.}, J = 3.6 Hz), 5.74 (brs, 2H, NH₂, exchangeable with D₂O). Anal. Calcd. for C₁₀H₈N₆OS (260.28): C, 46.15; H, 3.10; N, 32.29; S, 12.32. Found: C, 46.03; H, 2.98; N, 32.11; S, 12.21.

Synthesis of 4-[6-(thiophen-2-yl)-5,6-dihydro[1,2,4]triazolo[3,4-b][1,3,4-thiadiazol-3-yl] phthalazin-1(2H)-one, 5

A mixture of **4** (1 g, 3 mmol), thiophene-2-aldehyde (0.4 mL, 3 mmol) and catalytic amount of *p*-toluene sulphonic acid (0.3 g) in DMF (20 mL) was heated under reflux for 16 hrs. The reaction mixture was concentrated and then poured onto cold water and the deposited solid was collected by filtration and recrystallized from EtOH/dioxane to give **5** as pale yellow crystals; mp: 334-336 °C, yield: 72 %. IR (ν/cm⁻¹): 3142, 3101 (NH), 1649 (C=O). MS m/z (%): 354 (M⁺; 7.3), 245 (100), 109 (93.1), 101 (16.3). ¹H-NMR (DMSO-d₆) δ (ppm): 14.2 (s, 1H, NH, exchangeable with D₂O), 13.2 (s, 1H, NH, exchangeable with D₂O), 9.9 (brs, 1H), 8.3 (d, 1H, C₄-H_{thiophene ring}, J = 1.2 Hz), 8.0-7.75 (m, 4H_{arom.}), 7.7 (d, 1H, C₂-H_{thiophene ring}, J = 1.2 Hz), 7.2 (dd, 1H, C₃-H_{thiophene ring}, J = 3.6 Hz). Anal. Calcd. for C₁₅H₁₀N₆OS₂ (354.41): C, 50.83; H, 2.84; N, 23.71; S, 18.09. Found: C, 50.77; H, 2.63; N, 23.55; S, 18.12.

Synthesis of 4-(5H-spiro-1,2,4-triazolo[3,4-b][1,3,4-thiadiazole-6,9'-fluorene-3-yl]phthalazin-1(2H)-one, 6

A mixture of **4** (1 g, 3 mmol), fluorenone (0.69 g, 3 mmol) and catalytic amount of *p*-toluene sulphonic acid (0.3 g) in DMF (20 mL) was heated under reflux for 18 hrs. The reaction mixture was concentrated and then poured onto cold water and the precipitated product was filtered off, dried and recrystallized from dioxane/DMF to give **6** as yellow crystals; mp: >300 °C, yield: 78 %. IR (ν/cm⁻¹): 3372 (NH), 1700 (C=O), 1666 (C=N). MS m/z (%): 422 (M⁺; 0.8), 421 (72.9), 366 (67), 173 (100), 145 (58.7). ¹H-NMR (DMSO-d₆) δ (ppm): 12.9 (s, 1H, NH, exchangeable with D₂O), 11.3 (s, 1H, NH, exchangeable with D₂O), 8.8-7.6 (m, 12H_{arom.}). Anal. Calcd. for C₂₃H₁₄N₆OS (422.46): C, 65.39; H, 3.34; N, 19.89; S, 7.59. Found: C, 65.45; H, 3.23; N, 19.76; S, 7.49.

Synthesis of 3-(4-oxo-3,4-dihydrophthalazin-1-yl)-5H-spiro-1,2,4-triazolo[3,4-b][1,3,4-thiadiazole-6,3'-indolin-2'-one, 7

A mixture of **4** (1 g, 3 mmol), isatin (0.56 g, 3 mmol) and catalytic amount of *p*-toluene sulphonic acid (0.3 g) in DMF (20 mL) was heated under reflux for 3 hrs. The deposited solid on hot was filtered off, dried and recrystallized from DMF to give **7** as white crystals; mp: >300 °C, yield: 55 %. IR (ν/cm⁻¹): 3157, 3113 (NH), 1671 (C=O). MS m/z (%): 387 (M-2; 75), 245 (50), 172 (87.5), 129 (87.5), 102 (75), 57 (100). ¹H-NMR (DMSO-d₆) δ (ppm): 13.2 (s, 1H, NH, exchangeable with D₂O), 11.0 (s, 1H, NH, exchangeable with D₂O), 9.1 (s, 1H, NH, exchangeable with D₂O), 8.8-7.4 (m, 8H_{arom.}). Anal. Calcd. for C₁₈H₁₁N₇O₂S (389.39): C, 55.52; H, 2.85; N, 25.18; S, 8.23. Found: C, 55.46; H, 2.72; N, 25.03; S, 8.15.

Synthesis of 4-(6-ethoxy-[1,2,4]triazolo[3,4-b][1,3,4]thiadiazol-3-yl)phthalazin-1(2H)-one, 8

A mixture of **4** (1 g, 3 mmol), triethyl orthoformate (10 mL) and freshly distilled acetic anhydride (10 mL) was heated under reflux for 10 hrs.

The reaction mixture was concentrated and the deposited product was filtered off, washed with petroleum ether (b.p. 60-80°C), dried and recrystallized from dioxane to give **8** as beige crystals; mp: > 300 °C, yield: 48 %. IR (ν/cm^{-1}): 3214, 3159 (NH), 1667 (C=O). MS m/z (%): 314 (M^+ ; 23.6), 286 (17.7), 270 (38.8), 171 (91.3), 145 (100), 119 (12.6). $^1\text{H-NMR}$ (DMSO- d_6) δ (ppm): 13.3 (s, 1H, NH, exchangeable with D_2O), 8.96 (d, 1 H_{arom} , $J = 7.8$ Hz), 8.35 (d, 1 H_{arom} , $J = 6.9$ Hz), 8.06 (d, 1 H_{arom} , $J = 3.7$ Hz), 7.9 (d, 1 H_{arom} , $J = 2.9$ Hz), 3.38 (q, 2H, CH_2 , $J = 7.5$ Hz), 1.4 (t, 3H, CH_3 , $J = 7.5$ Hz). Anal. Calcd. for $\text{C}_{13}\text{H}_{10}\text{N}_6\text{O}_2\text{S}$ (314.32): C, 49.67; H, 3.21; N, 26.74; S, 10.20. Found: C, 49.55; H, 3.11; N, 26.60; S, 10.03.

Synthesis of 4-(6-(phenylamino)-[1,2,4] triazol[3,4-b][1,3,4]-thiadiazol-3-yl)phthalazin-1(2H)-one, **9**

A mixture of **4** (1 g, 3 mmol), phenylisothiocyanate (0.4 mL, 3 mmol) and sodium hydroxide (0.8 g) in DMF (25 mL) was heated under reflux for 4 hrs. The reaction mixture was acidified with cold dilute hydrochloric acid and the precipitated solid was filtered off, dried, and recrystallized from dioxane to give **9** as beige crystals; mp: >300 °C, yield: 51 %. IR (ν/cm^{-1}): 3160 (NH), 1687 (C=O). MS m/z (%): 361 (M^+ ; 13.5), 171 (35.1), 128 (70.3), 102 (37.8), 92 (21.6), 91 (45.9), 64 (100). $^1\text{H-NMR}$ (DMSO- d_6) δ (ppm): 13.1 (s, 1H, NH, exchangeable with D_2O), 9.8 (s, 1H, NH, exchangeable with D_2O), 8.9-7.6 (m, 9 H_{arom}). Anal. Calcd. for $\text{C}_{17}\text{H}_{11}\text{N}_7\text{OS}$ (361.83): C, 56.50; H, 3.07; N, 27.13; S, 8.87. Found: C, 56.39; H, 2.97; N, 27.02; S, 8.72.

Synthesis of 4-(6-chloro-6-(furan-2-yl)-5,6-dihydro-[1,2,4]triazolo[3,4-b][1,3,4] thiadiazol-3-yl)phthalazin-1(2H)-one, **10**

To a solution of **4** (1 g, 3 mmol) and triethyl amine (0.5 mL) in DMF (10 mL), furoyl chloride (0.3 mL, 3 mmol) was added dropwise in ice bath and the mixture was stirred at room temperature for 2 hrs. The reaction mixture was acidified with cold dilute hydrochloric acid and the precipitated product was filtered off, dried, and then recrystallized from EtOH/dioxane to give **10** as beige crystals; mp: 290-292 °C, yield: 43 %. IR (ν/cm^{-1}): 3160, 3108 (NH), 1688 (C=O). MS m/z (%): 370 ($M-2$; 2), 246 (100), 186 (58.2), 145 (15.2), 102 (52.0). Anal. Calcd. for $\text{C}_{15}\text{H}_9\text{N}_6\text{O}_2\text{SCl}$ (372.79): C, 48.33; H, 2.43; N, 22.54; S, 8.60; Cl, 9.51. Found: C, 48.23; H, 2.29; N, 22.48; S, 8.50; Cl, 9.44.

Synthesis of ethyl 2-(4-amino-5-(4-oxo-3,4-dihydrophthalazin-1-yl)-4H-1,2,4-triazol-3-ylthio) acetate, **11**

A mixture of **4** (1 g, 3 mmol), ethyl chloroacetate (0.37 mL, 3 mmol) in dioxane (20 mL) in the presence of fused sodium acetate (0.5 g) was heated under reflux for 2 hrs. The reaction mixture was concentrated and then poured onto cold water and the precipitated product was filtered off, dried and recrystallized from EtOH/dioxane to give **11** as beige crystals; mp: 194-196 °C, yield: 80 %. IR (ν/cm^{-1}): 3315, 3217, 3160, 3106 (NH₂, NH), 1734 (C=O_{ester}). MS m/z (%): 346 (M^+ ; 20.4), 300 (21.7), 273 (100), 172 (55.4), 145 (16.5), 130 (21.8), 115 (31.1). $^1\text{H-NMR}$ (DMSO- d_6) δ (ppm): 13.38 (s, 1H, NH, exchangeable with D_2O), 8.93 (d, 1 H_{arom} , $J = 7.8$ Hz), 8.3 (d, 1 H_{arom} , $J = 7.8$ Hz), 8.07-7.9 (dd,

2 H_{arom}), 6.1 (s, 2H, NH₂, exchangeable with D_2O), 4.3 (s, 2H, SCH₂), 4.21-4.14 (q, 2H, CH₂, $J = 7.2$ Hz, $J = 3.6$ Hz), 1.23 (t, 3H, CH₃, $J = 7.2$ Hz). Anal. Calcd. for $\text{C}_{14}\text{H}_{14}\text{N}_6\text{O}_3\text{S}$ (346.36): C, 48.55; H, 4.07; N, 24.26; S, 9.26. Found: C, 48.31; H, 3.97; N, 24.13; S, 9.11.

Synthesis of 4-[6-amino-6,7-dihydro-5H-1,2,4-triazolo[3,4-b]-1,3,4-thiadiazin-3-yl]phthalazin-1(2H)-one, **14**

A mixture of **4** (1 g, 3 mmol), chloroacetonitrile (0.22 mL, 3 mmol) in dioxane (20 mL) in the presence of fused sodium acetate (0.5 g) was refluxed for 10 hrs. The reaction mixture was concentrated and then poured onto cold water and the precipitated product was filtered off, dried and recrystallized from dioxane/DMF to give **14** as white crystals; mp: 254-256 °C, yield: 59 %. IR (ν/cm^{-1}): 3347, 3287, 3161 (NH₂, NH), 1662 (C=O). MS m/z (%): 299 (M^+ ; 70.8), 283 (63.2), 258 (11), 228 (14.7), 198 (24.6), 172 (100), 130 (34.2), 114 (70), 88 (62.3), 50 (33.6). $^1\text{H-NMR}$ (DMSO- d_6) δ (ppm): 13.9 (s, 1H, NH, exchangeable with D_2O), 8.38-7.93 (m, 4 H_{arom}), 6.17 (s, 2H, NH₂, exchangeable with D_2O), 4.39 (s, 2H, CH₂). Anal. Calcd. for $\text{C}_{12}\text{H}_9\text{N}_7\text{OS}$ (299.31): C, 48.15; H, 3.03; N, 32.76; S, 10.71. Found: C, 48.03; H, 2.91; N, 32.58; S, 10.64.

Synthesis of 4-[6-(4-nitrophenyl)-7H-1,2,4-triazolo[3,4-b]1,3,4-thiadiazin-3-yl]phthalazin-1(2H)-one, **15**

A mixture of **4** (1 g, 3 mmol) and *p*-nitro-2-bromoacetophenone (0.73 g, 3 mmol) in dioxane (20 mL) was heated under reflux for 6 hrs. The reaction mixture was cooled and the deposited solid was filtered off, dried and recrystallized from dioxane/DMF to give **15** as beige crystals; mp: 246-248 °C, yield: 71 %. IR (ν/cm^{-1}): 3301 (NH), 1674 (C=O). $^1\text{H-NMR}$ (DMSO- d_6) δ (ppm): 13.36 (s, 1H, NH, exchangeable with D_2O), 8.9-8.3 (dd, 4 H_{arom}), 8.3-7.9 (m, 4 H_{arom}), 5.3 (s, 2H, CH₂). Anal. Calcd. for $\text{C}_{18}\text{H}_{11}\text{N}_7\text{O}_3\text{S}$ (405.39): C, 53.33; H, 2.73; N, 24.19; S, 7.91. Found: C, 53.24; H, 2.62; N, 24.03; S, 7.80.

Conclusion

From the foregoing survey, it seems that functionalities in 4-amino-5-mercapto-3-substituted-1,2,4-triazoles provide a useful and convenient strategy for synthesis of numerous fused heterocyclic compounds containing 1,2,4-triazolo[3,4-b]1,3,4-thiadiazole and 1,3,4-thiadiazine derivatives. The subject of such reactions is still ongoing and undoubtedly will provide new fused functionalized 1,3,4-thiadiazoles of both industrial and biological interests.

References

- Wang, J., Song, Y. H. *J. Heterocycl. Chem.* **2013**, *50*, 603.
- Zanatta, N., Amaral, S. S., Santos, J. M. D., Fernandes, L. D. S., Bonacorso, H. G., Martins, M. A. P. *J. Heterocycl. Chem.* **2011**, *48*, 1085.
- Demibas, N., Ugurluoglu, D. A. *Bioorg. Med. Chem.* **2002**, *10*, 3717.
- Mathew, V., Keshavayya, J., Vaidya, V. P., Giles, D. *Eur. J. Med. Chem.* **2007**, *42*(6), 823.

- ⁵Al-Masoudi, N. A., Al-Soud, Y. A. *Nucleos Nucleot Nucleic Acids* **2008**, 27(9), 1034.
- ⁶Arunkumar, S., Ilango, K., Ravindar, B., Ramalakshmi, N. *Der Pharma Chem.* **2009**, 1, 70.
- ⁷El-Hashash, M. A., El-Kady, A. Y., Taha, M. A., El-Shamy, I. E. *Chin. J. Chem.* **2012**, 30, 616.
- ⁸Awadallah, F. M., El-Eraky, W. E., Saleh, D. O. *Eur. J. Med. Chem.* **2012**, 52, 14.
- ⁹Sriram, D., Yogeewari, P., Senthilkumar, P., Sangaraju, D., Nelli, R., Banerjee, D., Bhat, P., and Manjashetty, T. H. *Chem. Biol. Drug. Des.* **2010**, 75, 381.
- ¹⁰Abdalla, M. S. M., Hegab, M. I., Abo Taleb, N. A., Hasabelnaby, S. M., Goudah, A. *Eur. J. Med. Chem.* **2010**, 45, 1267.
- ¹¹Zhang, L., Guan, L. P., Sun, X. Y., Wei, C. X., Chai, K. Y., Quan, Z. S. *Chem. Biol. Drug. Des.* **2009**, 73, 313.
- ¹²Ryu, C. K., Park, R. E., Ma, M. Y., Nho, J. H. *Bioorg. Med. Chem Lett.* **2007**, 17, 2577.
- ¹³Del Olmo, E., Barboza, B., Ybarra, M. I., López-Pérez, J. L., Carron, R., Sevilla, M. A., Boselli, C., Feliciano, A. S. *Bioorg. Med. Chem Lett.* **2006**, 16, 2786.
- ¹⁴Mahmoud, M. R., Abu El-Magd, W. S. I., Abd El-Wahab, S. S., Soliman, S. A. *J. Chem. Res.* **2012**, 66.
- ¹⁵Mahmoud, M. R., Abu El-Magd, W. S. I., Derbala, H. A., Hekal, M. H. *J. Chem. Res.* **2012**, 75.
- ¹⁶Mahmoud, M. R., Abu El-Magd, W. S. I., Abd El-Wahab, S. S., Soliman, S. A. *Synth. Commun.* **2013**, 43, 1484.
- ¹⁷Mahmoud, M. R., El-Ziaty, A. K., Abu El-Azm, F. S. M., Ismail, M. F., Shiba, S. A. *J. Chem. Res.* **2013**, 80.
- ¹⁸Mahmoud, M. R., Abu El-Azm, F. S. M. *J. Chem. Res.* **2013**, 535.
- ¹⁹Mahmoud, M. R., Abu El-Magd, W. S. I., Derbala, H. A., Hekal, M. H., *Chin. J. Chem.* **2011**, 29(7), 1446.
- ²⁰Ghorab, M. M., El-Sharief, A. M. S., Ammar, Y. A., Mohamed, S. I. *Il Farmaco* **2000**, 55(5), 354-361.
- ²¹Shi, H., Wang, Z., Shi, H., *J. Heterocycl. Chem.* **2001**, 38(2), 355-357.
- ²²Ghattas, A. A. G., Moustafa, H. M., Hassanein, E. A. A., Hussein, B. R. M. *Phosphorus Sulfur Silicon* **2012**, 187(12), 1469-1481.

Received: 16.05.2014.

Accepted: 11.06.2014.



KINETICS OF THE OXIDATIVE DECOLORIZATION OF AMARANTH RED BY ACIDIC BROMATE

Z. M. Abou-Gamra,^{[a]*} and H. A. A. Medien^[a]

Keywords: Amaranth Red; decolorization; kinetics; bromate.

The kinetics of the oxidative decolorization of amaranth with KBrO_3 acidified by H_2SO_4 was followed up by monitoring the decrease of the absorbance of amaranth at $\lambda_{\text{max}} = 520$ nm. The reaction was carried out under pseudo-first-order conditions. The concentration of BrO_3^- was ca 300 greater than that of amaranth. The rate of reaction increased with increasing concentration of H_2SO_4 and BrO_3^- , while amaranth had no effect on the rate of reaction. The effects of the ions, Cl^- , Br^- and SO_4^{2-} were investigated and the reaction rate increased with increasing concentrations of chloride and bromide while it decreased with increasing concentration of SO_4^{2-} . A reaction mechanism has been proposed.

* Corresponding Authors

E-Mail: zanibabougamra@yahoo.com

[a] Chemistry Department, Faculty of Science, Ain-Shams University, Abbassia, Cairo, Egypt

Introduction

Wastewater treatment is one of the major problems facing the chemical, petrochemical, pharmaceutical, and textile industries. These industries generate large quantities of organic pollutants that cause environmental and health problems. Biological (biodegradation),¹ physical² and chemical methods (chlorination, ozonation)³ are the most frequently used methods for removal of dyes from effluent water streams. But, these traditional processes for treatment of the effluents prove to be insufficient to purify waste water after the different operations of waste waters dyeing and washing.

Advanced oxidation processes (AOPs) are alternative methods for the complete degradation of dye. The usage of the advanced oxidation processes (AOPs) have improved during the last decade since they are able to eliminate the problem of dye destruction in aqueous systems. AOPs were based on the generation of very reactive species such as hydroxyl radicals ($\bullet\text{OH}$) ($E = 2.8\text{V}$ vs NHE) that oxidize a broad range of pollutants quickly and non-selectively. AOPs such as Fenton and Photo-Fenton catalytic reactions,⁴⁻⁶ $\text{H}_2\text{O}_2/\text{UV}$ processes.⁶

Potassium bromate is powerful oxidizing agent.⁷ It is used in oxidation of organic and inorganic compounds.⁸⁻⁹ Literature survey shows that bromate is used as an oxidizing agent for various dyes. The oxidation of dyes received attention for last decade.¹⁰⁻¹² Although previous studies have taken important steps forward in generating empirical rules for oxidation, further intensive study is still required to understanding the mechanism of oxidation by bromate.

Azo dyes are used extensively in textile industry. Amaranth as example for azo dyes is used as cosmetic dye and can applied for natural and synthetic fibers, leather, paper, phenol formaldehyde resins.¹³

Number of studies is published on oxidation of amaranth by various oxidizing agents.¹⁴⁻¹⁶ Quick look in literature oxidation of amaranth by bromate has not yet reported.

The aim of this study is investigation of the kinetic aspects of the oxidative decolorization of amaranth with acidic bromate solution. It also describes the effect of temperature, and foreign ions on the oxidation of amaranth by bromate.

Experimental

Materials

All chemicals were of high grade quality, they were used as received. The standard solutions and dilution were made using bidistilled water. Amaranth, trisodium(4*E*)-3-oxo-4-[(4-sulfonato-1-naphthyl)-hydrazono]-naphthalene-2,7-di-sulfonate, was obtained from Aldrich. For the daily kinetic runs a stock solution of dye (10^{-3} mol dm^{-3}) was prepared. The flask containing the dye solution was wrapped in aluminium foil and stored in the dark to minimize exposure to light. KBrO_3 was supplied from Merck and its initial concentration was standardized iodometrically using starch as an indicator.¹⁷ The desired concentration of KBrO_3 was obtained by successive dilutions from the standard stock solution.

Kinetic measurements

The kinetic measurements were carried out spectrophotometrically using 292 Cecil spectrophotometer was equipped with constant temperature cell holder attached to thermostatic controlled bath with temperature stability of $\pm 0.1^\circ\text{C}$.

The kinetics of reaction were carried out by mixing solutions of (KBrO_3 & H_2SO_4) and placed in a thermostatic bath at desirable temperature. The reaction started by adding thermostatted dye solution. The progress of the reaction was monitored at $\lambda_{\text{max}} = 520$ nm. Pseudo first-order conditions were maintained in all runs by using a large excess of bromate over amaranth.

Results and discussion

In the present study the oxidizing property of the acidified KBrO_3 (redox potential of 1.5 V at 25 °C was considered as a tool for color removal of organic dyes in the industrial wastewater stream.

When amaranth was added to the acid-free KBrO_3 solution no changes in the absorbance spectra have been observed. The reaction was initiated when the dye solution was allowed to react with the acidified KBrO_3 . The absorbance of amaranth at $\lambda_{\text{max}} = 520 \text{ nm}$ decreased with time as shown in Figure 1.

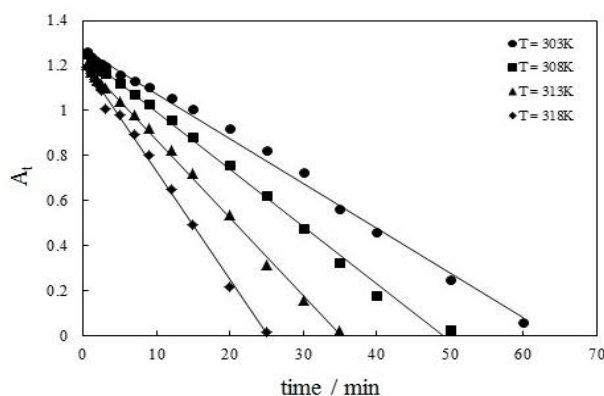


Figure 1. Zero order plots for the decolorization of amaranth by acidified KBrO_3 at different temperatures. $[\text{dye}] = 5 \times 10^{-5} \text{ mol dm}^{-3}$, $[\text{KBrO}_3] = 1.5 \times 10^{-2} \text{ mol dm}^{-3}$, $[\text{H}_2\text{SO}_4] = 8 \times 10^{-2} \text{ mol dm}^{-3}$

The plot of the absorbance vs. time was linear as shown in Figure 1. This indicates the zero-order kinetics of the reaction with respect to the amaranth concentration.

Effect of potassium bromate concentration

The effect of the initial concentration, $[\text{KBrO}_3]_0$, on the reaction rate was investigated at constant [amaranth], $5 \times 10^{-5} \text{ mol dm}^{-3}$, and in the presence of 0.08 mol dm^{-3} of H_2SO_4 . Figure 2 shows linear relation between rate constant and $[\text{BrO}_3^-]_0$, which indicates that the reaction follows first-order kinetics with respect to the $[\text{KBrO}_3]$ (plotting of $\ln k_o$ versus $\ln[\text{BrO}_3^-]$ yields straight line of slope equals the unity). This is in good agreement with earlier results¹⁸⁻¹⁹ while Nasiruddin Khana et al²⁰ reported that the reaction followed zero order kinetics with respect to the $[\text{KBrO}_3]$.

The intercept of abscissa means that no reaction takes place at $[\text{BrO}_3^-]$ below $0.015 \text{ mol dm}^{-3}$. This means that the concentration of the generated active species is very small and unable to oxidize the amaranth. It has been reported that the system involved various acidified oxybromo species such as: H_2BrO_3^+ , BrO_2^- , HOBr and BrO_2^- .²¹⁻²³ These species could be competed with bromated ion in the oxidation and decolorization of organic dyes.

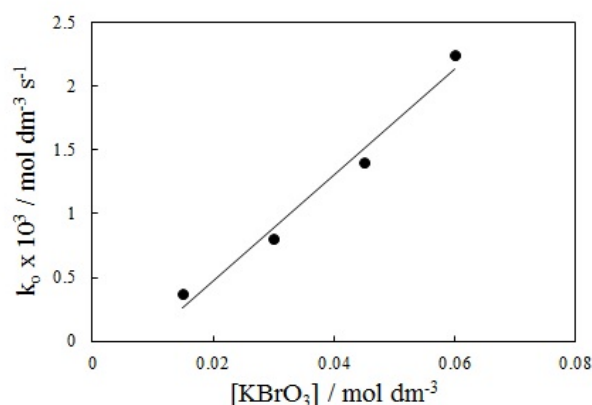


Figure 2. Variation of observed rate constant with $[\text{KBrO}_3]$. $[\text{dye}] = 5 \times 10^{-5} \text{ mol dm}^{-3}$, $[\text{H}_2\text{SO}_4] = 8 \times 10^{-2} \text{ mol dm}^{-3}$, at 35 °C

Effect of sulfuric acid concentration

The effect of $[\text{H}_2\text{SO}_4]$ on the reaction rate was investigated by keeping the [amaranth] and $[\text{KBrO}_3]$ constant while the concentration of the acid was varied in range of $0.04\text{--}0.4 \text{ mol dm}^{-3}$, Figure 3.

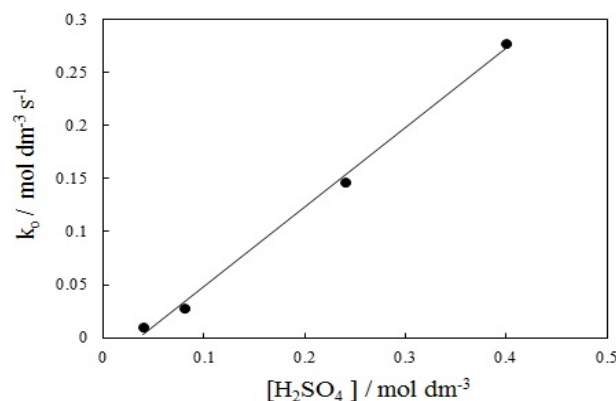


Figure 3. Variation of observed rate constant with $[\text{H}_2\text{SO}_4]$. $[\text{dye}] = 5 \times 10^{-5} \text{ mol dm}^{-3}$, $[\text{KBrO}_3] = 1.5 \times 10^{-2} \text{ mol dm}^{-3}$, at 35 °C

Figure 3 shows that the reaction rate is very slow at $[\text{H}_2\text{SO}_4]$ lower than about 0.04 mol dm^{-3} , and then it is gradually increased. Plot $\ln k_o$ versus $\ln [\text{H}_2\text{SO}_4]$ yields straight line with slope of unity indicates that the order of reaction with respect to the H_2SO_4 is first order.

Again, the slower rate obtained at lower concentrations of the acid can be attributed to the formation of the intermediates active species contributed in the oxidation reaction needed a high acid concentrations, i.e., the acid/bromate ratio should be equal to or more than 3 as can be seen from Figure 4.

Effect of amaranth concentration

The influence of the initial concentration of dye on the reaction rate was investigated, in range of $3 \times 10^{-5} - 8 \times 10^{-5} \text{ mol dm}^{-3}$. The $[\text{KBrO}_3]$ and $[\text{H}_2\text{SO}_4]$ were kept constant at 0.03 mol dm^{-3} and 0.08 mol dm^{-3} respectively.

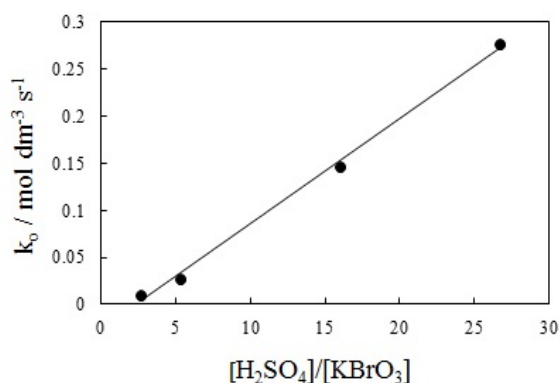


Figure 4. Variation of observed rate constant with $[\text{H}_2\text{SO}_4]/[\text{KBrO}_3]$ ratio. $[\text{dye}] = 5 \times 10^{-5} \text{ mol dm}^{-3}$, at 35°C

Under this condition, the reaction obeyed zero-order kinetics with respect to [amaranth]. As shown in Figure 5, increasing the [amaranth] led to soft increase in the reaction rate.

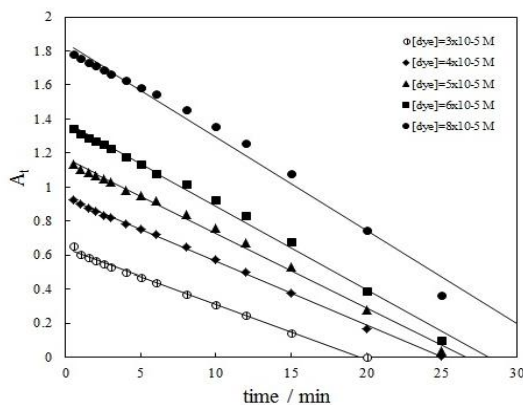


Figure 5. Zero order plots for the decolorization of amaranth by acidified KBrO_3 at different dye concentrations. $[\text{KBrO}_3] = 3 \times 10^{-2} \text{ mol dm}^{-3}$, $[\text{H}_2\text{SO}_4] = 8 \times 10^{-2} \text{ mol dm}^{-3}$ at 35°C

It was reported earlier that the reaction obeyed first order kinetics,¹⁸⁻¹⁹ while other study showed that reactions obeyed third order kinetics.²⁰

Effect of some additive ions

It is well known in the textile industry that in order to accelerate or increase the fixation of dyes onto the fibers, it is necessary to use high electrolyte concentration in dye bath to decrease the negative charged barrier between the cellulose and anionic dyes.²⁴ Therefore, the textile industry wastewaters are almost heavily charged with unconsumed dyes, different types of electrolytes and other chemicals. Taking into consideration that in effluents of textile dye industry, chloride and sulfate ions are naturally occurring anions, the oxidative decolorization reaction of amaranth was monitored in the presence of NaCl , NaBr and Na_2SO_4

Effect of sodium chloride concentration

The influence of chloride ions, NaCl , on the reaction rate was studied. The $[\text{NaCl}]$ was varied in range of the 0.4×10^{-2} – $2 \times 10^{-2} \text{ mol dm}^{-3}$, whereas the concentrations of the other reactants were kept constant. A plot of k_0 vs. $[\text{NaCl}]$ gave

straight line which indicates the first-order kinetics with respect $[\text{Cl}^-]$. Furthermore, the increase k_0 with increasing $[\text{Cl}^-]$, Figure 6, indicates that the reaction is catalyzed by Cl^- . Increasing the concentration of NaCl increases the ionic strength which indicates the reaction between species of the same charge. Also the great increase in rate constant as the $[\text{Cl}^-]$ increased can be attributed to the formation of active chloride species such as: Cl^- , Cl_2 , HOCl and ClO^- , which could work as powerful oxidizing species.¹⁸

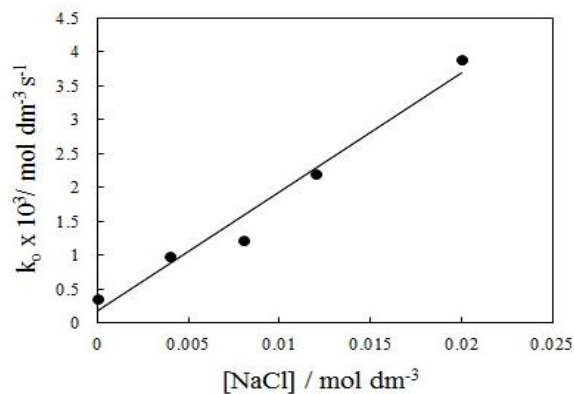


Figure 6. Variation of observed rate constant with $[\text{NaCl}]$. $[\text{dye}] = 5 \times 10^{-5} \text{ mol dm}^{-3}$, $[\text{KBrO}_3] = 1.5 \times 10^{-2} \text{ mol dm}^{-3}$, $[\text{H}_2\text{SO}_4] = 8 \times 10^{-2} \text{ mol dm}^{-3}$, at 40°C

Effect of sodium bromide concentration

The effect of the initial concentrations of bromide ion as common ion effect on the reaction rate was also studied. The $[\text{KBrO}_3]$, $[\text{H}_2\text{SO}_4]$, and [amaranth] were kept constant at $0.015 \text{ mol dm}^{-3}$, 0.08 mol dm^{-3} , and $5 \times 10^{-5} \text{ mol dm}^{-3}$, respectively, while the $[\text{NaBr}]$ was varied from 1.2×10^{-5} to $4 \times 10^{-5} \text{ mol dm}^{-3}$, Figure 7. Figure 7 shows that the oxidation rate of amaranth is greatly accelerated with increasing $[\text{Br}^-]$. This is good evidence that the $[\text{Br}^-]$ catalyzed the decolorization of amaranth. The experimental value of observed rate constant in absence of bromide ($0.43 \times 10^{-3} \text{ mol dm}^{-3} \text{ s}^{-1}$) is coincident with the intercept of Figure 7 ($0.391 \times 10^{-3} \text{ mol dm}^{-3} \text{ s}^{-1}$). It has been reported that the addition of $[\text{Br}^-]$ in the reaction medium containing acidified KBrO_3 facilitated the generation of bromine and hypobromous acid species¹¹ which work as oxidizing species.²⁵

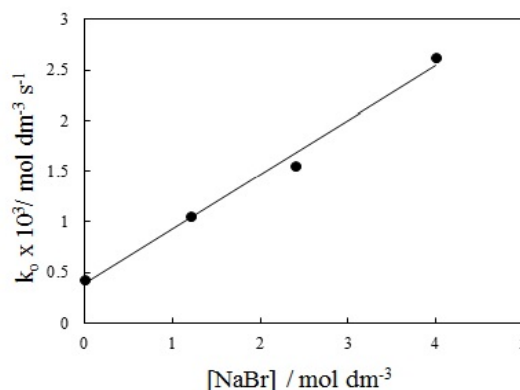


Figure 7. Variation of observed rate constant with $[\text{NaBr}]$. $[\text{dye}] = 5 \times 10^{-5} \text{ mol dm}^{-3}$, $[\text{KBrO}_3] = 1.5 \times 10^{-2} \text{ mol dm}^{-3}$, $[\text{H}_2\text{SO}_4] = 8 \times 10^{-2} \text{ mol dm}^{-3}$, at 40°C

Effect of sodium sulfate concentration

The effect of the initial concentrations of sulfate ions was also investigated. The concentration of the reactants was held constant, while the concentration of Na_2SO_4 was varied from 0.004 to 0.024 mol dm^{-3} . The value of k_0 in absence sulphate (8.62×10^{-4} mol $\text{dm}^{-3} \text{s}^{-1}$) decreased to 4.1×10^{-4} mol $\text{dm}^{-3} \text{s}^{-1}$ in presence of 0.024 mol dm^{-3} of Na_2SO_4 . This could be ascribed to the decreasing hydrogen ions concentration in the reaction medium through the decrease of ionization constant of H_2SO_4 with increasing $[\text{SO}_4^{2-}]$.¹⁸

Effect of temperature

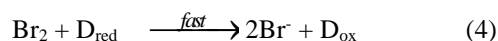
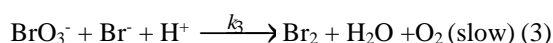
The kinetic measurements of the reaction were carried out at various temperatures in 303-318 K range. A plot of Arrhenius equation was applied and the activation energy, E_a was deduced. The other activation parameters were determined and are listed in Table 1. The ΔH^* positive value indicates that the oxidative decolorization of amaranth is endothermic.

Table 1. Thermodynamic parameters for decolorization of Amaranth by bromate

Parameters	Value
E_a	71.5 kJ mol ⁻¹
ΔH^*	68.94 kJ mol ⁻¹
ΔS^*	-85.24 J mol ⁻¹ K ⁻¹
ΔG^*	95.22 kJ mol ⁻¹

Reaction mechanism

Based on the above results and discussion, the proposed mechanism of the oxidation of amaranth red, (D), by acidified bromate is



where (red) and (ox) are reduction and oxidation reactions respectively.

The rate of reaction can be written as

$$\text{Rate} = k_3[\text{Br}^-][\text{BrO}_3^-][\text{H}^+] \quad (5)$$

Applying steady state approximation principle for HBrO_3 and Br_2 , Eqn. 5 becomes

$$\text{Rate} = k_1[\text{H}^+][\text{BrO}_3^-] \quad (6)$$

This is in good agreement with the experimental findings that the reaction follows first-order kinetics with respect to BrO_3^- , H^+ and zero-order kinetics with respect to the [dye].

Conclusion

The oxidative decolorization of amaranth red dye by potassium bromate acidified with H_2SO_4 was studied. The reaction followed zero-order kinetics with respect to amaranth and first order with respect to both KBrO_3 and H_2SO_4 . The decolorization rate was enhanced with increasing the concentrations of Br^- and Cl^- while it decreases with increasing SO_4^{2-} concentration.

References

- Ghodake, G., Jadhav, U., Tamboli, D., Kagalkar, A., Govindwar, S., *Indian J. Microbiol.*, **2011**, 51(4), 501–508.
- Abou-Gamra, Z. M., Medien, H. A. A., *Eur. Chem. Bull.*, **2013**, 2(7), 417–422.
- Burkinshaw, S. M., Kabambe, O. *Dyes Pigm.*, **2009**, 83, 363–374.
- Abou-Gamra, Z. M., *Eur. Chem. Bull.*, **2014**, 3(1), 108–112.
- Medien, H. A. A., Khalil, S. M. E., *J. King Saud Univ. (Sci.)*, **2010**, 22, 147–153.
- Elmorsi, T. M., Riyad, Y. M. Z., Mohamed, H., Abd El Bary, H. M. H., *J. Hazard. Mater.*, **2010**, 174, 352–358.
- Vogel, “*Quantitative Chemical Analysis*”, ELBS with Longman (**1991**), 405.
- Ajaya Kumar Singh, Ashok Kumar Singh, Vineeta Singh, Ashish, Surya Prakash Singh, Singh, B., *The Open Catal. J.*, **2013**, 6, 8–16.
- Sreekantha, B., Jonnalagadda, Reuben H.S., *J. Chem. Soc. Perkin Trans II*, **1988**, 1111–1115.
- Absalan, G., Alipour, Y., *Anal. Sci.*, **2003**, 19(4), 635.
- Jonnalagadda, S. B., Salem, M. A., *Phys. Chem. Chem. Phys.*, **1999**, 1, 821–826.
- Keyvanfar, M., Abedi, N., *E-J. Chem.*, **2010**, 7(4), 1612–1620.
- Shu, H.Y., Huang, C.R., *Chemosphere*, **1995**, 31, 3813–3825.
- Nadupalli, S., Koorbanally, N., Jonnalagadda, S. B., *J. Phys. Chem. A*, **2011**, 115(27), 7948–7954.
- Chung-Hsin Wu, Chung-Liang Chang, Chao-Yin Kuo, *React. Kinet. Catal. Lett.*, **2005**, 86(1), 37–43.
- Dachipally, P., Jonnalagadda, S. B., *J. Environ. Sci. Health, Part A*, **2011**, 46(8), 887–897.
- Sullivan, J. C., Thompson, R. C., *Inorg. Chem.* **1979**, 18, 2375–2379.
- Gemeay, A. H., El-Ghrabawy, G. R., Zaki, A. B., *Dyes Pigm.*, **2007**, 73, 90–97.
- Adetoro, A., Iyun, J. F., Idris, S.O., *Arch. Appl. Sci. Res.*, **2010**, 2(6), 177–184.
- Khana, M. N., Siddiqui, Z., Uddin, F., *J. Iran. Chem. Soc.*, **2009**, 6(3), 533–541.
- Swawunyama, P., Jonnalagadda, S. B., *J. Phys. Org. Chem.*, **1995**, 8, 175–185.
- Orban, M., Dekepper, F., Epstein, I. R., *J. Am. Chem. Soc.*, **1982**, 104, 2657–2658.

- ²³Foersterting, H., Varga, M., *J. Phys. Chem.*, **1993**, 97, 7932-7938. ²⁵Bagheri, H., Saber-Tehrani, M., Shishehbore, M. R., Shahvazian, M., *Prog. Color Colorants Coat.*, **2010**, 3, 58-65.
- ²⁴Carneiro, P. A., Osugi, M. E., Sene, J. J., Anderson, M. A., Zanoni, M. V. B., *Electrochim. Acta*, **2004**, 49, 3807-3820.

Received: 20.05.2014.
Accepted: 13.06.2014.



INFLUENCE OF Na₂WO₄ AND SUCCINIC ACID ON THE CORROSION RESISTANCE OF GALVANIZED STEEL IN SIMULATED CONCRETE PORE SOLUTION PREPARED IN SEA WATER.

S. Rajendran,^{[a],[b]*} C. Nathiya,^[c] P. Prabhakar,^[c] P. Shanthi,^[d] S. Umadevi,^[e] and M. Pandiarajan^[a]

Keywords: simulated concrete pore solution; galvanised steel; sodium tungstate; succinic acid.

Corrosion resistance of galvanized steel (GS) in Simulated concrete pore solution (SCPS) prepared in sea water, in the presence of sodium tungstate and succinic acid has been investigated by polarization study. Inclusion of sodium tungstate and also succinic acid in SCPS reduces the corrosion resistance of GS, Hence it is concluded use of sodium tungstate or succinic acid shall be avoided while GS rebar are used in construction of buildings, bridges especially in marine environment.

* Corresponding Authors

E-Mail: pandiarajan777@gmail.com

- [a] Corrosion Research Centre, PG and Research, Department of Chemistry, GTN Arts College, Dindigul- 624005, Tamil Nadu, India
 [b] Corrosion Research Centre, Department of Chemistry, RVS School of Engineering and Technology, Dindigul- 624005, Tamil Nadu, India
 [c] Research Department of Chemistry, APA College of Arts and Culture, Palani, Dindigul, India
 [d] Kunthavai Naachiar Government Arts College, Thanjavur- 613007, India
 [e] Sri GVG Vishalakshi College for Women, Udumalpet- 642124, India

Introduction

Several methods have been used in order to reduce the concrete reinforcement corrosion. They include cathodic protection, coatings, addition of inhibitors to concrete and a combination of these methods.¹ Corrosion inhibitors have been successfully used in steel pipelines, tanks etc, for many decades.^{1,2} Their use in concrete field is more recent, but is of an increasing interest³⁻⁷ since it can be considered as a promising technique offering an easy practice with reduced costs. For this reason, a large range of inhibitors is, nowadays, available for the customer. However, there is still a controversy regarding the inhibitors protection efficiency.⁸ Some authors reports that inhibitors are effective in reducing corrosion rate in concrete contaminated with chlorides.⁸ The most frequently used technique is adding the inhibitors to the mixing water of concrete as admixtures for new structures. Calcium nitrite was the most extensively tested corrosion inhibitor.⁹ Nitrite acts by stabilizing the passive film and its effectiveness had interestingly been proved however environmental limitations have highly reduced its use.¹⁰ Laboratory studies of the preventive inhibitive action carried out on monofluorophosphate (MFP) showed that a critical concentration ratio MFP/chlorides greater than 1 had to be achieved; otherwise the reduction in corrosion rate was not significant.¹¹ Furthermore, in solutions based on Ca(OH)₂ MFP is reported to react with the calcium ion and as a result, its active substance disappears from solution due to precipitation.

The amino-alcohols are common inhibitors based on mixtures of alkanolamines and amines or alternatively on organic acids.⁴ They were widely applied and rapidly established in the market since they are non toxic and cost attractive. Furthermore, amino-alcohols can be applied for different purposes. In fact, Wombacher et al.¹² reported that amino-alcohols based mixed inhibitors can be used either as concrete admixtures or in repair products for existing structures.¹² They transport mechanism through the concrete cover had been studied by Tritthart¹³ who demonstrated that the amino-alcohol compound is not bound by cement but remains largely dissolved in the pore liquid which provides optimal conditions for high mobility. However, according to another study carried out by Tritthart¹⁴ on cement paste samples, he found that in the case of surfaces application only a very small amount of amino-alcohol penetrated from mixed inhibitors which suggested that the penetration is inhibited by some mechanisms such as the clogging of the pores by solidification of other compounds of the mixed inhibitor.

Experimental

Preparation of Simulated Concrete pore solution (SCPS)

Simulated concrete pore solution is mainly consisted of saturated calcium hydroxide (Ca(OH)₂), sodium hydroxide (NaOH) and potassium hydroxide (KOH) with the pH ~ 13.5.¹⁵ However in numerous studies of rebar corrosion, saturated Ca(OH)₂ has been used as a substitute for pore solution.¹⁶ A saturated calcium hydroxide solution is used in present study, as SCP solution with the pH ~ 12.5.

Metal specimen

Galvanized Steel (18% Cr, 12% Ni, 2.5% Mo < 0.03 C) and balance iron wires of 1mm diameter are used in the present study.

The parameter of sea water used in the present study is given in Table 1.

Table 1. Parameters of sea water

Parameter	Results
pH	7.06
Total dissolved solids	30539 ppm
Electrical conductivity	44910 $\mu\Omega^{-1}\text{cm}^{-1}$
Total Hardness as CaCO ₃	100ppm
Calcium as Ca	19ppm
Magnesium as Mg	12ppm
Chloride as Cl	11400ppm
Fluoride as F	0
Sulphate as SO ₄	6708ppm

Result and Discussion

Analysis of Polarization curves

Corrosion resistance of galvanized steel (GS) in simulated concrete pore solution (SCPS) prepared in natural sea water, in presence of sodium tungstate and succinic acid has been evaluated by polarization method. Polarization study has been used to evaluate the corrosion resistance of metals. If corrosion resistance increases, linear polarization resistance (LPR) value increases and corrosion current (I_{corr}) value decreases.¹⁷⁻³⁰

Table 2. Corrosion parameters of galvanized steel (GS) in simulated concrete pore solution (SCPS) prepared in natural sea water, in presence and absence of inhibitors, obtained from polarization study.

System	E_{corr}	b_c	b_a	LPR	I_{corr}
	mV	mV decade ⁻¹			
	vs.SCE				
SCPS	-843	150	267	18561	2.249×10^{-6}
SCPS+A	-887	148	301	11985	3.603×10^{-6}
SCPS+B	-874	146	246	4975	8.020×10^{-6}

A=sodium tungstate 50 ppm, B=succinic acid 50 ppm

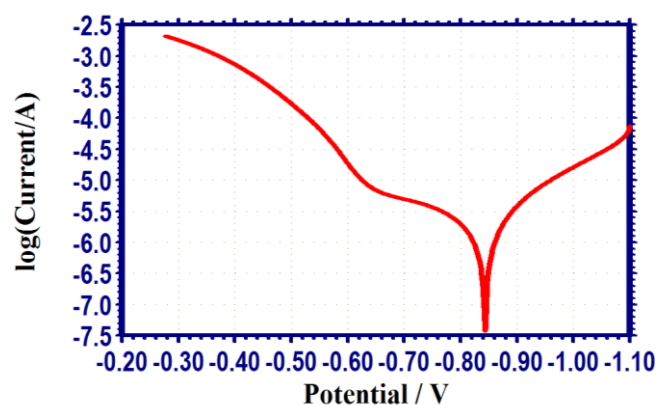


Figure 1. Polarisation curve of galvanized steel immersed in SCPS

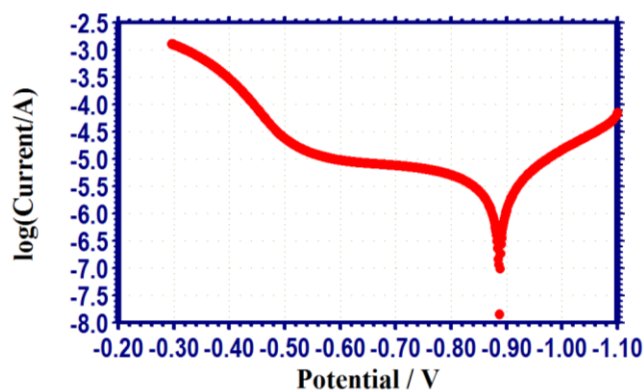


Figure 2. Polarization curve of galvanized steel immersed in SCPS+ sodium tungstate 50 ppm

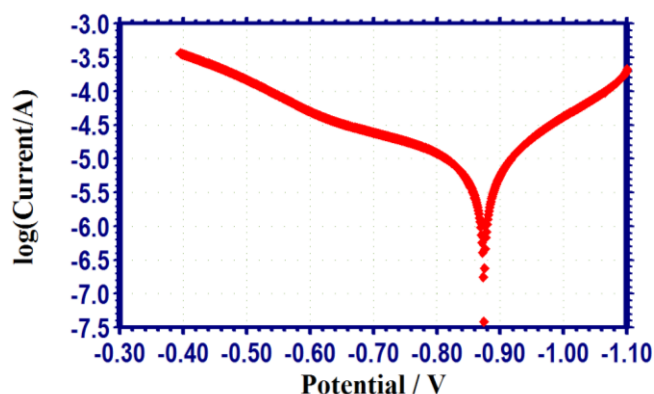


Figure 3. Polarization curve of galvanized steel immersed in SCPS+ succinic acid 50 ppm

The polarization curves of GS, immersed in SCPS in the absence and presence of inhibitors, namely sodium tungstate and succinic acid are shown in Figure 1 to 3. The corrosion parameters, namely corrosion potential (E_{corr}), Tafel slope (b_c =cathodic; b_a =anodic) linear polarization resistance (LPR) and corrosion current (I_{corr}) values are given in Table 2.

When GS is immersed in SCPS prepared in sea water, the corrosion potential is -843 mV vs SCE. The LPR value is 18561 ohmcm² and the corrosion current is 2.249×10^{-6} Acm⁻².

Influence of sodium tungstate on corrosion resistance of GS

When 50 ppm of sodium tungstate is added to the SCPS, the corrosion resistance of GS decreases. This is revealed by the fact that LPR value decreases from 18561 to 11985 ohmcm². Further, the corrosion current value increases from 2.249×10^{-6} to 3.603×10^{-6} A cm⁻². This may be attributed to the fact that when sodium tungstate is added to SCPS which is a saturated solution of Ca(OH)₂ (pH=13.9), calcium is precipitated as calcium tungstate. Hence calcium is not available for the formation of CaCO₃ and CaO on the metal surface, which is the usual case in the absence of any foreign inhibitors. This accounts for the weakening of the protective layer, decrease in LPR value and increase in corrosion current value. Another factor to be considered is that the protective film formed on the metal surface is porous and amorphous.

Through the pores of the film the corrosive ions, such as chloride ion, present in sea water diffuse towards the metal surface and enhance the corrosion of the metal. Hence decreases in LPR value and increase in corrosion current value.

Another aspect to be considered is that the experimental condition, dezincification may take place from galvanized steel, which may be enhanced due to the formation of zinc tungstate.

Influence of succinic acid on the corrosion resistance of GS

When succinic acid is added to SCPS, the corrosion resistance further decreases to a great extent and the corrosion current increases from 2.249×10^{-6} to 8.020×10^{-6} A cm⁻². This is attributed to the fact that, succinic acid, being a dicarboxylic acid, consists of succinate anions in the basic medium (pH=13.9). Moreover it forms insoluble salt of calcium succinate in the bulk of the solution. Hence calcium is not available to be transported towards the metal surface, to form Ca(OH)₂, CaO and CaCO₃. Other Factors include porous and amorphous nature of the protective film and dezincification process of galvanized steel which is enhanced by the formation of Zinc succinate is the bulk of the solution.

Analysis of the corrosion potential values indicate that in the presence of sodium tungstate and also at succinic acid, the corrosion potential is shifted to the cathodic side. This is due to the release of Zn²⁺ ion from galvanized steel because of dezincification process. The cathodic Tafel slopes and not affected very much. That is reduction of oxygen molecules into hydroxide ion is not altered very much during polarization process. However, the anodic slopes are very much. This is due to the dissolution of protective films formed on the anodic sites of the metal surface by addition of sodium tungstate and also succinic acid. The ion tungstate and ion succinate formed as protective film formed on the anodic sites go in to the solution. Hence the anodic slopes are changed when sodium tungstate and succinic acid are added to SCPS which galvanized steel is used as rebar.

Conclusion

Corrosion resistance of galvanized Steel (GS) in simulated concrete pore solution (SCPS) prepared in sea water, in the presence of sodium tungstate and succinic acid has been investigated by polarization study. Inclusion of sodium tungstate and also succinic acid in SCPS, reduces the corrosion resistance of GS, Hence it is concluded that use of sodium tungstate or succinic acid shall be avoided while GS rebar are used in construction of buildings, bridges especially in marine environment.

Acknowledgement

The authors are thankful to their management and St. Joseph's Research and Educational Trust, Dindigul for their help and encouragement.

References

- ¹Batis, G., Pantazopoulou, P., Routoulas, A., *Cement, Concrete Compos.*, **2003**, 25(3), 371.
- ²Elsener, B., Corrosion inhibitors for reinforced concrete. In: Banas, J., Filippek, R., Zurek, Z., editors. Proc. 7th Polish Corr. Conf., *J. Ochr. Prezed. Koroz.*, **2002**, 25-23.
- ³Dhouibi, L., Triki, E., Raharinaivo, A., *Cement, Concrete Compos.*, **2002**, 24(1), 35-43.
- ⁴Trepanaier, S. M., Hope, E. E., Hansson, C. M., *Cement, Concrete Compos.*, **2001**, 31(5), 713.
- ⁵Gouda, V. K., Halaka, W. Y., *Brit. Corros. J.*, **1970**, 5, 204.
- ⁶Al-Amoudi, O. S. B., Maslehuddin, M., Lashari, A. N., Almusallam, A. A., *Cement, Concrete Compos.*, **2003**, 25(4), 39.
- ⁷Montecelli, C., Frignani, A., Trabaneli, G., Brunoro, G. A., *Proc. 8th Eur. Symp. Corros. Inhib.*, Univ. Ferrara, Italy, 18-28, September, **1995**, 609.
- ⁸Jamil, H. E., Montomer, M. F., Boulif, R., Shiri, A., Ferreira, M. G. S., *Electrochim. Acta*, **2003**, 48, 3509.
- ⁹Berke, N. S., Weli, T. G., Worldwide review of corrosion inhibitors in concrete. In Malhotra, V. M., editor, *Adv. Concr. Technol.*, CAMET Ottawa. **1994**, 899.
- ¹⁰El-Jazairi, B., Berke, N. S., *The use of calcium nitrite as a corrosion inhibiting admixture to steel reinforcement in concrete*. In: Page, C. L., Treadaway, K. W. J., Bamforth, P. B., editors, *Corrosion of Reinforcement in Concrete Construction*. London: Elsevier, **1990**, 571.
- ¹¹Alonso, C., Andrade, C., Argiz, C., Malric, B., *Cement, Concrete Compos.*, **1996**, 26(3), 405.
- ¹²Wombacher, F., Maeder, U., Marazzani, B., *Cement, Concrete Compos.*, **2004**, 26(3), 209.
- ¹³Tritthart, J., *Cement Concrete Res.*, **2003**, 33, 829.
- ¹⁴Tritthart, J., *COST 521 Workshop, Belfast*, 28-31, August, **2000**, 205.
- ¹⁵Hansoon, C. M., *Cement Concrete Res.*, **1984**, 14, 574.
- ¹⁶Nakayama, N., Obuchi, A., *Corros. Sci.*, **2003**, 45, 2075.
- ¹⁷Pandiarajan, M., Prabhakar, P., Rajendran, S., *Eur. Chem. Bull.*, **2012**, 1(7), 238.
- ¹⁸Nagalakshmi, R., Rajendran, S., Sathiyabama, J., Pandiarajan, M., Lydia Christy, J., *Eur. Chem. Bull.*, **2013**, 2(4), 150.
- ¹⁹Rajendran, S., Anuradha, K., Kavipriya, K., Krishnaveni, A., Thangakani, J. A., *Eur. Chem. Bull.*, **2012**, 1(12), 503.
- ²⁰Vijaya, N., Regis, A. P. P., Rajendran, S., Pandiarajan, M., Nagalakshmi, R., *Eur. Chem. Bull.*, **2012**, 2(5), 275.
- ²¹Antony, A., Benita Sherine, H., Rajendran, S., *Port. Electrochim. Acta*, **2010**, 28(1), 1-14.
- ²²Mary Anbarasi, C., Rajendran, S., Manivannan V. N. and Shanthi, T., *The Open Corros. J.*, **2012**, 5, 1.
- ²³Sahaya Raja, A. S., Rajendran, S., *J. Electrochem. Sci. Eng.*, **2012**, 2(2), 91.
- ²⁴Mary Anbarasi, C., Rajendran, S., *Chem. Eng. Commun.*, **2012**, 199, 1596.
- ²⁵Thangam, Y. Y., Kalanithi, M., Anbarasi, C., Rajendran, S., *Arab. J. Sci. Eng.*, **2009**, 34, 49.
- ²⁶Leema Rose, A., Pascal Regis, P., Rajendran, S., Krishnaveni, A., Selvarani, F. R., *Arab. J. Sci. Eng.*, **2012**, 37, 313.
- ²⁷Anthony, N., Benita Sherine H. and Rajendran, S., *Int. J. Eng. Sci. Techn.*, **2002**, 2, 2774.

²⁸Rajendran, S., Chitradevi, P., Johnmary, S., Krishnaveni, A., Kanchana, S., Christy, L., Nagalakshmi, R. and Narayanasamy, B., *Zastit. Mater.*, **2010**, *51*, 149.

³⁰Rajendran, S., Kalpana Devi, M., Peter Pascal Regis, A., John Amalraj, A., Jeyasundari, J., Manivannan, M., *Zastit. Mater.*, **2009**, *50*, 131.

²⁹Anthony, N., Benita Sherine, H. and Rajendran, S., *Arab. J. Sci. Eng.*, **2010**, *35*, 41.

Received: 29.05.2014.
Accepted: 17.06.2014.